Leibniz-Institut für Gewässerökologie und Binnenfischerei

Dissertation

Studies of Turbulent Flow in Vegetated River Reaches with Implications for Transport and Mixing Processes

zur Erlangung des akademischen Grades
***Doctor rerum naturalium* (*Dr. rer. nat.*)**
im Fach Geographie

eingereicht an der
Mathematisch-Naturwissenschaftlichen Fakultät II
der Humboldt-Universität zu Berlin

von Dipl.-Phys. Tatiana Sukhodolova
geb. am 25.09.1968 in Chisinau, Republik Moldau

Präsident der Humboldt-Universität zu Berlin
Prof. Dr. Dr. h. c. Christoph Markschies

Dekan der Mathematisch-Naturwissenschaftlichen Fakultät II
Prof. Dr. Wolfgang Coy

Gutachter:

1. Prof. Dr. Gunnar Nützmann	Leibniz-Institut für Gewässerökologie und Binnenfischerei, Berlin
2. Prof. Gerhard H. Jirka, Ph. D.	Institut für Hydromechanik, Universität Karlsruhe
3. Prof. Angela M. Gurnell	Department of Geography, King's College London

Eingereicht am: 11. März 2008
Datum der Promotion: 9. April 2008

ZUSAMMENFASSUNG

Die vorliegende Dissertation befasst sich mit den komplexen physikalischen und biologischen Prozessen in Flachlandflüssen, die mit der saisonalen Entwicklung submerser aquatischer Vegetation im Zusammenhang stehen. Vorrangige Ziele der durchgeführten Arbeiten waren sowohl Untersuchungen zum Einfluss elastischer submerser Vegetation auf die Struktur der turbulenten Strömung, als auch die damit verbundenen Effekte auf Transport- und Mischungsprozesse sowie mögliche Auswirkungen auf Morphodynamik und Ökologie.

Erkenntnisse zur Struktur der turbulenten Strömung, die sich über Beständen submerser elastischer Vegetation entwickelt, konnten aus originären Feldexperimenten gewonnen werden. Die Resultate wurden mit der hydrodynamischen Modellierung der Entwicklung einer Mischungsschicht verglichen. Theoretische Analysen der Mischungsschicht über submerser Vegetation führten zu einer Erweitung des Modells. Dabei zeigt sich, in welcher Weise die Interaktion zwischen Strömung und Pflanzen die Entwicklung der Scherschicht und der Turbulenz beeinflusst. Die abgeleiteten theoretischen Lösungen stehen in engem Zusammenhang mit der theoretischen Beschreibung der biomechanischen Eigenschaften elastischer Vegetation.

Die Dissertation beschäftigt sich vorwiegend mit Effekten der Wechselwirkung von Strömung und Bewuchs in Bezug auf eindimensionale Ansätze der Modellierung von Transport und Vermischung in Flüssen. In der Arbeit werden quantitative Ansätze zur Modellierung der longitudinalen Dispersion für einen bestimmten Typ von Vegetation vorgeschlagen, die die komplexe Struktur der Strömung bei Bewuchs berücksichtigen. Darüber hinaus wird gezeigt, wie die entwickelte Theorie zur Wechselwirkung von Strömung und Vegetation mit einem phänologischen Modell für das Wachstum der Pflanzenbiomasse gekoppelt werden kann, womit ein nahezu geschlossener Lösungsansatz für die behandelte Fragestellung vorliegt.

Schlagwörter:
Makrophyten, Flussströmung ,Turbulenz, longitudinale Dispersion.

SUMMARY

The thesis is focused on complex physical and biological processes occurring in natural lowland streams due to the seasonal development of submerged aquatic vegetation. The primary goal of the studies was an exploration of the effects that submerged flexible vegetation sets upon turbulent flow structure, their consequences for transport and mixing processes, and implications for morphodynamics and ecology.

A deeper insight into the structure of turbulent flow evolving over a patch of flexible submerged vegetation was gained completing an original field experimental study which results were examined in a context of a hydrodynamic model of the mixing layer. The model was expanded by theoretical analysis of evolution of the mixing layer over the vegetation patch yielding knowledge on how do interactions of flow and vegetation produce the velocity shear and turbulence across the flow. The obtained theoretical solutions are linked to the theoretical description of biomechanical properties for flexible buoyant vegetation.

The thesis is concentrated on examining the consequences of flow – plants interactions in respect to the one-dimensional approach to the modeling of transport and mixing in rivers. In this study the longitudinal dispersion model was re-examined to account for the complex structure of flow in vegetation mosaic and possible quantitative approaches are proposed to infer the model parameters for a known type of vegetation. It was also shown how the developed theory of flow-plants interactions can be coupled with a phenological model of biomass growth providing a nearly complete approach to the problem.

Keywords:

macrophytes, river flow, turbulence, longitudinal dispersion.

CONTENTS

PREFACE

Last century was the time of a culmination in the thousands years struggle of humanity for natural resources, the time when there suddenly appeared an understanding for necessity to get in peace with nature by obeying its laws. However, many natural laws and subtle mechanisms by which nature operates are still the secrets that humans need to learn and to comprehend. This is why studies dedicated to the ecological problems boomed over last decades producing an immense body of literature in different branches of science. As most of the traditional sciences were beginning with collection of facts and some, sometimes completely false, beliefs, ecological studies presently are greatly relying on empirical approaches. Limits to short observations, inconsistencies difficult to interpret, and contradictions between different data are the attributes of the empirical approach which require theoretical generalizations. Unfortunately many theoretical approaches treat the problems with superficial idealizations that lack particular practical value. To achieve a compromise between these extremes, at least for a very tiny part of the general problem, was the general idea and the leitmotiv of the present research.

This study was focused on the understanding of complex bio-physical interactions occurring in the natural channel flows (brooks, streams, and rivers) subjected to the seasonal development of submerged macroscopic plants. Macrophytes, a conventional term referring to aquatic plants, establish dense colonies capable of dramatic alteration of the flow current and formation of stagnated areas where intense sedimentation processes lead to accumulation of the transported substances including valuable nutrients and harmful pollutants. The colonies, or patches of vegetation themselves are the habitats for different species of the aquatic life as invertebrates and fish. Complexity of the phenomena is explained by the fact that the flow in rivers is turbulent while the submerged vegetation is flexible and adjusting itself to the flow structure altered again by the presence of vegetation. Therefore studies of vegetated turbulent flows are almost always a challenging task with little hope for complete success. Methodologically it required both empirical evidence through field experiments and measurements, and a comprehensive knowledge of the processes allowing for some valuable theoretical advances.

Tatiana Sukhodolova,
Berlin-Friedrichshagen, 17 February 2008.

1 INTRODUCTION

Vegetation proliferates in the fluvial ecosystems - it colonizes floodplains, banks (riparian vegetation), and riverbeds (aquatic vegetation). Presence of the plants in a stream causes mechanical obstruction to the flow by redistributing velocity fields, and, as a consequence, vegetation alters the hydraulic regime of a stream, and its transport and mixing processes which are crucial for both morphodynamics and ecology of the fluvial system. As a biotic component of the system, vegetation is a source of food, it provides diverse habitat and refuge for numerous micro- (bacteria) and macro-organisms (invertebrates, fish). Because of multi-dimensional effects caused by vegetation, the seasonal dynamics of the vegetation cover is perceived either undesirable or beneficial. Water resources managers consider the uncontrolled growth of vegetation a nuisance due to reduced transport capacity of a river system because of the fact that the mechanical removal of vegetation is costly and increases turbidity of waters (Kouwen and Unny 1973). Champion and Tanner (2000) report that for the same water level in a lowland stream the water discharge was about seven times larger during the unvegetated period. The unfavorable hydraulic consequence of the abundant vegetation growth is also pronounced through the significant increase in the levels of ground waters with possible negative effects for the agriculture. However, the macrophytes are very important for maintaining the quality of water in rivers because of their efficiency for the nutrient purification through the absorption, sedimentation, and biochemical functions of microbes around plants stems and roots (Peifang and Chao 2007).

The macrophytes are generally classified in hydraulic studies as emergent and submerged. Among submerged macrophytes, which are mainly concerned in the present study, two groups are distinguished: meadow formers and canopy formers (Madsen et al. 2001). The morphology of plants comprising these two groups is different: the meadow forming plants have basal stems and homogeneous distribution of biomass over the depth while the canopy forming plants have an apical stem with biomass concentrated near the top of the plants. Moreover, the rooted macrophytes maintain upright postures in the flow by two bio-mechanical properties, namely by rigidity (stiffness) and buoyancy. A predominance of one of those properties defines a strategy of the plant in respect to maintenance of the optimal photosynthetic rates and adaptation to the physical forcing. The buoyant plants, or the certain submerged forms of the plants, tend to be flexible, and by these properties (buoyancy and flexibility) to achieve the upright positions with the maximum photosynthesis and the minimum hydrodynamic forcing while avoiding the investments of additional resources into the structural support typical for rigid plants (Stewart 2006).

Individual plants are seldom growing alone – more often they form communities called patches. Although the effect of an individual plant on the flow can be very local and relatively minor, communities are capable of generating significant changes in the environment for the benefit of comprising individuals. Physiologically the patches are perceived as the result of dominance of vegetative spread over sexual reproduction and habitat heterogeneity (Clarke 2002). Statzner and Higler (1986), and Statzner (1987) demonstrated that in fluvial systems discontinuities in the hydraulic stress are related to the flow patterns, substratum conditions, and morphology. Those factors cause and control the formation of patchiness. Even when the plants distribution seems to be fairly uniform, the biological activity of plants may have a considerable spatial variability related to current patterns (Pringle et al. 1988). A high level of patchiness in the streams is associated with the alteration of riffles and pools because of the difference in slopes, flow velocities, substratum type, and accumulation of the particulate organic matter.

Different patches together with the free spaces between them form the vegetative mosaic. Viewing streams as the mosaics of patches provides possibility for exploring the topology of mosaics and their dynamics in a quantitative manner (Pringle et al. 1988). Mechanics of spatial and temporal complexity can be investigated in a manageable fashion on the variety of scales by examining interrelationships between the basic building blocks of the system, Figure 1.1.1.

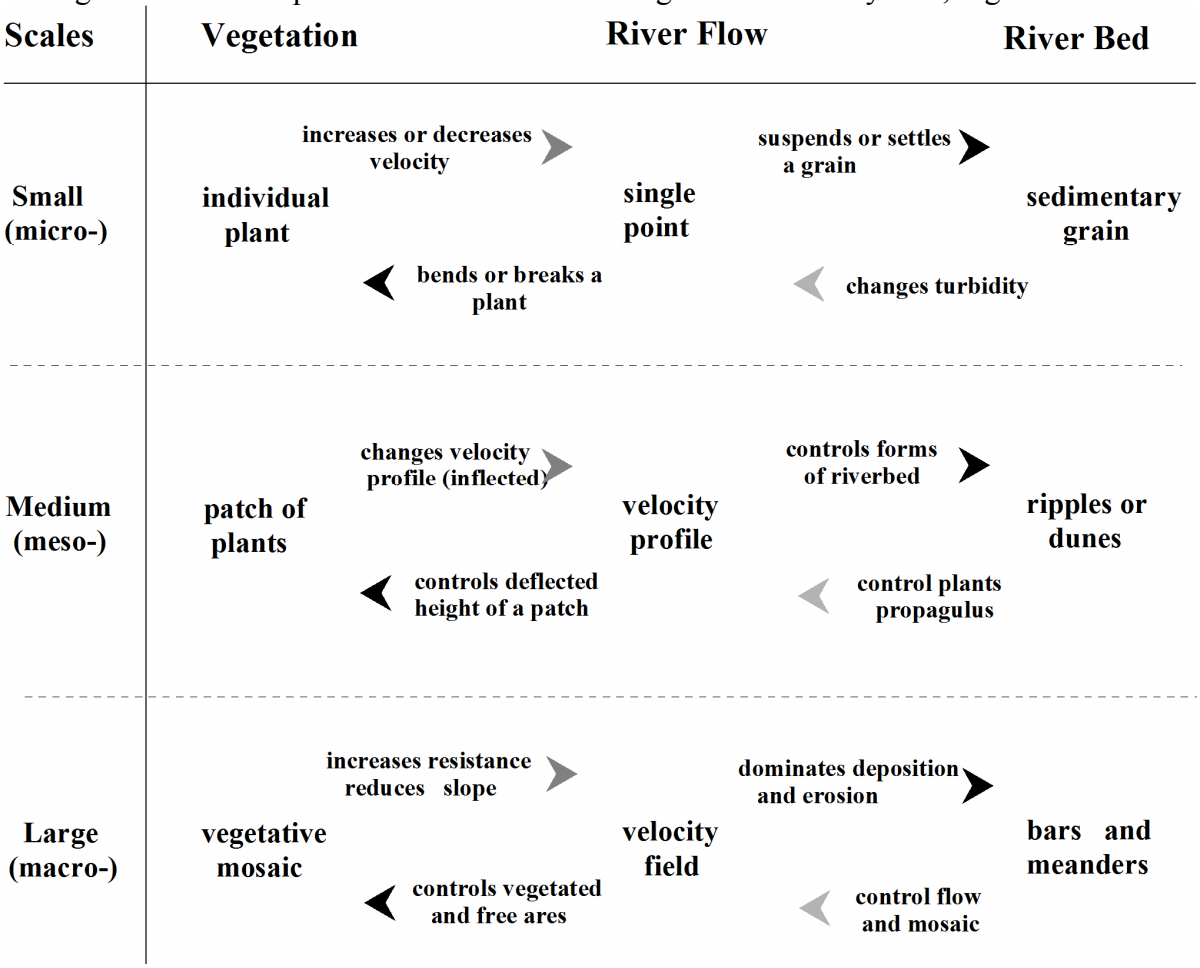

Figure 1.1.1 Schematic relationships between principal components of a fluvial ecosystem across different scales.

Because of the involvement of physical and biological components, the problem of vegetation in streams is complex and requires multidisciplinary approach to be understood and comprehended quantitatively. However, until recently only particular case problems were approached by the certain disciplines. Thus, river engineers were concerned mainly with the effects of increased resistance to the flow due to seasonal growth of vegetation and hence they approached the problem using principles of empirical hydromechanics (hydraulics). Aquatic botanists have studied various species of plants in the context of plants systematic and they regarded the physio-geographical conditions of plants habitats by the mean values of principal physical parameters as temperature, substrate, current, and depth. During the last decades the ecological issue of the problem gained broader recognition and inspired studies of more subtle mechanisms as mass exchange, transport and spiraling of nutrients in river continuum (Webster 1975, Vannote et al. 1980). The value of understanding of these complex mechanisms is dictated also by the increased demands of addressing various environmental issues in a global context of the climatic change and its consequence for the fluvial systems in different regions. Therefore both the curiously driven research and the pragmatic management have to explore the synergies of multidisciplinary approaches to integrate the expertise of environmental fluid mechanics, eco-hydraulics, fluvial geomorphology, bio-mechanics, aquatic botany, and freshwater ecology in

order to develop the practical tools for assessing the ecological integrity in fluvial environments and for guiding both the contemporary river management and the river restoration projects. The ecological integrity here is perceived through the capacity for supporting and maintaining a balanced, integrated, adaptive biologic system possessing the full range of elements and processes expected in a natural habitat of a region (Clarke 2002).

Before formulating objectives for the present research we present a state of the art review for the approaches developed in different branches of science relevant to the problem. Nowadays the bibliography on the particular aspects of the problem is ample and continuously multiplying, thus making difficulty for any review to be up-to-date and completely representative of all sources. Therefore in this review only most important works that are crucial for development of the theory are presented. The aim of this review is to give a synoptical panorama of the problem while the details of theoretical approaches will be given in the following chapter. For every involved discipline a short outline of historical prospective of development is given because it helps better understanding the lacunae in the multidisciplinary knowledge

1.1 State of the Art Review

A necessity to describe the effect of vegetation on the water flows emerged first as a consequence of the intensive hydro-engineering constructions in the second quarter of the last century. That period was characterized by the worldwide development of irrigational networks and hence demanded a design for morphodynamically stable channels accounting for the seasonal growth of aquatic vegetation. An empirical technique known as *n-Uh* retardance curves was developed to predict the resistance of grassed open-channel beds (Cox and Palmer 1948; Ree and Palmer 1949; Eastgate 1966). The technique, essentially 1D- modeling, provides the relationships for resistance coefficient of Chezy-Manning equation n as a function of bulk flow velocity U and depth h. Initially the technique was developed as a purely empirical relation, which nevertheless captured the fundamental hydrodynamic property – dependency of the friction factor on the Reynolds number. This fact explains the success and long-term relevance of the method as it is still widely used in the engineering practice hitherto. The technique was also the basis for the first attempt to incorporate bio-mechanical properties of plants into the resistance computational scheme (Kouwen and Unny 1973; Kouwen and Li 1980; Kouwen 1992) and it is still recognizable in the more recent schemes (Green 2005; 2006; Carollo et al. 2005; Wilson 2007). Although the *n-Uh* method is an effective approach in engineering applications, it contains several limitations emerging from the conceptual schemes underlying the method and the restrictions of the empirical material upon which it has been validated. Indeed, the Chezy-Manning equation and hence *n-Uh* method are strictly valid only for the steady uniform flow in which effect of vegetation is presented by homogeneous characteristics of the flow. In general *n-Uh* curves are applicable for flows causing appreciable bending of plants that result in a complete submergence of the vegetation layer and the slopes of flow surface greater than 1-2%.

More elaborated, 2D modeling schemes, were developed first for the atmospheric flows over terrestrial vegetation (Goldstein 1938; Plate and Quraishi 1965), and later applied to the aquatic submerged vegetation (Haber 1982; Murota et al. 1984; Stephan and Gutknecht 2002). This class of models, conventionally called perturbed boundary layer approach, treats the flow as a domain composed of two layers – the vegetation layer, and the overlaying boundary layer with the characteristic logarithmic velocity profile. Additional frictional force, vegetative drag, in these models was parameterized through the drag coefficients of individual plants and related to the population density of vegetation thus making a big stride toward a physically tractable solution of the problem (Thom 1971; Stewart and Thom 1973). Indeed, the models of this class allowed the description for vertical fluxes of the momentum and substances with distinction for the plant species forming the vegetation layer. However, it is appeared that the models, when applied to

analyze the results of measurements, exhibited some inconsistencies especially strong in a description of turbulence statistics (Raupach and Thom 1981).

A comprehensive analysis and comparison of experimental data coupled with the development of an accurate theoretical method of double time-space average (Wilson and Shaw 1977) allowed Raupach et al. (1989) to come up with a conclusion that the structure of flow over terrestrial vegetation is better represented by the model analogous to hydrodynamic mixing layer model rather than by a perturbed boundary layer model. It was radical and very productive proposition stimulated particularly by the deeper understanding of the structure of turbulence and its core elements – organized motions called coherent structures (Brown and Roshko 1974; Cantwell 1981; Finnigan 2000; Harman and Finnigan 2007). Recently these ideas were fruitfully adapted to the studies of the flows with aquatic vegetation (Nepf and Vivoni 2000; Ghisalberti and Nepf 2002; 2004). In contrast to the perturbed boundary layer, the model of the analogous mixing layer, or vegetated shear layer, provided a single mathematical expression for the vertical profile of time-mean velocity across both the vegetated layer and the overlying flow. This velocity profile has a distinctive inflection point which existence is a precondition for generation of the Kelvin-Helmholz instabilities that evolve into the large-scale coherent structures (Brown and Roshko 1974; Ho and Huerre 1984; Ghisalberti and Nepf 2002). Presently this approach represents a frontier for many ongoing theoretical and laboratory studies and is intensively exploited and further developed in this study.

There were also attempts to derive analytical models for the universal velocity profile over submerged vegetation using double time-space average technique and the Prandtl's mixing length hypothesis (Righetti and Armanini 2002; Carollo et al. 2002). Carollo et al. (2002) obtained an arctangent velocity profile which is in fact essentially the same as the widely used hyperbolic tangent distribution (Mischalke 1964; Ghisalberti and Nepf 2002).

Apart of the theoretical and experimental investigations, mathematical modeling of the vegetation effect was always valuable for the development of the numerical computational codes which are important for the practical applications and represent an arsenal of modern engineering tools. The obstructions to the surface flows, similar to vegetation, were first introduced into the two-equation $k-\varepsilon$ models by Burke and Stolzenbach (1983), and later used by Shimizu and Tsujimoto (1993), Naot et al. (1996), López and García (2001), Fischer-Antze et al. (2001), Neary (2003), Uittenbogaard (2003), and Choi and Kang (2004). Though these studies reveal capabilities of such computational tools in general, they also indicated particular problems associated with selection or evaluation of model parameters and usage of empirical constants.

Recently, because of expanding capabilities of modern computers, the application of direct numerical methods to solve Navier-Stokes equations became for many cases possible. Especially popular became large eddy simulation technique (LES) which appears now to be powerful enough to resolve the flow domain on a scale of a typical laboratory setup (Nadaoka and Yagi 1998; Cai and Neary 2002; Stoesser and Rodi 2004; Stoesser et al. 2006). The approach was already applied to the vegetated flow phenomena and most probably in the nearest future will became one of the primary tools in the scientific investigations.

The research activities described above were mainly carried out by the engineers and relay heavily on an idealization and high degree schematization of both the plants morphology and the flow conditions. When the models were routinely applied to study in the natural conditions, their performance was often hampered by the complexity of the natural phenomenon. This fact was most probably the reason why freshwater ecologists mostly selected purely empirical approach to the study of flow in the vegetated streams (Sand-Jensen 1998; Sand-Jensen and Pedersen 1999; Champion and Tanner 2000; Gantes and Sánchez Caro 2001; Schulz et al. 2003). The empiricism of these studies was recently a source of debate (Sand-Jensen 2003; 2005; Sukhodolov 2005; Green 2005; Statzner et al. 2006) the conclusion of which was that for the characterization of flow-plants interactions the conventions grounded on the physical principles are strictly necessary (Statzner et al. 2006). Nevertheless, the field studies completed on different

species of macrophytes were valuable to indicate that physiological and phenological properties of plants determine bio-mechanical properties and result in the flow effect.

The fluvial systems are the transport agents for various dissolved and suspended substances many of which are crucial for the aquatic life, for example nutrients, organic carbon, minerals, and oxygen. The transport rates, through the retention of substances, define the rates of the biological cycles (uptake and release) and hence directly influence a trophic state of the ecosystem. Retention of the particulate matter plays a central role in a number of stream processes including morphological changes of the riverbed and the composition of the riverbed material. Another example, a coarse particulate organic matter (CPOM) is generally available to shredders (invertebrate group) only after it is retained in the benthic zone and pre-processed by bacteria. The concept of the nutrient spiralling is essentially based on the retention processes of dissolved nutrients in the certain zones of the fluvial system. The retention of matter in streams is also a physical phenomenon, and therefore is influenced in part by the flow conditions, the properties of particles, and due to mechanical trapping of particles by macrophytes working as the nets for CPOM. A convenient mathematical framework for the transport processes of suspended and dissolved substances is provided by a model of dispersion which facilitate both practical computations and experimental field studies of the transport phenomena.

The longitudinal dispersion model was introduced in the middle of the last century by the seminal works of Sir Geoffrey Taylor (1953; 1954). Since that time the model was tested in laboratory (Elder 1959; Fischer 1967; Fukuoka 1971) and natural open-channel flows (Thomas 1958; Glover 1964; Godfrey and Frederick 1970; Day 1975; Beltaos 1980; Sukhodolov et al. 1997). These studies have indicated that the measured distributions of concentration systematically deviate from the predicted by the model of longitudinal dispersion. The deviations are pronounced in a decreased maximum of concentrations and in relatively larger trailing edges. These differences were addressed to the accumulation and the delayed release of the transported substances in non-transit zones of the flow, popularly called “dead-zones” (Nordin and Troutman 1980). Respectively, to account for the effect, an extension of the classical longitudinal model with additional terms and equation describing balance of mass in the dead zone was introduced and studied theoretically, numerically, and experimentally (Thackston and Schnelle 1970; Pedersen 1977; Valentine and Wood 1977; Young and Wallis 1986; Bencala et al. 1990; Runkel and Chapra 1993; Czernuszenko and Rowinski 1997). Recently the dispersion processes attracted attention in respect to the vegetated flows (Nepf 1999), and the model of longitudinal dispersion with dead zones was applied to interpret the seasonal dynamics of transport and mixing processes in a lowland river (Sukhodolova et al. 2006). The model uses four parameters: bulk flow velocity, dispersion coefficient, relative volume of dead zones, and a characteristic residence time in the zone. In vegetated flows all these parameters are affected or formed by the vegetation and hence substantially vary during the vegetation season. The relations between parameters of the model, the characteristics of aquatic vegetation and the turbulent flow are presently unknown and only started to be examined (Nepf 1999; Lightbody and Nepf 2006; Sukhodolova et al. 2006).

Systematic studies of vegetation began since 1730 by the famous Swedish naturalist Carl Linné. In the last quarter of nineteenth century the comprehensive taxonomic studies of aquatic vegetation with clear emphasis on plants ecology were already completed. Approximately at the same time appears a first quantitative theory describing growth of vegetation – the classical logistic growth equation of Verhulst that has been used as a basis for several extended models (Tsoularis 2001). During the last decades the interest to the aquatic plants ecology is greatly increased because of the growing understanding of the effect of vegetation on the physical components in the freshwater ecosystems (Wright et al. 1982; Madsen 1993; Gurnell and Midgley 1994; Sand-Jensen 1998; Nepf 1999; Champion and Tanner 2000; Nepf and Vivoni 2000; Lightbody and Nepf 2006). Three main directions can be outlined as relevant for the present research: investigations of spatial patterns of macrophytes abundance and composition

(Madsen 1993), the studies of freshwater macrophytes biomass growth (Best et al. 2001), and the development of a theory for bio-mechanical properties of individual plants (Niklas 1992).

The studies of abundance and composition of macrophytes as well as biomass growth and seasonal changes require accurate spatial mapping and sampling techniques. Wright et al. (1981) examined the detailed and simplified techniques of mapping and concluded that a reasonable compromise in the accuracy (10-15%) can be attained on a double fold gain in the sampling time when using rectangle technique. The most effective methods of sampling of freshwater macrophytes are relying on snorkeling or scuba-diving techniques (Downing and Anderson 1985; Madsen 1993). These techniques were shown to be superior to indirect methods employing rakes, grapnels, and various dredges. For example the sampling from a boat was only 68% as effective as the underwater sampling by a diver (Capers 2000). The size of a sampling guide template also matters and more accurate results are obtained with the larger guides for less sample replications (Downing and Anderson 1985). However, sampling and mapping are still non-standardized procedures requiring special considerations and the pilot tests prior to running the large-scale field sampling programs.

The aquatic plants, as all living organisms, are the subject to the natural life cycle which includes germination, growth, maturation as flowers are produced, senescence as the plants begin to die and decay, and dormancy (often in tubers) during the winter time. The phenological cycles are usually expressed by the concept of day-degree as an integral representative parameter of environment (Thornley and Johnson 1990). The biomass (dry weight of plants per square meter) growth is modeled by the mass-balance of the plants productivity due to photosynthetic gains and losses because of respiration and decay (Carr et al. 1997). Available models (Tsoularis 2001) require the knowledge on relative growth rates which are apparently the functions of temperature, solar irradiance, and nutrients availability (Toerien et al. 1983). Mostly these functions are obtained in the respiratory chambers in the laboratory mesocosms (Carr et al. 1997) while in-situ studies are scarce (Davis and McDonnel 1997). Movement of water has a significant effect on macrophytes growth (Madsen et al. 2001). It stimulates the abundance and diversity at low and moderate velocities, but reduces it at high velocities. Actually modifications of environment by macrophytes due to reduction of flow velocity and increased sedimentation result in an increase of light availability because of the reduction of the water turbidity. Although the theoretical grounds for modeling the biomass dynamics are significantly advanced, they provide practically no information on spatial distribution of macrophytes in terms of population density and its dynamics.

An observation that anatomy of plants is principally different for the organs experiencing different physical loads comprises a fundamental paradigm of the modern-biomechanics (Niklas 1992). Indeed, anatomical differences between the organs and the structural properties of the plants tissue can be examined to infer the nature and forces experienced by the plants. Typically in aquatic systems plants location is space (posture, bending, orientation of blades) is the result of the balance between weight, buoyancy, drag, and lift forces. Presence of the significant buoyancy force is a distinctive feature differencing the submerged aquatic vegetation from the terrestrial and emerged vegetation. Buoyancy for the flexible plants creates an accurately balanced self-regulating mechanism preventing the plants from breaking and dislodgement during the high flow events and maintaining maximally possible light conditions (Stewart 2006).

The upright posture of plants is also maintained by a flexural rigidity of the plants tissue. The flexural rigidity is defined as a multiplication of elasticity modulus to the second moment of plant section area and can be studied by the means of tensile stress-extension tests (Niklas 1992; Stewart 2006). The flexural rigidity of the aquatic plants must be highly dependent on a phenological phase and significantly influenced by the epiphyte communities. Although flexural rigidity is one of the principal parameters for predicting deflected height of submerged vegetation (Kouwen and Unny 1973) and for specification of the similarity criteria in laboratory modeling (Nepf and Vivoni 2000), it was investigated very seldom for natural aquatic

vegetation. At the same time there were numerous studies deducing simple and effective express-tests of flexural rigidity in practice of textile industry: cantilever, sliding cantilever, and heart-loop (Stuart 1966; Takatera and Shinohara 1994).

Over the last few decades there has been continuously increasing recognition of the role of aquatic vegetation in fluvial geomorphology. Initially morphodynamics processes, mainly erosion, were studied to address the problem of riverbed protection by the grass linings using the method of permissible velocities to determine erosion rates (Kouwen 1992). Particular attention in the studies was also given to the vegetation as a stabilizing factor of the riverbanks (Gregory and Gurnell 1988). The focus of more recent research was projected toward the sedimentation and deposition processes in vegetated patches. Sand-Jensen (1998), and Schulz et al. (2003) reported results of the field observations and have documented a significant increase of sedimentary deposits composed of fine cohesive material beneath the vegetative canopies is lowland rivers. Tsujimoto (1999) elaborated two-dimensional morphodynamics model and used it to study the morphodynamics processes around a patch of vegetation. The modeling results were compared to the laboratory observations and also revealed development of characteristic bedforms around the vegetated patches. Interesting field observation of morphodynamics processes induced by sparse vegetation in an ephemeral fluvial system is reported by Tooth and Nanson (2000). They demonstrated that in the landscapes with an extremely variable hydrological regime, the in-stream vegetation can form specific bedforms in three distinctive steps. In the beginning, over randomly and sparsely distributed vegetation on a flatbed, appear tear-shaped bedform with a planar form of a lemniscate and a longitudinal scale about three time of the width of a vegetation patch. After development of a tear-shaped form the interactions between neighboring patches begin by means of flow deflection and enhancement of the secondary currents which result in extending the length of individual bedforms and complete removal of some neighboring forms with their vegetation. On the final stage the relief is composed of the long parallel ridges. Some recent observations of morphodynamic processes in vegetated lowland river also indicate presence of similar bedforms (both tear-shaped and longitudinal ridges) even in typical lowland rivers (Sukhodolov and Sukhodolova 2005). Formation of these bedforms can have important implications for roughness of the riverbed after vegetation decay.

Morphodynamic processes and bedforms dynamics are particularly important for the succession of the macrophytes population. Many species of freshwater macrophytes winter in the form of tubers which are buried into the riverbed. Propagation of bedforms during winter turns over the sediments and entrains the tubers into the flow which transports them downstream where they became again deposited.

1.2 Summary of the Review

Over the last century the theories developed in different branches of engineering became a profound basis for quantitative assessment of complex interactions between turbulent flow and macroscopic plants. However, the knowledge deduced theoretically and obtained by completing idealized laboratory experiments only helps to understand processes rather than delivers a final result – this knowledge explains how processes evolve, but is incapable to predict what actually happens in the nature. On the other hand, reported field investigations mainly captured a momentary picture of the natural processes, thus giving a portrait of what has already happened but leaving obscure the question of how it has happened. Obviously the further progress can be achieved by performing field experimental studies which will bring together the theoretical grounds, the reality of nature, and a certain control of the variables which is essential of any experimentation.

Available theories of transport processes and mixing in the fluvial systems provide possibilities for describing the effect of vegetation through the dead zone parameters. However,

presently there is a lack of knowledge on the mechanisms of dead zone formation by the vegetation patches which can be only comprehended through the knowledge of details on the structure and dynamics of turbulent flow around and within the vegetation patches.

Though coupling of the transport and mixing theories with the hydrodynamic description of the flow-vegetation interaction will yield a deeper insight into the problem, an exciting prospective can emerge when such coupled theory could be further expanded with a theoretical construct describing the phenological dynamics of the vegetative patches. A resultant multidisciplinary theory will establish then an advanced predictive model for the essential mechanisms in the fluvial ecosystems.

1.3 Objective of the Study

The study described in this thesis challenges the development of a coupled theory by linking phenological dynamics of the aquatic plants to the theory of transport and mixing in a fluvial system. The link between the biological and physical components of the system will be obtained through the detailed hydromechanical analysis of complex interactions between turbulent flow and vegetation applied to the field experimental data. To make this ample task feasible, the study is limited to a particular river reach and considers only the dominant vegetation species; however the developed theory and methodology could be applied and expanded further to different macrophyte species and different rivers.

1.4 Novelty and Contribution

By providing a mathematically based model which couples formalized description for the seasonal growth of biomass and its spatial distribution with the model of bio-mechanical interactions with turbulent river flow and its consequence for flow structure and hence mixing and transport processes, the study contributes to the development of theoretical grounds of modern fluvial ecology, eco-hydraulics, and physical geography. The developed model links:

- an analytical solution of biomass growth equation describing the seasonal dynamics of the area occupied by submerged macrophytes and their population density;
- a hydrodynamic model of vegetated shear layers providing detailed information on mean and turbulent flow structure inside and above vegetation patches and allowing for quantitative objective assessment of slow transit areas within vegetation area (dead zones);
- the longitudinal dispersion model with the dead zones expanded with the closures accounting for mechanistic dispersion of substances by the patchy structure of vegetation mosaic, and allowing for prediction of transport, mixing, and retention of substances in natural streams.

The developed model and its parts were tested using the results of the original experimental and measurement studies completed in the field conditions in a typical lowland river reach subjected to the seasonal growth of aquatic vegetation. Therefore the study also provides unique experimental data set comparable in accuracy and detail to the modern laboratory studies and hence allowing for the rigorous verification of the recently developed theoretical concepts and empirical relationships. Another important aspect of the completed research is elaboration of an advanced methodology for field experiments exploiting modern acoustic methods of measurements in turbulent flows together with the novel underwater video-recording systems and expanded by methods of studies of bio-mechanical properties.

1.5 Practical Relevance

This study was completed partly in a frame of the research projects BU 1442/1 “Aggregation processes and transport of cohesive sediment in a lowland river” and SU 405/2-1 “A Fluid Mechanics Laboratory in the Field: studies of mixing layers and re-circulating flows in natural yet simplified conditions” both financed by Deutsche Forschungsgemeinschaft (DFG), with a limited support provided by the budget program of IGB. Though this research was not formally included into the budget program of IGB for the period when it was carried out, it succeeded the first and really profound attempt to establish a solid theoretical basis for multidisciplinary research carried out in IGB on the ecology and eco-hydraulics of lowland rivers. The developed theory sets the grounds for the quantitative assessment of bi-stability concept – a concept that represents a paradigm in modern freshwater ecology which assumes that freshwater ecosystem can be dominated either by phytoplankton or macrophytes. When phytoplankton is abundant the turbidity is greatly increased and limits light availability for the macrophytes and this way sets up the control over macrophytes dynamics. Vise versa, the abundance of macrophytes causes substantial decrease in phytoplankton because of enhanced sedimentation. The bi-stability concept seems to be a reasonable explanation for changes in the ecosystem of the lower Spree River where for period before 1995 the submerged macrophytes were not abundant, but presently grow intensely. To advance understanding of how bi-stability concept captures processes in the lower Spree River the developed theory will require one additional step – enclosure of a sub-model for the phytoplankton. Ecology and dynamics of phytoplankton as well as hydrodynamical aspects of phytoplankton have been the topic of intensive research in IGB, and therefore the development of the unified theory which will additionally include phytoplankton phenology and transport is reliable.

1.6 Thesis Layout

The thesis is composed of 9 chapters following abstract and introduction, and includes 132 illustrations, 20 tables, and 199 references to literature sources. The Chapter 2 is dedicated to the introduction of theoretical backgrounds of the study. The chapter is subdivided by sections according to the scientific discipline: hydrodynamics, transport and mixing, bio-mechanics and ecology, hydraulics and morphodynamics. Description in each subsection begins with essentials represented by differential equations and followed by modeling approaches. The closing subsection summarizes the relevant content and describes conceptual framework of present research. In the Chapter 3 the methodology of the study is presented together with extended description of the geographical object of the research and experimental techniques applied during the study. The Chapter 4 presents the results of field experimental and measurement studies of flow hydrodynamics over single patch of submerged vegetation, and flow structure in a river cross-section with vegetation patches, and the results of theoretical analysis of the flow structure. Bio-mechanical properties of individual plants, the growth of biomass and the formation of vegetation mosaic is described in the Chapter 5 together with development of analytical solution for a dynamical model of vegetation growth and its spatial distribution. The results of field experiments on longitudinal dispersion are presented in the Chapter 6 with the theoretical developments regarding the effect of vegetation on longitudinal dispersion coefficient. The Chapter 7 presents the results and interpretation of field observations for river flow hydraulics (bulk characteristics) and morphodynamics processes, their seasonal changes, and role of submerged vegetation in sedimentation/re-suspension processes and retention of nutrients and coarse organic matter. The Chapter 8 illustrates the developments on some practical applications including interpretation of results of studies of retention of nutrients, and

dynamics of population of juvenile fish. Short discussion of the study and main conclusions are presented in the Chapter 9 and followed by the list of references, and used symbols.

2 THEORETICAL BACKGROUND

In this Chapter theoretical background essential for the disciplines involved in the study is presented in detail. This forms both the framework for the development of a coupled theory and the interpretational analytical layout for experimental studies and observations. Each section begins with an overview of the partial differential equations governing the dynamics of a system, and continues with considerations of modeling principles, scaling relations, useful classifications and particular relevance for the fluvial systems.

2.1 Turbulent Flows

Substantial part of our study is designed to assess the flow properties in a typical lowland river and to address changes in those properties by the effect of a seasonal growth of submerged vegetation. Following presentation of the general theory (Subsection 2.1.1), the description is focused on the boundary layer theory and basics of the open-channel flows as the essentials of the flow dynamics in a non-vegetated river channel (Subsection 2.1.2). Theoretical background and considerations on mixing layer analogy for flow over submerged vegetation are represented in the Subsection 2.1.3. Basics of statistical hydromechanics bridging the theory with the practice of turbulence measurements are given in the Subsection 2.1.4.

2.1.1 Governing equations, modelling, and classification

Motion of water is completely described by the system of partial differential equations called Navier-Stokes equations (Monin and Yaglom 1971)

$$\frac{\partial u_i}{\partial t} + \sum_j u_j \frac{\partial u_i}{\partial x_j} = \frac{1}{\rho} X_i + \frac{1}{\rho}\frac{\partial p}{\partial x_i} + \nu \nabla^2 u_i, \;\; i, j = 1, 2, 3 \tag{2.1.1}$$

$$\sum_i \frac{\partial u_i}{\partial x_i} = 0 \tag{2.1.2}$$

where ρ is density of water, u is instantaneous velocity, t is time, X is body forces, x is coordinate, p is pressure, ν is kinematic viscosity, ∇^2 is a Laplacian operator. Equations (2.1.1-2.1.2) are derived considering flux balances for a control unit volume and describe dynamics of momentum (2.1.1) and conservation of mass (2.1.2). Averaging of system (2.1.1-2.1.2) in accordance with the Reynolds decomposition scheme

$$u_i = \bar{u}_i + u'_i, \;\; p = \bar{p} + p' \tag{2.1.3}$$

yields the system of Reynolds equations

$$\frac{\partial \bar{u}_i}{\partial t} + \sum_j \bar{u}_j \frac{\partial \bar{u}_i}{\partial x_j} = \frac{1}{\rho} X_i - \frac{1}{\rho}\frac{\partial \bar{p}}{\partial x_i} - \frac{1}{\rho}\frac{\partial p'}{\partial x_i} - \sum_j \frac{\partial \overline{u'_i u'_j}}{\partial x_j} + \nu \nabla^2 \bar{u}_i, \tag{2.1.4}$$

$$\sum_i \frac{\partial \bar{u}_i}{\partial x_i} = 0 \tag{2.1.5}$$

where $\bar{u}_i$ is mean velocity, and u'_i is turbulent fluctuation. Reynolds equations differ from Navier-Stokes equations by additional terms $\overline{u'_i u'_j}$ called Reynolds stresses. Multiplying the terms of equation (2.1.1) with u_i, performing Reynolds averaging, and after simple transformations one obtains equations of turbulent kinetic energy conservation

$$\frac{\partial}{\partial t}\left(\frac{\overline{u_i'^2}}{2}\right)+\underbrace{\bar{u}'_j\frac{\partial}{\partial x_j}\left(\frac{\overline{u_i'^2}}{2}\right)}_{\text{turbulent convection}}+\underbrace{\frac{\partial}{\partial x_j}\overline{u'_j\left(\frac{p'}{\rho}+\frac{u_i'^2}{2}\right)}}_{\text{pressure transport}}-\underbrace{\nu\frac{\partial}{\partial x_j}\overline{u'_i\left(\frac{\partial u'_i}{\partial x_j}+\frac{\partial u'_j}{\partial x_i}\right)}}_{\text{viscous diffusion}}=$$
$$\underbrace{-\frac{1}{2}\nu\overline{\left(\frac{\partial u'_i}{\partial x_j}+\frac{\partial u'_j}{\partial x_i}\right)^2}}_{\text{dissipation}\,(\varepsilon)}\underbrace{-\overline{u'_i u'_j}\frac{\partial \bar{u}_i}{\partial x_j}}_{\text{production}\,(\Pi)} \tag{2.1.6}$$

Equation (2.1.6) specifies important terms of turbulent kinetic energy balance such as energy dissipation ε, production Π, convection, diffusion, and transport. As it can be shown later, the terms in equation (2.1.6) are specific for different types of the flows and their study could provide deeper insight into the structure of flows and possibilities of its quantitative assessment.

Navier-Stokes equations are presently solved directly by means of numerical simulations (DNS). However, DNS methods are still limited to the very small flow domains and are only possible for simplified geometries, thus giving insight into purely academic problems (Nezu and Nakagawa 1993). Although the system (2.1.1-2.1.2) cannot be solved *exactly* for practical applications, it can be substituted by a set of equations that approximate the system (2.1.1-2.1.2) and is respectively called mathematical *model*.

Mathematical modelling is focusing on obtaining a solution of the boundary value problem of a system of partial differential equations (PDE) with given initial and boundary conditions. Reynolds equations (2.1.4-2.1.5) represent a convenient and most often used analytical framework for models development. Unfortunately, because of additional turbulent stresses $\overline{u'_i u'_j}$, Reynolds equations contain more unknown variables than the number of equations, and therefore require provision of additional (so-called closing) equations. Coupled with closing equations the system (2.1.4-2.1.5) is no more exact analogue of Navier-Stokes equations but their model with the consequences to be good or bad, appropriate or inappropriate depending on the complexity of investigated flow and choice of initial and boundary conditions.

The main goal of the mathematical modelling of turbulent flows is to solve a closure problem for the system (2.1.4-2.1.5) by providing adequate equations for turbulent stresses $\overline{u'_i u'_j}$. A simplest model assumes a relationship between mean flow and turbulence

$$-\overline{u'_i u'_j}=\nu_T\frac{d\bar{u}_i}{dx_j} \tag{2.1.7}$$

where ν_T is the turbulent viscosity. Advanced models employ more complicated schemes, for example $k-\varepsilon$ model is based on a simplified equation of kinetic energy conservation (2.1.6)

$$\frac{\partial k}{\partial t}+\bar{u}_i\frac{\partial k}{\partial x_i}=\frac{\partial}{\partial x_i}\left(\frac{\nu_T}{\mu_2}\frac{\partial k}{\partial x_i}\right)+\Pi-\varepsilon \tag{2.1.8}$$

$$\frac{\partial \varepsilon}{\partial t}+\bar{u}_i\frac{\partial \varepsilon}{\partial x_i}=\frac{\partial}{\partial x_i}\left(\frac{\nu_T}{\mu_3}\frac{\partial \varepsilon}{\partial x_i}\right)+\frac{\varepsilon^2}{k}\left(\mu_4\frac{\Pi}{\varepsilon}-\mu_5\right) \tag{2.1.9}$$

where $k=\sum\overline{u_i'^2}/2$ is turbulent kinetic energy, and $\mu_{1,2,..5}$ are empirical constants (Kolmogorov 1942; Grinvald and Nikora 1988; Rodi 1993).

The knowledge of a specific type of the flow for which a model is developed permits in many cases further simplifications of the PDE system down to the level at which the model can be solved analytically. Though analytical treatments provide exact solution for the model equations, obtained results are not necessarily the same as the exact solutions of the full system. Therefore mathematical models are always requiring *validation* of results by means of comparison with experimental data. Indeed, equations (2.1.7-2.1.9) are the good illustrations of the fact that mathematical modelling of turbulent flows requires a substantial empirical knowledge on the turbulent velocity and pressure fluctuations and their relationships to the mean flow characteristics.

Navier-Stokes equations (2.1.1-2.1.2) are represented in the physical space-time coordinate system that for a particular implementation requires specification of units and the size of the domain under investigation. The specification can be eliminated if the dimensionless coordinate system $t^* = t/t_0$, $x_i^* = x_i/l_0$, and $u_i^* = u_i/u_0$ is considered, where t_0, l_0, and u_0 are characteristic time, length, and velocity scales. In this coordinate system, with body forces typically presented by gravity force $X_i = \rho g_i$, the dimensionless momentum equation (2.1.1) will be written as

$$St\frac{\partial u_i^*}{\partial t^*} + \sum_j u_j^* \frac{\partial u_i^*}{\partial x_j^*} = \frac{1}{Fr^2} + \frac{\partial p^*}{\partial x_i^*} + \frac{1}{\mathrm{Re}}\nabla^2 u_i^* \tag{2.1.10}$$

where g is specific gravity, $St = l_0 t_0^{-1} u_0^{-1}$ is Strouhal number, $Fr = u_0 g^{-1/2} l_0^{-1/2}$ is Froude number, $p^* = p\rho^{-1}u_0^{-2}$ is dimensionless pressure, and $\mathrm{Re} = l_0 u_0 \nu^{-1}$ is Reynolds number. Dimensionless equation (2.1.10) is composed of dimensionless variables t^*, x^*, and u^*, and the dimensionless parameters St, Fr, and Re. As the dimensionless variables are not anymore dependent on the system of units or the size of the domain, the solution of the system (2.1.10) will depend solely on the dimensionless parameters. Particularly, equation (2.1.10) shows that two flows will be similar or identical if their dimensionless parameters are equal. The Strouhal number indicates if the flow is unsteady $(St \neq 0)$ or steady $(St = 0)$. The Froude number reveals if the flow regime is subcritical $(Fr < 1)$, critical $(Fr = 1)$, or supercritical $(Fr > 1)$. Reynolds number represents a relationship between inertia and viscous forces and thus is a main indicator of the flow state. At significantly large Re numbers flow is turbulent and at small Reynolds numbers it is laminar. Typically flow in lowland rivers is characterized as steady $(St \approx 0)$, subcritical $(Fr \approx 0.1)$, but almost always turbulent, $\mathrm{Re} > 10^4$ and higher.

In the previous paragraph it was anticipated that the knowledge of the flow type significantly reduces the efforts for mathematical modelling. To assist the selection of an appropriate prototype for the turbulent flow under investigation a hydrodynamical classification was developed (Tennekes and Lumley 1972). In this classification the flows are subdivided into two basic categories: *free* and *confined* flows. For free flows further classification distinguishes *mixing layers, jets,* and *wakes* while confined flows are usually represented by *boundary layer.* Schematically this classification is depicted in Figure 2.1.1.

Assumption on flow steadiness allows to eliminate the time derivatives from initial system of equations and to limit the task only into the spatial domain. Further simplifications are achieved by considering the flow away from the solid boundaries or free surface (free turbulent flows). In free turbulent flows velocity gradients are maintained inside the flow domain and the specification of certain characteristic flow properties allows for significant reductions of equations of motion.

Canonical flow patterns (Figure 2.1.1) are mainly created and observed in the laboratory facilities. In geophysical flows, and particularly in fluvial systems, these patterns are seldom presented alone. As a rule these flow patterns are superimposed and interact with each other. Recent studies suggest that the flow over submerged vegetation canopy could be also better

represented by an analogous mixing layer model which is in general a combination of boundary and mixing layers (Nepf and Vivoni 2000; Ghisalberti and Nepf 2002; 2004).

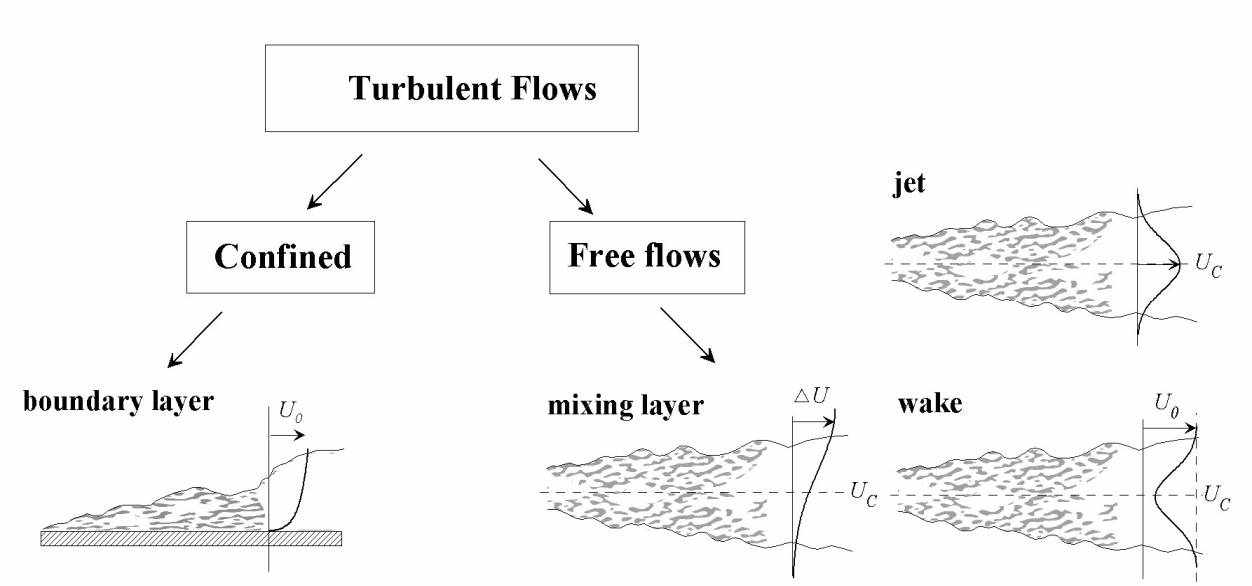

Figure 2.1.1 Hydrodynamic classification of turbulent flows after Tennekes and Lumley (1972)

2.1.2 Fluvial channel flow

Let us consider a coordinate system with the streamwise axis x parallel to the line of mean change in riverbed elevation (Figure 2.1.2a), the transverse axis y normal to the riverbanks and originating at the river centreline and positively directed toward the right bank (Figure 2.1.2b). The coordinate system also includes the vertical axis z with the origin at the mean riverbed elevation and positive direction towards the free surface (Figure 2.1.2). The riverbed is inclined at an angle α in respect to the horizontal axis so that its mean slope is $i_0 \approx \sin\alpha$.

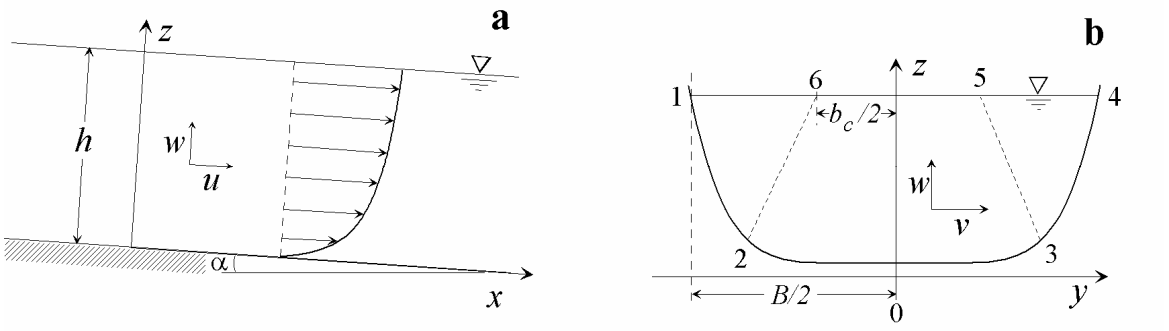

Figure 2.1.2 Schematic representation of the flow in a river

Further analysis is concentrated on a typical for many natural streams conditions: a steady turbulent flow gradually varying in the streamwise direction and with vertical scales of motion much smaller than horizontal scales. The projections of gravity force are $g_x = g\sin\alpha = g\,i_0$, $g_y = 0$, and $g_z = g\cos\alpha = -g$. For such flow the assumption that vertical accelerations are negligibly small as compared to the horizontal allows omitting the vertical accelerations in Reynolds equations (2.1.4-2.1.5). For fully developed turbulent flow the terms related to viscous effects can be also dropped because they are negligibly small as compared to others, and the equations (2.1.4-2.1.5) can be rewritten as

$$\bar{u}\frac{\partial \bar{u}}{\partial x}+\bar{v}\frac{\partial \bar{u}}{\partial y}+\bar{w}\frac{\partial \bar{u}}{\partial z}=g i_0-\frac{1}{\rho}\frac{\partial \bar{p}+p'}{\partial x}-\frac{\partial \overline{u'u'}}{\partial x}-\frac{\partial \overline{u'v'}}{\partial y}-\frac{\partial \overline{u'w'}}{\partial z} \tag{2.1.11}$$

$$\bar{u}\frac{\partial \bar{v}}{\partial x}+\bar{v}\frac{\partial \bar{v}}{\partial y}+\bar{w}\frac{\partial \bar{v}}{\partial z}=-\frac{1}{\rho}\frac{\partial \bar{p}+p'}{\partial y}-\frac{\partial \overline{u'v'}}{\partial x}-\frac{\partial \overline{v'v'}}{\partial y}-\frac{\partial \overline{v'w'}}{\partial z} \tag{2.1.12}$$

$$0=-g-\frac{1}{\rho}\frac{\partial \bar{p}+p'}{\partial z}-\frac{\partial \overline{u'w'}}{\partial x}-\frac{\partial \overline{v'w'}}{\partial y}-\frac{\partial \overline{w'w'}}{\partial z} \tag{2.1.13}$$

$$\frac{\partial \bar{u}}{\partial x}+\frac{\partial \bar{v}}{\partial y}+\frac{\partial \bar{w}}{\partial z}=0 \tag{2.1.14}$$

The normal components of Reynolds stresses tensor can be absorbed into the modified pressure term $\bar{p}$ because they represent turbulent pressure, and for a uniform flow ($\partial \bar{u}_i / \partial x = 0$) with stable free surface ($p' \approx 0$), the system (2.1.11-2.1.14) reduces to

$$\bar{v}\frac{\partial \bar{u}}{\partial y}+\bar{w}\frac{\partial \bar{u}}{\partial z}=g i_0-\frac{1}{\rho}\frac{\partial \bar{p}}{\partial x}-\frac{\partial \overline{u'v'}}{\partial y}-\frac{\partial \overline{u'w'}}{\partial z} \tag{2.1.15}$$

$$\bar{v}\frac{\partial \bar{v}}{\partial y}+\bar{w}\frac{\partial \bar{v}}{\partial z}=-\frac{1}{\rho}\frac{\partial \bar{p}}{\partial y}-\frac{\partial \overline{v'w'}}{\partial z} \tag{2.1.16}$$

$$0=-g-\frac{1}{\rho}\frac{\partial \bar{p}}{\partial z}-\frac{\partial \overline{v'w'}}{\partial y} \tag{2.1.17}$$

$$\frac{\partial \bar{v}}{\partial y}+\frac{\partial \bar{w}}{\partial z}=0 \tag{2.1.18}$$

Multiplying continuity equation (2.1.18) with $\bar{u}_i$ and adding it respectively to the left side of equations (1.1.15-17) yields

$$\frac{\partial \bar{u}\bar{v}}{\partial y}+\frac{\partial \bar{u}\bar{w}}{\partial z}=g i_0-\frac{1}{\rho}\frac{\partial \bar{p}}{\partial x}-\frac{\partial \overline{u'v'}}{\partial y}-\frac{\partial \overline{u'w'}}{\partial z} \tag{2.1.19}$$

$$\frac{\partial \bar{v}\bar{v}}{\partial y}+\frac{\partial \bar{v}\bar{w}}{\partial z}=-\frac{1}{\rho}\frac{\partial \bar{p}}{\partial y}-\frac{\partial \overline{v'w'}}{\partial z} \tag{2.1.20}$$

$$0=-g-\frac{1}{\rho}\frac{\partial \bar{p}}{\partial z}-\frac{\partial \overline{v'w'}}{\partial y} \tag{2.1.21}$$

Additional normal components of the Reynolds stresses appearing in (2.1.20-2.1.21) due to the mean motion can be also absorbed into modified pressure terms. Restricting the interest to only straight river reach allows further simplifications as terms $\overline{v'w'}$ and $\bar{v}\bar{w}$ will be zero in the absence of secondary currents and the system (2.1.19-2.1.21) rewrites to

$$\frac{\partial \bar{u}\bar{v}}{\partial y}+\frac{\partial \bar{u}\bar{w}}{\partial z}=g i_0-\frac{1}{\rho}\frac{\partial \bar{p}}{\partial x}-\frac{\partial \overline{u'v'}}{\partial y}-\frac{\partial \overline{u'w'}}{\partial z} \tag{2.1.22}$$

$$\frac{\partial \bar{p}}{\partial z}=-\rho g \tag{2.1.23}$$

Integrating equation (2.1.23) over distance from riverbed yields $\overline{p} = -\rho g z + f(x,y)$ where function $f(x,y)$ can be obtained using the boundary condition on the free surface z_s: $\overline{p}(z_s) = 0$, and respectively $f(x,y) = \rho g z_s$. Obtaining the derivative for the longitudinal pressure gradient and substituting it into equation (2.1.23) finally provides equation of momentum conservation

$$\frac{\partial\left(\overline{u}\,\overline{v} + \overline{u'v'}\right)}{\partial y} + \frac{\partial\left(\overline{u}\,\overline{w} + \overline{u'w'}\right)}{\partial z} = g\left(i_0 - \frac{\partial h}{\partial x}\right) \tag{2.1.24}$$

where $h = z_s - z_0$. Equation (2.1.24) shows that the weight of water per unit volume in the cross-section of a river channel is balanced by the stresses (mean and turbulent) exerted by the flow friction over the banks and riverbed. River flow represents a symmetric type of flow because it is confined between opposing banks (Figure 2.1.2) and therefore the transverse components of the shear stress necessarily vanish at the axis of symmetry. Defining the total Reynolds stresses as $-\overline{u}\,\overline{w} - \overline{u'w'} = \tau_{xz}/\rho$, one obtains two-dimensional equation describing momentum dynamics in the central part of the flow

$$\frac{\partial \tau_{xz}}{\partial z} = -\rho g\left(i_0 - \frac{\partial h}{\partial x}\right) \tag{2.1.25}$$

and after integration (2.1.25) with the boundary condition $\tau_{xz}(z_s) = 0$ yields

$$\frac{\tau_{xz}}{\rho} = u_*^2\left(1 - \frac{z}{h}\right),\ u_*^2 = g\,h\,I,\ I = i_0 - \frac{\partial h}{\partial x} \tag{2.1.26}$$

where u_* is characteristic velocity scale called shear or friction velocity, and I is energy gradient.

Now, knowing the distribution of shear stresses over the depth, one can obtain relations for the other flow quantities using turbulence models. Applying simplest closure (2.1.7) rewritten as $\tau_{xz} = \rho \nu_T\, d\overline{u}/dz$ together with (2.1.26) yields

$$\frac{d\overline{u}}{dz} = \frac{u_*^2\left(h - z\right)}{\nu_T} \tag{2.1.27}$$

Obviously, to integrate (2.1.27) requires specification of turbulent viscosity distribution. A simple guess on $\nu_\tau(z) = const$ provides parabolic velocity distribution known as Basen formulae. However, validation of the constant turbulent viscosity model using experimental observations indicated incapability of the model. The reliable result can be obtained using parabolic distribution of turbulent viscosity with mixing-length concept of Prandtl-Karman

$$\nu_\tau = \kappa U_* z\left(1 - \frac{z}{h}\right) \tag{2.1.28}$$

where κ is von Karman parameter. Integrating (2.1.27) together with (2.1.28) leads to the well-known logarithmic law

$$\frac{\overline{u}}{u_*} = \frac{1}{\kappa}\ln\left(\frac{z}{z_0}\right) \tag{2.1.29}$$

where z_0 is hydrodynamic roughness parameter appearing from the constant of integration at the solid boundary.

Modeling of turbulence characteristics such as turbulent kinetic energy and dissipation rates is possible only with the application of more advanced turbulence closure as $k-\varepsilon$ model (Nezu and Nakagawa 1993) which for 2-D steady and uniform flow from (2.1.8-2.1.9) writes as

$$\Pi = \varepsilon + \frac{d}{dz}\left(\frac{\nu_T}{\mu_2}\frac{dk}{dz}\right),\ \nu_T = C_\mu \frac{k^2}{\varepsilon} \tag{2.1.30}$$

Assuming local equilibrium $(\Pi = \varepsilon)$ equation (2.1.30) is transformed to

$$\nu_T \frac{dk}{dz} = const \tag{2.1.31}$$

and with an approximation for turbulence viscosity

$$\nu_T \approx \frac{k^2}{\varepsilon} \approx \frac{L_x}{k}\left(\frac{k}{\sqrt{\overline{u'^2}}}\right) \approx \frac{u_*^3 h}{k} \tag{2.1.32}$$

(here L_x is integral length scale of turbulence), can be finally rewritten as follows

$$\frac{1}{k}\frac{dk}{d\eta} = const = -2C_k \tag{2.1.33}$$

where $\eta = z/h$ and C_k is empirical constant. Integrating (2.1.33) and performing simple transformations one obtains scaling relationship describing distribution of turbulent kinetic energy over the river depth

$$\frac{k}{u_*^2} = D_k \exp\left(-2C_k \frac{z}{h}\right) \tag{2.1.34}$$

where D_k is a parameter emerging from a constant of integration. Another useful scaling relationship was deduced for the dissipation rate of turbulent energy (Nezu and Nakagawa 1993)

$$\frac{\varepsilon h}{u_*^3} = E\sqrt{\frac{h}{z}}\exp\left(-3\frac{z}{h}\right),\ E = 12.2K_x/B_x \tag{2.1.35}$$

where K_x and B_x are some functions of integral scales of turbulence.

Analysis described in the previous paragraph is applicable to the central part of the river located sufficiently far from the banks influence or where the opposing effect of banks diminishes directional fluxes (Figure 2.1.2b). Actually, for many natural streams, especially for mountain rivers, the central part of the river represents about 80 to 90% of the river section area due to the fact that river width can be 100 times larger than the river depth. However, in small lowland rivers and trained reaches the influence of the banks can attain 2/3 of the river width and should be taken into account.

Considering the area of the flow close to the free surface where τ_{xz} stress component is close to zero, one can from (2.1.24) obtain the horizontal stresses $-\overline{u}\,\overline{v} - \overline{u'v'} = \tau_{xy}/\rho$

$$\frac{\partial \tau_{xy}}{\partial z} = \rho g I \tag{2.1.36}$$

and integrating with the condition on the delimiting line $\tau_{xy} = 0$ (points 5, and 6 in Figure 2.1.2) yields

$$\frac{\tau_{xy}}{\rho} = v_*^2\left(1 - \frac{\hat{b}-\hat{y}}{\hat{b}}\right),\ v_*^2 = gI\hat{b} \tag{2.1.37}$$

where v_* is side-wall (bank) shear velocity, $\hat{y} = y - b_c/2$, and $\hat{b} = \left(B - b_c\right)/2$ is the area of flow affected by the flow friction over the bank.

Effect of vegetation is traditionally modelled by the drag force concept in frame of which the pressure gradient is represented as

$$\frac{\partial \overline{p}}{\partial x} = \rho C_D a \frac{\overline{u}^2}{2} \tag{2.1.38}$$

where C_D is drag coefficient of the plants, a is projected area of the plants, and $\overline{u}$ is mean velocity in the vegetated layer. Respectively equation (2.1.25) can be rewritten as

$$\frac{\partial \tau_{xz}}{\partial z} = -g\rho \left(i_0 - C_D a \frac{\overline{u^2}}{2} \right) \tag{2.1.39}$$

Opening the brackets in (2.1.39) and considering that slope of the river has a negative sign in the downstream direction, one after integration obtains

$$\frac{\tau_{xz}}{\rho} = ghS + C_D a h_{ve} \frac{\overline{u}_v^2}{2} \tag{2.1.40}$$

where h_{ve} is the effective height of the vegetation layer.

In contrast to the vertical (2-D) boundary layer examined in previous section, 3-D boundary layer near the bank of the river is more complicated because the location (extent) of the layer is not known a priory. Indeed, the fully developed vertical boundary layer is limited in the river by the free surface. As the research was concentrated on 2-D boundary layers an immense empirical material was available for validation of turbulence model and deduction of logarithmic velocity law. For 3-D boundary flows near river banks all information that is necessary for carrying out analytical treatment is presently unavailable and the solutions are generally obtained numerically accounting to only one evident boundary condition – zero velocity at the water edge. Obviously, the necessary knowledge can only be obtained from detailed studies of 3-D turbulence patterns in the near bank region with unambiguous determination of transversal stress components τ_{xy} and spatial scales of organized turbulent motions (*coherent structures*) responsible for stresses formation. The following paragraph introduces some basics of coherent structures theory.

Implicitly the introduction of turbulence models implied a certain degree of determinedness in the turbulence, and recognizing of the fact that some experimental studies in canals were completed shortly after Reynolds (Rümmelin 1913). Explicitly the determinedness of turbulence was postulated in the concept of triple decomposition proposed by Velikanov (1946), and evidenced in the experimental research by Townsend (1956). These works and their ideas preceded the development of the contemporary concept of spatially coherent, temporally evolving vortical motions, popularly called coherent structures (Cantwell 1981; Lumley 1981; Nezu and Nakagawa 1993; Schoppa and Hussain 2000). Term coherent outlines a specific feature of the structures: the correspondence between components of the velocity vector and pressure distinguishing the structure from surrounding liquid. This peculiarity provides a possibility for visual observing of some simple structures. The structures developing near the riverbed and lifted toward the free surface, so-called *boils* (Matthes 1947) were shown to appear in a quasi-periodic manner (Jackson 1976) and can be documented with a camera (Figure 2.1.3).

However, because of irregular geometry of river and unsteadiness of water discharge, the instantaneous velocity patterns in rivers can be extremely complex.

Coherent structures manifest the governing mechanisms of energy extraction from the mean flow and hence it is naturally expected that their understanding could lead to the further development of models for the turbulence statistics. Despite intensive studies on coherent structures over the last half century only few quantitative theories had been proposed. The

situation mainly accounts for the fact that large-scale energy containing structures are extremely dependent on the flow geometry and universal theories can not be principally developed.

Figure 2.1.3 Boil on a flow free surface in the Wesenitz River

Velicanov (1946) has proposed a theoretical model for vertically two-dimensional open-channel flow. He suggested that the large-scale turbulent structures originate due to vertical velocity gradients and following Rümmelin (1913) can be represented by helical motions with the spatial scales comparable to the flow depth and transported with the mean convective velocity that equals to the bulk flow velocity. This kinematical model for coherent structures has found further experimental confirmation (Klaven 1968). Implying determinedness in turbulence, Velicanov suggested to expand Reynolds decomposition into triple decomposition $\mathbf{u} = \overline{\mathbf{u}} + \tilde{\mathbf{u}} + \mathbf{u}'$ where $\overline{\mathbf{u}}$ is mean velocity, $\tilde{\mathbf{u}}$ is structural velocity, and $\mathbf{u}'$ is random velocity. A streamline for structural component Velicanov represented with periodic function $\psi = c\cos\left(2\pi\left[\chi + f(\eta)\right]\right)$, $\chi = x/L_C$, $\eta = z/h$, where x is streamwise coordinate, L_C is average length of large-scale structure. Considering streamwise and vertical components $u = -\partial\psi/\partial z$, $w = -\partial\psi/\partial x$ together with Lorenz equation, Velicanov obtained $f(\eta) = 1-\eta$, $c = \sqrt{g\,h\,i_0\,\pi^{-2}}\sqrt{L_C\,h/2}$, and deduced expressions for turbulence intensity and turbulent stresses

$$\frac{\overline{\tilde{u}\tilde{w}}}{u_*^2} = 1-\eta \tag{2.1.41}$$

$$\frac{\sqrt{\tilde{u}^2}}{u_*} = \sqrt{\frac{L_C}{h}}(1-\eta) \tag{2.1.42}$$

$$\frac{\sqrt{\tilde{w}^2}}{u_*} = \sqrt{\frac{L_C}{h}} \tag{2.1.43}$$

The model of Velicanov includes length scale parameter L_C which has to be determined to provide the closure for the model (2.1.41-2.1.43). A simple relationship was proposed by Grishanin (1979). Assuming a relationship between large-scale structures and flow depth, from a phenomenological relation $T_C = \left(h^2/\overline{\varepsilon}\right)^{1/3}$, Grishanin obtained

$$\frac{L_C}{h} = \left(\frac{C^2}{g}\right)^{\frac{1}{3}} \tag{2.1.44}$$

where T_C is mean period of large-scale structures, $\bar{\varepsilon} = g\overline{U}I$ is depth-averaged dissipation rate, and $C = \overline{U}/\sqrt{hI}$ is Chezy parameter.

2.1.3 Mixing layers: general theory and special cases

As it was shown in the Subsection 2.1.1 mixing layer represents a fundamental, and apparently simplest, class of turbulent flow patterns (Tennekes and Lumley 1972). The family of mixing layers derives from a canonical mixing layer – a free turbulent flow maintained by internal velocity gradients and evolving independently of solid boundaries (Monin and Yaglom 1971; Brown and Roshko 1974). Typically canonical mixing layers evolve in the co-flowing liquids of different densities or flows of different mean velocities, for instance downstream of a splitter plate, Figure 2.1.4.

For incompressible, stationary, and uniform coflowing streams, Navier-Stokes equations can be reduced to (Tennekes and Lumley 1972; Pope 2000)

$$\frac{\partial \bar{u}}{\partial x} + \frac{\partial \bar{v}}{\partial y} = 0 \tag{2.1.45}$$

$$\bar{u}\frac{\partial \bar{u}}{\partial x} + v\frac{\partial \bar{u}}{\partial y} + \frac{\partial \overline{u'v'}}{\partial y} = 0 \tag{2.1.46}$$

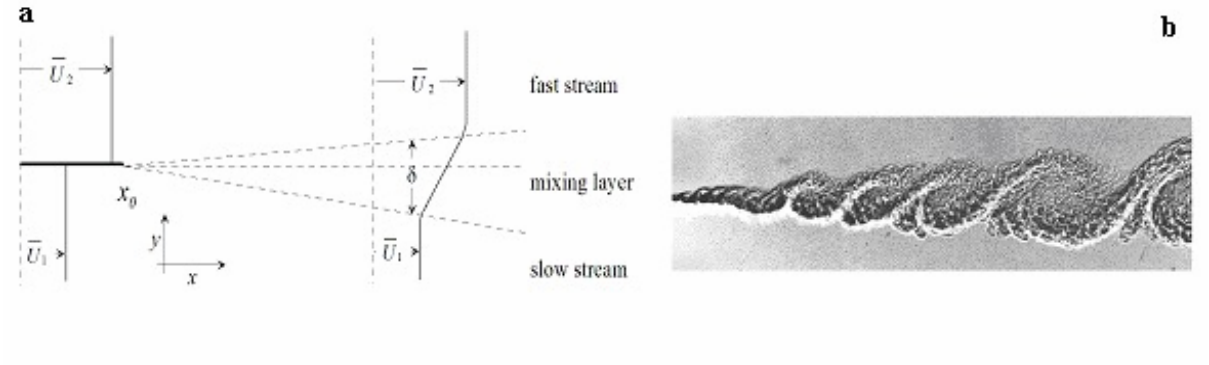

Figure 2.1.4 A sketch of a canonical mixing layer (a), and a photograph from laboratory experiments by Brown and Roshko, 1974 (b).

Two characteristic velocity scales are defined for the mixing layer - convective velocity $u_C = \left(\bar{u}_1 + \bar{u}_2\right)/2$, and velocity difference $\Delta u = \bar{u}_2 - \bar{u}_1$. The width of the mixing layer is a cross-flow distance between locations where velocities inside the mixing layer attain the values of the ambient flows (within 10% accuracy) $\delta(x) = y_{0.9}(x) - y_{0.1}(x)$, and its centreline is positioned at $\bar{y}(x) = \left(y_{0.9}(x) + y_{0.1}(x)\right)/2$. Respectively, the scaled cross-flow coordinates are defined by $\xi = \left(y - \bar{y}(x)\right)/\delta(x)$, the scaled velocities by $F(\xi) = \left(\bar{u} - u_C\right)/\Delta u$, and the scaled Reynolds stresses by $\tau_n(\xi) = \overline{u'v'}/\Delta u^2$ (Pope 2000). Supposing the similarity for canonical mixing layers (assumption is confirmed by experimental evidence), one can represent the system (2.1.45-2.1.46) as

$$\frac{u_C}{\Delta u}\frac{d\delta}{dx}\left(\xi + \frac{\Delta u}{u_C}\int_0^{\xi} F(\xi)d\xi\right)F' = \tau_n'. \tag{2.1.47}$$

Equation (2.1.47) clearly illustrates that the condition of self-similarity in the canonical mixing layer is attained only if scaling variables vary linearly along the principal direction of the flow

$$\frac{u_C}{\Delta u}\frac{d\,\delta}{d\,x} = \alpha_c = const \tag{2.1.48}$$

where α_c is spreading coefficient. The spreading coefficient is the quantity that has to be determined empirically. Available experimental studies report values in the range from 0.06 to 0.12, and the observed scatter is attributed to the initial conditions on the splitter plate (Pope 2000).

Applying turbulence-viscosity hypothesis $\tau_n = -\nu_T F'$, and considering uniform turbulent viscosity across the flow, one reduces equation (2.1.47) to

$$\alpha_c \xi F' = -\nu_T F'' \tag{2.1.49}$$

which readily provides the solution for the scaled velocity profile

$$F(\xi) = \frac{1}{\sqrt{2\pi\nu_T/\alpha_c}}\int_0^{\xi}\exp\left(-\frac{\xi^2\alpha_c}{2\nu_T}\right)d\xi = \frac{1}{2}erf\left(\frac{\xi}{\sqrt{2\nu_T/\alpha_c}}\right). \tag{2.1.50}$$

Though exponential mean velocity profile (2.1.50) has solid theoretical basis, an empirical hyperbolic tangent function is used in many theoretical and experimental studies (Michalke 1965)

$$F(\xi) = 0.5\tanh\left(\frac{2y}{\delta}\right) \tag{2.1.51}$$

Equation (2.1.51) is a good approximate to (2.1.50) which fits experimental data as well, and is conventional for analytical studies.

Detailed laboratory studies have reported that the mean velocity profile (2.1.50) evident on the time-averaged patterns actually never exists at any given instant (Wygnanski and Fiedler 1970). The instant interface between merging flows appears to be sharp and corrugated due to the presence of large-scale vortex structures, Figure 2.1.4b (Ho and Huerre 1984). Initially, close to the splitter, the downstream development of the mixing layer is dominated by a linear instability mechanism. The basic vorticity distribution in parallel flows of different velocities has a distinctive maximum and hence is inviscidly unstable to small perturbations via the Kelvin-Helmholtz instabilities which grow exponentially with distance and roll up into vortices (Ho and Huerre 1984). The characteristic period T_C of instabilities and vortices in the mixing layer is related to bulk flow characteristics by the Strouhal number

$$St = f\frac{\delta_m}{U_C}, \quad \delta_m = \frac{\delta}{4\sqrt{\pi}} \tag{2.1.52}$$

where δ_m is momentum thickness, $f = 1/T_C$ is a frequency. The linear stability analysis completed using (2.1.51) provided the critical value of the Strouhal number $St = 0.032$ which corresponds to so-called natural frequency f_n of the unforced mixing layers between parallel flows and was validated through experimental studies (Ho and Huerre 1984). Despite the fact that f_n appeared to be independent of velocity difference, in non-parallel flows and forced mixing layers its value was shown to deviate significantly ($St =$ 0.076) from the nominal.

As it was described above, the vortices of the mixing layer grow exponentially with the distance while the width of the mixing layer is growing linearly. This contradicting feature is explained by the fact that instabilities and vortices appear randomly in space and time and the observations of ensembles in averaging procedures smears distinctive boundaries imposed by certain structures. In result the sharp gradients in the mean flow appear to be smooth and the

mean flow complies with the exponential mean velocity profile (2.1.50) and its hyperbolic tangent approximate (2.1.51).

Canonical mixing layers provide the prototype flow pattern and the analytical framework (2.1.45-2.1.52) for somewhat more applied types of flows (shallow mixing layers) that create a basis for quantitative description of complex geophysical flows. Shallow mixing layers appear in depth restricted environments where flows of different velocities are merging in horizontally unconfined domain. In fluvial systems these flows are found at river confluences and near engineering constructions. They were explored in laboratory facilities (Chu and Babarutsi 1988; Uijttewaal and Tukker 1998; Uijttewaal and Booij 2000) and recently in the field (Schnauder et al. 2007). The studies have shown that dynamics of the mixing layers is governed by the friction on the flow bed which produces stabilizing effect upon the spatial growth of the mixing layer at the larger downstream distance from the mixing layer origin. For the shallow mixing layers the spreading coefficient α_c is usually defined differently than (2.1.48) and is represented as follows

$$\alpha_c = \frac{d\delta}{dx}\frac{2u_C}{\Delta u} \tag{2.1.53}$$

The spreading coefficient in the shallow mixing layers is no more constant as in the free mixing layers where $\alpha_c = 0.18$, but depends on the stabilizing effect of the bottom shear on the large scale structures and therefore is decreasing with distance from the origin. The stabilizing effect of the bottom shear is presented by the flux bed friction number S_{flux} that is determined by the ratio between the loss $\Lambda = 0.5 c_f \bar{u} \left(2\overline{u'}^2 + \overline{v'}^2 \right) / h$ of large scale kinetic energy due to the bottom friction and the production $\Pi = -\overline{u'v'}\frac{\partial \bar{u}}{\partial y}$ of the large scale turbulence

$$S_{flux} = \frac{\Lambda}{\Pi} \tag{2.1.54}$$

Assuming proportionality between turbulent stresses, the flux bed friction number S_{flux} can be simplified to the gradient bed friction number S

$$S = c_f \frac{\delta}{h}\frac{u_c}{\Delta u} = \frac{\delta}{h}\frac{c_f}{2\lambda},\ c_f = 2\frac{\tau_0}{\rho \bar{u}^2} \tag{2.1.55}$$

where c_f is friction factor, and $\lambda = 0.5\Delta u / u_c$. Relation between α_c and S based on the experimental data was suggested by Chu and Babarutsi (1988)

$$\begin{aligned} &\alpha_c = \alpha_{C0}\left(1 - \frac{S}{S_{crit}}\right) \quad for\ S < S_{crit} \\ &\alpha_c = 0 \qquad\qquad\qquad for\ S > S_{crit} \end{aligned} \tag{2.1.56}$$

with $\alpha_c = 0.36$. However, Tukker (1997) found initial spreading coefficient to be identical to the spreading coefficient of free mixing layers $\alpha_c = 0.18$.

Recently the mixing layer analogy was successfully applied to describe the dynamics of atmospheric flows over terrestrial vegetation, for instance over the woods of considerable area (Raupach et al. 1996; Finnigan 2000), and in laboratory studies of submerged flexible aquatic vegetation (Gisalberti and Nepf 2002). Obviously, the analogy was promoted by the inflected mean velocity profile (2.1.51) that is inviscidly unstable to the small perturbations and is the source of the enhanced turbulence. Unlike the perturbed boundary layer model, the mixing layer analogy offers complete solution for flow above, in the interface, and inside the vegetation canopy. Mostly the studies exploiting the mixing layer analogy consider the region of fully developed uniform flow, where the mixing layer growth is either stabilized by the friction effects

or restricted by the flow boundaries (Ghisalberti and Nepf 2002). The dynamical properties of the mixing layers evolving in flows over vegetation canopies were not explored in detail hitherto. However, some information was gained through the studies of coherent structures populating the interface between the flows over and inside the canopy (Ghisalberti and Nepf 2002). Particularly, those studies indicated that large scale organized fluid motions generate *monami* motions of the vegetative canopy that significantly affect momentum transfer into the canopy. The characteristic frequencies of coherent structures were reported to scale in accordance with (2.1.52) for $St = 0.032$ revealing thus that the structure of the flow over vegetation is similar to that of canonical mixing layers.

In analogous mixing layers over vegetation the layer width grows only to a finite thickness. Thereby the canopy drag is simultaneously a source of appearance and the culprit of the suppression of the mixing layer. Stability parameter for the vegetated mixing layers can be evaluated from the condition of equilibrium between shear scale turbulent kinetic energy and the dissipation due to canopy drag within the shear layer (Ghisalberti and Nepf 2004)

$$\int_{z_1}^{z_2} -u'w'\frac{\partial u}{\partial z}dz = \int_{z_1}^{h}\frac{1}{2}C_D a\,\overline{u}\left(2\overline{u'}^2+\overline{v'}^2\right)dz \tag{2.1.57}$$

where z_1 and z_2 are lower and upper boundaries of the vegetative layer respectively. The integral conservation of shear turbulent energy (2.1.57) can be simplified (Ghisalberti and Nepf 2004) by application of the eddy viscosity concept and assumption on the self-similarity approximate of the velocity profile to yield

$$\Delta u^2 \approx (h-z_1)\,C_D\,a\,(u_h^2-u_1^2) \tag{2.1.58}$$

Stability parameter was determined by Ghisalberti and Nepf (2004) as the ratio between the production of the large-scale turbulence energy and the canopy drag dissipation

$$\Omega = \frac{(\Delta u)^2}{(h-z_1)\,C_D a(u_h^2-u_1^2)} \tag{2.1.59}$$

The critical value of Ω was found experimentally to be equal $\Omega = 8.7 \pm 0.5$.

2.1.4 Statistical description of turbulent flows

In the previous sections the turbulent flows were examined using the partial differential equations and respectively considering the flow as a *deterministic* continuum. We have also demonstrated that in turbulent flows are always present unavoidable perturbations in initial, boundary conditions, and material properties which cause turbulent fluctuations and therefore make flow variables (velocities, pressure) *random*. Typical records of instantaneous velocity vector components are shown in Figure 2.1.5.

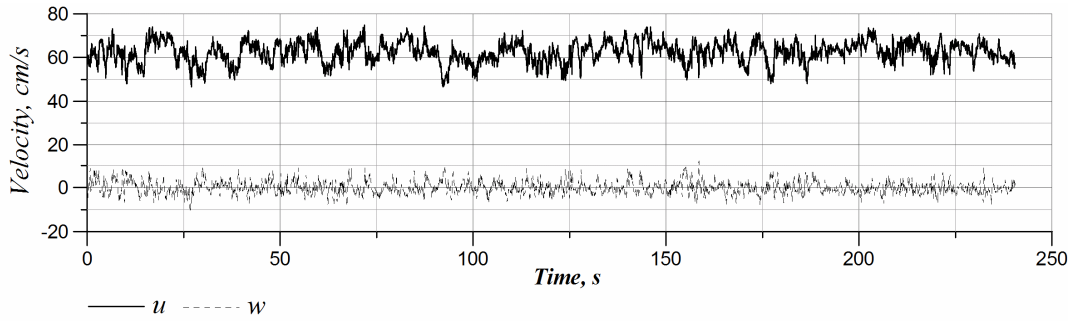

Figure 2.1.5 Instantaneous velocity records measured in the Spree River

Seemly random fluctuations about certain mean value are evident on these records. It is also evident that to subtract comprehensive information on random variables one needs to apply statistical methods (Monin and Yaglom 1971; Pope 2000).

Let us consider a random flow variable u which in general can be any component of velocity vector or pressure. A probabilistic event that a certain instantaneous value of the variable u is smaller than a certain threshold U is $B \equiv \{u < U\}$, and respectively the probability of the event is defined as $P(B) = P\{u < U\}$. To characterize the probability of any event one should examine cumulative distribution function $F(U) \equiv P\{u < U\}$. A *probability density function* (PDF) is derivative of $F(U)$

$$f(U) = \frac{dF(U)}{dU} \tag{2.1.60}$$

and represents a complete characteristic of the random variable u. PDF is usually constructed to satisfy normalization condition $\int_{-\infty}^{\infty} f(U)dU = 1$, $f(U) \geq 0$, and $f(-\infty) = f(\infty) = 0$. For any PDF characteristic parameters called statistical moments μ_n can be defined as

$$\mu_n = \int_{-\infty}^{\infty} (U)^n f(U)dU, \; n = 1, 2, 3 \ldots m \tag{2.1.61}$$

A PDF of completely random variable is represented by a Gaussian or normal function

$$f(U) = \frac{1}{\sqrt{2\pi\mu_2}} \exp\left[-\frac{(U-\mu_1)^2}{2\mu_2}\right] \tag{2.1.62}$$

The first statistical moment of distribution is simply the mean value

$$\mu_1 = \overline{U} = \int_{-\infty}^{\infty} U f(U)dU \tag{2.1.63}$$

and the root square from the second centred moment is standard deviation or fluctuation

$$\mu_2 = \overline{U'^2} = \int_{-\infty}^{\infty} \left(U - \overline{U}\right)^2 f(U)dU \tag{2.1.64}$$

Obviously, $U = \overline{U} + \sqrt{\overline{U'^2}}$ represents statistically the random variable and provides the essence of the Reynolds decomposition (Section 2.1.1). The moments of higher order μ_3, and μ_4 represent the features of the PDF shape, thus the third moment (skewness) indicates the asymmetry of the PDF, and the fourth moment (kurtosis) characterizes flatness of the distribution.

In practice the continuous fields of random variables are represented by discrete functions and respectively integrals are replaced by sums for determination of the statistical moment for the discrete functions. The PDF functions then are approximated by histograms in which the empirical frequencies n/N (n is number of samples in a certain interval, and N is total number of samples in the record) are plotted versus respective intervals of the random variable. An example of empirical distribution for the streamwise velocity component (u) of the record presented in Figure 2.1.5 is shown in Figure 2.1.6. The solid line on the plot indicates normal distribution (2.1.62). Although the deviations of the measured PDF from the normal distribution seemed to be small, they are characteristic for the river turbulence. It indicates that there were distinctive fluctuations of velocity larger than mean (peaks larger than normal line on the right side) and smaller than mean (peaks on the left side).

For two random flow variables u and w, for example, one can similarly define a *joint* cumulative probability distribution function $F^*(U,W) \equiv P\{u < U, w < W\}$ and respectively a joint probability density function $f^*(U,W)$ the second moment of which called co-variance

$$\mu_2^* = \overline{U'W'} = \int_{-\infty}^{\infty}\int_{-\infty}^{\infty}\left(U-\overline{U}\right)\left(W-\overline{W}\right)f^*(U,W)\,dU\,dW \qquad (2.1.65)$$

is an essence of the shear stresses defined in the Section 2.1.1.

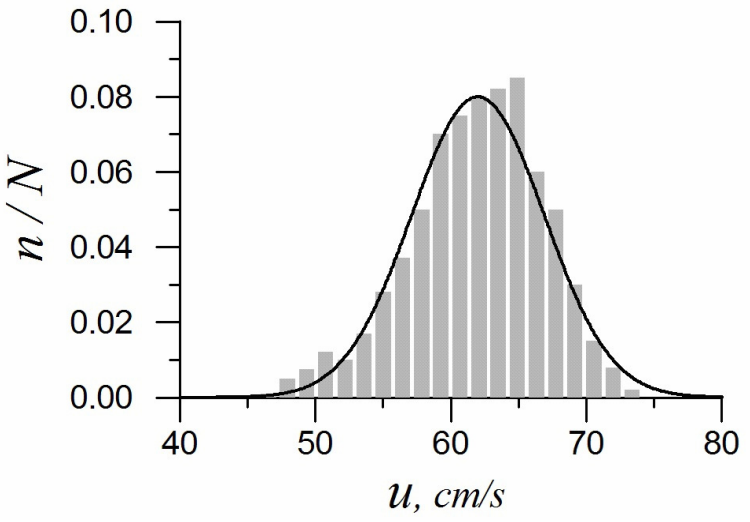

Figure 2.1.6 Example of velocity histogram and its approximation with normal distribution

The theory of random variables introduced briefly in this paragraph provides statistical description for one-point observations and considers the random variable irrespective of time. However, the turbulent signal is a result of certain motions that pass the point of observation as flow evolves in space and time. Obviously, the complete insight into the statistical properties should also include the relation of random signals to the space and time or the knowledge of *random processes*.

To introduce definition of a random process we should consider the random variable *u* as a function of time *u(t)*. Formally speaking *u(t)* is now a random process completely characterized by its one-time probability distribution function $\hat{F}(U,t) \equiv P\{u(t) < U\}$ and respectively by its derivative or one-time probability density function $\hat{f}(U,t)$. Although strictly speaking for characterization of a random process we need to know $\hat{f}$ for all times, which is of course impossible, for statistically *stationary* random processes one-time PDF is representative for the whole ensemble realizations of the random process.

A turbulent flow, after an initial transient period, can reach a statistically stationary state, in which, even though the flow variable vary in time, the statistical moments became independent of time. This means that for sufficiently long sampling periods measured moments will be stable values which change no more with an increase of the sampling period. This property is illustrated in Figure 2.1.7 for the second moments of velocity records shown in Figure 2.1.5. One can see that after initial period of about 60 seconds the records converged to statistically stable values that didn't change significantly for longer sampling periods.

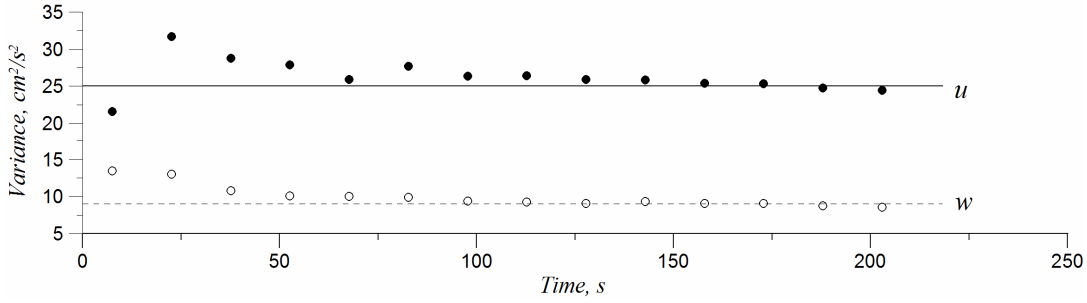

Figure 2.1.7 Statistical variance as function of sampling period.

For statistically stationary processes it is possible to define multi-time statistic called *auto-covariance* $r(\tau)=U(t)U(t+\tau)$ and respectively auto-covariance function as

$$r(\tau)=\int_{-\infty}^{\infty}\int_{-\infty}^{\infty}\left(U(t)-\overline{U}\right)\left(U(t+\tau)-\overline{U}\right)\hat{f}\left(U(t),U(t+\tau),\tau\right)dU_t\,dU_{t+\tau}$$
$$\approx\lim_{T\to\infty}\frac{1}{2T}\int_{-T}^{T}u'(t)u'(t+\tau)dt \qquad (2.1.66)$$

where T is sampling period, and τ is the time lag. Normalizing auto-covariance function with the variance of random variable yields auto-correlation function of the process $R(\tau)=r(\tau)/\mu_2$ which possesses the following properties: $R(0)=1$, $R(\tau)\le 1$. For a periodic process $u(t)$ the correlation is also periodic, but for turbulent signals $R(\tau)$ it diminishes as the lag time increases (Figure 2.1.8a). Usually this decrease is pronounced enough to insure the convergence of an integral

$$L_T=\int_0^{\infty}R(\tau)d\tau \qquad (2.1.67)$$

where L_T is integral time scale. Examples of the auto-correlation functions for the velocity records presented in Figure 2.1.5 are shown in Figure 2.1.8a. Although both functions are quickly decaying with lag time, the auto-correlation for the vertical component exhibits much faster decay rate in comparison with the streamwise component. Convergence of the integral (2.1.67) is illustrated for the same data in Figure 2.1.8b.

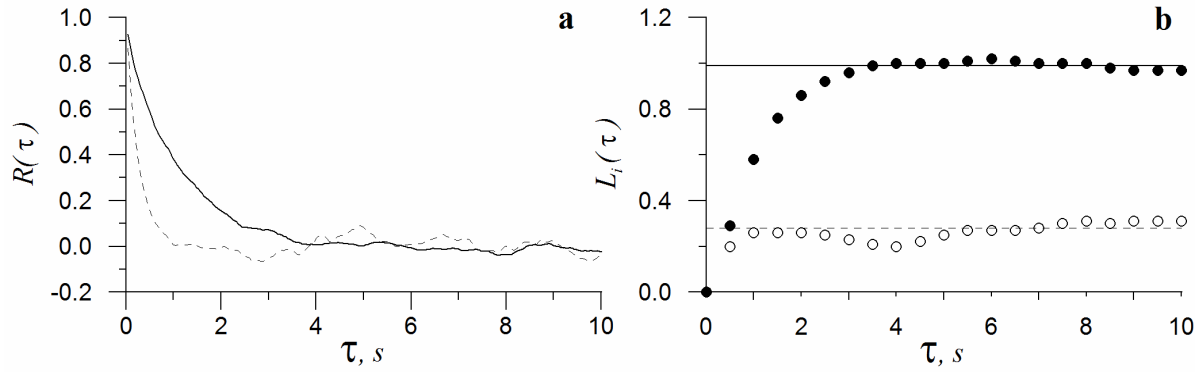

Figure 2.1.8 Auto-correlation functions (a), and convergence of the integral (equation 2.1.67).

A stationary random process, and respectively records of instantaneous flow velocities, can be approximated by Fourier series, and the variance of random variable then is the sum of contributing Fourier modes. Therefore the variance can be decomposed into spectrum of Fourier modes *S(f)* by applying Fourier transformation to auto-covariance function

$$S(f)=2\int_{-\infty}^{\infty}r(\tau)e^{-i2\pi f\tau}d\tau=2\int_{-\infty}^{\infty}r(\tau)\cos(2\pi f\tau)d\tau \qquad (2.1.68)$$

For isotropic turbulence $S_u(f)=S_w(f)$, turbulence spectrum is related by Kolmogorov's theoretical relationship (Kolmogorov 1942; Monin and Yaglom 1971)

$$S(f)=C_0\,\varepsilon^{2/3}\left(\frac{\overline{u}}{2\pi}\right)^{2/3}f^{-5/3} \qquad (2.1.69)$$

where $C_0=0.48$ is universal constant. Spectra computed for velocity records (Figure 2.1.5) are shown in Figure 2.1.9.

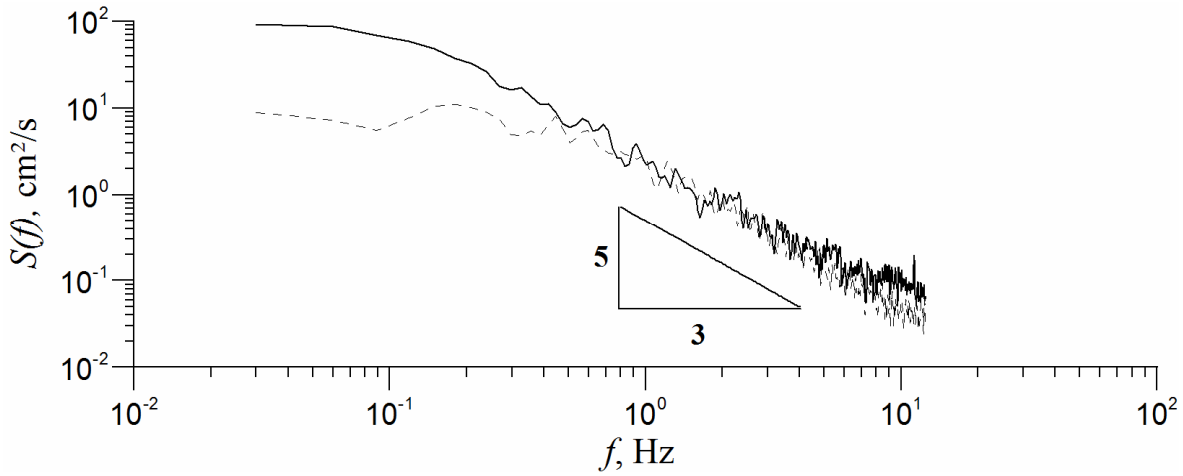

Figure 2.1.9 Examples of spectral density functions.

The triangle drown in this plot indicates the trend (2.1.69). Though condition $S_u(f) = S_w(f)$ is approximately satisfied in the range from 0.6 to 5 Hz, the spectrum of streamwise component appears to be about 10 times larger than spectrum of vertical component in the range from 0.01 to 0.6 Hz. Therefore river turbulence is always considered as *locally isotropic*. Local here means that this property is satisfied at some high frequency part of the spectrum called *inertial interval.* Respectively the low frequency range of the spectrum characterized by anisotropic spectra density is called productive interval. The essential property of turbulence in the inertial interval (2.1.69) is used for practical computations of the dissipation rate. In mixing layers because of vortex pairing mechanism a distinctive *inverse* turbulence cascade with $S(f) \sim f^{-3}$ can be also observed. Spatial distributions of flow variables represented by the random processes $u(x,t)$ form the fields of random variables. Understanding of structural properties requires analysis of statistical properties for these fields and can be achieved by the analysis of multi-point statistical functions called cross-covariance functions

$$r_{1-2}(\Delta x,\tau) = \lim_{T\to\infty} \frac{1}{2T} \int_{-T}^{T} u'(x_0,t)\, u'(x_0+\Delta x, t+\tau) dt \qquad (2.1.70)$$

which can be normalized by a pair of standard deviations (root square of variances) of the variable at each point $1(x_0)$ and $2(x_0+\Delta x)$ to obtain cross-correlation function.

2.2 Transport and Mixing of Dissolved Substances

Theory of transport and mixing of dissolved conservative substances forms a conventional framework for the quantitative description of more complex processes as transport and sedimentation of the suspended particulate matter (SPM) or the coarse particulate organic matter (CPOM), and dynamics of fluvial phytoplankton. Basics of turbulent diffusion are presented in the Subsection 2.2.1 with an introduction to the principles of their mathematical modeling. In the Subsection 2.2.2 the three-dimensional system of equations is reduced to one-dimensional longitudinal dispersion model convenient for many practical applications. The concept of dead zones – a crucial concept for this study is introduced in the Subsection 2.2.3, and a statistical approach is outlined in the Subsection 2.2.4.

2.2.1 Governing equations, modelling, and classification

For dissolved conservative substance transported by moving water equation of mass conservation can be written as (Monin and Yaglom 1971; Rutherford 1994)

$$\frac{\partial c}{\partial t} + \sum_i u_i \frac{\partial c}{\partial x_i} = e_m \nabla^2 c, \;\; i = 1, 2, \text{ and } 3 \tag{2.2.1}$$

where c is concentration of the substance (dimensionless variable), and e_m is coefficient of molecular diffusivity. Similarly to (2.1.10) by introducing the same dimensionless variables in equation (2.2.1) one obtains dimensionless equation

$$\frac{\partial c}{\partial t^*} + \sum_i u_i^* \frac{\partial c}{\partial x_i^*} = \frac{1}{Pe} \nabla^2 c \tag{2.2.2}$$

where $Pe = e_m^{-1} u_0 l_0$ is Peclet number which is in fact the ratio between molecular diffusion and advection. Applying Reynolds decomposition scheme (2.1.3) and $c = \bar{c} + c'$ to equation (2.2.1) yields

$$\frac{\partial \bar{c}}{\partial t} + \sum_i \bar{u}_i \frac{\partial \bar{c}}{\partial x_i} = e_m \nabla^2 \bar{c} - \sum_i \frac{\partial \overline{u'_i c'}}{\partial x_i} \tag{2.2.3}$$

expressing the dynamics of mean concentration of a substance $\bar{c}$ and containing additional terms – turbulent fluxes $\overline{u'_i c'}$.

Averaging procedure applied to (2.2.1) again, as in case with averaging of Navier-Stokes equations, creates the problem of closure and hence plaguing the issue of turbulence modeling. A simple relationship is often used by analogy with molecular diffusion

$$\overline{u'_i c'} = -e_T \frac{\partial \bar{c}}{\partial x_i} \tag{2.2.4}$$

where e_T is coefficient of turbulent diffusion. In fact there is direct analogy between equation (2.1.7) and (2.2.4) because the turbulent structures that transport momentum are, at the same time, the transport agents of mass, and hence $e_T = \nu_T$. The analogy, conventionally termed Reynolds analogy, has important practical implications because turbulent diffusion coefficients can be obtained from the turbulence models

$$e_T = \overline{u'_i u'_j} \Big/ \frac{d\bar{u}_i}{d x_j} \tag{2.2.5}$$

and therefore understanding of mechanisms of mixing and transport phenomena is tightly connected to the understanding of turbulent flows.

Characteristics of substance sources define boundary conditions for the boundary value problem (2.2.1) that in many cases can lead to significant simplifications of the system and allows for analytical treatment of the problem. The general classification of sources subdivides them into *instantaneous*, and *continuous* depending on the time of the source activity. The sources can be further classified considering spatial characteristics of sources, and *point, line, sheet,* and *distributed* sources are generally distinguished as the basic elements (Rutherford 1994).

2.2.2 Transport and mixing in rivers

Mechanism of turbulent diffusion appears to be much more effective mixing agent than the molecular diffusion. Indeed, many studies report that concentrations of substances released from

continuous point source in the mid-depth of the river flow became uniformly distributed over the flow depth at distance about fifty times of river depth (Rutherford 1994; Jirka 2004). Uniform distribution of concentration in the river cross-section is attained at distances of one hundred times of the river channel width from the instantaneous sheet ejection across the flow (Sukhodolov et al. 1997). These experimental observations reveal the fact that because of turbulence the so called *well-mixed* condition is attained in river cross-sections relatively close to the sources and further mixing processes can be considered only in longitudinal direction.

One-dimensional model describing mixing and transport is obtained by performing spatial averaging of equations (2.2.3-2.2.4). At the first step it is assumed that molecular diffusion is much smaller than turbulent and the correspondent term in (2.2.3) is simply neglected, and the resulting equation is integrated over the river depth (Rutherford 1994)

$$h\frac{\partial \bar{c}_h}{\partial t}+\frac{\partial h\bar{u}_x\bar{c}_h}{\partial x}+\frac{\partial h\bar{u}_y\bar{c}_h}{\partial y}=-\frac{\partial h\langle u'_x c'_h\rangle}{\partial x}+he_x\frac{\partial \bar{c}_h}{\partial x}-\frac{\partial h\langle u'_y c'_h\rangle}{\partial y}+he_y\frac{\partial \bar{c}_h}{\partial y} \tag{2.2.6}$$

where $\bar{c}_h$ is depth averaged concentration of the substance, $\bar{u}_x$, and $\bar{u}_y$ are depth averaged mean streamwise and transverse flow velocities, u'_x, u'_y, and c'_h indicate fluctuations of mean velocity and concentrations due to inhomogeneous spatial distribution, and the angle brackets indicate averaging over the depth. The depth averaging procedure eliminated the two terms associated with the vertical turbulent fluxes, but introduced two additional fluxes due to non-uniformity of mean velocity and concentration fields. These additional fluxes are called *dispersive* and are again modeled analogously to the molecular and turbulent diffusion as $\langle u'_i c'_h\rangle=-E_i\partial\bar{c}_h/\partial x_i$, and after substitution into (2.2.6) the resulting coefficients $K_i=E_i+e_i$ became the coefficients of dispersion. Similarly to the depth averaging, equation (2.2.6) can be now averaged across the channel width yielding

$$A\frac{\partial C}{\partial t}+\frac{\partial AUC}{\partial x}=-\frac{\partial A\langle U'C'\rangle}{\partial x}+AK_x\frac{\partial C}{\partial x} \tag{2.2.7}$$

where $A=hB$ is area of a cross-section, U and C are cross-sectional mean velocity and concentration, and $U'C'$ additional dispersive flux due to non-homogeneity of velocity and concentration fields.

The longitudinal dispersion model is obtained from spatially averaged equation (2.2.7) by modeling dispersive flux as $\langle U'C'\rangle=-K\partial C/\partial x$, and respectively introducing a longitudinal dispersion coefficient $D=K+K_k$. For uniform flow one obtains one-dimensional longitudinal dispersion equation

$$\frac{\partial C}{\partial t}+U\frac{\partial C}{\partial x}-D\frac{\partial^2 C}{\partial x^2}=0 \tag{2.2.8}$$

Equation (2.2.8) can be solved analytically, and for instantaneous injection over the cross-section at $x=0$ and $t=0$ the solution is the following function

$$C=\frac{M_T}{2A\sqrt{\pi Dt}}\exp\left[-\frac{(x-Ut)^2}{4Dt}\right] \tag{2.2.9}$$

At a first glance equation (2.2.9) resembles the normal distribution (2.1.62), however, significant difference is that the variable time present in all parts makes the distribution (2.2.9) asymmetrical. Applying the Laplace transformation to (2.2.8) with the boundary condition representing a sheet instantaneous injection one obtains the moments of distribution

$$\mu_1=\bar{t}=\frac{2D}{U^2}+\frac{x}{U} \tag{2.2.10}$$

$$\mu_2 = \sigma_t^2 = \frac{8D^2}{U^4} + \frac{x}{U}\frac{2D}{U^2} \tag{2.2.11}$$

$$\mu_3 = Sk\,\sigma_t^3 = \frac{64D^3}{U^6} + \frac{x}{U}\frac{12D^2}{U^4} \tag{2.2.12}$$

where Sk is skewness. At large distance from the source the second terms of the right sides of equations (2.2.11-2.2.12) became much greater than first terms which describe initial values of moments ($x = 0$). Neglecting them, and scaling skewness as $Sk = \mu_3 / \sigma_t^3$ yields

$$Sk \approx \left(\frac{D}{U}\right)^{1/2} x^{-1/2} \tag{2.2.13}$$

indicating that skewness is decreasing with the distance from source.

Although many experimental and field studies showed that concentration distributions indeed obey behaviour predicted by (2.2.10-2.2.11), almost all studies reported the phenomenon of persistent skewness meaning that skewness of distributions in many cases was constant or even growing with distance from source. The culprit of this discrepancy was attributed to the presence of a small, asymptotically approaching zero trailing edges of distribution conventionally called tails.

2.2.3 Dead zone modeling concept

The tales in the concentration distributions had been presumed to appear as a result of the temporal trapping of substances in the non-transit (stagnant) parts of the channel called *dead zones*. Substances accumulated in the dead zones are slowly released back to the transit flow after the passage of the substance cloud. Characterizing the dead zone area A_d as a portion of the river cross-section area $э = A_d / A$, and assuming that a characteristic time of residence for the substances in a dead zone is T_d, from the balance of mass one can derive a system

$$\frac{\partial C}{\partial t} + U\frac{\partial C}{\partial x} - D\frac{\partial^2 C}{\partial x^2} = \frac{э}{T_d}\left(C_d - C\right) \tag{2.2.14}$$

$$\frac{\partial C_d}{\partial t} = \frac{\left(C - C_d\right)}{T_d} \tag{2.2.15}$$

where C_d is substance concentration in the dead zone. The system (2.2.14) and (2.2.15) transforms to (2.2.8) when $э \to 0$, and $T_d \to \infty$. To solve dead zone balance equations (2.2.14) and (2.2.15) one again needs to specify boundary and initial conditions (Czernuszenko et al. 1997)

$$C_d(x, 0) = C(x, 0) = 0, \quad 0 < x < \infty \tag{2.2.16}$$

$$C(0, t) = C_0(t), \quad \lim_{x\to\infty} C(x, t) = 0 \tag{2.2.17}$$

Although hitherto analytical solutions of the boundary value problem (2.2.14)-(2.2.17) have been not found, the temporal moments of the concentration distributions were proposed recently (Czernuszenko and Rowinski 1997)

$$\mu_1 = \bar{t} = \frac{2D}{U^2} + \frac{x}{U}\left(1 + э\right) \tag{2.2.18}$$

$$\mu_2 = \sigma_t^2 = \frac{8D^2}{U^4} + \frac{x}{U}\frac{2D}{U^2}\left(1+ э\right) + 2\frac{x}{U} э T_d \tag{2.2.19}$$

$$\mu_3 = Sk \times \sigma_t^3 = 2\frac{x^2 D}{U^4}\left(1+ э\right)^2 э + 64\frac{D^3}{U^6} + \frac{x}{U}\left[12\frac{D^2}{U^4}\left(1+ э\right)^2 + 4 э T_d \frac{D}{U^2} D\left(э +2\right) + 6 э T_d^2 \right] \tag{2.2.20}$$

The difference between the moments of longitudinal dispersion model (2.2.10-2.2.12) and the dead zones model (2.2.18-2.2.20) is illustrated on the example of the numerical solution of the boundary value problem (2.2.14-2.2.17), Figure 2.2.1.

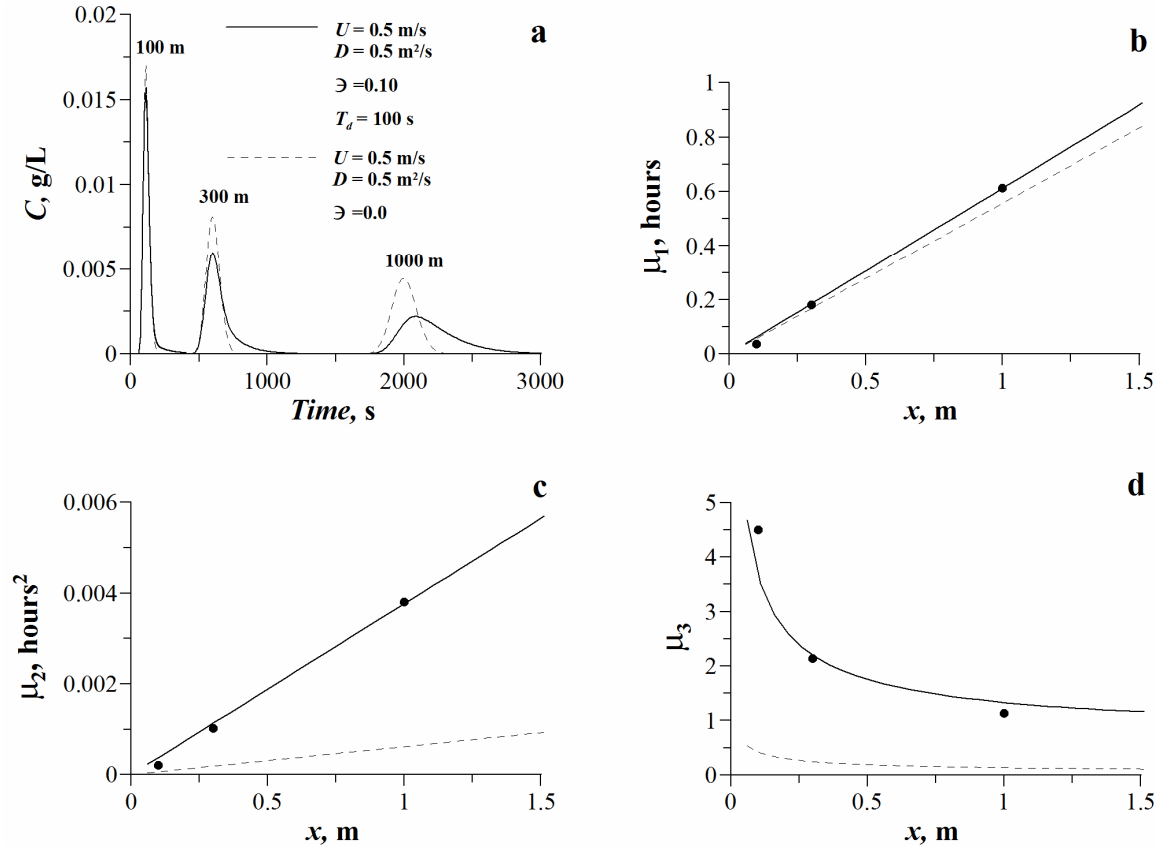

Figure 2.2.1 Examples of numerical solutions of (2.2.15-2.2.18) and their comparisons with the longitudinal dispersion model (a), and moments of its distribution (b-d).

Validation of the model (2.2.14)-(2.2.15) on results of experimental and numerical studies shows that dead zone model adequately describes spatial evolution for temporal moments of concentration distribution (Czernuszenko et al. 1998). The moments (2.2.18)-(2.2.20) can be used to determine parameters of the dead zone model U, D, $э$ and T_d from results of tracer studies by means of nonlinear optimization procedure similar to the methods of moments in the classical dispersion model. Determination of model parameters can be achieved by solving optimization problem in respect to the central moments (2.2.18) and (2.2.20)

$$\lim_{u,D,э,T_d}\left\{ F\left(u, D, э, T_d\right) = \sum_{i=1}^{3}\sum_{k=1}^{N}\left[\mu_{i\,m}\left(x_k\right) - \mu_i\left(x_k\right)\right]^2 \right\} \tag{2.2.21}$$

where F is criterion function, k is the number of measured sections of the tracer cloud. This method to determine the parameters of the dead zone model may be less accurate than the solving of optimizing problem by fitting measured concentration curves with the numerical

solutions of boundary value problem (2.2.14)-(2.2.17). However, accurate numerical solution would require detailed information on the flow and river channel geometry for the entire river reach. In the absence of that information the performance of the moments method (2.2.21) is expected to be the same as for advanced techniques (Czernuszenko et al. 1998).

2.2.4 Lagrangian statistics and dispersion coefficient

Let us consider the trajectories of particles in a field of homogeneous turbulence, Figure 2.2.2.

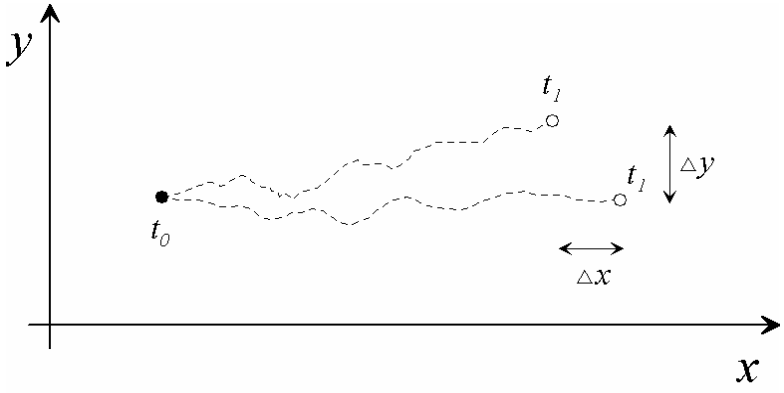

Figure 2.2.2 Trajectories of a particles pair in the field of uniform turbulence.

Adopting Lagrangian system of coordinates moving with the bulk flow velocity, a streamwise coordinate of a particle can be described as

$$x(t) = \int_0^t u'(\tau)\, d\tau \tag{2.2.22}$$

introducing a measure of a scatter for the ensemble of particles released from the same point x_0, y_0, t_0 around the center of mass of the particle cloud $\sigma_x^2 = \left\langle \left(x - \bar{x}\right)^2 \right\rangle$ one can show that

$$\sigma_x^2 = 2\overline{u'^2} \int_{\tau=0}^{t} R_x(\tau)(t-\tau)\, d\tau \tag{2.2.23}$$

where $R_x(\tau)$ is Lagrangian auto-correlation function analogous to Eulearian auto-correlation function introduced in the Section 2.1.4. Respectively the properties of this function are $R_x(0) = 1$, and $R_x(\infty) = 0$, and integrating (2.2.23) for those two limiting cases one obtains

$$\sigma_x^2 \approx \overline{u'^2}\, t^2 \text{ at small } \tau \text{ (or short distances from source)} \tag{2.2.24}$$

$$\sigma_x^2 \approx 2\overline{u'^2}\, T_x\, t \text{ at large } \tau,\ T_x = \int_0^\infty R_x(\tau)\, d\tau \tag{2.2.25}$$

where T_x is Lagrangian integral time scale. On the other hand, taking into account the Reynolds analogy for the mass transport, it can be shown that

$$e_x = \frac{1}{2}\frac{d\sigma_x^2}{dt} \tag{2.2.26}$$

The longitudinal dispersion coefficient can be presented similarly to equation (2.2.26) as

$$D = \frac{1}{2}\frac{d\sigma_x^2}{dt} = \int_0^\infty \overline{U'(t)U'(t+\tau)}\, d\tau \tag{2.2.27}$$

where U' is deviation of the instant longitudinal velocity of the particle from its averaged velocity. As it was shown in (2.2.1), the velocity deviation U' can be considered as a sum of two

components: turbulent U'_T, and stipulated by heterogeneity of the mean velocity field U'_A. After simple transformations and neglecting correlations between mean and turbulent quantities, equation (2.2.27) transforms to

$$D = \sigma_T^2 T_T + \sigma_A^2 T_A \tag{2.2.28}$$

where σ_T^2, σ_A^2 and T_T, T_A are variance and Lagrangian time scales of turbulent and mean quantities. In river flows the impact produced by heterogeneity of the mean velocity fields is generally much larger (about 10 times) than contribution of turbulent component and respectively (2.2.28) can be further simplified to $D = \sigma_A^2 T_A$. Assuming that velocity variance can be related to mean (bulk) velocity of the river flow (U) as $\sigma_A^2 = \alpha_u^2 U^2$, and Lagrangian time scale is related to the bulk flow width and mean velocity as $T_A = \beta_B B / U$, one obtains

$$D = \alpha_u^2 \beta_B U B \tag{2.2.29}$$

Coefficients α_u and β_B were interpreted as variations in flow attributed to the presence of bed forms, but most of the field studies due to the lack of information represent them as a multiple parameter which value was shown to vary from 0.8 to 3 (Rochusaar and Paal 1970; Sukhodolov et al. 1997; Rowinski et al. 2004).

2.3 Plants Biomechanics and Ecology

Complexity of the flow-macrophytes interactions stems from the interplay of biomechanical, physiological, and ecological aspects of the vegetation lifecycles. As far as functioning of an individual plant in the natural environment is related via physical laws to its shape, macrophytes developed advanced methods of adaptation to variable environmental conditions (Niklas 1992). Highly competitive species produce both terrestrial and aquatic forms and reproduce by tubers and seeds in order to maintain sustainable population. Although an individual plant causes virtually no effect on the flow, abundant population may drastically change hydraulic regime of a river or a stream. Apparently biophysical, hydrodynamic, and transport processes in the river will be different for various macrophyte species and different scales.

To clarify the relationship between different scales, processes and scientific disciplines addressing particular problems, a following scheme is presented in Figure 2.3.1. The scales, on which the macrophytes and their interaction are considered, vary from small (individual plant) to large (vegetative mosaic), with intermediate scales represented by vegetative patches. On the scale of an *individual plant* the life cycle and ecological functioning of the individual is governed by biophysical processes and can be clarified by methods of plants biomechanics, physiology, environmental fluid mechanics, and biogeochemistry. V*egetative patches* are assemblages of plants growing in relatively uniform physical conditions and characterized by the presence of defined spatial boundaries. Thus a vegetation patch can be characterized by a dominant species of a certain characteristic size, depth and velocity of a flow. The distribution of riverbed material over the patch area can be considered as uniform and its geochemical composition varies insignificantly. At the same time the characteristics of environment surrounding the patch may differ substantially. Assembling of individual plants into patches means establishing certain interactions between plants and assumes an increased level of interaction with the flow. As the patch represents a biotope from the prospective of plants ecology its understanding requires studies of biotope dynamics, ecohydraulics, and certainly involves understanding of sedimentological processes. On the scale of a uniform river reach the vegetation patches form distinctive patterns called *vegetation mosaics*. The mosaics represent more diverse communities that obviously are linked to the terrestrial and in-flow factors and therefore necessitate studies of biocenoses dynamics, fluvial hydraulics, and morphodynamics.

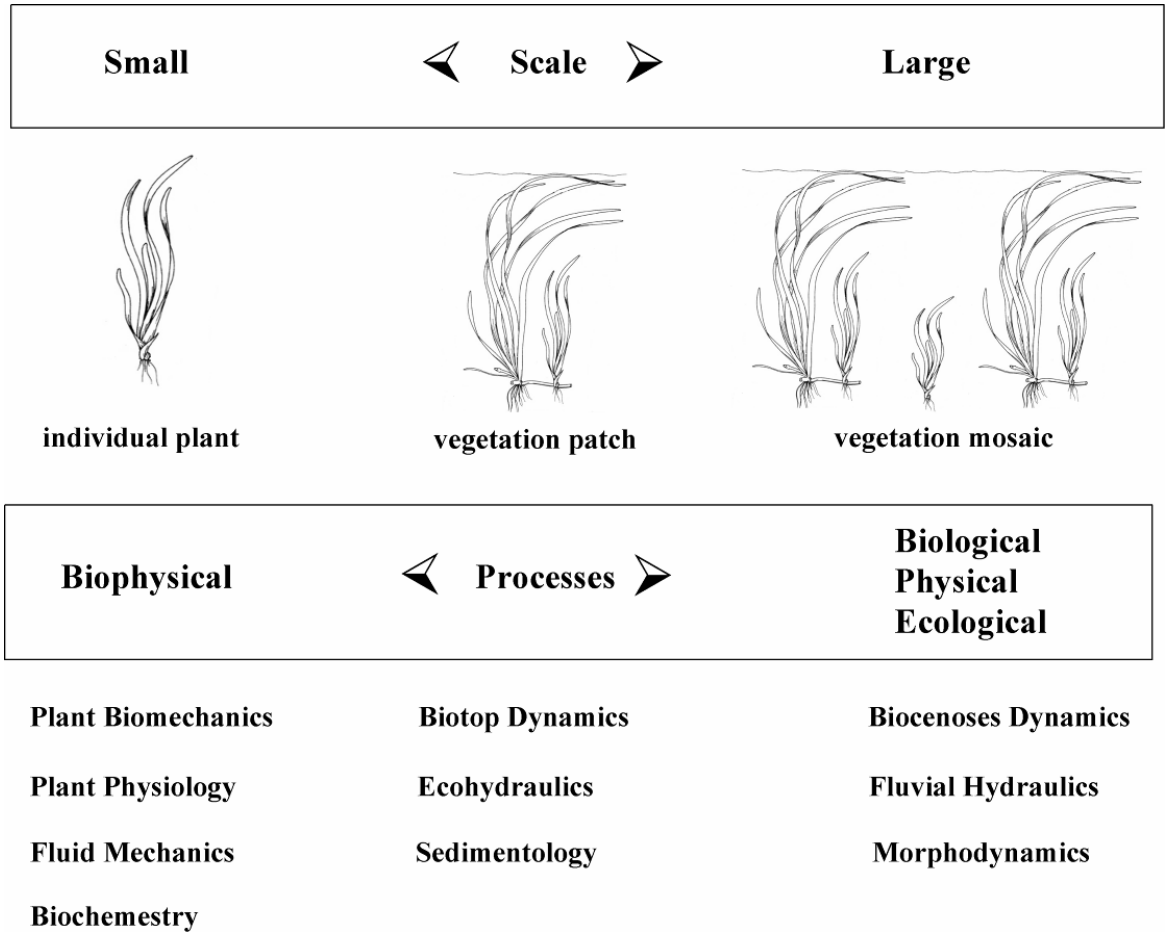

Figure 2.3.1 Scales, processes, and scientific disciplines related to the problem

The following content of this part of the chapter is arranged in accordance with the presented scheme. Biomechanical properties of the individual plants are discussed in the Subsection 2.3.1 prior to characterization of the integral properties of vegetation growth represented by biomass, Subsection 2.3.2. Spatial arrangement of vegetation into patches and mosaics is discussed in the Subsection 2.3.3.

2.3.1 Biomechanical properties of plants

Macroscopic rooted aquatic plants, being typical photosynthetic organisms, struggle during their life cycle for optimal light and nutrients uptake rate conditions. In fluvial systems with running waters individual plants achieve the optimum by maintaining an upright posture that exposes the plants to lighter, nutrient and oxygen richer layers in water column. However, the upright posture is maintained on expense of exposure to the action of higher hydrodynamic forces with a risk of mechanical destruction or dislodgement of the plant. Obviously, the sustainable plants counteract hydrodynamic forces by the internal mechanisms – flexural rigidity and buoyancy. For flexible freshwater macrophytes forming submerged vegetation in the streams, low flexural rigidity enables bending of the plants or their blades and by this bending streamlines the shape of the plants, reduces their projected area and hence decreases hydrodynamic force. The buoyancy maintains upward force that supports suspended state of the plants in the water column and counteracts the downward weight force. A balance of hydrodynamic forces on the one hand and rigidity and buoyancy on another determines the deflected height of the vegetation cover in the stream which is one of principal parameters for

description of flow-vegetation interactions. To understand how this balance is maintained we need to describe the forces with certain theoretical models and also to comprehend scaling ratios of these forces that regulate positions of plants in the flow. Flexural rigidity EI_a is a measure of the capacity of an object to resist bending. It depends both on the cross-sectional dimensions of the object measured as the second moment of area I_a and on the elastic modulus of the material E. Elasticity theory is usually applied to a loaded cantilever beam which is considered to be an analogue to aquatic plants and allows quantitative assessment of the ability of plant tissues to withstand drag force (Velasko et al. 2005; Erduran and Kutija 2003).

To review essentials of this theory let us consider a cantilever with a free end characterised by the length L and flexural rigidity EI_a under dominant lateral load applied at the free end (Figure 2.3.2).

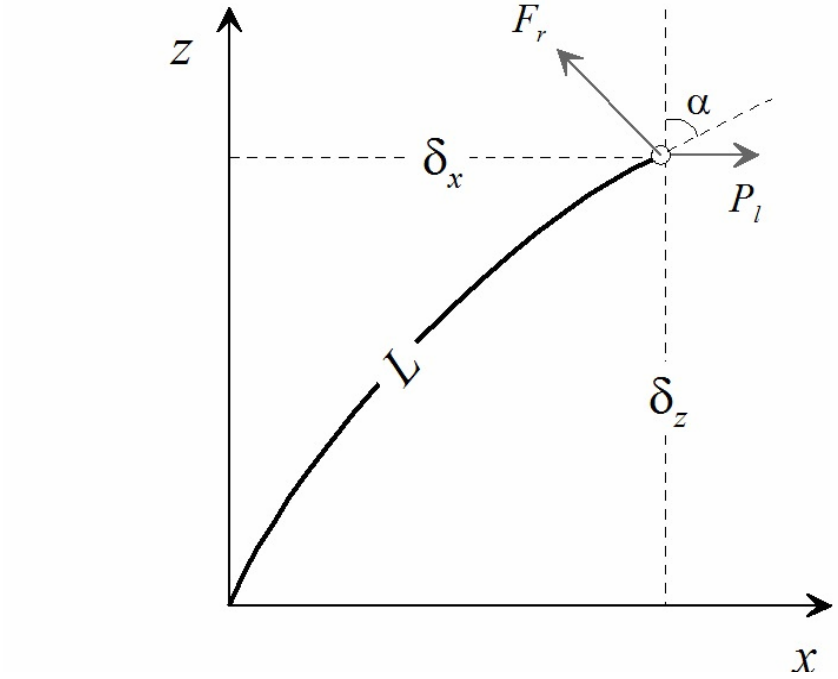

Figure 2.3.2 Schematic representation of a cantilever beam and forces balancing its bending.

The differential equation describing the behavior of a beam is (Niklas 1992)

$$M = -K\,E\,I_a \tag{2.3.1}$$

where M is the moment of bending force, and K is the curvature of the cantilever

$$K = \frac{\dfrac{d^2z}{dx^2}}{\left(1+\left(\dfrac{dz}{dx}\right)^2\right)^{3/2}} \tag{2.3.2}$$

where x is longitudinal coordinate, and z is vertical coordinate originating at the basis of the cantilever. For small deflections ($\delta_z \approx L$) K can be approximated only with d^2z/dx^2 and equation (2.3.1) simplifies to

$$P_l(L-x) = \frac{d^2z}{dx^2} EI_a \tag{2.3.3}$$

where P_l is lateral load. Integration of (2.3.3) for the lateral load applied to the free end of the beam yields a deflection distance δ_x (Figure 2.3.2)

$$\delta_x = \frac{P_l L^3}{3 E I_a} \tag{2.3.4}$$

Integrating (2.3.3) for condition of the lateral load being uniformly distributed along the beam provides different coefficient to the elasticity modulus

$$\delta_x = \frac{P_l L^3}{8 E I_a} \tag{2.3.5}$$

Representing the bending angle as $\delta_x / L \approx \sin\alpha$ and rearranging (2.3.4)-(2.3.5) into general form, one obtains relation between load and bending angle as a function of beam size and biomechanical properties of the tissue

$$P_l = \frac{1}{C_b}\frac{EI_a}{L^2}\frac{\delta_x}{L} \cong \frac{1}{C_b}\frac{EI_a}{L^2}\sin\alpha \tag{2.3.6}$$

where C_b is a coefficient depending on the type of load application and in average can be taken as 0.2. Comparison of the beam deflections computed according to the simplified bending beam theory (small deflections) with more general non-linear theory developed for large deflections (Gaylord and Denny 1997) indicated that the simplified approach (2.3.6) is reasonable for the range of relative deformations $0 < \delta_x / L < 0.3$ that corresponds to the bending angles in the range $0° < \alpha < 20°$.

Buoyancy provides an upward force on the object. The magnitude of this force equals to the weight of the displaced fluid. The buoyancy of an object depends, therefore, only upon two factors: the object's submerged volume, and the density of the surrounding fluid. The greater the object's volume and surrounding density of the fluid are the more buoyant force it experiences. The buoyant force F_B can be expressed using the following equation

$$F_B = \rho V g \tag{2.3.7}$$

where ρ is the density of the fluid, V is the volume of the submersed body and g is the acceleration due to gravity. The buoyancy of floating objects exceeds their weight F_G, while objects with weight excess over buoyancy sink. The buoyancy acts against the gravity force and makes objects seem lighter. To represent this effect it is common to define a relative density ρ_r of an immersed object by relating density of the object ρ_p to the density of the fluid ρ

$$\rho_r = \rho\left(1 - \frac{\rho_p}{\rho}\right) \tag{2.3.8}$$

The resulting force experienced by immersed body can be expressed using following equation

$$F_B - F_G = g V \rho_r \tag{2.3.9}$$

The buoyancy of the aquatic plants is produced by air chambers (lacunae) in the tissues of plants. These chambers, valuable part of respiratory system of the plants, are needed for delivery of oxygen derived by leaves from the surrounding water to the roots and rhizomes. Freshwater aquatic plants have a system of internal lacunae that often occupies large proportions of the plant volume (Sand-Jensen *et al*. 1982; Smith *et al*. 1988). Comparison of the terrestrial and submerged leaves of the same plants revealed that the leaves developed during submergence were elongated and thin in comparison with terrestrial leaves grown completely in air, but still contained well-developed air spaces (Mommer et al. 2005). The leaf mass per unit area in terrestrial leaves was approximately twice higher as compared to leaves of submerged plant form. Submerged aquatic species thus have an advantage on the effect of reduced weight.

Although buoyancy is important biomechanical property of aquatic vegetation, the studies and data on the buoyancy or density of certain plant species are scarce to find in literature. A pioneer study on the rigidity and buoyancy as mechanisms allowing seaweeds to maintain an upright posture in the flow (Stewart 2006) revealed that their combination resulted in the lower hydrodynamic forces experienced by the plants. The impact of the buoyancy to the balance of forces acting on the aquatic plants was not considered in the hydrodynamic studies on submerged vegetation hitherto. Mainly rigidity of plants was assumed to be the dominating counteracting force (Velasko et al. 2005; Erduran and Kutija 2003). In biological studies the flexural rigidity of the plants was neglected and the buoyancy force only has been recognised to counteract to the drag force in the case of the submerged highly flexible vegetation (Green 2005).

2.3.2 Biomass dynamics: equations and modeling

The biomass is a conventional quantitative integral measure of vegetation defined as the dry weight of the plants per square meter of the area on which the plants are growing on. At every instant the biomass represents a state of the plants, individual or community, as a respective stage in the phenological cycle influenced by external factors such as light and nutrients availability, physical effects of flow, and biological and ecological processes - losses of biomass due to respiration and grazing. The dynamics of biomass as a scalar quantity B is conventionally comprehended through the mass balance approach (Carr *et al.* 1997)

$$B = P - R - L \tag{2.3.10}$$

where P is photosynthetic production of biomass, R and L are biomass losses due to respiration and decay respectively.

The biomass dynamics models are based mostly on an assumption that the production and loss rates at any moment of time t are proportional to the available biomass $B(t)$ (Herb and Stefan 2003)

$$\frac{dB}{dt} = \left(\mu - \lambda - \delta \right) B \tag{2.3.11}$$

where $\mu(t)$, $\lambda(t)$, $\delta(t)$ are growth, respiration and loss rate coefficients. Accordingly, detailed modeling of biomass requires provision of rate coefficients $\mu(t)$, $\lambda(t)$, $\delta(t)$ for every phase of the phenological cycle including germination, growth, maturation, senescence, and dormancy. In general these coefficients have to be determined experimentally as the functions of temperature, solar irradiance and nutrients availability (Toerien *et al.* 1983; Davis and McDonnell 1997).

However, the detailed modeling of rate coefficients in many cases is impossible or even impractical because of laborious techniques and necessity of *in situ* calibration for the rates obtained in laboratory mesocosms. Therefore more often detailed rates are substituted by net rate $r(t)$

$$\frac{dB}{B\ dt} = r \tag{2.3.12}$$

allowing for easy curve-fitting in practical applications and for various models exploring different approaches to represent net rates. Indeed, based on equation (2.3.12) a variety of growth curves have been developed to model population dynamics and biological growth. Classical growth models were developed by Compertz (1825), Verhults (1838), and Richards (1959).

Simplest exponential growth function is obtained assuming a constant growth rate and integrating equation (2.3.12)

$$B = B_0 \exp(r\,t) \tag{2.3.13}$$

where B_0 is the constant of integration representing initial biomass. Simplicity of the solution (2.3.13) has an obvious disadvantage as the growth in this model is unrestricted in time, and therefore it makes impossible description of biomass dynamics in maturation phase when the growth rate of biomass is sharply reduced. To confide the exponential growth at the upper bound, Verhulst (1838) introduced a corrective to the net rate called *carring capacity* K_c. This corrective is simply multiplicative factor $1 - B/K_c$ that can be interpreted as a limiting factor in physical dimension, and applied to (2.3.12) gives a characteristic logistic equation

$$\frac{dB}{B\,dt} = r\left(1 - \frac{B}{K_c}\right) \tag{2.3.14}$$

which after integration yields a solution

$$B = \frac{K_c\,B_0}{(K_c - B_0)\exp(-r\,t) + B_0} \tag{2.3.15}$$

Although the model (2.3.15) is one step closer to reality than (2.3.13) and it is useful for predicting growth of many agricultural plants harvested at maturation phase, it is still not appropriate for description of the senescence phase. Logistic function can be rewritten as

$$B = \frac{B_{\max}}{1 + \exp[-k(t - t_m)]} \tag{2.3.16}$$

where k is a constant representing modified growth/decay rate, $B_{\max}$ is maximum value of biomass at time moment t_m, that corresponds to the inflection point. Function (2.3.16) is symmetrical around the inflection point at t_m. However, the observations of biomass growth indicate that in many cases observed curves are asymmetrical, and therefore Richards (1959) devised a more flexible relation by introducing asymmetry parameter β

$$\frac{d\,B}{B\,d\,t} = r\left(1 - \frac{B}{K_c}\right)^{\beta} \tag{2.3.17}$$

integration of (2.3.17) yields the following solution

$$B = K_c\left(1 - \exp(\beta\,r\,t)\left[1 - \left(\frac{B_0}{K_c}\right)^{-\beta}\right]\right)^{1/\beta} \tag{2.3.18}$$

or modifying similarly to (2.3.16)

$$B = \frac{B_{\max}}{(1 + \beta\exp[-k(t - t_{\max})])^{1/\beta}} \tag{2.3.19}$$

At t_m the absolute growth rate is maximal and the relative growth rate equals to $k/(1+\beta)$, and for $\beta = 1$ the function (2.3.17) converts to logistic equation.

Presently there is a family of logistic-based functions originating from the classical one (2.3.14). An extended review of these logistic functions is presented by Tsoularis (2001). Most recent functions proposed by Werker and Jaggard (1997), and Wilson et al. (2007) are presented here as the reference for the later usage. All of these functions differ by the way of representing the relative growth rate. Werker and Jaggard (1997) introduced two models with exponential

$$\frac{d\,r}{d\,t} = -k(r - r_{\min}) \tag{2.3.20}$$

and quadratic decline of relative growth rate

$$\frac{d\,r}{d\,t} = -k\left(r - r_{\min}\right)\frac{r_{\max} - r}{r_{\max} - r_{\min}} \tag{2.3.21}$$

Applying (2.3.20) to (2.3.14) yields the following solution

$$B = \frac{K_c}{1 + \frac{K_c - B_0}{B_0}\exp\left(-U\right)}$$
$$U = r_{\min}\left(t - t_0\right) + \frac{r_0 - r_{\min}}{k}\left(1 - \exp\left[-k\left(t - t_0\right)\right]\right) \tag{2.3.22}$$

Wilson et al. (2007) proposed two simpler relations: a Gaussian like

$$B = B_{\max}\exp\left[-0.5\left(\frac{T - T_{B\max}}{C_w}\right)^2\right] \tag{2.3.23}$$

and a log-normal

$$B = B_{\max}\exp\left[-0.5\left(\frac{\ln T / T_{B\max}}{C_w}\right)^2\right] \tag{2.3.24}$$

where T is day-degree sum or thermal time, $T_{B\max}$ is thermal time corresponding to the maximum of biomass, and C_w is a constant. Equations (2.3.23) and (2.3.24) utilise a day-degree concept (Thornley and Johnson 1990) which needs more attention here.

Thornley and Johnson (1990) proposed to characterize particular stages in phenological cycle by a day-degree sum T

$$T = \sum_{i=1}^{j}\overline{T_i} - T_b \tag{2.3.25}$$

where $\overline{T_i}$ is daily mean temperature which is above certain threshold value T_B. Day-degree or thermal time thus represents an index of accumulated energy that functions as a biological "clock" guiding plants to develop from one stage to another. Certain values of the day-degree sum characterize transition between the phases in the macrophytes growth. Example of the phenological cycle of the Wildcelery *Vallisneria americana* obtained by Best et al. (2001) is presented in the Table 2.3.1.

Table 2.3.1 Phenological cycle of Wildcelery *Vallisneria americana* (Best et al. 2001)

Developmental phase	Julian day	$T(T_B = 3°C), °C$
tuber sprouting	0-105	1-270
leaf expansion, maturation	106-227	271-2072
max biomass	227	2072
senescence	228-365	2073-3167
senesced	365	3167

Though the seasonal dynamics of the plant characteristics is well depicted by the described models, coupling of these equations with hydrodynamic or transport models for analytical treatment can be problematic because of their complicated form. In other words, it may be

difficult to use the derivatives of the models like (2.3.19), (2.3.22) in analytical deductions and hence it is desirable to find a model with the structure more appropriate for analytical treatment.

2.3.3 Patchiness and mosaics in rivers

In contrast to the patches, formation of which reflects a certain self-organizing mechanism and mainly depends on flow-plant interaction, formation of a mosaic involves larger scale factors controlling the physiology of plants. Those most important factors are: light availability (shadowing by terrestrial vegetation, light attenuation in the water column), nutrients supply, and substrates. Some of those factors, like light attenuation in the water column and substrate, in many respects are dependent on the river morphology and channel processes that impose a relationship between transported amount of water and solids and display that relation integrally as the turbidity of water. Water turbidity sets (by light attenuation) the limits upon the river depth that can be colonized by the certain species of macrophytes and thus together with the river morphology (as a distribution of river depths imposed by bedforms) forms the specific patterns of vegetation cover - a mosaic. A simple classification of the vegetative mosaic patterns can be deduced considering river morphology together with the possible depth limit attributed to light attenuation, Figure 2.3.3.

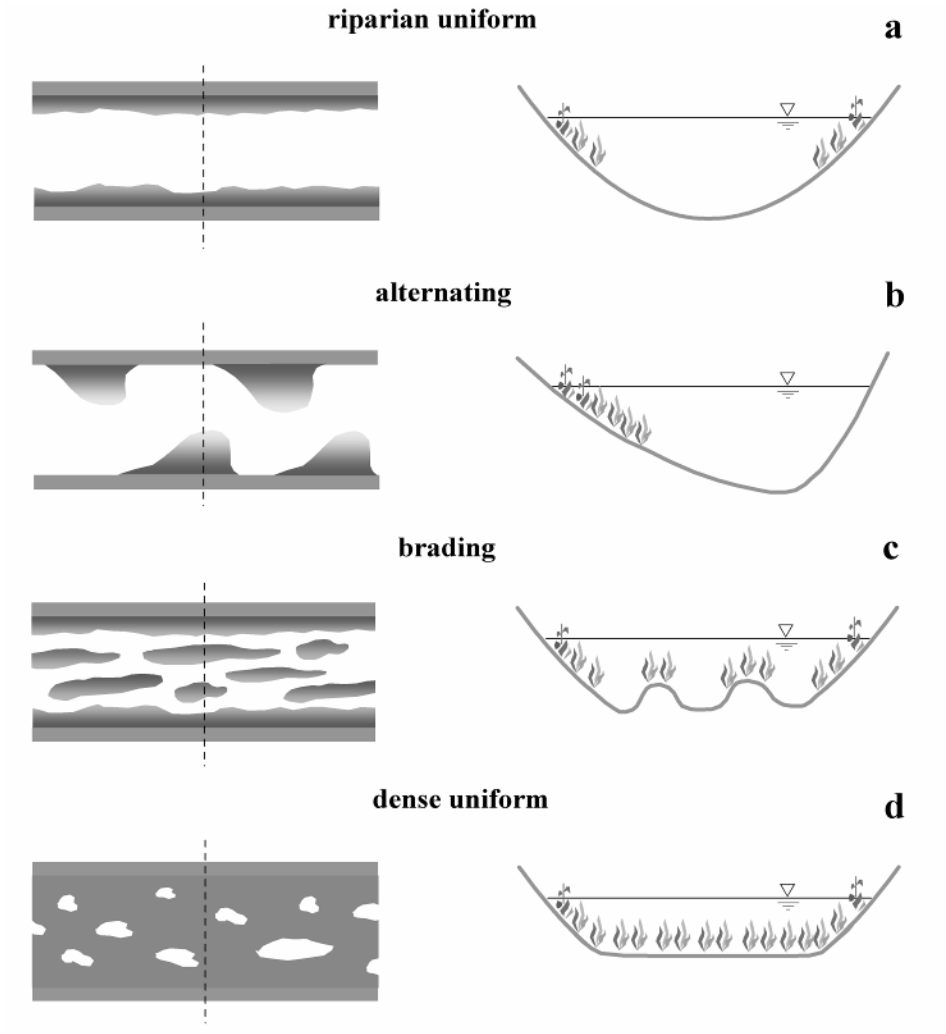

Figure 2.3.3 Classification of vegetative mosaic patterns, a) riparian uniform canopy, b) alternating riparian canopy, c) dense incomplete, and d) dense complete.

Thus, in relatively straight reaches of rivers with regular river bed morphology represented by a parabolic profile (Figure 2.3.3a) with the depth maximum significantly below the limit set by the light attenuation for certain species, one can expect only riparian uniform mosaic to develop. As the large scale morphological structures of riverbed are often represented by alternate or point bars, specific alternating patterns of vegetation canopy can develop on such river reaches, Figure 2.3.3b. Vegetation grows abundantly at the bars and is scarce on the opposing banks because of enhanced forcing and scouring induced by the flow. In the relatively shallow river channels, where the depth of the river is smaller than the depth limit imposed by the light attenuation dense vegetative canopies can develop (Figure 2.3.3c, d). There two types of mosaic can be distinguished – incomplete dense where the vegetation patches are separated by the paths of freely flowing water (Figure 2.3.3c), and dense complete canopy relatively uniform over the most of cross-sections of the channel (Figure 2.3.3d). Obviously, that basic patterns described on the classification scheme (Figure 2.3.3) can be superimposed and complicated by other factors mentioned above.

2.4 Fluvial Hydraulics and Morphodynamics

In contrast to detailed hydrodynamical description of the flow (Subsection 2.1.2) fluvial hydraulics concerns one-dimensional, bulk representation of flow. It operates on the large scales where local non-uniformities became insignificant. The central problem of hydraulics is the assessment of resistance to the flow motion. In alluvial channels hydraulic resistance is controlled by morphodynamic processes, therefore both of these issues are considered in this Section. The problems of channel resistance are discussed in the Subsection 2.4.1 and followed by description of relevant details of morphodynamics (Subsection 2.4.2).

2.4.1 Resistance of river channels

In contrast to hydrodynamic methods described in Section 2.1, river hydraulics focuses on the one-dimensional schematization of the problems and their semi-empirical and even purely empirical solutions providing practically relevant results. However, hydrodynamic theory provides the theoretical background of river hydraulics and particularly for one-dimensional approximation of equation

$$\frac{d\tau_{xz}}{dz} = -\rho g\left(i_0 - \frac{\partial h}{\partial x}\right) = \rho g I \tag{2.4.1}$$

assuming that the effect of banks is negligibly small in relatively wide fluvial channels and hence $\tau \approx \tau_{xz}$. Integrating equation (2.4.1) over river depth yields

$$\tau = \rho g I\left(h - z\right) \tag{2.4.2}$$

and for boundary conditions on the riverbed $z = 0$, and $\tau\left(0\right) = \tau_0$ one obtains

$$\tau_0 = \rho g I h \tag{2.4.3}$$

In a uniform flow potential energy of flow $\rho g h$ is transformed into the kinetic energy of flow $\rho U^2/2$ where U is bulk flow velocity. Considering the work of gravitational force against friction for a unit length of a channel one obtains definition for a bulk friction factor c_f of the channel equating bed shear stress in (2.4.3) as $\tau_0 = 0.5\rho c_f U^2/2$, and hence

$$c_f = \frac{2gIh}{U^2} = \frac{2u_*^2}{U^2} \tag{2.4.4}$$

The friction factor is a dimensionless parameter which has a sound physical meaning though in (2.4.4) strongly related to the concept of flow uniformity.

Historically the first hydraulic relation between bulk flow characteristics was Chezy formula (1776) deduced empirically

$$U = C\sqrt{hI} \tag{2.4.5}$$

where C is Chezy coefficient. Apparently Chezy coefficient is related to the bulk friction factor as $C = \sqrt{2g/c_f}$, but contrary to c_f, the Chezy coefficient has a dimension $\left[\sqrt{m}/s\right]$. Later Manning, attempting to account for experimental observation that resistance depend on submergency of the channel, has proposed an expression for the Chezy coefficient

$$C = \frac{1}{n}h^{1/6} \tag{2.4.6}$$

where n is Manning coefficient for the roughness related to the bulk friction factor as $n = h^{1/6}\sqrt{c_f}/\sqrt{2g}$. Though both empirical friction factors are suffering the dimension problem and empirical ambiguities, they are still actively used in hydraulic computations because the experimental material on the resistance in natural flows was usually generalized in terms of those coefficients.

Experimental studies indicated that friction factor in the uniform channel flows are dependent on the density of water ρ, viscosity μ, its bulk velocity U, dimension of the flow h, and on geometry of roughness elements Δ

$$c_f = f\left(\rho,\quad \mu,\quad U,\quad h,\quad \Delta\right) \tag{2.4.7}$$

Applying theory of dimensionless variables, equation (2.4.7) can be simplified to the relation of two principal parameters

$$c_f = f\left(\mathrm{Re} = \frac{\rho U h}{\mu},\ \frac{\Delta}{h}\right) \tag{2.4.8}$$

thus indicating that friction depends on Reynolds number, and relative submergence of the roughness elements.

In two-dimensional open channel flow velocity was shown to obey logarithmic distribution (2.1.29). With some transformations equation (2.1.29) can be rewritten to provide the description of the bulk friction factor

$$\frac{1}{\sqrt{c_f}} = \frac{1}{k}\left[\ln\left(\mathrm{Re}\sqrt{c_f}\right)+1\right] \tag{2.4.9}$$

where k is Karman parameter. Relation of c_f with the relative submergence is also dependent on the flow regime and the character of roughness elements. Usually different types of roughness elements are experimentally tested to obtain empirical relationship (2.4.8).

Hydraulic resistance in vegetated channels considers quasi-uniform turbulent (viscous drag smaller than turbulent) open-channel flow over uniformly distributed vegetative canopy (Figure 2.4.1).

Hydraulic resistance in vegetated channels can be described by equation derived from (2.1.40) and introducing bulk friction factor in non-vegetated channel $\tau_0 = 0.5\rho c_f U^2$, yields relation of the plants drag coefficient to the bulk friction factor

$$c_f = 2\frac{g h_0 I}{U^2} + C_D a\, h_{ve}\frac{u_v^2}{U^2} = \underbrace{c_{fb}}_{\text{bed friction}} + \underbrace{C_D a h_{ve}\upsilon}_{\text{vegetation friction}},\quad \upsilon = \frac{u_v^2}{U^2} \tag{2.4.10}$$

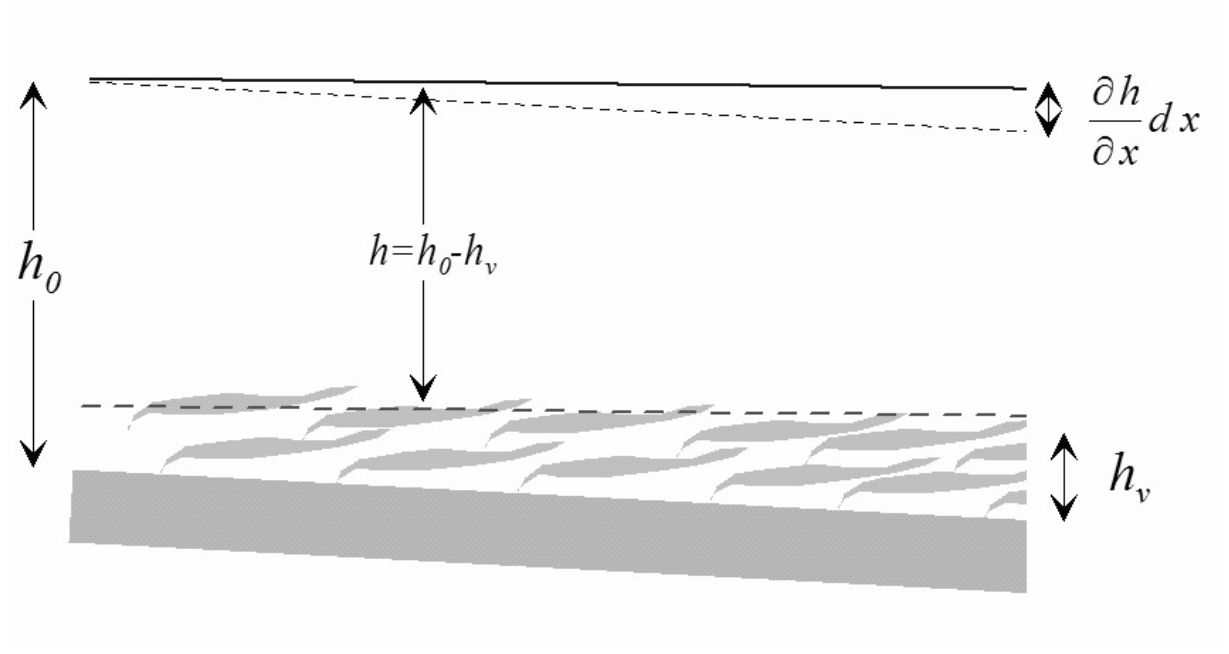

Figure 2.4.1 Schematic representation for open-channel flow in vegetated channel

For dense vegetation and small surface slopes it is also assumed that vegetative drag dominates resistance, and hence

$$c_f \approx C_D a h_{ve} \upsilon \tag{2.4.11}$$

The following important implications follow from the described theoretical considerations:

- with increase of population density of vegetation the slope of the free surface will be reduced because pressure gradient and riverbed slope have opposite signs

$$I_v = I - C_D a \frac{h_{ve}}{h_0} \frac{u_v^2}{2g};$$

- drag coefficient and projected area of the plants for flexible vegetation depend on flow characteristics (due to reconfiguration).

Reduction of the slope corresponding to the increase of vegetation density reduces mean velocity of the flow and results in the increase of the total flow depth on the river reach.

2.4.2 Morphodynamic processes

Rivers flow in the channels composed by the alluvium – loose or compacted – once transported by river flow and accumulated in river valleys. Interactions of flow with its own channel and feedback effects of the channel on the flow dynamics create sequential patterns of erosion and deposition of loose alluvium generally referenced as *bedforms*. Systematic changes in morphology of the river beds because of evolution of bedforms in response to changes in supplies of water and sediment are called *morphodynamic processes*. In this section we briefly describe essentials of river morphodynamics, effect of morphodynamic processes on aquatic vegetation, and the feedback from aquatic vegetation.

The morphodynamic changes of alluvial riverbeds are described by the two-dimensional equation of balance of mass which relates dynamics of riverbed relief to the sedimentary fluxes

$$\left(1-\lambda_p\right)\frac{\partial z}{\partial t} = -\frac{\partial\left(q_b+q_s\right)}{\partial x} - \frac{\partial\left(q_b+q_s\right)}{\partial y} \tag{2.4.12}$$

where λ_p is porosity of sediment deposits, q_b is volume bedload transport rate per unit width of the channel (unit bedload discharge), and q_s is volume suspended sediment transport rate per unit width of the channel (unit suspended sediment discharge). To solve (2.4.12) we need to provide description for transport rates of bedload and suspended sediment and to model conservation of suspended sediments.

Balance of physical forces acting upon a sediment grain resting at equilibrium on a riverbed is maintained by drag force $F_d = 0.5\rho\pi C_d \left(d/2\right)^2 u_f^2$ and friction force $F_f = 4\mu\left(\rho_s - \rho\right)\pi\left(d/2\right)^3 g/3$, where ρ_s is density of sediment, d is diameter of a grain, u_f is effective flow velocity, and μ is friction coefficient. Relating the forces $F_d = F_f$ and assuming that velocity near the riverbed obeys the logarithmic law (2.1.29), one obtains

$$\frac{u_*^2}{\rho^* g d} = \frac{4}{3}\frac{\mu}{C_d F_u^2} \tag{2.4.13}$$

where $\rho^* = \left(\rho_s - \rho\right)/\rho$ is relative density of sediments, and $u_f = u_* F_u$, F_u can be obtained from (2.1.29). The left hand side of (2.4.13) is dimensionless bed shear stress τ^*, and the right hand side (2.4.13) is the threshold value of the bed shear stress τ_c^* called critical shear stress. Critical means here that when the shear stress exceeds the critical value the grain will be entrained into motion. As the drag coefficient C_d for the grain depends on the flow regime expressed by characteristic Reynolds number $\mathrm{Re}_* = u_* d/\nu$, the shear stresses τ^* are considered as the function $\tau^* = f\left(\mathrm{Re}_*\right)$ expressed in graphical form in Shields diagrams. Physical consideration of the riverbed stability described above, were used to construct many practical formulae for computations of bedload discharge. Most widely used is Meyer-Peter and Müller (1948) formula

$$q_b = 8\sqrt{\rho^* g d}\, d\left(\tau_s^* - \tau_c^*\right)^{3/2} \tag{2.4.14}$$

where $\tau_c^* = 0.047$, and τ_s^* is the skin friction portion of the total shear stress $\tau_s^* = 0.06 + 0.4\left(\tau^*\right)^2$ (Engelund and Hansen 1972).

The discharge of suspended sediment can be obtained by integration of suspended sediment concentration over the flow depth. In contrast to dissolved substances considered in the section 2.2, the sediments are characterized by their buoyancy, represented by settling velocity u_s, and equation (2.2.3) will be modified as

$$\frac{\partial \bar{c}}{\partial t} + \bar{u}\frac{\partial \bar{c}}{\partial x} + \bar{v}\frac{\partial \bar{c}}{\partial y} + \left(\bar{w} - u_s\right)\frac{\partial \bar{c}}{\partial z} = e_m \nabla^2 \bar{c} - \sum_i \frac{\partial \overline{u_i' c'}}{\partial x_i} \tag{2.4.15}$$

For steady, longitudinally and transversally uniform distributions of concentration, and neglecting the molecular diffusion, one simplifies equation (2.4.15) to

$$u_s \frac{\partial \bar{c}}{\partial z} = \frac{\partial \overline{w'c'}}{\partial z} \tag{2.4.16}$$

and modeling turbulent flux by introducing turbulent viscosity concept (2.2.4) yields

$$u_s \frac{\partial \bar{c}}{\partial z} = e_T \frac{\partial^2 \bar{c}}{\partial z^2} \tag{2.4.17}$$

The simple analytical solution of (2.4.17) is provided for the case of two-dimensional open channel flow with parabolic distribution of turbulent viscosity (2.1.28). Imposing boundary

condition $\bar{c}_b$ (concentration at the reference elevation z_b) near the riverbed and integrating (2.4.17) leads to Rouse (1939) concentration profile

$$\frac{\bar{c}}{\bar{c}_b} = \left[\frac{\xi_b}{\xi} \frac{(1-\xi)}{(1-\xi_b)} \right]^{\frac{u_s}{\kappa u_*}}, \quad \xi = \frac{z}{h}, \text{ and } \xi_b = \frac{z_b}{h} \tag{2.4.18}$$

When the distribution of suspended sediment concentration over the flow depth is provided it can be integrated to obtain discharge of suspended sediments as

$$q_s = \int_0^h \bar{u}(z)\bar{c}(z)\,dz \tag{2.4.19}$$

Both approaches (2.4.13-2.4.14 and 2.4.15-2.4.18) to treat sediment fluxes in the alluvial systems are illustrative to show the relationship between turbulent flows and mixing and transport models described in previous sections. They show that turbulence characteristics, and particularly shear velocity, are the basic parameters for quantitative description of morphodynamic processes.

Although equation (2.4.12) represents the morphodynamic processes in continuous form, in turbulent flows these processes cumulatively appear in discrete dynamically behaving instances - bedforms. Although alluvial bedforms in fluvial systems are widely ranging in their sizes and shapes, they can be subdivided into some classes. Most widely accepted classifications of bedforms in lowland rivers include ripples and dunes (micro-forms), alternate and point bars (meso-forms), and river meanders (macro-forms), Figure 2.4.2. Essential feature of bedforms is their ability for directional motion due to sequential spatio-temporal deposition/erosion processes. However, the rates of motion are different for different bedforms, and furthermore, different processes dominate the bedforms dynamics.

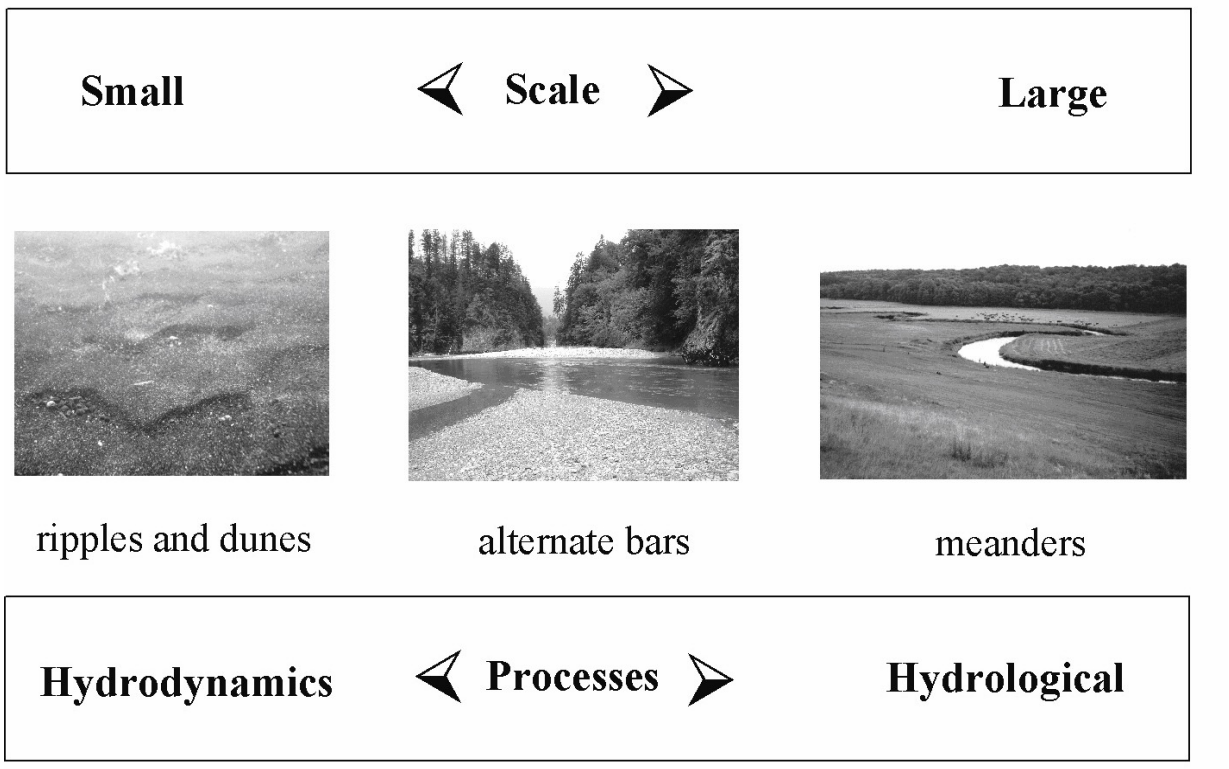

Figure 2.4.2 Scales, bedforms and dominating processes in fluvial morphodynamics

2.5 Formulation of the Problem

The aim of this Section is to expand in details the general description for the objective of the study already introduced in the Section 1.3. Having expanded description of the theoretical background in the previous sections makes it easy to specify the points where the lack of knowledge requires improvement and what are the steps should be made to pursue the goals of the study.

The **focus** of the study is set on the development of a complete theory describing longitudinal transport and mixing of substances in a fluvial system subjected to the seasonal growth of submerged vegetation. A complete theory means here that theoretical description of seasonal dynamics of vegetation cover should provide the parametric field for longitudinal dispersion model with dead zones. The main working **hypothesis** in this study is that transformation of the output from the vegetation growth model to the parameters of the dispersion model can be achieved through the hydrodynamical description of the complex flow-vegetation interactions. To test this hypothesis we need first to create a conceptual model of the phenomena which on the next step will evolve into a certain theoretical scheme, and finally will be verified by comparing predictions of theory to the observations in nature.

2.5.1 Conceptual model

The longitudinal dispersion model with dead zones presented in the Subsection 2.2.3 is a convenient theoretical scheme capable of accurate prediction of solutes concentrates but requiring knowledge of the four principal parameters: bulk flow velocity U, dispersion coefficient D, dead zone relative area э, and dead zone residence time T_d for running practical applications. Though the way to obtain bulk velocity is straightforward from the hydraulic approaches described in the Section 2.4, the parameterization schemes for the other three parameters are less obvious and only recently became concerned. Nepf and Vivoni (2000) suggested subdivision of flow over submerged vegetation into two layers: the zone of vertical exchange and the longitudinal exchange zone. The lower boundary of the vertical exchange zone, so-called penetration depth, is the horizon in the water column to which turbulence generated on the boundary between vegetation and free flow is practically disappearing. Thus the zone of longitudinal exchange became decoupled from the overlying flow and hence mostly produces the effect of slow exchange.

Therefore it is hypothesised here that:

- the dead zones in flow with submerged vegetation are formed by a substantial parts of the longitudinal exchange zones;
- the residence time in a vegetative dead zone is defined by the characteristic longitudinal scale of the dead zone and the mean streamwise velocity inside the longitudinal exchange zone;
- the length of the dead zone is proportional to the longitudinal length of an average vegetative patch while its height equals to the difference between bulk depth of the flow and the penetration depth;
- to account for the effect of vegetation, the longitudinal dispersion coefficient should describe the phenomenon of mechanistic dispersion in vegetative mosaics.

It can be seen that parameters of the longitudinal dispersion model with dead zones are related explicitly or implicitly to the characteristics of vegetation by this conceptual model. The most important variables thus are the following: area covered by vegetation, deflected height in the water column, vegetation population density. These variables explicitly became dependent on interactions with the flow and seasonal changes due to phenological dynamics.

Complete approach to the description of transport and mixing in river reaches with submerged vegetation would mean: 1) prediction of vegetation biomass and its spatial distribution in terms of average size of a patch in vegetative mosaic; 2) prediction of characteristics size of individual plant, its morphology, and population density; 3) prediction of flow resistance using information on vegetative characteristics, and thus bulk flow velocity; 4) prediction of flow interactions with patches of macrophytes by means of determining the penetration depth and characteristic dimensions of the dead zone and their characteristic velocity scale in the longitudinal direction; 5) assessing the effect of enhanced retentivity of particulate matter in dead zones on river morphology and composition. The conceptual scheme of the approach is depicted in Figure 2.5.1.

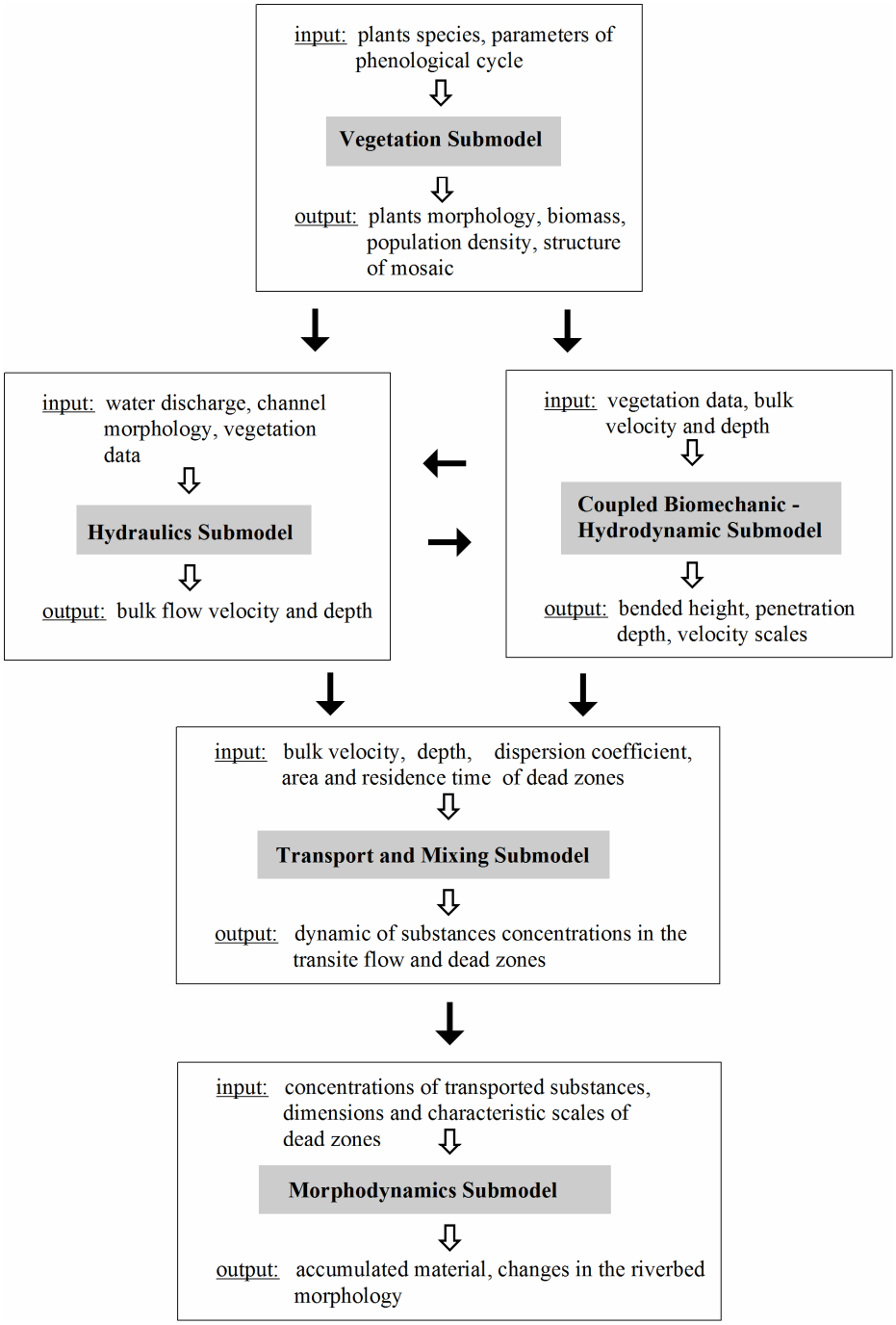

Figure 2.5.1 A scheme depicting concept of the complete approach to the problem.

2.5.2 Knowledge gaps and possible ways of bridging

Though an immense body of knowledge pertaining to the problem is already available, many important links necessary for building a complete approach are still missing and respectively need further theoretical consideration, an experimental assessment or observation. Here we outline specific problems and the ways they can be resolved.

The review of quantitative theoretical and empirical methods designed to assess vegetation growth is operating with the biomass of the plants rather than with characteristics of its spatial distribution (Subsection 2.3.2). Little is known about formation of vegetative patches and their mosaics. Quantitative description of bio-mechanical properties of individual plants was mainly focused on the rigidity as the primary mechanisms by which plants maintain the upright posture by balancing drag force of the flow (Subsection 2.3.1). However, for flexible submerged vegetation rigidity most probably impose a minor effect while the balance with drag is maintained by buoyancy. Therefore to expand the vegetation submodel – a crucial element of the approach (Figure 2.5.1) – the following problems should be clarified:

- the effect of buoyancy on maintaining the upright position and respectively bending angle of the flexible submerged plants;
- the theoretical description should be developed for predicting phenological dynamics of an average area occupied by plans in a cross-section, the population density of vegetation, and dimensions of an average individual plant;
- dynamics of vegetative mosaics patterns and mechanisms controlling dimensions of the vegetative patches.

Resistance of vegetated river channels is presently predicted with large uncertainties for conditions of typical lowland rivers with small slopes and flexible submerged vegetation.

Available semi-theoretical schemes relate bended angle of the plants to their rigidity while the effect of buoyancy can dominate the counterbalance part for flexible submerged plants. Effect of vegetation on water slope in rivers and its seasonal dynamics is not examined. Respectively, for hydraulic submodel (Figure 2.5.1) we consider following improvements:

- re-examination of semi-empirical and empirical relationships for flow resistance parameters such as Chezy, and Manning coefficients and their dependency on buoyancy in *n-Uh* or more general $c_f = f\left(\mathrm{Re}, \theta\right)$ methods;
- investigation of seasonal dynamics of water slope on a river reach with submerged vegetation.

The complex interactions between turbulent flow and flexible vegetation are comprehended through the hydrodynamics approach relaying on the flow analogy to free mixing layers. However, most of available studies consider the flow only in the domain of dynamical equilibrium where growth of the mixing layer is stabilized and its spatial growth rates are insignificant. Evolution of the vegetated shear layer (Subsection 2.1.3) from the leading edge of vegetation cover and downstream to the zone of fully developed dynamically stable zone was not examined theoretically or experimentally hitherto. Obviously, an understanding of flow structure in and above the patches of submerged flexible vegetation will be only possible when the following problems will be addressed:

- the evolution of flow in and above a patch of submerged flexible vegetation and the effect of population density on this dynamics;
- scaling relationships providing further relations between penetration depths, bulk flow characteristics, vegetation density, and bio-mechanical properties of individual plants (represented by buoyancy for flexible submerged vegetation);

- knowledge on spatial dynamics of turbulent flow in vegetative mosaics for better understanding of principal mechanisms governing flow in vegetation-free areas between the vegetation patches and their consequence for transport and mixing processes.

Hydraulic and hydrodynamic submodels (Figure 2.5.1) should be running in the complete model iteratively because of feedback mechanisms between turbulent flow and vegetation response to it (plants bending). On the first step the bulk flow characteristics supplied by hydraulic model based on some initial assumptions on plants bending should be corrected in the hydrodynamical model and used for refined computations by the hydraulic submodel.

The longitudinal dispersion model with dead zones requires provision of theoretical and experimental assessment for dynamics of the model parameters during vegetative period. Presently the knowledge on seasonal dynamics of transport and mixing in vegetated rivers is mostly lacking any rigorous experimental or theoretical evaluation. Therefore a quantitative assessment should include:

- experimental studies of longitudinal dispersion in a lowland river with submerged vegetation to outline trends and amplitudes of variation in parameters;
- to explain the trends and if possible observed amplitudes theoretically based on the knowledge of vegetation cover dynamics (vegetation submodel, Figure 2.5.1) and flow hydrodynamics (hydrodynamics submodel, Figure 2.5.1).

On the final stage the implications of complex interaction of flow and submerged vegetation can be considered in respect to morphodynamics aspect of transport and mixing problems – sedimentation, retention of nutrients in vegetated riverbeds and their further remobilization by mechanisms of resuspension.

Morphodynamic submodel (Figure 2.5.1) will be considered here as an example of implication of research results rather than advanced submodel. The topics that morphodynamic modeling is covering are so numerous that most of them we need to leave behind the scopes of the detailed study. Here we only will examine to some extent implications of our study for retention of nutrients and some other substances in vegetated riverbeds, and also conditions for their resuspension. Morphodynamics of bedforms evolving on the riverbed during winter period and crucial for maintenance of vegetation succession will be also investigated by field measurement studies.

As it can be seen from the content of this section, the task set for this research is ample and challenging. It requires significant theoretical and experimental work which had little precedents in scientific practice and hence requires additional methodological, technological, and logistical efforts. To make the general task possible to achieve, we will limit our study to the investigations for only one species of submerged plants dominating particular river reach.

3 METHODS AND TECHNIQUES

Field studies completed for this research project represent the factual basis for the deeper understanding of investigated physical and biological phenomena, validation of theoretical concepts and for verification of available and developing mathematical models. The program of the field studies and its components is conceptually depicted in Figure 3.1. Accordingly, the studies can be subdivided into two main categories: field measurements and field-scale experiments.

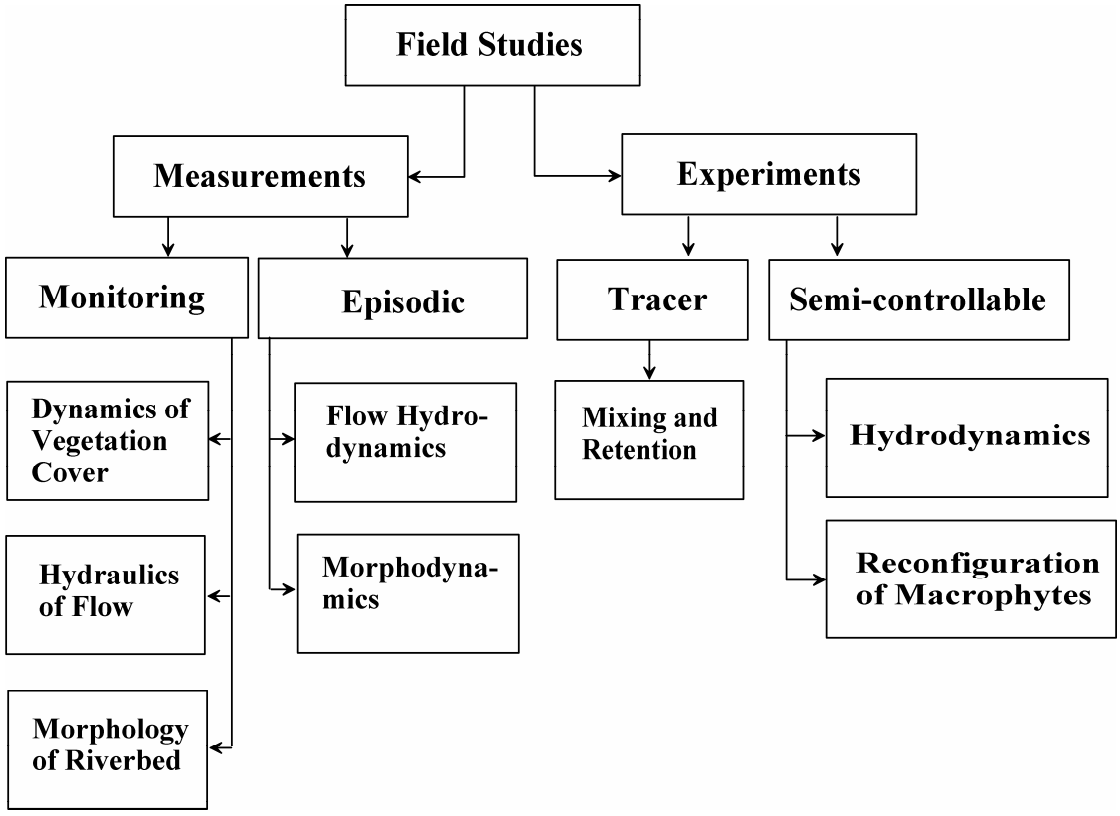

Figure 3.1 Components of the program for field studies and relations between them

The field measurements comprised of the monitoring measurements for parameters characterizing dynamics of vegetation cover simultaneously with the observations of hydraulic characteristics and riverbed morphology. The program of these observations was relatively simple, relatively fast to perform and allowing for systematic, approximately biweekly, measurements. The monitoring program was extended with the detailed episodic field measurements for flow hydrodynamic characteristics and morphodynamic processes. These measurements were more complicated and time consuming (lasting for about one week with subsequent logistics) and respectively were only conducted during the periods of notable difference in the flow, vegetation, and riverbed morphology. The results of these measurements provide possibilities for direct comparison of flows in vegetated and unvegetated areas of the same river section and for verification of mathematical models.

The field-scale experimental studies comprised of the tracer studies and of detailed semi-controllable experiments. Tracer studies were designed to investigate transport, mixing, and

retention of dissolved substances and the effect of vegetation on those processes. The program of tracer experiments assumed repetition of the experiments at characteristic conditions. They were performed in a channel free of vegetation (winter and early spring), and two times at different stages of vegetation cover development thus providing insight into the evolution of the processes. Semi-controllable experiments assumed active control on the experimental conditions similarly to laboratory experiments (Nepf 1999; Ghisalberti and Nepf 2002). The advantages of such experimental studies are: 1) possibility to apply theoretical models for analysis of experiments, 2) to make direct comparison with laboratory experiments and to explore the scale effects, and 3) they provide direct estimates of model parameters. However, such experiments are so extremely difficult and time consuming, that they were performed only once in this study.

3.1 Experimental River Reaches

The field measurements and experiments of this study were completed on the Spree River. The Spree River is a typical lowland river about four hundred kilometers in length, running from the Lusatian mountains through several shallow lakes to Berlin, were it joins the Havel River (Figure 3.1.1a).

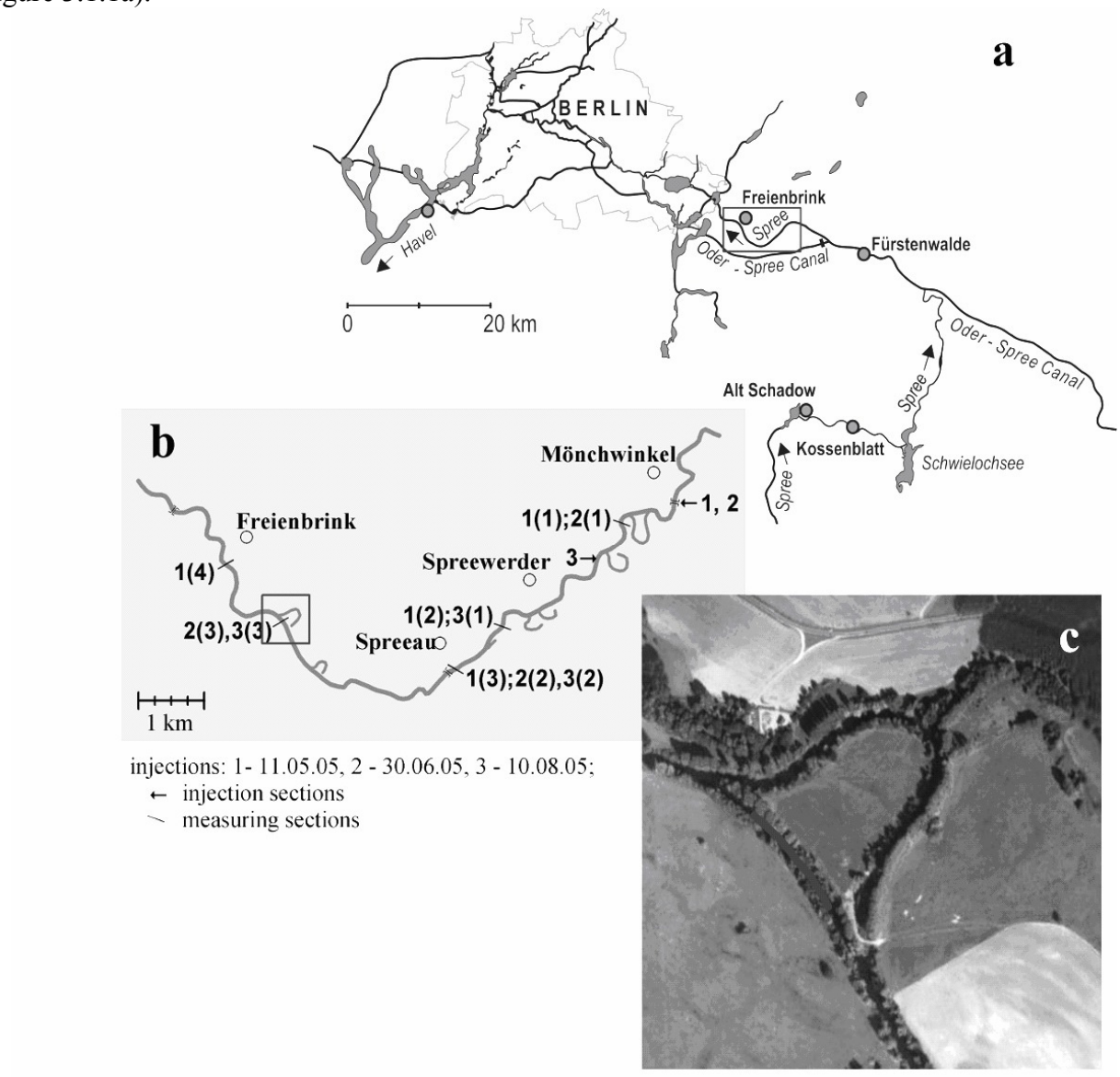

Figure 3.1.1 Study area (a), enlarged is the area of investigations on longitudinal dispersion (b), and the airborne picture of the experimental river reach near the village of Freienbrink (c).

The part of the river stretching downstream from the village Mönchwinkel till the eastern border of Berlin was used as the experimental river reach for studies of transport and mixing processes (Figure 3.1.1b, the highlighted area on Figure 3.1.1a). The river channel on the reach is canalized with banks armored by a rip rap. The remnants of meanders are still connected in their outlets with the modern canalized channel (Figure 3.1.1b,c). The canalized channel is mildly sinuous with trapezoidal shape of a cross-section that measures from 20 to 35 m wide at a bank full level (Figure 3.1.2). Annually, during the period from May to September, aquatic and riparian vegetation grows abundantly on the river reach and intensively affects the flow (Figure 3.1.2, Figure 3.1.3).

Figure 3.1.2 The Spree River downstream of Mönchwinkel.

Figure 3.1.3 Experimental river reach of the Spree River near Freienbrink

A river reach near the village of Freienbrink (Figure 3.1.1, Figure 3.1.3) served as the experimental river reach for studies of flow hydrodynamics and detailed investigations of complex interactions between turbulent flow and submerged vegetation. The river reach is straight on the distance about 1 km (Figure 3.1.1b). The remaining meander on the reach is separated from the river by a bridge and the inlet of the meander was completely silted with sedimentary deposits and woody debris so that no water was moving through the remnant meander. This river reach was the study site for the previous field investigations of IGB (Sukhodolov et al. 1998, Sukhodolov et al. 1999). Detailed maps of riverbed elevations on the experimental reach are presented in Figure 3.1.4a, and the spatial distribution of d_{50} as the representative riverbed material parameter is shown in Figure 3.1.4b.

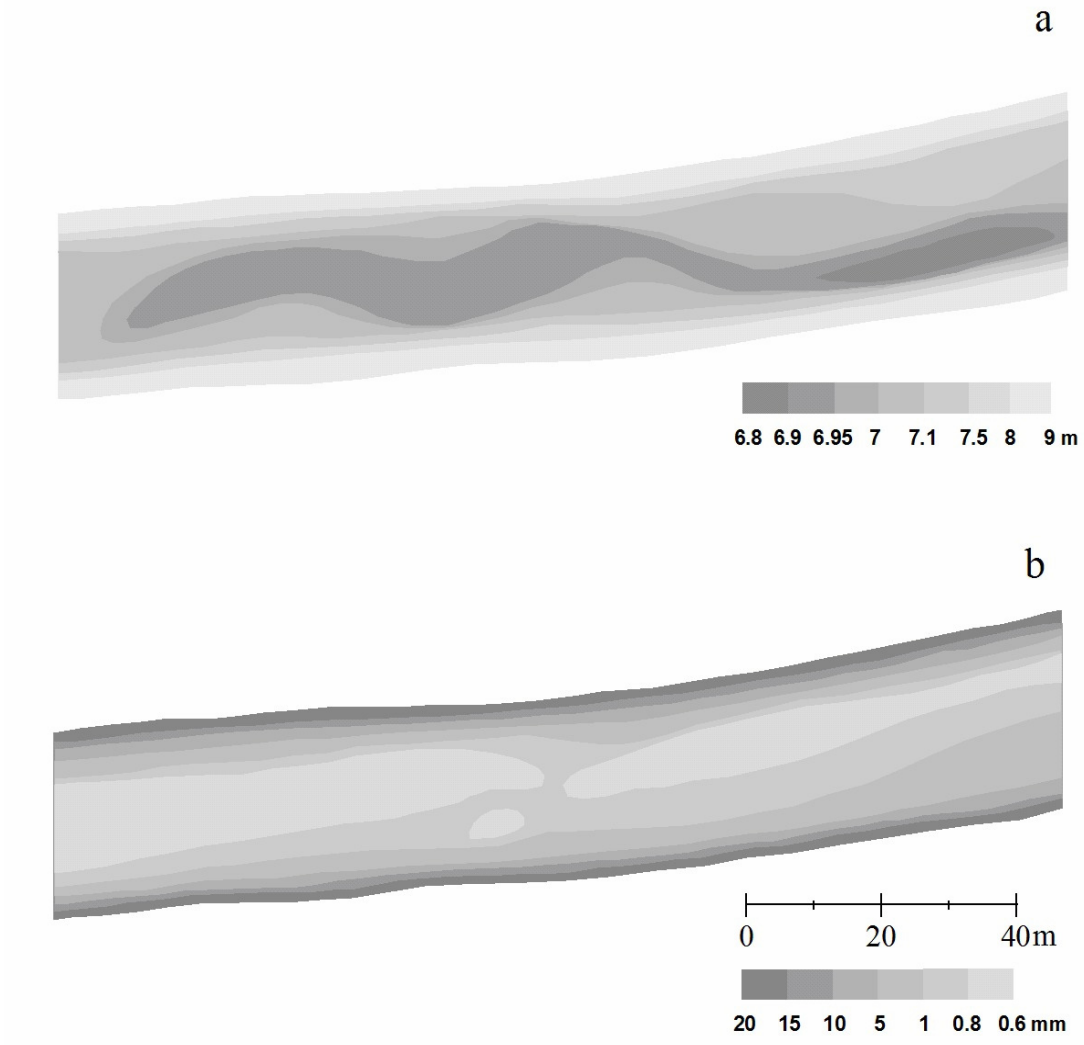

Figure 3.1.4 Riverbed elevations above arbitrary datum (a), and spatial distribution of d_{50} (b) on the experimental river reach of the Spree River near Freienbrink

3.2 Apparatuses and Equipment

3.2.1 Acoustic Doppler velocimeter

Flow velocities were sampled with Nortek Doppler velocimeters (NDV, Oslo, Norway). NDV are acoustic devices in functionality analogous to acoustic Doppler velocimeters (ADV) produced by SonTek Inc. (San Diego, USA). Presently devices of both firms are widely used in

different laboratory and field applications worldwide and represent inexpensive alternatives for the laser Doppler velocimeters (LDV). Brief descriptions of the device, principles of its operation, characteristics of accuracy are presented in this subsection.

NDV (Figure 3.2.1) unit comprises of sensor (1), signal conditioning module (2), and a processor (3). In our field studies a 3-D probe on a flexible 1 meter cable, with 5 cm distance from the tip to the sampling volume was employed. The cable connects the probe to the signal conditioning module which transmits the signal to the processor in a splashproof case by 20 meter long high frequency cable. Transformed signal is delivered to a communicating port of a portable computer by which the NDV unit is operated.

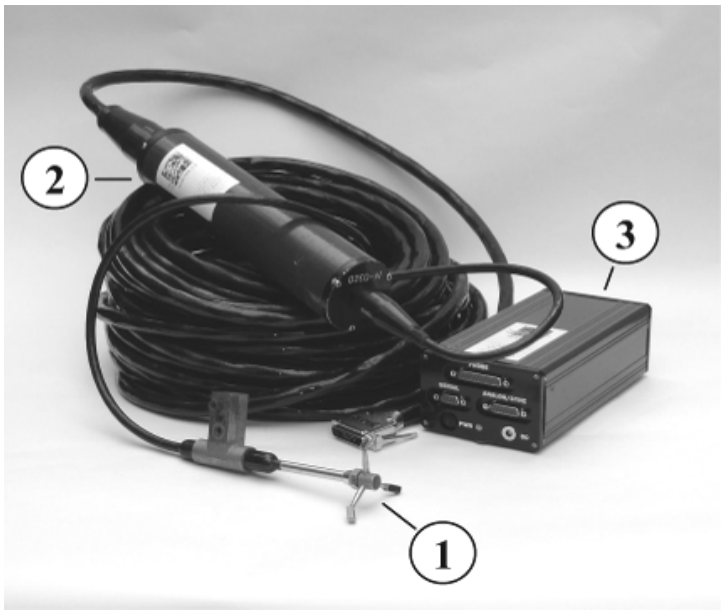

Figure 3.2.1 Nortek Doppler Velocimeter.

A NDV probe represents a bi-static Doppler sonar with a separated 10 MHz transmitter and three receivers. In 3-D probe the transmitter is located in the center, on the probe's tip, and aligned with the vertical axes of the stem. The receivers are surrounding the transmitter on the sectors of 120º and connected with the stem by short arms. An imaginary line orthogonal to the plane of transducers intersects the probes axis at 30º focusing the receivers on the intersection. The point of intersection has a certain volume depending on the parameters of the transmitted signal and is respectively called *sampling volume.* The sampling volume, cylindrical in shape and coaxial with the principal axis of the probe, has the diameter of 6 mm and the height that can be programmatically changed in the range from 0.5 to 7.2 mm (Lohrmann et al. 1994).

NDV is using the pulse-to-pulse coherent Doppler technique which minimizes errors in velocity estimates during high frequency sampling in variable flow within velocity range 0-2.5 m/s. In this operating technique short phase coherent acoustic impulses are transmitted to the flow where they are scattered on small particles (about 10μm) moving with the velocities close to the local velocities of flow and the scattered signals are intercepted by receivers. Receivers register appearance of a pair of successive impulses and calculate the phase difference $\Delta\Phi$ which is converted to the velocity as

$$V_i = \frac{C_s}{4\pi f}\frac{\Delta\Phi}{\tau} \tag{3.2.1}$$

where C_s is speed of the sound in water, f is nominal operating frequency, and τ is lag time between impulses. Velocity components V_i measured in the system of coordinates aligned with

the directions of reflected signals are transformed into orthogonal system of coordinate with the use of a calibration matrix

$$\begin{bmatrix} u \\ v \\ w \end{bmatrix} = \begin{bmatrix} a_{11} & a_{12} & a_{13} \\ a_{21} & a_{22} & a_{23} \\ a_{31} & a_{32} & a_{33} \end{bmatrix} \times \begin{bmatrix} V_1 \\ V_2 \\ V_3 \end{bmatrix} \tag{3.2.2}$$

where *u, v,* and *w* are orthogonal velocity components in the system of coordinates aligned with the stem axis of the probe, and a_{ij} are the components of the transformation matrix (Lohrmann et al. 1994). The calibration matrix is obtained by propagating the probe in a still water tank. Accurate calibration provides velocity error within ±1%.

Because the scheme of pair-to pair coherent Doppler shift calculates the phase difference for acoustic impulses separated by the lag time the effective frequency is $1/\tau$. When the registration frequency is higher than effective then there is a situation that acoustic signals could be superimposed. Another critical situation occurs when the registration frequency is smaller than effective. In this case $\Delta\Phi > \pm\pi$ that sets the limits on registration of maximal velocities of the flow. To avoid those two critical situations in operational scheme of the device the whole range of velocities (0÷2.5 m/s) is subdivided into five subranges with the specific lag times set for each subrange (±3, ±10, ±30, ±100, and ±250 cm/s). Operating of NDV near the solid boundaries or the flow free surface creates conditions favorable for interference of the acoustic signal. However this problem can be solved by programmatically changing of the velocity subrange.

Besides the problem associated with operational scheme, the measurements with NDV are affected by rapid changes in velocity structure because of turbulence and presence of acoustic noise. Experiments had shown that acoustic noises registered by NDV are nonsystematic, uncorrelated (Voulgaris and Trowbridge 1998), and represented by a flat spectrum similar to those of the white noise (Nikora and Goring 1998). The effect of the acoustic noise is additive in respect to the statistical characteristics of turbulence and can be described as (Lohrmann et al. 1994)

$$\overline{u_i'^2} = \overline{\hat{u}_i'^2} + a_{ij}^2\sigma^2 \tag{3.2.3}$$

$$\overline{u_i' u_j'} = \overline{\hat{u}_i' \hat{u}_j'} + a_{ik}a_{jk}\sigma^2 \tag{3.2.4}$$

where σ is standard deviation of the noise, and a_{ij} are components of the transformation matrix (3.2.2). Characteristic values of a_{ij} are: $a_{1j}^2 \approx a_{2j}^2 \approx 10$, $a_{3j}^2 \approx 0.3$, $a_{1k}a_{2k} \approx -1$, $a_{1k}a_{3k} \approx 0.1$, and $a_{2k}a_{3k} \approx 0.1$. These values indicate that vertical velocity component is resolved more accurately (roughly an order of magnitude) in respect to acoustic noises than horizontal components and that distortions due to acoustic noises are particularly small for non-diagonal components of velocity correlation tensor.

Different factors contribute to the acoustic noise: uncertainties in resolving the difference in Doppler phase, inaccuracy in its determination, and non-uniformity of velocity distribution in the sampling volume. The uncertainties of Doppler phase are produced by electronics of the device and can be experimentally determined by measurements in still water for specific velocity subrange at certain concentration of suspended particles (Nikora and Goring 1998). The inaccuracy of determination of Doppler phase is produced by systematic widening of the reflected signal while velocity non-uniformity in the volume is solely attributed to the effect of turbulence on measurements. The value of the acoustic noise can be determined by methods of spectral analysis. However, the precondition for using these methods is the presence of inertial subrange in the measured spectra. The level of noise than can be determined by the values of spectral density at high frequency band of the spectra where spectra are transformed to white

noise. The contribution of the spectra can be estimated by integrating spectra over the high frequency bend with subtraction of the portion of inertial contribution.

3.2.2 BackScat fluorometer

The concentrations of uranin AT solutions, used as the tracer for experiments on mixing processes, were measured with the use of a BackScat fluorometer (Haardt, Germany). BackScat fluorometer (model 1301) employed in this study is *in-situ* highly sensitive device that resolves 8 ng/L of uranin dye solution within 120 ms response time, Figure 3.2.2.

Figure 3.2.2 BackScat in-situ fluorometer.

The device utilizes the physical phenomenon called fluorescence, a form of luminescence. Fluorescent substances emit light at instant after irradiation from an external source. Essentialy and particularly important for the method is that for fluorescent substances emitted light has longer wavelengths and lower frequencies than the absorbed light because some portion of energy is lost in the sequence "excitation-emission". The difference between excitation and emission spectra individual for each fluorescent substance makes fluorometry an accurate and sensitive method (Wilson et al. 1986).

In contrast to the laboratory fluorometers, *in-situ* (field) fluorometers need modulated excitation to compensate for background (daylight) sources. The compensation is achieved by processing the detected signal generated with Xenon flashlight. Another particular feature of BackScat fluorometer is a 180º optical geometry between axes of excitation and detection. *Measuring volume,* which in laboratory devices (90º schemes) is defined as the volume at the intersect of excitation and detection rays, for the BackScat fluorometer is defined as the area in front of the optical window (Figure 3.2.2) illuminated by a flash-lamp. The emitted and scattered signals are separated by the system of filters and reflecting mirrors in the such 180º scheme. Therefore specific filters are necessary for different types of tracing fluorescent dyes.

Fluorescent properties of the dye solutions vary directly with the concentration of a dye and depend on a certain setup of a fluorometer; therefore calibration of device is necessary in all practical applications. Several factors can affect accuracy of the measurements. Aside the concentration, the most significant factor affecting fluorescence is the temperature. In general fluorescence activity is inversely proportional to the temperature. The temperature effect can be accounted by making calibration for the different temperature ranges. Fluorescence depends also on a chemical composition of the solution: mineralization, pH, dissolved oxygen content, and

hence necessitates calibration of the device to be conducted in the water sampled in the river where field tracer studies are planned. Additionally a permanent reduction in fluorescence can be caused by the photochemical decay, or photodecomposition. Bright sunlight has this effect on the uranin dye, and the effect increases gradually with the time. Stream depth, turbidity of water, ice cover, and cloudy skies tend to minimize photodecomposition (Wilson et al. 1986).

3.2.3 Underwater video system UVS-RAY

To measure the deflected height of the vegetative canopy *in-situ* an underwater video system UVS-RAY purposely developed in IGB was employed in this study (Figure 3.2.3). The system consists of a digital camera Olympus C-5060 with a wide angle lens converter WCON-07 in an underwater housing IKELITE (1, Figure 3.2.3) and an underwater lighting system Werner Videolight 100 (2). The camera was installed on a platform (3) aligned with a wire screen (4). The mesh of the screen (10 cm) provides a reference coordinate enabling further calibration and processing of the obtained digital video records.

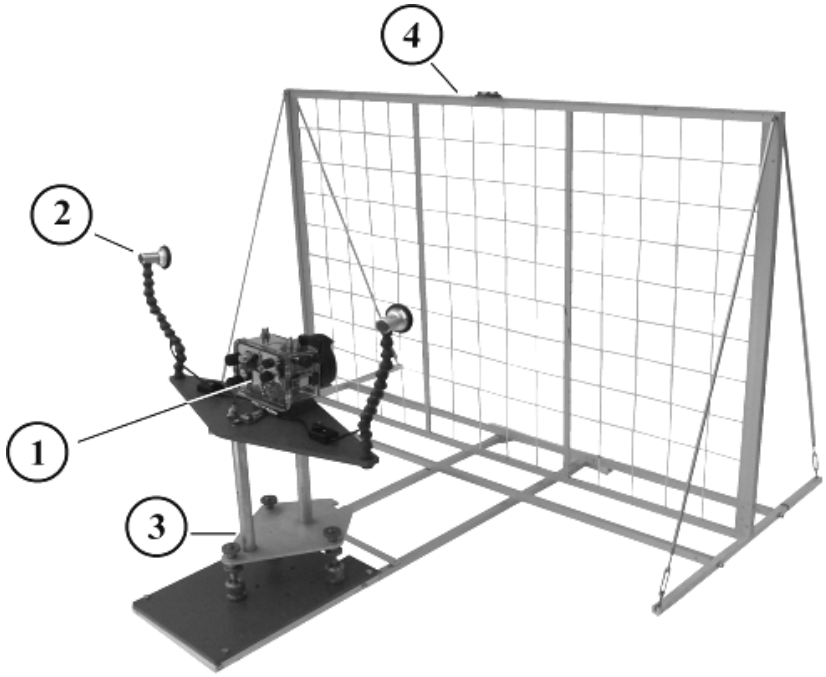

Figure 3.2.3 A scheme of the UWS-RAY system.

3.2.4 Field Equipment

Though field studies with application of ADV/NDV became increasingly popular, commercial equipment suitable for fluvial hydraulics applications is still unavailable. Respectively researches have to manufacture field equipment customarily and need to account for the following requirements that the equipment has to meet: 1) the mounting system should be stable and prevent flow-induced vibrations; 2) it should provide known orientation of the sensors; and 3) keep the sensors away from the area of interaction of flow with the submerged parts of the equipment. Field equipment should be light weighted, easy to transport, and simple to operate.

The field mounting equipment used in this study was designed and manufactured in IGB, Figure 3.2.4. The basis of the mounting system is represented by portable platform made of

aluminum ⊥ -profiles (1). Mounting blocks (2) are attached to the platform and enable traversing of the devices along the platform and positioning with a proper heading. Elevating screws (3) provide an accurate vertical alignment of a guiding rod (4) and respectively of the NDV sensors (8) parallel to the rod. A 50 cm long consol (5) perpendicular to the rod keeps the sensor away from the area of possible backwater effect from the flow-device interactions. Another end of the consol houses the NDV signal conditioning module (9). The consol can be moved up and down along the guiding rod using a deploying rod (6), and fixed at the desired flow depth with the fixing screw (7). Lateral vibration of the sensor can appear when flow depth is more than 2 m and the flow velocity is larger than 20 cm/s. Chains (10) attached to the sides of the consol and tightened to the platform are effective in preventing the lateral vibration of the sensor.

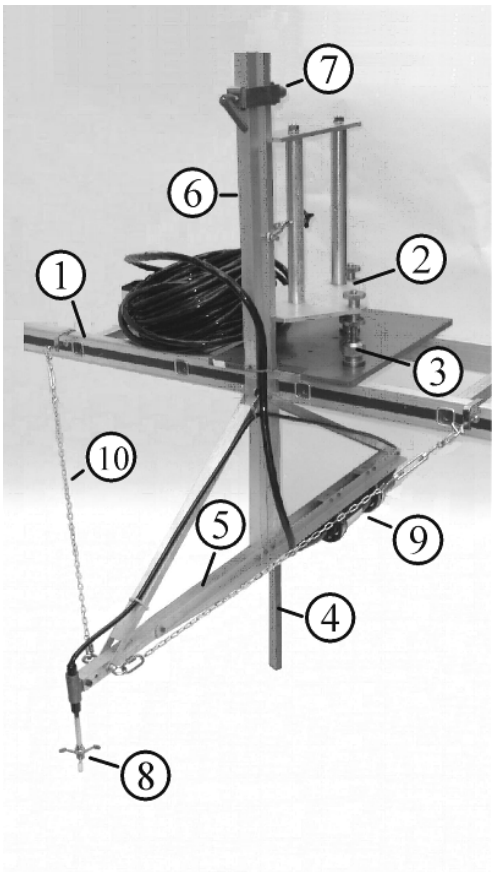

Figure 3.2.4 Scheme of NDV mounting equipment.

Geodetic measurements and accurate positioning and orienting of NDV sensors were completed with a total station ELTA R55 (Carl Zeiss Geodetic Systems, Germany). The device is utilizing a laser system for measuring distances and is equipped with a specialized built-in computer allowing for coordinates and elevations determination directly during the measurements. Three standard mirror targets with field tripods comprised the set of accessory equipment for the geodetic measurements.

Measurements of river depth were performed with a portable mono-static sonar system SonarLite (OHMEX Instruments, UK). The transducer of the sounder (∅ 7 cm) was mounted on a rod and aligned with a vertical axis by a bubble level. Signal processing block of the device is housed in a splash proof box with a liquid crystal display for data representation as a graphic or text.

The riverbed material was collected with a manual sampler and dried for some days at room temperature. Then samples were dried again at 104°C for 48 hours shortly before the granulometric analysis and processed with the standard sieving equipment.

Submerged vegetation was harvested manually using light underwater equipment (diving wet suits, masks, snorkels, and fins). The wet weight of the plants was determined with the portable electronic scales. The harvested plants were dried at shadow places on the special grids and later dried again at 110°C for 24 hours before weighting on the laboratory scales for determination of a dry weight of biomass.

For operating devices during the measurements as well as for installation of the equipment in field conditions small boats (rodeo-kayaks) and a floatable catamaran platform were used. Rodeo kayaks are compact boats enabling easy deployment and repositioning of NDV units. The customary built floatable catamaran platform serves as the carrier for NDV operating/powering equipment, and supportive vessel for installations and hydrometrical works.

3.3 Measuring and Experimental Setups

The measurement and experimental setups were arranged according to two principal schemes: transversal setup for measurements in a river cross-section (Figure 3.3.1), and a longitudinal alignment in field experiments (Figure 3.3.2). In the transversal setup the measuring platform (2) was installed across the river between the monuments (5) of a cross-section (Figure 3.3.1).

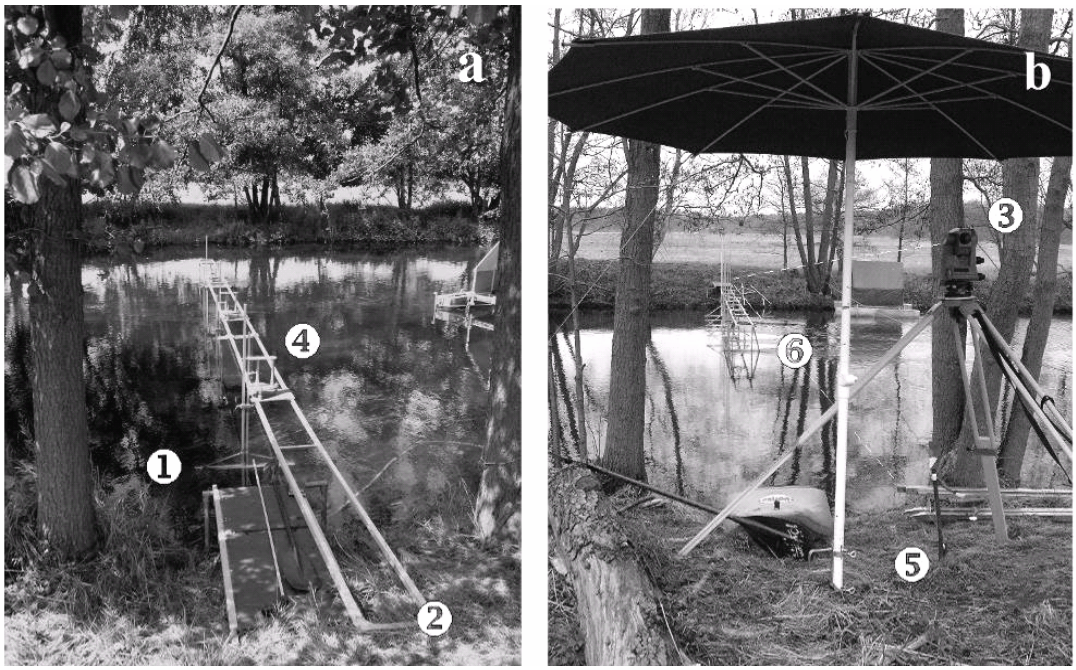

Figure 3.3.1 A scheme of measurement setup in a river cross-section

The total station (3) positioned at one of the monuments was used to orient NDV sensors (1) parallel to the vertical plane (6) of the cross-section. During the measurements NDV devices were moved across the stream by repositioning the mounting blocks (4). For field experiments on evolution of flow over vegetation patches and studies of coherent structures the platform (1) was positioned in the streamwise direction (Figure 3.3.2). The upstream end of the platform was fixed at a bar spanned across the river on the vertical poles and secured by chains (5) to the riverbed. In the experiments one NDV unit (2) was set upside down in stationary mode on the riverbed, and another one (3) was traversed along the platform. NDVs were operated from a floatable catamaran platform (4) equipped with a shelter. As the field measurements and experimental investigations were performed during relatively long period it was necessary to

adopt the specific conditions on the river – for example navigation of recreational boats. Thus measurements in the river cross-sections were performed in two sets spanning only a half a river at one time and leaving the path for the kayaks, canoes and motor boats. To prevent accidental collisions of the boats with the equipment during the night time the setup was illuminated with signaling lights.

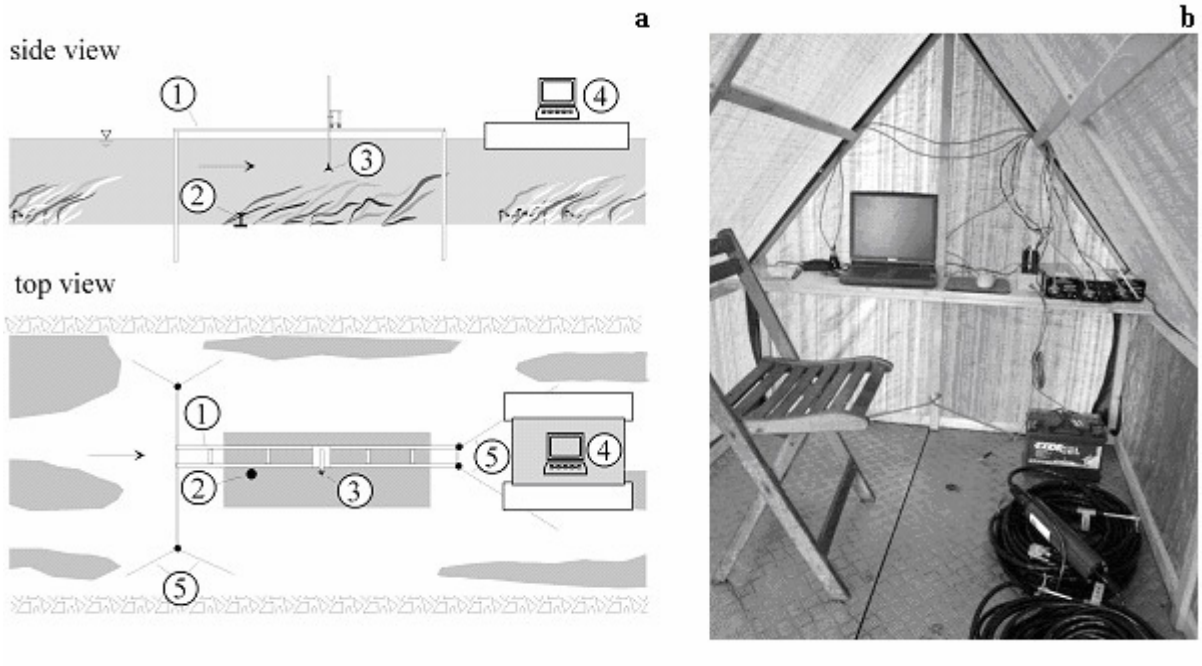

Figure 3.3.2 A scheme of the streamwise experimental setup (a), and the equipment of the measuring platform (b).

3.4 Data Collecting and Processing

NDV were operated by CollectV 3.3 software developed in Nortek AS. This software runs under Windows 98, NT, XP operating platforms and provides visual graphical environment for multi-channel operation of arrays of NDV. Additionally to velocity measurements, CollectV 3.3 allows using of NDVs as boundary sonar recorders – an advanced and very important feature for field investigations of relatively fast morphodynamic processes.

Time series of velocity measurements were processed with a versatile commercial software package ExploreV 1.5, Nortek AS, Norway. The software provides interactive graphical environment enabling fast and comprehensive data treatment. It allows editing, clipping, filtering of row data, as well as stationarity, spectral, cross-spectral and other advanced methods of analysis including the data processing on a spatial grid. With ExploreV measured time series were inspected visually to identify possible problems, such as spikes, trends or abrupt discontinuities in the time series. Frequency distributions of the velocity data were also examined to identify outliers. Examination of these distributions is especially valuable for determining errors associated with large spikes resulting from interruption of the acoustic signal by large pieces of debris moving through the sampling volume. Spikes always generated velocity values more than 3 standard deviations from the mean (3σ). These spikes were removed and replaced with values generated by linear interpolation between adjacent data using a 3σ filter in the time series option of ExploreV. In all cases this post-processing procedure did not greatly affect the values of means, producing changes of only few mm/s.

Customarily developed software (DOS operating platform) was used to register analogous output (volts) from BackScat fluorometer. Voltage time-series were converted to uranin concentration records by calibration relationships using Excel spreadsheets. The accuracy of

records and calibration was checked calculating balances of released and retrieved mass of the tracer.

Underwater video records were converted into a sequence of digital images in the format JPEG with the specialized software DVD Create. JPEG images were imported into GRAPHER 6 software and the boundaries between free flow and macrophytes were digitalized. The physical coordinates of the boundaries were computed using calibration screen marks and averaged over the sequence of the frames to obtain double time-spatial averages of variable flow boundaries.

Geodetic and bathymetric surveys were registered manually in the field and later converted into digital form. Interpolated results of those surveys were processed with specialized mapping and graphical software (Surfer 8.0 and Grapher 6.0) to obtain digital elevation models of the experimental river reaches.

The riverbed samples were processed automatically on a sieving apparatus with a sieve grade set of 0.063, 0.09, 0.125, 0.315, 0.45, 0.63, 1.0, 1.4, 2.8, 4.0, 6.3, and 19 mm. The separated fractions were weighted on analytical scales in laboratory and obtained granulometric distributions were analyzed with Grain Analyzer 1.0 software customarily developed in IGB.

3.5 Testing Bio-mechanical Properties of Plants

Flexural rigidity of the material is the measure of its ability to resist bending. There are many methods for measurements of the flexural rigidity and a plenty of commercially manufactured instruments implementing those methods. However, they all are based on the same principle of relating the measure of deformation (bending) of the material to a force caused the deformation. For a piece of material, which can bend under its own weight there were developed convenient methods allowing estimates of elastic properties performing very simple measurements without supplementary instrumentation. In our study we used two methods of that kind – the cantilever and the loop tests.

The cantilever method requires testing of deformations in a horizontal beam of a fabric piece bended by its own weight. A coordinate of a free end, and an angle between horizontal line and the straight line connecting the fixed and free ends of the cantilever ϕ are used to estimate bending rigidity (Figure 3.5.1).

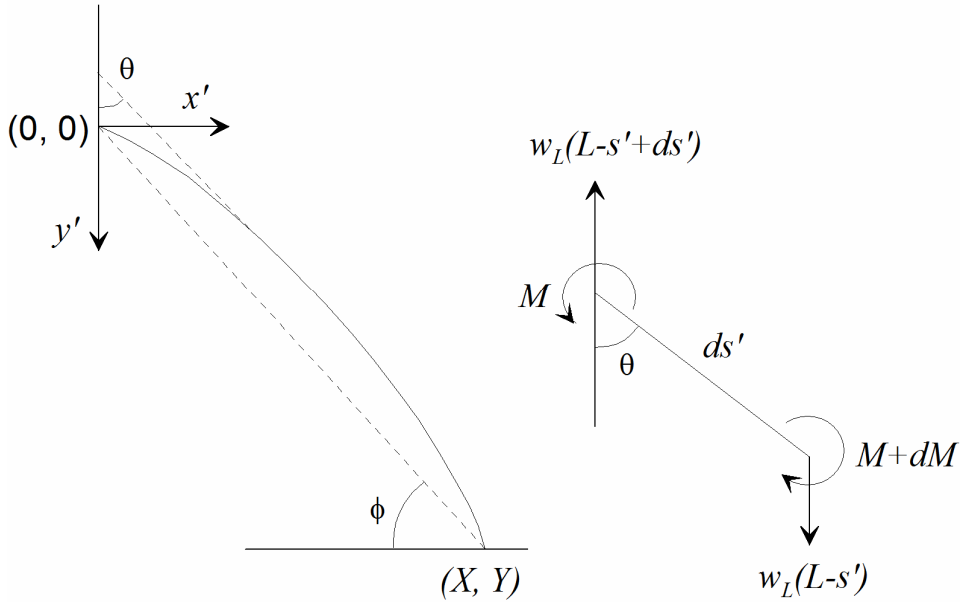

Figure 3.5.1 Forces related to the cantilever test (after Takatera and Shinohara, 1994)

For a horizontal cantilever of a length L, the weight per unit length w_L, flexural rigidity EI_a, and the moment of a small segment s' are related by the following partial differential equation

$$\frac{dM}{ds'} = -EI_a \frac{d^2\theta}{ds'^2} = w_L(L - s')\sin\theta \tag{3.5.1}$$

or in a normalized form

$$\frac{d^2\theta}{dq^2} = q\sin\theta; \quad s = \frac{s'}{L}; \quad q = K_b(1 - s) \tag{3.5.2}$$

here parameter K_b is a non- dimensional value defined by

$$K_b = \left(\frac{w_L}{EI_a}\right)^{1/3} L \tag{3.5.3}$$

Equation (3.5.2) was numerically integrated by Takatera and Shinohara (1994) using Runge-Kutta method and obtained solution for cantilever equilibrium was approximated by the polynomial functions to express relationship between ϕ and K_b

$$K_b = 3.4698\times10^{-5}\,\phi^3 - 0.0049422\,\phi^2 + 0.36316\,\phi - 2.8774 \tag{3.5.4}$$

We applied equation (3.5.4) to calculate parameter K_b from measured angle ϕ. Flexural rigidity was calculated then from equation (3.5.3) as

$$EI_a = w_L\left(\frac{L}{K_b}\right)^3 = w_L L_b^3 \tag{3.5.5}$$

where $L_b = L / K_b$ is bending length.

The loop method was proposed by Stuart (1966). A test implementing the method consists in laying down a loop of a stripe on a horizontal surface, Figure 3.5.2.

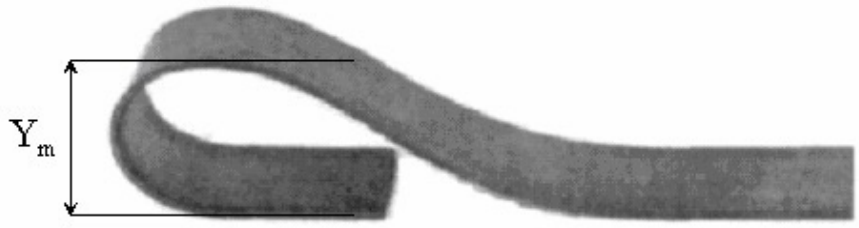

Figure 3.5.2 A loop of the stripe material (after Stuart 1966).

The curvature of the stripe at its ends is equal to zero and this condition allows integrating equations of equilibrium. In result of integration was established a proportionality factor of bending length L_b to the loop height Y_m as $L_b = 1.103\ Y_m$. Having bending length L_b defined as $L_b = (EI_a / w_L)^{1/3}$ provides the estimate of flexural rigidity EI_a according to

$$EI_a = w_L\,(1.103\ Y_m)^3 \tag{3.5.6}$$

For measurements of the flexural rigidity fresh plants were harvested and their shoots were clipped into three equal parts – lower (from roots), middle and upper (near ends), then tested for rigidity, and weighted on portable scales. The test consisted in successive positioning of samples, clipped parts of plants, into a cantilever beam (Figure 3.5.3) and a loop (Figure 3.5.4) and taking photographs. To assists accurate further digital processing of photographs a scaling screen was

placed in the background. After completion of the tests an additional photo of a sample was taken for determination of sample length and width. The photographs were digitalized with software tools and the bending parameters calculated.

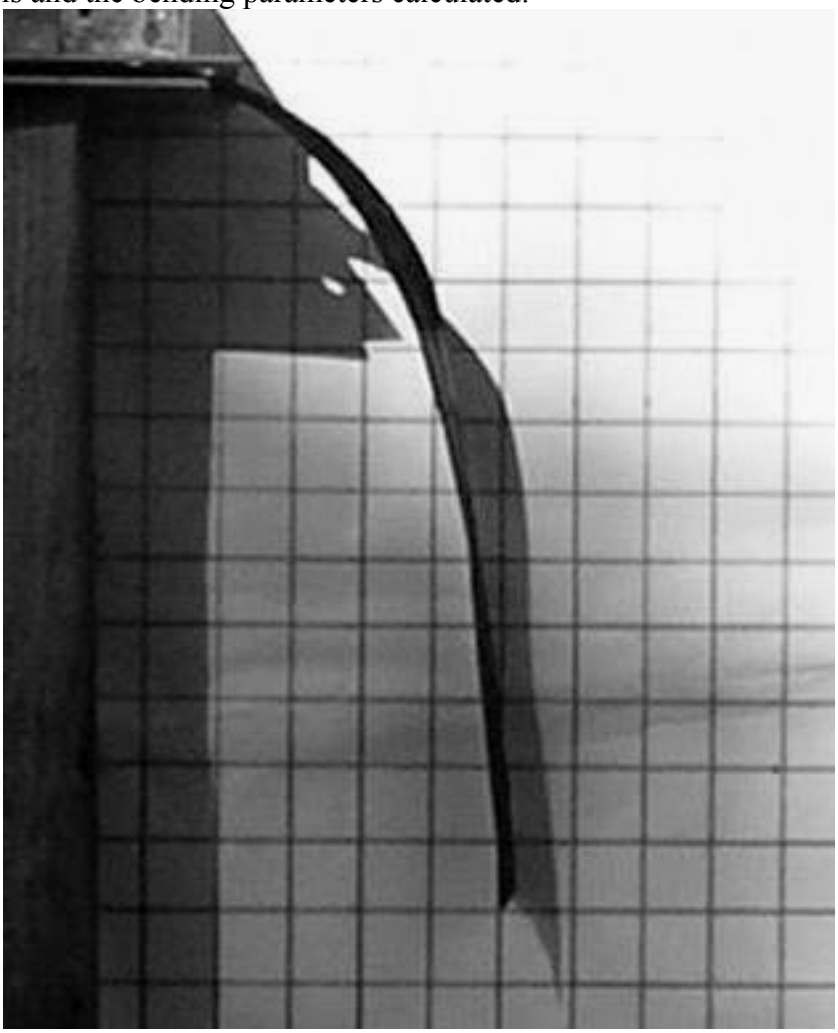

Figure 3.5.3 A band leaf of *Sagittaria sagittifolia* under the horizontal cantilever test.

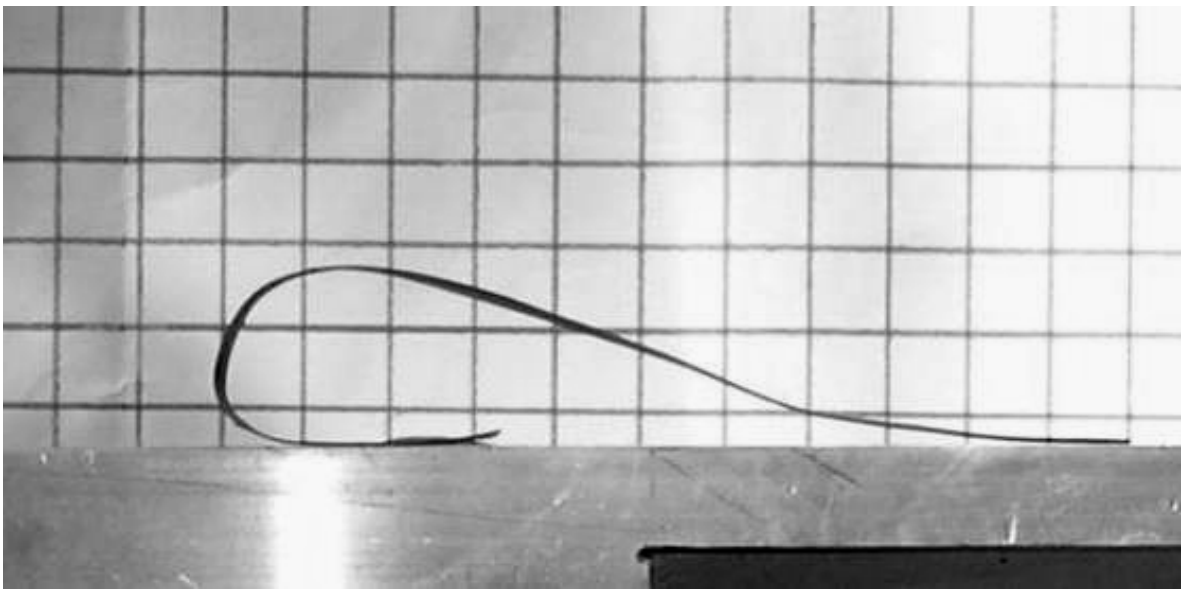

Figure 3.5.4 A band leaf of *Sagittaria sagittifolia* under the loop test

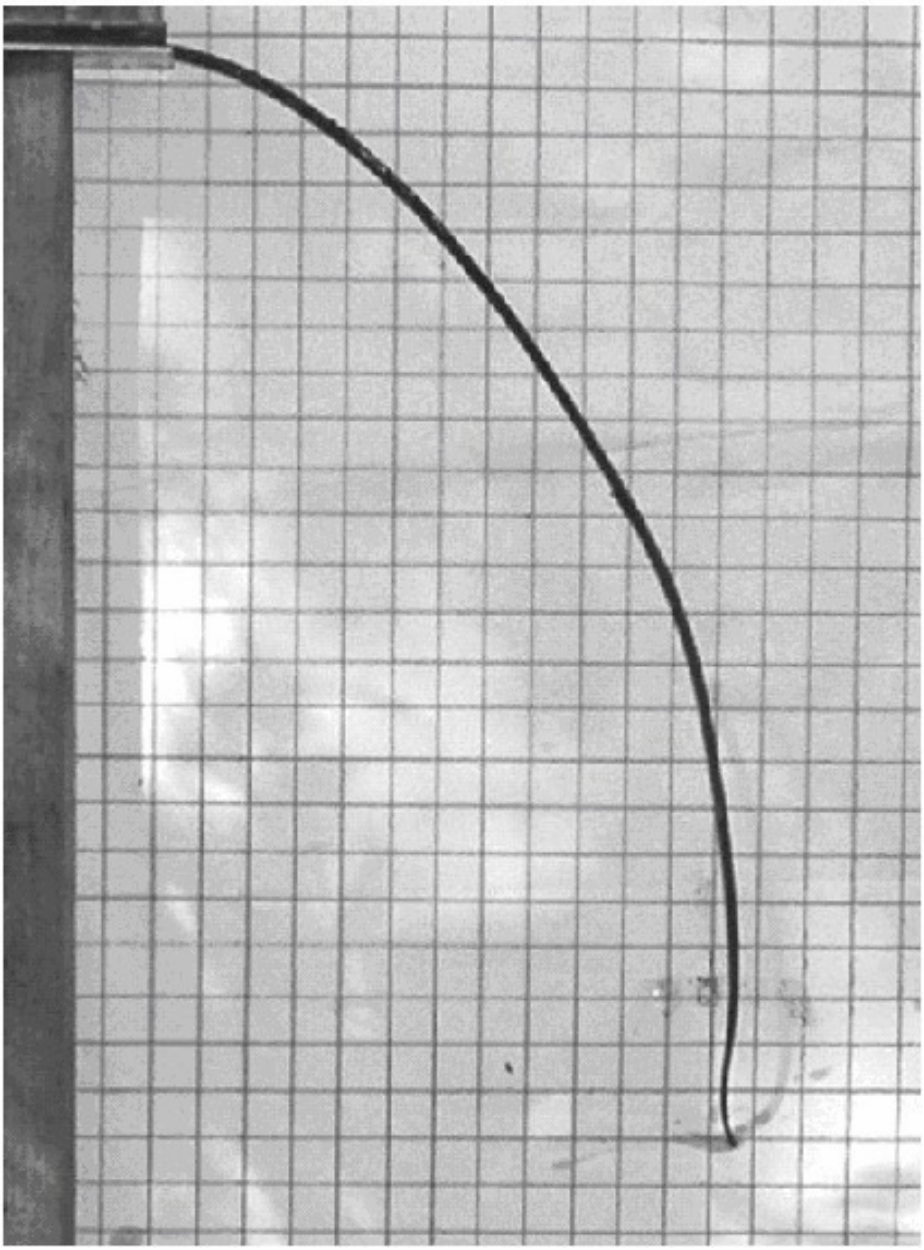

Figure 3.5.5 An air leaf of *Sagittaria sagittifolia* under the horizontal cantilever test.

Additionally to the tests performed on band leaves we also tested rigidity of air leaves of *Sagittaria sagittifolia* (Figure 3.5.5). These leaves with an arrowhead-shaped leaf blade above water surface appear in the maturation phase (Chapter 5, Subsection 5.1.1). Difference in the flexural rigidity of band and air leaves is caused by physiological reasons and can be explained by difference of leaves cross-sections. Band leaves are flat with elliptically shaped cross-section of about 1 mm in thickness, while cross-sections of air leaves are shaped to a circle about 5 mm in diameter. The second moment of elliptical area is $I_a = \pi d_p^{\,3} d / 64$ (Niklas 1992), and hence depends on the cube of thickness and the effect of shape (increased thickness) contributes to the resulting flexural rigidity characteristics. The thickness of the band and air leaves at their base is bigger then at the upper end – that determines decrease of the rigidity along the leaf. The results of completed bio-mechanical tests are summarized in Table 3.5.1.

The second important bio-mechanical property of plant tissue is its buoyancy, and the key parameter for determination of buoyancy is density of plant tissue. A simple displacement method of immersing the plants into a vessel with water and measuring displaced volume together with weight of the plant sample provides the value of density. For assessment of

density, fresh plants were harvested and their roots were clipped out. Then macrophytes samples were weighed at the portable scales (accuracy of 0.01g), and the volume of the shoots was measured by displacement method. Density of the plants was estimated as the ratio of the mass of each sample to its volume. The mean value of density determined for a total amount of 15 plants resulting 645±72 kg/ m^3 was used further for the calculation of the buoyancy of the plants with certain volume.

Table 3.5.1 Flexural rigidity of the band and air leaves of *Sagittaria sagittifolia*

N	Leaf	Leaf Part	X, cm	Y, Y_m, cm	ϕ, °	L, cm	W, N	w_L, N m^{-1}	L_b, cm	K_b	EI_a, $*10^5$ N m^2	EI_a mean, $*10^5$ N m^2
Cantilever test												
1	band	lower	27.0	26.7	45	38.4	0.029	0.075	5.8	6.57	1.51	2.53
2			19.8	55.0	70	61.0	0.048	0.079	5.9	10.3	1.66	
3			12.5	56.5	78	58.0	0.088	0.152	4.9	11.7	1.84	
4			21.3	32.5	57	39.0	0.030	0.077	4.8	8.17	0.84	
5			30.7	21.8	35	39.0	0.079	0.202	7.3	5.31	7.99	
6			22.7	29.8	53	37.9	0.041	0.109	5.0	7.61	1.34	
7		middle	18.1	33.0	61	38.5	0.030	0.078	4.4	8.79	0.66	0.95
8			20.4	20.4	45	31.0	0.037	0.120	4.7	6.62	1.23	
9		upper	6.2	43.6	82	46.0	0.035	0.076	3.6	12.8	0.35	0.25
10			9.7	34.4	74	36.5	0.039	0.106	3.3	11.1	0.38	
11			4.0	35.2	83	37.0	0.028	0.075	2.8	13.2	0.17	
12			7.7	23.1	72	25.0	0.024	0.097	2.4	10.5	0.13	
13			8.7	25.5	71	30.0	0.028	0.092	2.9	10.4	0.22	
Loop test												
1	band	lower		5.6		38.5	0.025	0.065	6.2	6.2	1.55	2.78
2				7.3		41.0	0.031	0.076	8.1	5.1	4.01	
3		middle		3.2		34.0	0.024	0.070	3.5	9.8	0.29	1.68
4				4.7		35.0	0.017	0.048	5.2	6.7	0.67	
5				4.0		30.0	0.015	0.049	4.4	6.8	0.42	
6				8.7		33.2	0.020	0.060	9.6	3.5	5.35	
7		upper		3.2		21.6	0.010	0.047	3.5	6.2	0.20	0.43
8				2.8		10.5	0.009	0.084	3.0	3.4	0.24	
9				4.6		42.4	0.018	0.043	5.1	8.3	0.57	
10				4.4		29.3	0.019	0.065	4.8	6.1	0.73	
Cantilever test												
1	air	lower	34.7	10.4	17	37.0	0.070	0.188	18.9	1.95	128	128
2		middle	41.9	15.9	21	54.0	0.071	0.132	19.1	2.84	91.3	91.3
3		upper	29.9	36.0	50	52.2	0.058	0.110	7.15	7.30	4.03	4.03

4 DYNAMICS OF FLOW WITH SUBMERGED VEGETATION

Developments of the theory for the shear layers evolving over submerged vegetation and the results of the field experiments testing particular implications of this theory are presented in this chapter (Section 4.1). Direct comparison of turbulent flow structure measured in a river cross-section with and without submerged vegetation completes the analysis and provides possibility of testing for both developed theory and obtained empirical knowledge (Section 4.2).

4.1 Effect of Vegetation Density: theory and field experiments

An original advancement of the shear layers dynamics theory is presented in the Subsection 4.1.1. The theory is developed by analytical examination of the flow evolution over a patch of submerged vegetation. Additionally in the Subsection 4.1.2 the scaling properties for mean and turbulence characteristics distributions in the vertical plane are examined. A simple phenomenological model for the coherent structures populating the shear layer over a patch of submerged vegetated is introduced in the Subsection 4.1.3. To test developed theory a series of field experiments was performed in a natural lowland river. The program of experimental studies is described in the Subsection 4.1.4, and the results of field experiments, their analysis and comparison with theory are presented in the Subsection 4.1.5.

4.1.1 Theoretical analysis of vegetated shear layers

Terrestrial vegetation often covers considerable areas over the terrains, and nearly uniform conditions can be attained at some distances from the canopy origin (relatively small as compared to the whole length of the canopy) (Raupach et al. 1996). In contrast, vegetation patches in natural streams over which spatially uniform conditions can develop often are relatively small and the flow continuously evolves from patch to patch. For this reason the knowledge of spatial dynamics of mixing layers is particularly valuable and will be examined here with the analysis of governing equations.

Consider incompressible, stationary, and fully developed open-channel flow approaching a patch of macrophytes located in the central part of the river. The flow is assumed to be uniform in transversal direction, and respectively the analysis focuses on 2D schematization.

The flow domain in the streamwise direction can be subdivided into 3 distinctive zones: the zone of the approaching fully developed open-channel flow (1), the zone of the evolving flow over the canopy (2), and the zone of fully developed flow over the canopy (3), Figure 4.1.1. Although in Figure 4.1.1 the longitudinal inclination of the river channel is not shown, the analysis implies the scheme of the channel described in the subsection 2.1.2 and depicted in Figure 2.1.2. Considering analysis of 2-D boundary flow presented in subsection 2.1.2, the boundary layer momentum equations for these parts of the flow can be written as:

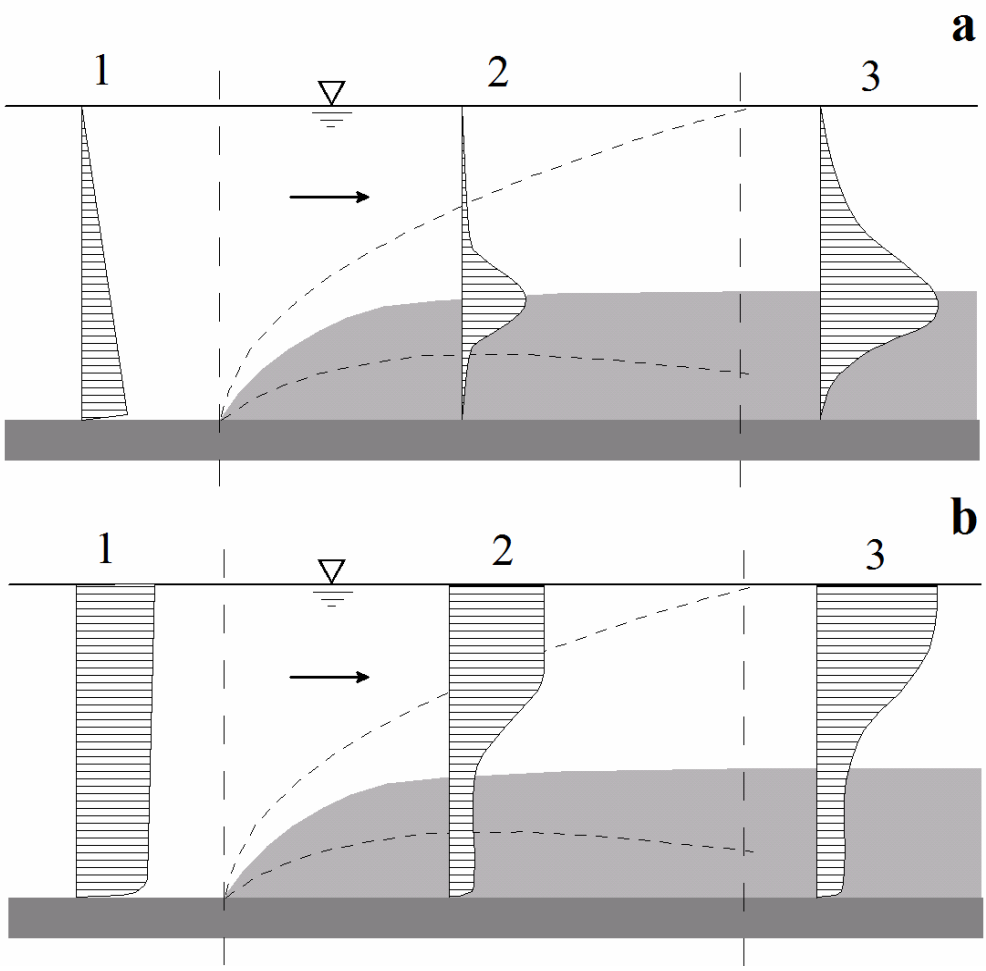

Figure 4.1.1 Schematic representation of Reynolds stresses (a), and the mean flow velocities (b) fields in flow with submerged vegetation.

$$0 = g\,i_0 - \frac{\partial \overline{u'w'}}{\partial z} \tag{4.1.1}$$

approaching fully developed flow (zone 1)

$$\bar{u}\frac{\partial \bar{u}}{\partial x} + \bar{w}\frac{\partial \bar{u}}{\partial z} = g\,i_0 - \frac{1}{\rho}\frac{\partial \bar{p}}{\partial x} - \frac{\partial \overline{u'w'}}{\partial z} \tag{4.1.2}$$

evolving vegetated flow (zone 2)

$$0 = g\,i_0 - \frac{1}{\rho}\frac{\partial \bar{p}}{\partial x} - \frac{\partial \overline{u'w'}}{\partial z} \tag{4.1.3}$$

fully developed vegetated flow (zone 3)

$$\frac{\partial \bar{u}}{\partial x} + \frac{\partial \bar{w}}{\partial z} = 0 \tag{4.1.4}$$

continuity equation

Expressing spatial pressure gradient due to vegetation drag force with conventional vegetation drag relation

$$\frac{\partial \bar{p}}{\partial x} = \rho C_D\, a\, \frac{\bar{u}^2}{2} \tag{4.1.5}$$

equations (4.1.1) and (4.1.3) can be rewritten as

$$\frac{\partial \tau_{xz}}{\partial z} = \rho g i_0 \tag{4.1.6}$$

$$\frac{\partial \tau_{xz}}{\partial z} - \rho \bar{u} \frac{\partial \bar{u}}{\partial x} = -\rho g i_0 + \rho C_D a \frac{\bar{u}^2}{2} \tag{4.1.7}$$

$$\frac{\partial \tau_{xz}}{\partial z} = -\rho g i_0 + \rho C_D a \frac{\bar{u}^2}{2} \tag{4.1.8}$$

In vertical plane the flow is subdivided into the zone of vegetation and the zone of free flow (Figure 4.1.1), while the analogous mixing, or simply shear layer occupies partly both zones of the flow.

Now let's examine the zone just above the river bed which is demarcated by the lower boundary of the shear layer $0 < z < z_1$ at distances were flow is already developed $x > x_d$ (where z_1 is elevation of the shear layer lower boundary, and x_d is distance from the patch origin over which the flow develops). Equation (4.1.8) in this zone can be further simplified because Reynolds stresses are zero there

$$0 = \rho g i_0 - \rho C_D a \frac{\bar{u}^2}{2} \tag{4.1.9}$$

Integrating (4.1.9) over the depth $0 < z < z_1$ yields

$$g i_0 = (C_D a)_1 \frac{\bar{u}_{1d}^2}{2}, \quad \bar{u}_{1d} = \sqrt{\frac{2 g i_0}{(C_D a)_1}} \tag{4.1.10}$$

where $(C_D a)_1$ is parameter averaged over the depth of the zone $0 < z < z_1$, and $\bar{u}_{1d}$ is mean velocity in this layer which is the slow stream velocity of the shear layer, index *d* stands there to indicate developed flow.

In the zone of evolving flow $0 < x < x_d$ integration of (4.1.7) over the layer $0 < z < z_1$ provides the following equation

$$\frac{1}{2} \frac{d \bar{u}_{1e}^2}{d x} = g \left(\frac{d z_1}{d x} + i_0 \right) - (C_D a)_1 \frac{\bar{u}_{1e}^2}{2} \tag{4.1.11}$$

that can be solved assuming $\frac{dz_1}{dx} = 0$ as

$$\bar{u}_{1e}^2 = \bar{u}_{1d}^2 + \left(\bar{u}_{0_1}^2 - \bar{u}_{1d}^2 \right) \exp\left[-(C_D a)_1 x \right] \tag{4.1.12}$$

where $\bar{u}_{1e}^2$ is mean velocity in the zone of evolving flow. The value $\bar{u}_{1d}$ defined in accordance with (4.1.10) was used as the right hand boundary value, and $\bar{u}_{0_1} \approx 0.9 \bar{u}_0$ - the mean velocity of the incoming flow was taken as the left hand boundary value.

Equation (4.1.12) can be used for the estimation of the distance x_d over which flow evolves. Determining it as the distance at which velocity $\bar{u}_{1e}(x_d) = 1.05 \bar{u}_{1d}$

$$(1.05 \bar{u}_{1d})^2 = \bar{u}_{1d}^2 + \left(\bar{u}_{0_1}^2 - \bar{u}_{1d}^2 \right) \exp\left[-(C_D a)_1 x_d \right] \tag{4.1.13}$$

x_d can be respectively assessed as

$$x_d = \frac{1}{(C_D a)_1} \ln\left(\frac{\bar{u}_{0_1}^2 - \bar{u}_{1d}^2}{0.1\bar{u}_{1d}^2} \right) \tag{4.1.14}$$

The next step in the theoretical analysis will be the examination of the flow in the near surface area $z_2 < z < h$, where z_2 is upper boundary of the shear layer. In the zone of evolving flow $0 < x < x_d$ integration of equation (4.1.7) over layer thickness $z_2 < z < h$ (neglecting $\frac{dz_2}{dx}$) yields

$$\frac{1}{2}\frac{d\bar{u}_{2e}^2}{dx} = gi_0 - \frac{\partial \tau_{xz}}{\partial z} \tag{4.1.15}$$

Taking in account that in the zone of evolution turbulence is starting to develop on account of internal shear due to mixing layer and hence $\frac{\partial \tau_{xz}}{\partial z} \approx 0$, equation (4.1.15) can be rewritten as

$$\frac{1}{2}\frac{d\bar{u}_{2e}^2}{dx} = gi_0 \tag{4.1.16}$$

and integration of (4.1.16) provide a solution with a boundary condition of incoming flow $\bar{u}_{02}$

$$\bar{u}_{2e}^2 = \bar{u}_{02}^2 + 2gi_0 x \tag{4.1.17}$$

In the zone of developed flow $x > x_d$ near the free surface $z_2 < z < h$, the longitudinal gradient of mean velocity vanishes and equation (4.1.15) takes the form

$$\frac{\partial \tau_{xz}}{\partial z} = gi_0 \tag{4.1.18}$$

and velocity can be deduced from equation (4.1.17) as

$$\bar{u}_{2d}^2 = \bar{u}_{0_2}^2 + 2gi_0 x_d \tag{4.1.19}$$

Inside the shear layer $z_1 < z < z_2$ in the zone of evolving flow $0 < x < x_d$, from equations describing evolution of flow velocities in the near bed region (4.1.12) and near the free surface (4.1.17), one can readily assess the mean velocity in the shear layer, the velocity difference, and their ratio λ

$$u_{ce} = \frac{1}{2}\left(\sqrt{\bar{u}_{0_2}^2 + 2g i_0 x} + \sqrt{\frac{2g i_o}{(C_D a)_1} + \left(\bar{u}_{0_1}^2 - \frac{2g i_o}{(C_D a)_1} \right) \exp\left[-(C_D a)_1 x \right]} \right) \tag{4.1.20}$$

$$\Delta u_e = \sqrt{\bar{u}_{0_2}^2 + 2g i_0 x} - \sqrt{\frac{2g i_o}{(C_D a)_1} + \left(\bar{u}_{0_1}^2 - \frac{2g i_o}{(C_D a)_1} \right) \exp\left[-(C_D a)_1 x \right]} \tag{4.1.21}$$

$$\lambda_e = \frac{\Delta u_e}{2u_{ce}} = \frac{\sqrt{\bar{u}_{0_2}^2 + 2g i_0 x} - \sqrt{\frac{2g i_o}{(C_D a)_1} + \left(\bar{u}_{0_1}^2 - \frac{2g i_o}{(C_D a)_1} \right) \exp\left[-(C_D a)_1 x \right]}}{\sqrt{\bar{u}_{0_2}^2 + 2gi_0 x} + \sqrt{\frac{2gi_o}{(C_D a)_1} + \left(\bar{u}_{0_1}^2 - \frac{2gi_o}{(C_D a)_1} \right) \exp\left[-(C_D a)_1 x \right]}} \tag{4.1.22}$$

In the zone of developed flow $x > x_d$ equations describing mean velocity in the shear layer, velocity difference, and parameter λ can be correspondently written as

$$u_{cd} = \frac{1}{2}\left(\bar{u}_{2d} + \bar{u}_{1d}\right) = \frac{1}{2}\left(\sqrt{\bar{u}_{0_2}^{\,2} + 2g\,i_0\,x_d} + \sqrt{\frac{2g\,i_o}{\left(C_D\,a\right)_1}}\right) \tag{4.1.23}$$

$$\Delta u_d = \bar{u}_{2d} - \bar{u}_{1d} = \sqrt{\bar{u}_{0_2}^{\,2} + 2g\,i_0\,x_d} - \sqrt{\frac{2g\,i_o}{\left(C_D\,a\right)_1}} \tag{4.1.24}$$

$$\lambda_d = \frac{\Delta u_d}{2u_{cd}} = \frac{\sqrt{\bar{u}_{0_2}^{\,2} + 2g\,i_0\,x_d} - \sqrt{\frac{2g\,i_o}{\left(C_D\,a\right)_1}}}{\sqrt{\bar{u}_{0_2}^{\,2} + 2g\,i_0\,x_d} + \sqrt{\frac{2g\,i_o}{\left(C_D\,a\right)_1}}} \tag{4.1.25}$$

The resulting velocity in the vegetated layer depends on the slope of the water surface reflecting the driving force of gravitation and on the bulk characteristics of the vegetation patch: projected area of plants per unit volume and the bulk drag coefficient. The bulk drag coefficient depends on the one hand on the velocity (through the Reynolds number defined at characteristic length of vegetation), and on another hand on the population density of vegetation because of sheltering effect. Effect of population density of vegetation is pronounced in the deceleration of the flow in the near bed part where flow penetrates through the vegetation. Therefore the larger vegetative density is - the smaller is velocity u_1 inside the patch, and the larger value attains the parameter λ which approaches the value of 1 at highest possible limit.

Having all necessary velocity scales and ratios deduced we are now in the position to analyze the evolution of the shear layer in the flow with submerged vegetation. At first approximate we assume that evolution of the shear layers in flow with vegetation can be characterized by the dependence of the spreading coefficient on the stability parameter by analogy with the shallow mixing layer. However, we will use the stability parameter Ω (2.1.59) proposed by Ghisalberti and Nepf (2002) because it was deduced from physical reasons and it accounts explicitly for characteristics of vegetation. The spreading coefficient than can be represented as

$$\begin{aligned} &\alpha_C = \alpha_{C0}\left(1 - \frac{\Omega}{\Omega_{crit}}\right) \quad &for\ \Omega < \Omega_{crit} \\ &\alpha_C = 0 \quad &for\ \Omega > \Omega_{crit} \end{aligned} \tag{4.1.26}$$

The main differences between canonical mixing layer and mixing layer analog over submerged vegetation canopy can be summarized as follows:

- two flows are evolving from the approaching fully developed open-channel flow: the fast stream in the area above the canopy and slow stream inside the canopy;
- the flows are initially non-parallel and the mean flux directed from the slow toward the fast stream;
- velocity difference and mean convective velocity of the analogous mixing layer are evolving along the vegetation canopy. Velocity difference is expected to grow with the distance while mean convective velocity is decaying, and depends on vegetation density;
- yet in the zone 3 where the flow reaches the developed stage, the main features characteristic for the mixing layers depend on the canopy properties cumulatively reflected in the drag coefficient. Particularly important is the population density which controls reconfiguration of macrophytes and forms the frontal area of the vegetation cover.

4.1.2 Scaling mean flow and turbulence characteristics

Property of self similarity of the mixing layers is a fundamental feature that serves as an efficient tool for analysis and interpretation of experimental and field measurements. The self-similarity of mean velocity profiles is expressed by equations (2.1.47 and 2.1.48). For turbulent flows the property of self-similarity implies also the similarity in turbulence characteristics. Here we derive similarity solutions for most important turbulence characteristics – turbulent stresses and dissipation rates.

To obtain the similarity solution for turbulent stresses we apply turbulent viscosity concept

$$\frac{\tau}{\rho} = -\overline{u'w'} = \nu_T \frac{d\bar{u}}{dz} \tag{4.1.27}$$

and velocity gradient from equation (2.1.51)

$$\frac{d\bar{u}}{dz} = \frac{\Delta u}{\delta} \frac{1}{\cosh^2 \eta}, \ \eta = \frac{2z}{\delta} \tag{4.1.28}$$

The scaled profile of turbulent stresses then will be written as

$$-\frac{\overline{u'w'}}{\Delta u^2} = \frac{\nu_T}{\delta \Delta u} \frac{1}{\cosh^2 \eta} \tag{4.1.29}$$

The self-similar profiles for dissipation rates of turbulent kinetic energy ε can be obtained using the hypothesis of local equilibrium of turbulence

$$\prod = -\overline{u'w'} \frac{d\bar{u}}{dz} = \varepsilon \tag{4.1.30}$$

where $\prod$ is turbulence production. As it was shown by numerical modeling of mixing layers (Pope 2000) the hypothesis of local equilibrium holds for such types of flows. Using equations (4.1.27-4.1.30) yields turbulence production

$$\prod = \nu_T \left(\frac{\Delta u}{\delta} \right)^2 \frac{1}{\cosh^4 \eta} \tag{4.1.31}$$

and the scaled profile of dissipation rates is then written as

$$\frac{\varepsilon \delta}{\Delta u^3} = \frac{\nu_T}{\delta \Delta u} \frac{1}{\cosh^4 \eta} \tag{4.1.32}$$

As it was shown for canonical mixing layers, an assumption that turbulent viscosity is constant agrees with the experimental observations. Therefore comparison of scaled profiles for turbulent stresses and dissipation rates will provide independent estimates of turbulence viscosity. On the other hand the obtained scaled values of turbulence viscosity can be compared to the values reported for canonical mixing layers (Pope 2000).

4.1.3 Coherent structures and their modeling

As it was anticipated earlier, dynamics of flow developing over submerged vegetation canopies dependents on the drug force imposed by vegetation and hence is related to the population density of the canopy. This dependency has to be reflected in the relation for the Strouhal number which for canonical mixing layers is represented by universal constant 0.032 in equation (2.1.52). Thus, the relation expresses (in the integral form) the structural properties of large-scale turbulence, or the relationship between large-scale vortices and space-time averaged characteristics of the flow described by the mixing layer model.

Instabilities and vortices evolving in the canonical mixing layers were shown to develop through the complex interactions periodically appearing along the mixing layers (Roshko 1992; Rogers and Moser 1992). A conceptual scheme of the principal interaction mechanism called *vortex pairing* is illustrated in Figure 4.1.2. Initial small wave-like Kelvin-Helmholtz instabilities evolve into spanwise vortex structures (rollers). Rollers appear to be conjugated by streamwise vortices contained in the braid regions between rollers, Figure 4.1.2.

The growth of the mixing layers is primarily associated with the repeated amalgamations of coherent structures into the large ones (Winant and Browand 1974). Intensive studies of coherent structures in the mixing layers completed during the last two decades indicate that nonlinear interactions of coherent structures as well as structural properties of flow upstream and conditions at junction are primarily responsible for properties of the mixing layers. However, this dependency on the initial conditions quickly disappears and self-similar development of the layers is observed after a region of secondary pairing.

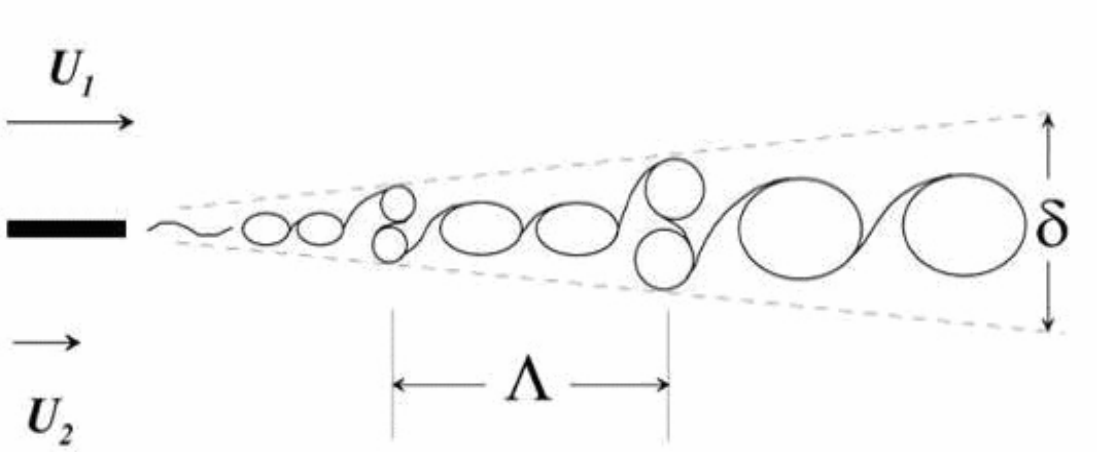

Figure 4.1.2 Conceptual model of the mixing layer structure and interactions between vortices.

In vegetated flows the coherent structures developing over submerged canopies experience additional interactions with vegetation represented in the model by the additional drag term (4.1.5). Though some laboratory studies indicate applicability of the Strouhal model with universal constant 0.032 (Ghisalberti and Nepf 2002), a more complex relation between vegetation drag, mean flow and turbulent structures can be intuitively perceived. Here we develop a simple analytical model indicating such relationship.

The analyses we want to perform necessitate the usage of an analytical relationship between characteristic spatial scale of turbulent structures and their characteristic temporal scale. For vertical structure characteristic temporal scale is evidently a time of the vortex revolution t_e which could be related to the radius of the vortex r via well known Richardson-Obukhov (Monin and Yaglom 1974) scaling law

$$t_e \approx \left(\frac{r^2}{\varepsilon} \right)^{1/3} \tag{4.1.33}$$

Assuming that in the mixing layers turbulence generation Π is in equilibrium dissipation rate

$$\varepsilon = \Pi = \frac{\tau}{\rho} \frac{\partial \bar{u}}{\partial z} = \frac{\tau}{\rho} \frac{\Delta u}{\delta} \tag{4.1.34}$$

relating the turbulent stress τ to the mean velocity in the mixing layer

$$\tau = 0.5 \rho c_f u_c^2 \tag{4.1.35}$$

and $r \approx \delta$, one obtains

$$t_e = \left(\frac{2\delta^3}{c_f u_c^2 \Delta u} \right)^{1/3} = \delta \left(\frac{2}{c_f u_c^2 \Delta u} \right)^{1/3} \tag{4.1.36}$$

where c_f is friction factor integrating skin and form drag of the vegetation layer. Obviously, the friction factor is related to the drag coefficient and if additional factors (bed friction, skin drag) are negligible, it is simply related to the drag coefficient as $c_f = C_D a h_v \varsigma$, where ς is squared ratio of velocity scales(2.4.10). Finally, applying Taylor's frozen turbulence hypothesis ($r \approx \delta \approx u_c t_e$) yields

$$f = \frac{u_c}{\delta} \left(\frac{2}{c_f} \frac{u_c}{\Delta u} \right)^{-1/3}, \; f = \frac{1}{t_e} \tag{4.1.37}$$

and it is readily seen that the structure of equation (4.1.37) resembles (2.1.52) as it includes the Strouhal number, though it shows that the universal constant of canonical mixing layers should be replaced by the function of the velocity scales ratio and the friction factor.

To summarize the subsections 4.1.1-4.1.3 it should be concluded that in these subsections an analytical framework was derived from the mixing layer theory and expanded with the analytical scaling relationships allowing for the analysis of turbulence statistics and structural properties measured in the field studies. This analytical framework is representing convenient basis for generalization of field measurements and observations and could be used for development of prognostic models.

4.1.4 Program of field experiments

The purpose of the field experimental studies was to obtain the detailed spatial patterns of mean and turbulent flow characteristics over a patch of submerged flexible aquatic plants in a natural stream. A monospecific patch composed of selected uprooted plants was purposely formed at the beginning of the study. Varying the population density of the patch through pruning between measurement runs made the experimental design of this field study complete and resembling detailed laboratory methods.

The plants of *Sagittaria sagittifolia* with filamentous blades (on average 12 blades, each blade about 1.6 m long, 1.5 cm wide, 5.3 grams dry weight per plant) were manually collected and replanted to form a rectangular patch (4×8 m) in the central part of the experimental river reach (Figure 4.1.3).

To prevent wash out of the plants from loose sediments each plant was moored by an aluminum rod (∅ 1cm, 20 cm long) attached to the plant near the root by a wire. Implanting procedure was guided by aluminum profiles marked on 20 cm intervals. The plants were uniformly distributed on a staggered pattern (Figure 4.1.4). A week later after planting, a control survey has indicated that the plants had perfectly adopted to their new grounds and even shot the fresh rhizomes. In total three runs of measurements were completed with different population densities (25, 7, and 2 plants per square meter) and an additional run over unvegetated riverbed. The population density of the patch was reduced between experimental runs through pruning. Figure 4.1.5 and Figure 4.1.6 illustrate the characteristic views of the experimental patch in the beginning and at the end of the experiments. All runs were identical in methodology and amount of measurements. An experimental run consisted of velocity measurements and underwater surveys of vegetation patch characteristics. Measurements of instantaneous velocity vectors were taken at a stationary point and ten verticals positioned along the longitudinal axis of the patch (Figure 4.1.7).

Figure 4.1.3 Implanting the vegetation patch by a diver.

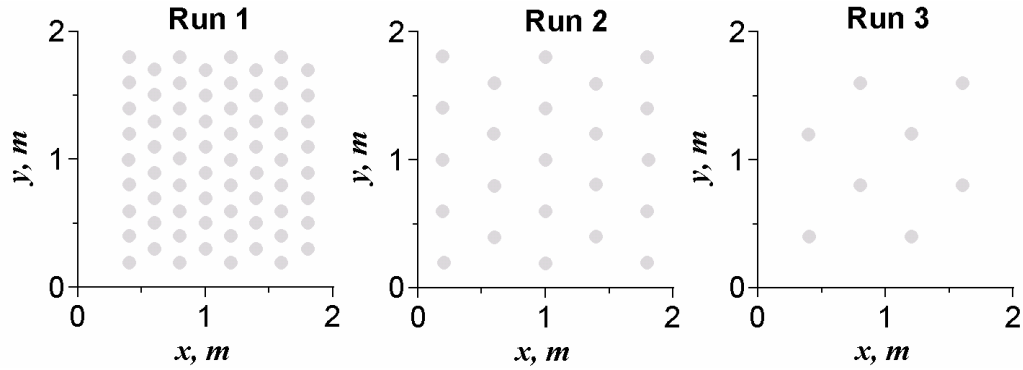

Figure 4.1.4 Patterns of plants spatial distributions in the field experiments.

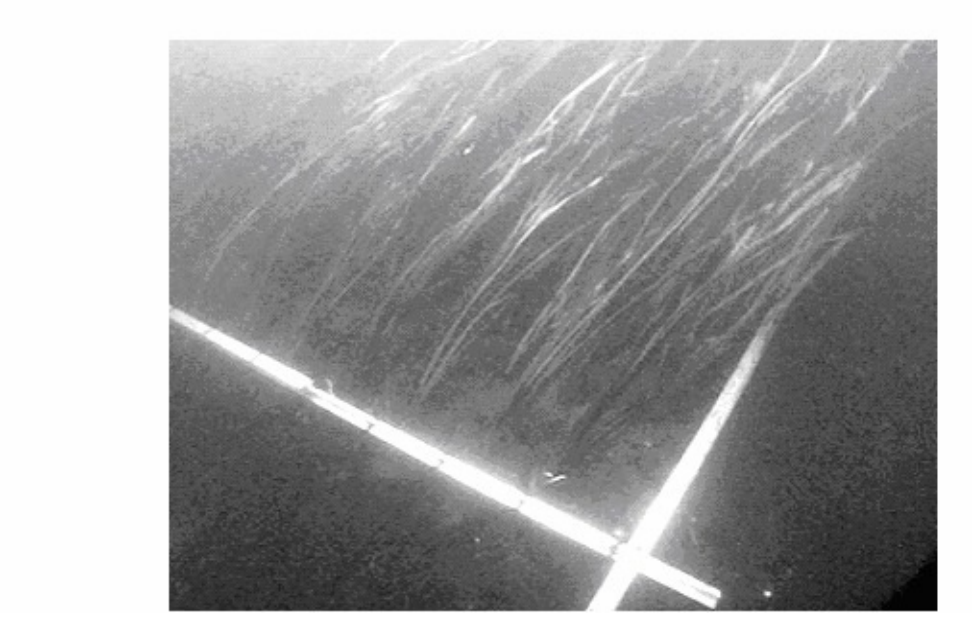

Figure 4.1.5 Experimental vegetation patch with maximal density of vegetation (Run 1).

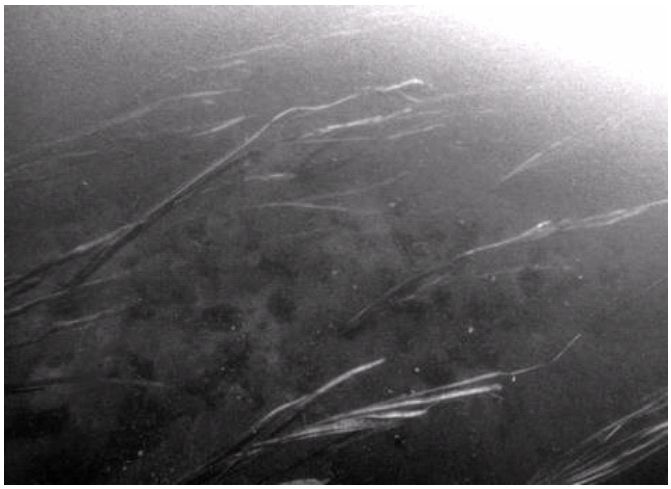

Figure 4.1.6 Experimental vegetation patch with minimal density of vegetation (Run 3).

Figure 4.1.7 Experimental setup and the floatable platform during experimental measurements.

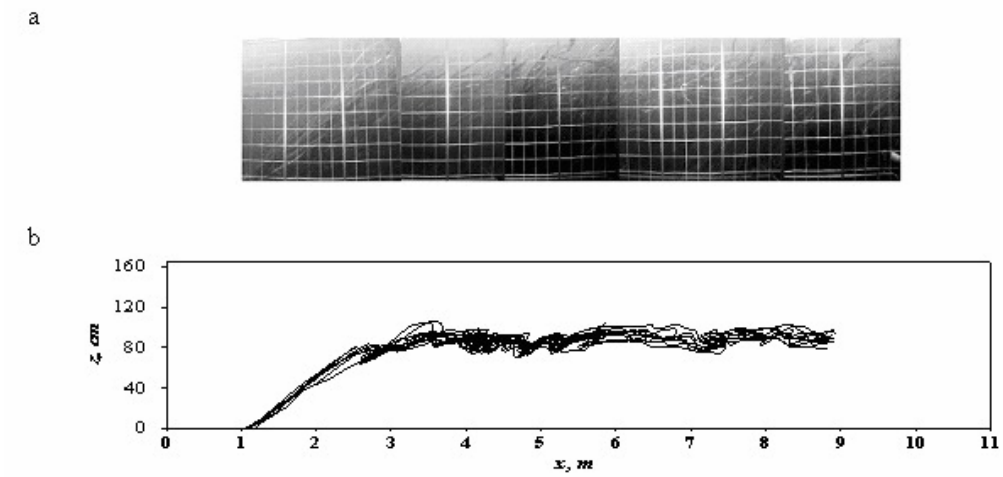

Figure 4.1.8 Examples of underwater video frames (a), and digitized averaged over 30 second time intervals boundaries of the vegetation canopy (b), experimental Run 1

Each vertical profile consisted of 7 points uniformly distributed over the depth. Velocities were recorded at 25Hz sampling rate in 300 s sampling periods for each point. Measurements were performed using three synchronized velocimeter units one of which was moored at the stationary point on the riverbed at the upstream edge of the patch and two others were traversed along the center line of the patch to take velocity measurements at the verticals. Vertical profiles were placed densely near the stationary point and were more sparse in downstream part of the patch were flow was changing less intensely. After completing velocity measurements the patch was surveyed by taking scaled underwater video records. Five frames (2×1.5 m) were recorded in digital format during 30 s at shutter speed of 25 Hz (Figure 4.1.8a). In the last frame, at the downstream part of the patch, video recording was synchronized with velocity sampling at 25 Hz by a NDV velocimeter positioned near the middle part of the frame. The sampling volume of the velocimeter was located at the upper boundary of the vegetation. Recordings were performed during 300 s.

Water levels and respectively the slope of free surface were monitored every hour during the period of velocity measurements. Fluctuations of water level were within 3-5 mm – a negligibly small value as compared to the mean depth of the flow.

After completing measurements and surveys for the run, the population density of the patch was reduced through pruning of every second row in the transverse and streamwise directions. Removed plants were collected, dried and weighted to determine a biomass density of the vegetation patch.

Video records were converted into a sequence of digital images in the format JPEG with the specialized software DVD Create. JPEG images were imported into GRAPHER 6 software and the boundaries between free flow and macrophytes were digitalized. The physical coordinates of the boundaries were computed using calibration screen marks (Figure 4.1.8b) and averaged over the sequence of the frames to obtain double time-spatial averages of variable boundaries of the vegetation in the patch.

Table 4.1.1 Bulk characteristic of the flow during field experiments.

Run	Q, m^3/s	U, m/s	H, m	h, m	I $\times 10^5$	ρ_p, kg/m^3	Fr	Re $\times 10^{-5}$	Symbol
1	5.08	0.18	1.23	1.65	8.98	0.132	0.06	2.18	●
2	5.10	0.18	1.24	1.65	9.13	0.048	0.06	2.19	○
3	5.24	0.18	1.27	1.68	9.15	0.014	0.06	2.29	✕
4	5.09	0.18	1.24	1.64	9.57	0.000	0.06	2.19	□

where Q is water discharge, and ρ_p is density of vegetative cover (dry weight of plans per volume of the canopy).

Table 4.1.2 Bulk characteristics of vegetation canopy in the experiments.

Run	N, per m^2	B, kg/m^2	h_v, m	$90-\alpha$, grad.
1	25	0.117	0.89	33
2	7	0.032	0.66	24
3	2	0.008	0.61	22

where N is number of plants per square meter, B is density of the canopy (dry weight per m^2), h_v is bending height of the canopy.

Hydraulic and morphologic characteristics of the bulk flow during experiments and experimental conditions for different runs are summarized in Table 4.1.1. The variations in water discharge were within 2% on account of variations of flow depth. At the same time bulk mean velocity was practically constant indicating that the small variations in depth had no effect upon the flow structure. The flow is characterized by high Reynolds numbers and very small Froude numbers.

Bulk characteristics of the vegetation patch in the experimental runs are presented in Table 4.1.2. Bended height as well as bending angle of the vegetation was determined using scaled underwater video records (averaging over 30 s periods).

4.1.5 Field experiments: results and analysis

Measured mean streamwise flow velocities are shown in Figure 4.1.9. Dense population of plants in the patch (Figure 4.1.9a) obviously indicates the flow pattern similar, at first glance, to the canonical mixing layer. However, as it was outlined theoretically, there are pronounced differences between the canonical and the mixing layers over vegetation patches. First, in the canonical mixing layer velocity difference Δu is constant along the whole length of the flow domain while measurements indicate systematic growth of Δu in the streamwise direction (Figure 4.1.9). Velocity patterns reveal an obvious effect of vegetation density on the flow structure. The lower boundary of the mixing layer is systematically decreasing in height as the vegetation density reduces and in the third run is almost coinciding with the riverbed surface. Second difference is the direction of the mean flow in the plane orthogonal to the streamwise direction. In the canonical flow faster stream accelerates the slower and therefore the mixing layer is progressively distorted in the vertical direction towards the slower flow. The data in Figure 4.1.9 indicate the opposite – the domain occupied by the faster flow progressively contracts towards free surface of the flow in the near field of the patch/mixing layers origin. Patterns of mean vertical velocities (Figure 4.1.10) also indicate directed fluxes toward the free surface at the beginning of the layer. In the far field (x > 5m), mean vertical velocities are directed toward the riverbed, thus from the fast to the slow flow, as in the canonical mixing layers. With the decrease of vegetation density the lower boundary of the layer is decreasing and at lowest density the mixing layer almost attaches the riverbed and became a perturbed boundary layer.

As it was discussed in the Chapter 2 and in the subsection 4.1.1, velocity difference Δu represents a principal parameter of the mixing layers which is constant along the whole flow domain in the canonical flows. Theoretical analysis completed in this Chapter has indicated that in the shear flow developing over vegetation canopy the velocity difference is evolving along the patch length (4.1.21, 4.1.24). Spatial variations of measured velocities u_1, u_2, and their comparison with the models (4.1.12) and (4.1.17) are shown in Figure 4.1.11.

It can be seen that velocity near the riverbed is decreasing with the distance and attains relatively stable values at distances $x > 4$ m from the origin of the vegetation patch. The measured data are reproduced satisfactory by the proposed model though at distances close to the patch origin stronger deviations occur. Velocity near the free surface of the flow slightly increases with the distance from the origin and is predicted by the model fairly well. The discrepancies near the upstream edge of the patch are most probably attributed to the fact that spatial characteristics of vegetation cover exhibit there strong spatial non-uniformity.

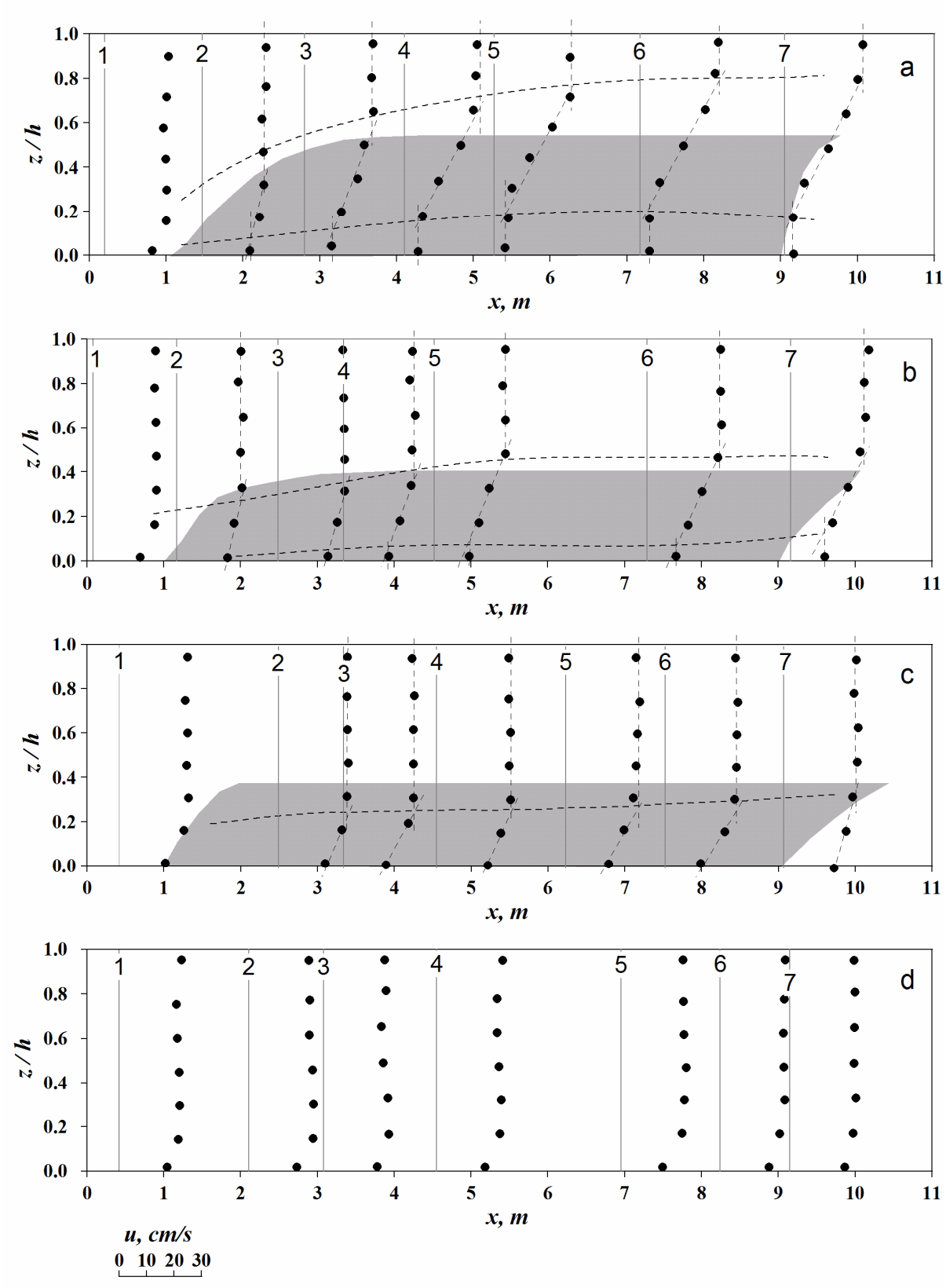

Figure 4.1.9 Vertical profiles of mean streamwise velocity as a function of position in the experimental vegetation patch: Run 1 (a), Run 2 (b), Run 3 (c), and Run 4 (d), the dashed lines mark the boundaries of the flow layers.

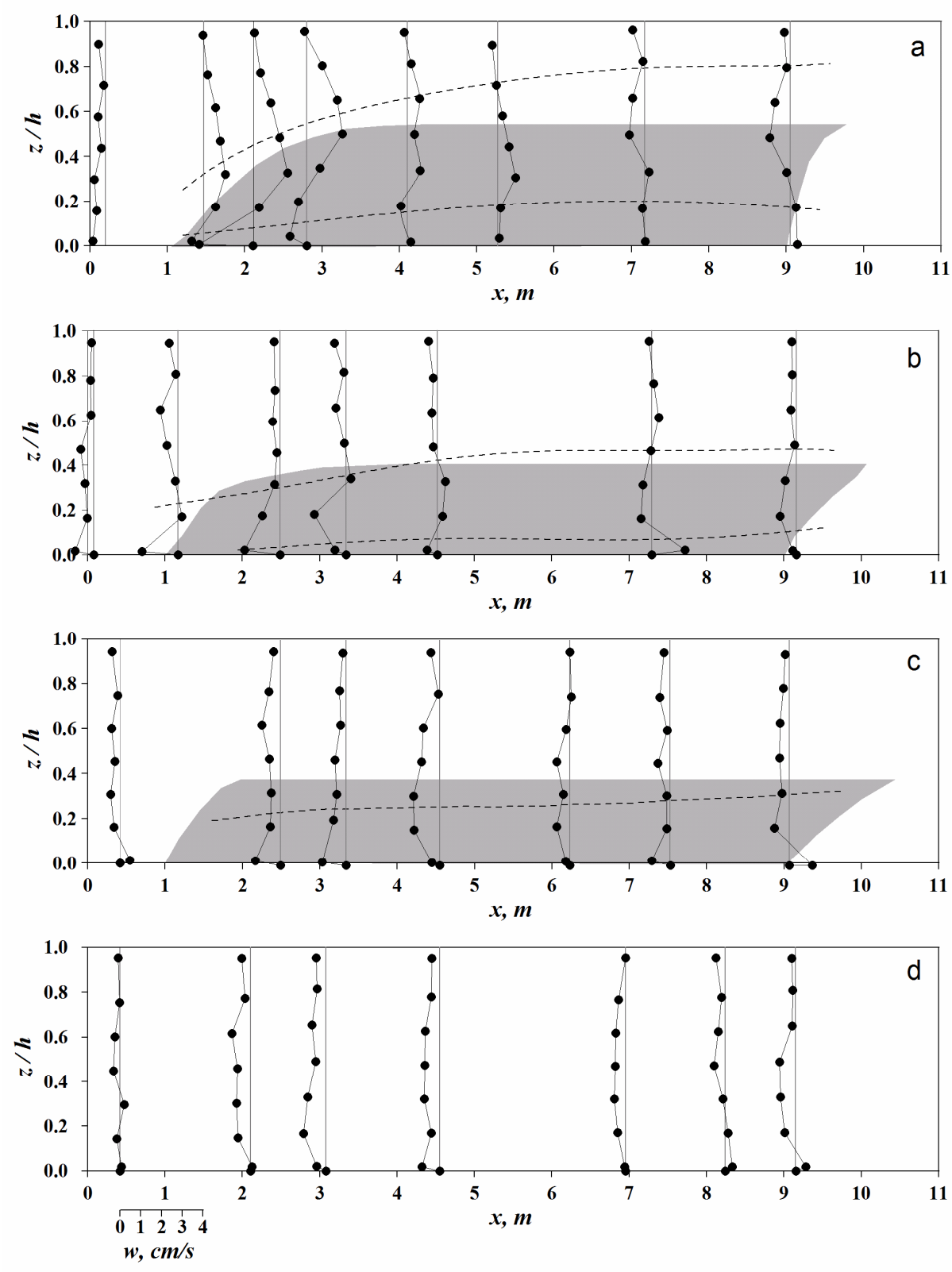

Figure 4.1.10 Vertical profiles of mean vertical velocity as a function of position in the experimental vegetation patch: Run 1 (a), Run 2 (b), Run 3 (c), and Run 4 (d), the dashed lines mark the boundaries of the flow layers

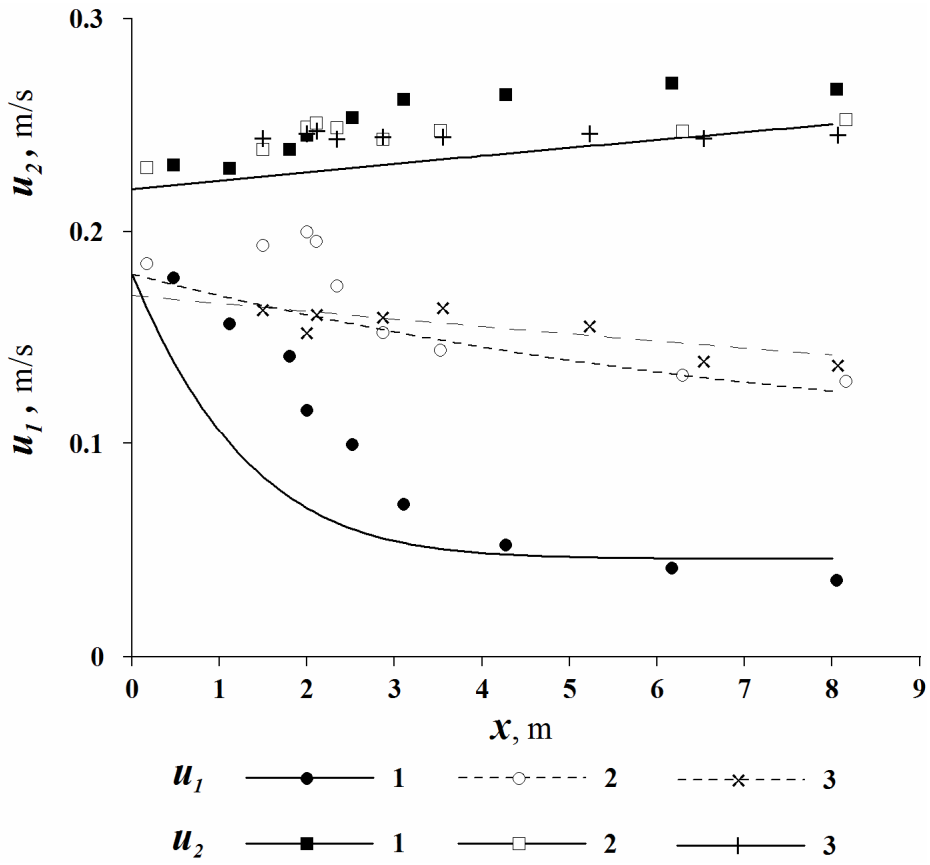

Figure 4.1.11 Measured distributions of mean velocities in the layer near the riverbed and near the free surface and their comparison with the theoretical predictions.

Measured and predicted by (4.1.21, 4.1.24) values of velocity difference are presented in Figure 4.1.12. For this parameter the model provides sufficiently accurate solution though some deviations are also characteristic at the upstream part of the patch. The spatial evolution of mean velocity of the shear layer is shown in Figure 4.1.13. One can see that values predicted by the model (4.1.20), (4.1.23) agree with measured data fairly well though indicating also systematic deviations at the upstream part of the patch.

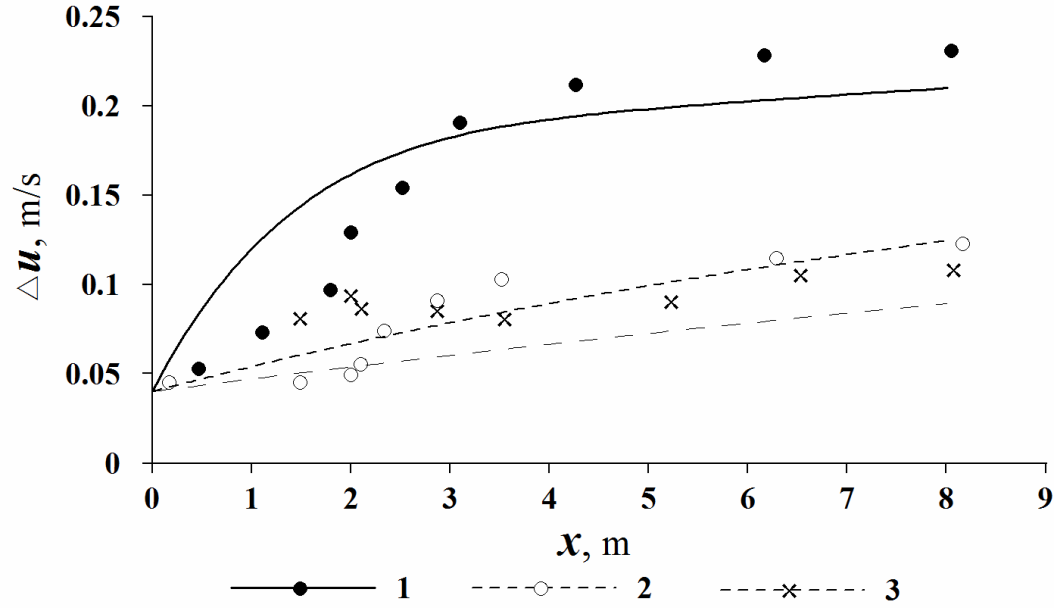

Figure 4.1.12 Evolution of the measured velocity difference along the patch centerline and its comparison with values predicted by the present theory.

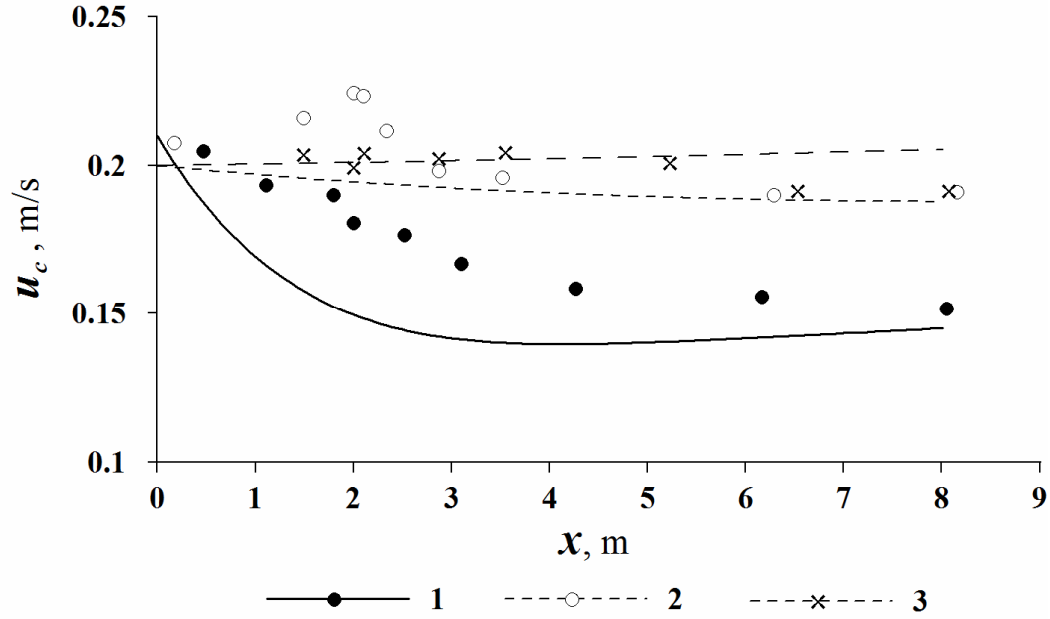

Figure 4.1.13 Measured distributions of mean velocities inside the shear (mixing) layer and their comparison with the theoretical predictions.

Described above velocities represent the components of the main scaling parameter of the mixing layer model – the relative shear $\lambda = \dfrac{\Delta u}{2u_c}$, therefore obtained experimental data should be also compared with the modeled data of this parameter. Normalized measured data and the results of modeling with (4.1.22) and (4.1.25) are shown in Figure 4.1.14. Comparison of measured and predicted values indicate general agreement for all experimental runs and allows concluding the applicability of the proposed theoretical solutions. At the same time some systematic deviations at the upstream part of the patch can be most probably accounted by introducing a transitional distance and offsetting the origin of the layer to the virtual location. However, this problem was not examined here in detail and left for further examination.

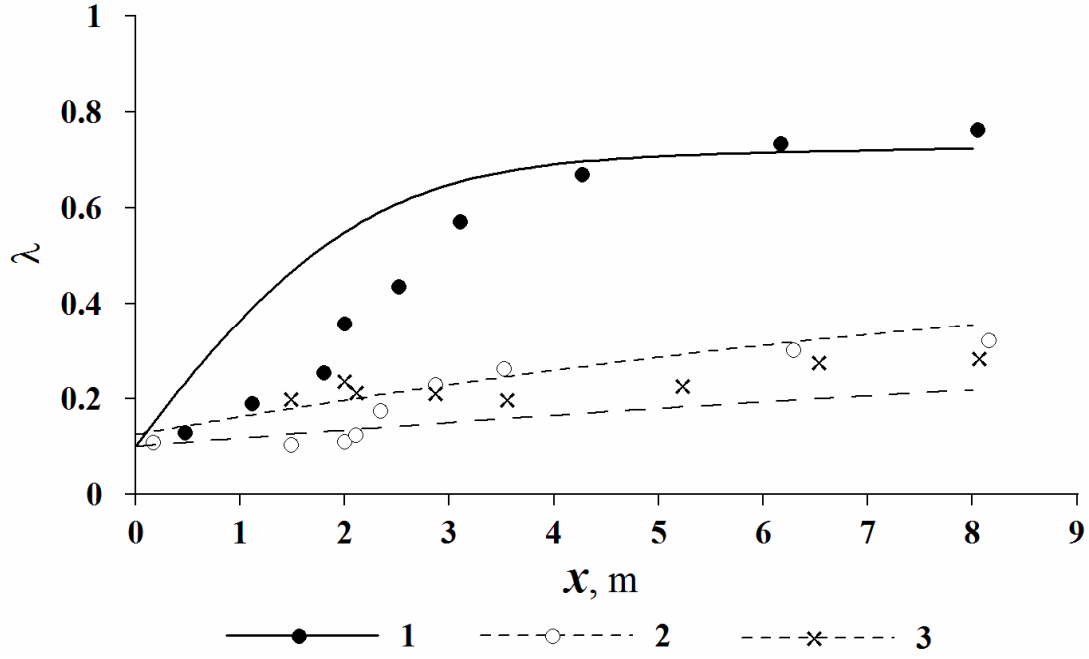

Figure 4.1.14 Evolution of the measured relative shear along the patch centerline and its comparison with values predicted by the present theory.

Analysis of correspondence between the theory developed in this study for characteristic velocity scales and the results of field experimental studies indicate general agreement between theory and experiments. The next important step is to explore the dynamics of the shear layer width and its location over the river depth.

Evolution of the shear layer width along the vegetation patch is shown in Figure 4.1.15.

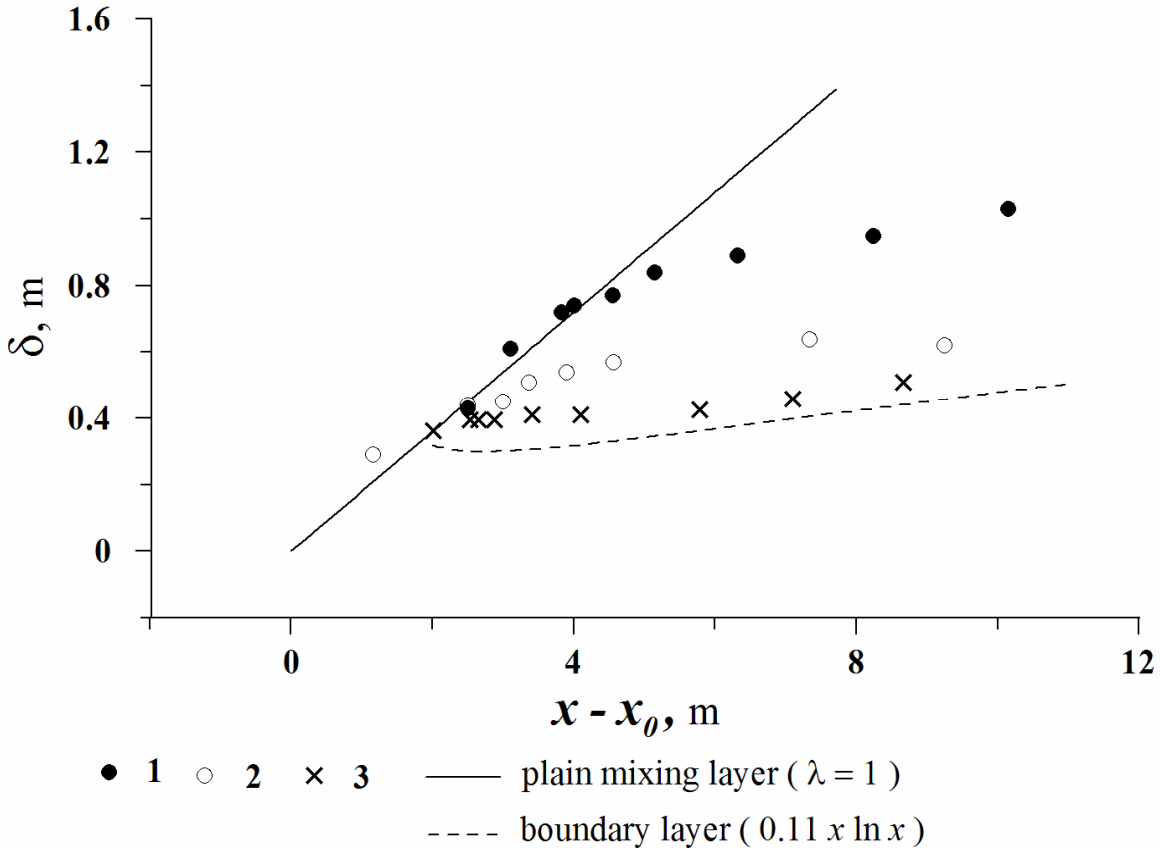

Figure 4.1.15 Evolution of the shear layer width.

For comparison the field experimental data are presented together with solutions of a canonical mixing layer at maximal possible relative velocity difference ($\alpha_C = 0.18$, $\lambda = 1$), and boundary layer development (Tennekes and Lumley 1972). One can see that experimental points on these plots are enclosed between those two limiting models though indicating systematic grouping of the points with different densities of vegetation. Obviously that experimental data do match neither mixing layer nor boundary layer model. From canonical mixing layer it differs by the tendency of the flow to attain stable state while from the boundary layer it differs by the behavior at close distances where the flow tends to the mixing layer model.

An attempt to adopt the corrected model for spreading rate analogously to shallow mixing layers (4.1.26) requires examination of dynamics of spreading rate and its comparison with a critical value which is shown in Figure 4.1.16.

In this figure we only show two first experimental runs because they exhibited more similarity with the mixing layer model. One can see from this plot that at large distances from the origin of the layer the data indicate correspondence with stabilization model and particular value for the critical stability parameter proposed by Ghisalberti and Nepf (2004). At distances close to the origin the model is incapable of reproducing the non-linear growth of the spreading rate.

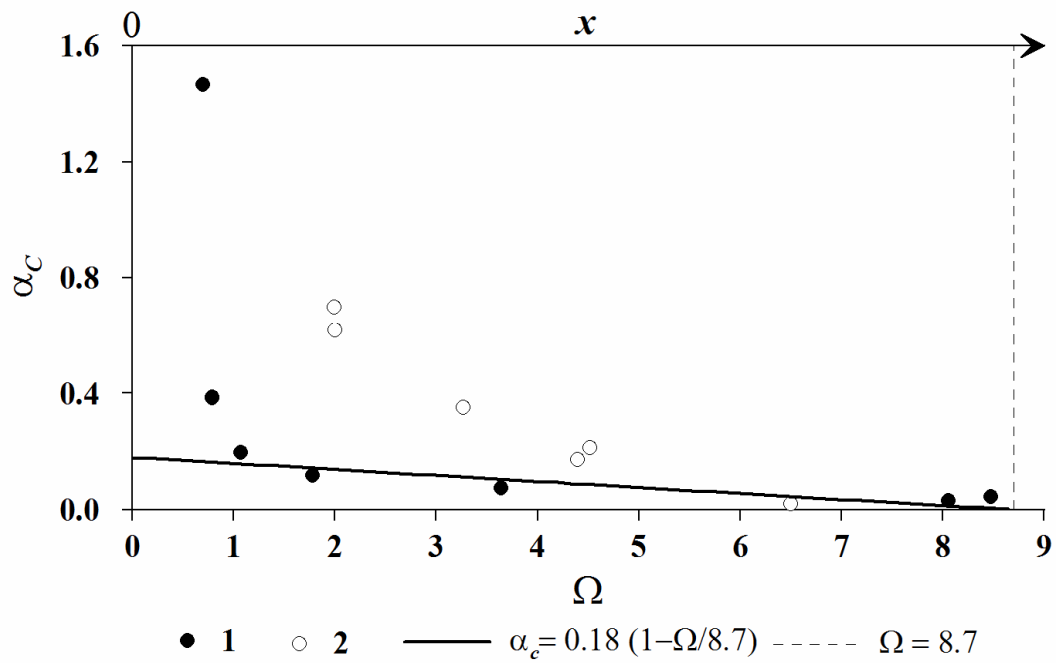

Figure 4.1.16 Dynamics of the spreading rate in the field experiments

The problem with adopting the analogous model for representation of evolution of the layer is most probably because of the principal difference between canonical, shallow and vegetated mixing layers. Indeed, in the canonical mixing layer velocity difference is defined and constant at the origin of the layer. In the shallow mixing layer it is defined at the origin of the layer and subjected to the effect of an additional factor which stabilizes the dynamics at certain distance. In vegetated shear layers the velocity shear and hence dynamics are starting to evolve at the origin of the vegetation patch and hence the width of the layer becomes dependent on the distance similarly to the boundary layers. Because velocity difference is also evolving over the distance it became interrelated to the layer width, Figure 4.1.17.

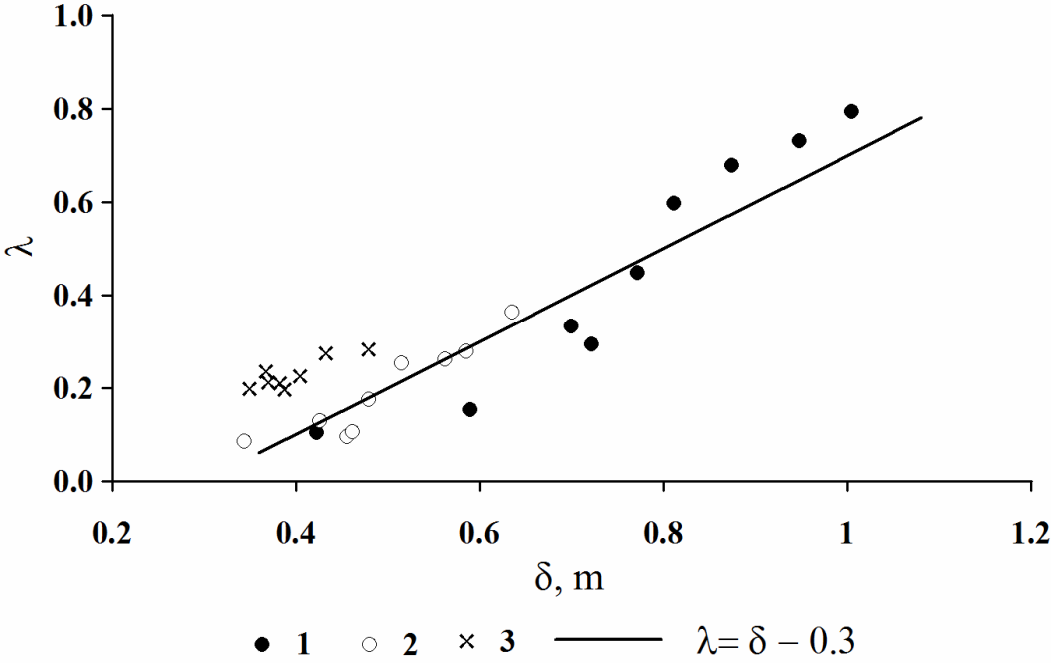

Figure 4.1.17 Relation between shear layer width and velocity ratio.

Therefore we need to reconsider the model of the vegetated shear layer width. As the first approach to the problem we propose to use analysis of dimensionless variables. The width of the shear layer appears to be dependent on the following factors: distance from the origin, depth of the flow, bended height of vegetation, vegetation type and morphology, and velocity scales

$$\delta = F\left(x,\ h,\ h_v,\ C_D a, \Delta u,\ u_h,\ u_1 \right) \tag{4.1.38}$$

or representing the variables in (4.1.38) in dimensionless form we obtain a scaling relationship similar to one widely used in the analysis of shallow mixing layers

$$\delta^* = \frac{\delta}{h} = F_1\left(x^* = \frac{x}{h},\ c_f^{'} = C_D a\, h_v,\quad u^* = \frac{u_h^2 - u_1^2}{\Delta u^2} \right) = F_2\left(c_f^* \times x^* \right) \tag{4.1.39}$$

where $c_f^* = c_f^{'} / u^*$. This relation can be now examined as a function $\delta^* = f\left(C_D\, a\, x \right)$ using experimental data, Figure 4.1.18. This figure shows that experimental data indicate perfect scaling on a line represented by a logarithmic function which was expected from the fact that the layer velocity difference is dependent on the distance from the path origin. The data indicate a perfect scaling for different densities of vegetation. The obtained function, though empirically evaluated, allows reconsideration of the dynamical equation for the shear layer and yields the following model

$$\frac{d\,\delta}{d\,x} = \frac{\alpha_C}{2} \chi^{-1},\ \chi = \frac{x}{h} \tag{4.1.40}$$

The model (4.1.39) apparently bridges the features of the canonical mixing layers – the fact that spreading rate represents a universal scaling parameter – and the characteristic behavior of the boundary layer – dependency of the layer width on the logarithm of the distance from the origin of the layer.

Similar consideration can be applied to the analysis of the vertical position of the shear layer over the flow depth, and the result can be a dependence of vertical position on the shear layer width. Simple comparison of observed values confirms this conclusion, Figure 4.1.19.

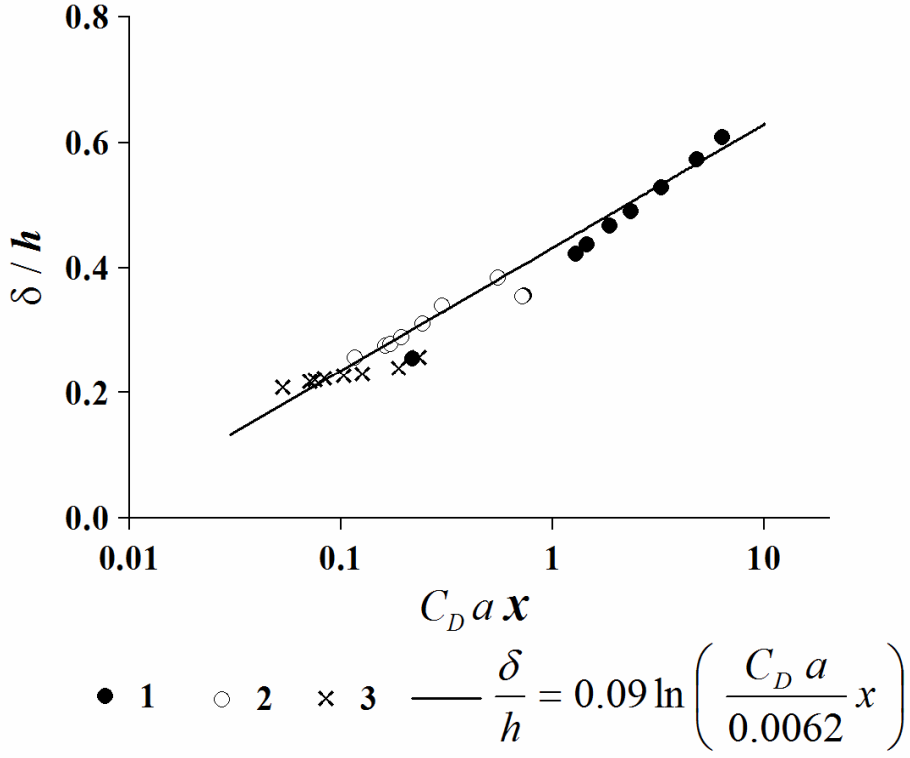

Figure 4.1.18 Dynamics of the shear layer width along the patch of vegetation.

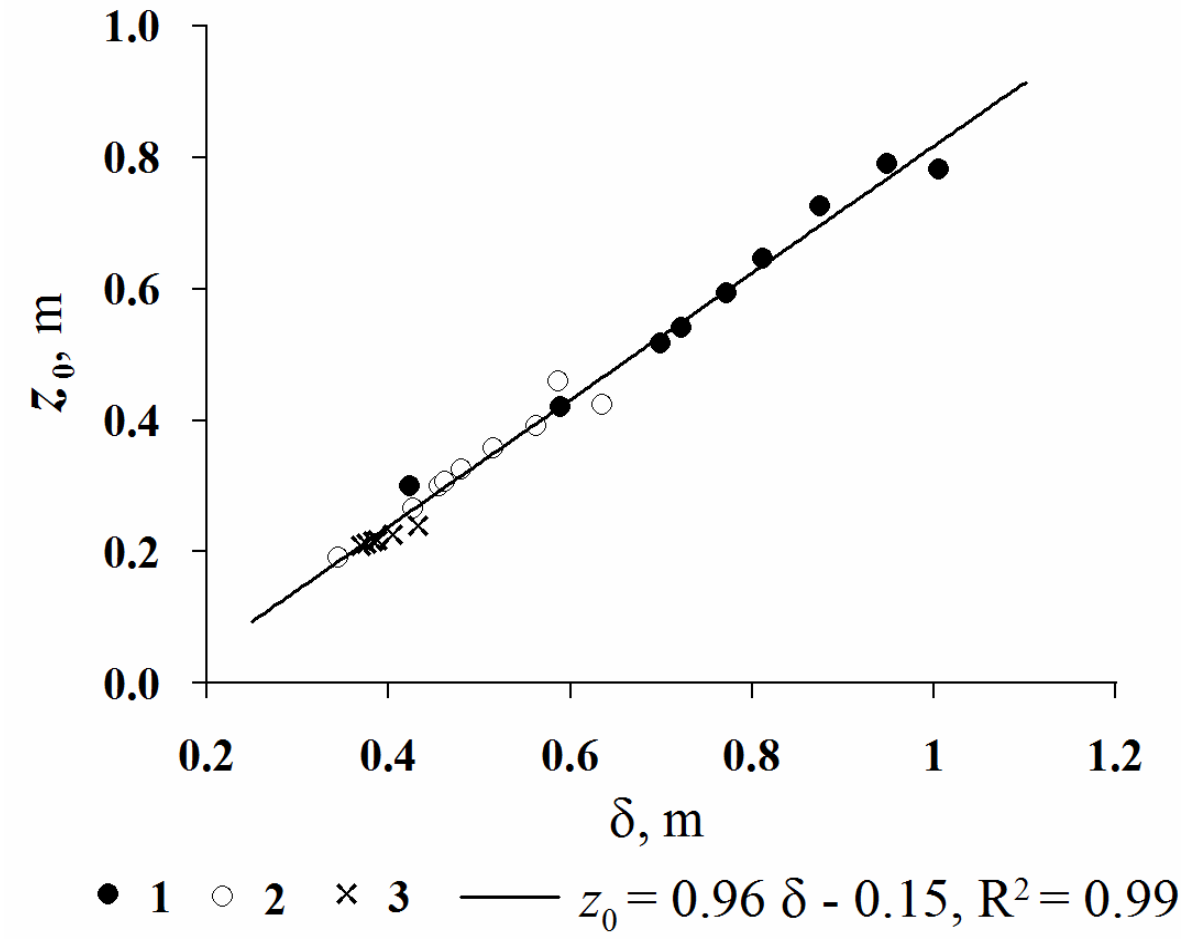

Figure 4.1.19 Relation between position of the shear layer center and its width along the patch of vegetation.

Measured spatial patterns of the principal component of the Reynolds stresses tensor $-\overline{u'w'}$ are shown in Figure 4.1.20. Dashed lines on this plot mark boundaries of the flow layers determined using the mean velocity patterns in accordance with the definition scheme (Subsection 2.1.3). The same lines are used on other figures showing distributions of turbulent kinetic energy and dissipation rates. Additionally, in Figure 4.1.20c is shown the upper limit of the boundary layer evolving over the river bed without vegetation.

The coordinates of that delimiting line were determined at intersects of zero (or nearly zero values) of Reynolds stresses with vertical axes. Near the origin of the mixing layer the maximum of Reynolds stresses is located somewhat below the average boundary of the patch. However, at far downstream from the origin the vertical position of maximum of Reynolds stresses coincides with the boundary of the vegetative canopy. The magnitude of the Reynolds stresses increases systematically along the vegetation patch, though its variations are relatively small in far downstream than near the origin of the patch. The maximal values of Reynolds stresses are attained in the dense vegetation canopy and are reduced proportionally to the decreases in population density. The effect of vegetation at lowest density is still present due to enlarged values of the stress, while the pattern of stresses distribution clearly indicates a region of linear decrease characteristic for the boundary layer. The slope of the upper boundary of the layer in Figure 4.1.20c is the same as in boundary layer without vegetation (Figure 4.1.20d).

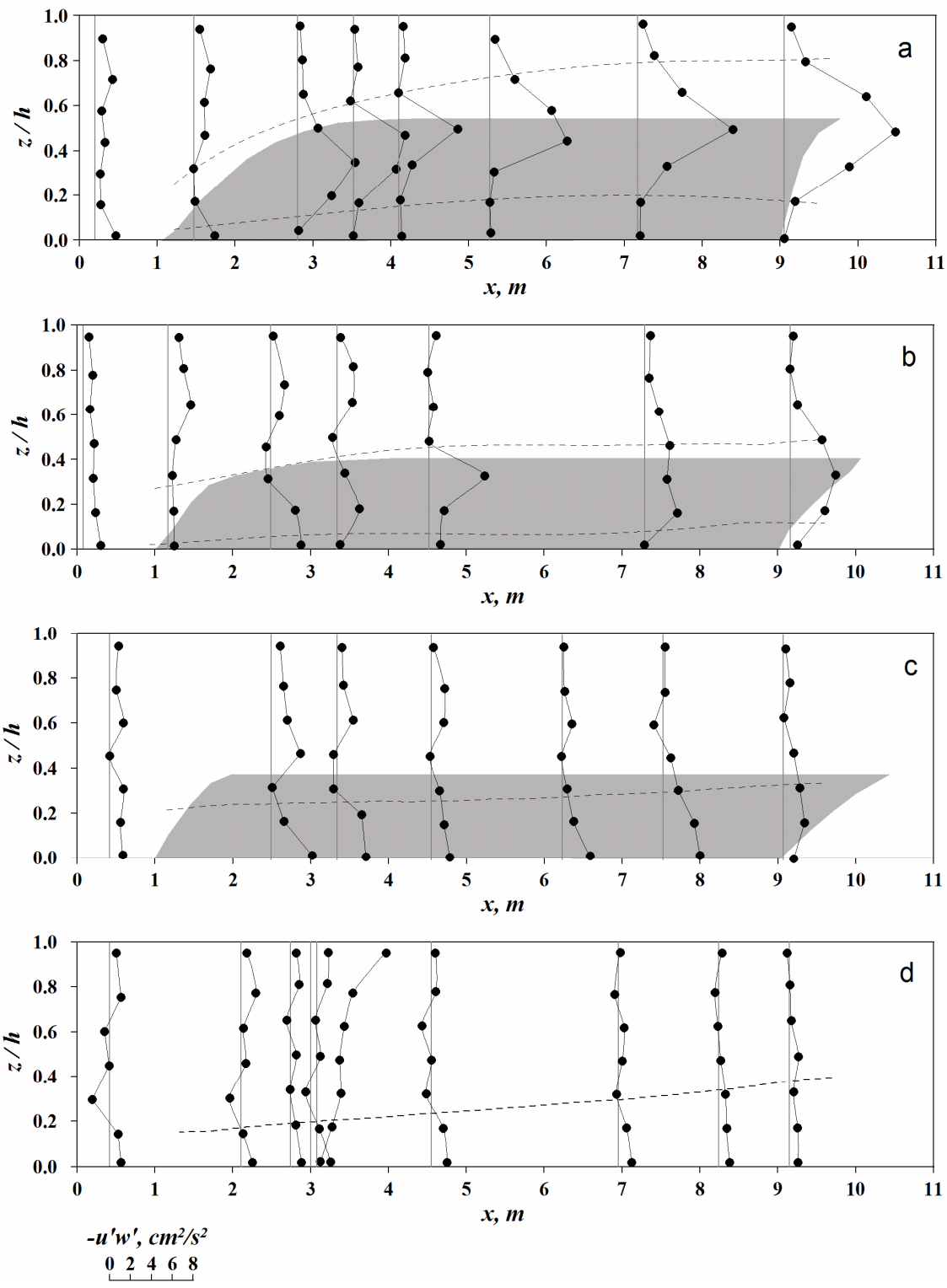

Figure 4.1.20 Vertical profiles of Reynolds stresses as a function of position in the experimental vegetation patch: Run 1 (a), Run 2 (b), Run 3 (c), and Run 4 (d), the dashed lines mark the boundaries of the flow layers.

Modeling of flow velocities around the vegetation patch presented above required provision of drag coefficients and projected area of the plants as the main input parameters of the model describing properties of vegetation in the patch. Drag coefficient of the flexible vegetation is a depth-dependent parameter, as the rigidity and thickness of the plants are decreasing with the plant's length from the roots to the upper part of the shoots. Near the roots plants of *Sagittaria sagittifolia* resemble cylinders with drag coefficient of the order of 1, in the upper part they are more like flat plates with drag coefficient about 0.05. Individual drag coefficients of the elements differ from the bulk drag coefficient of the vegetation patch because of the sheltering effect. The bulk drag coefficient is most important for describing flow characteristics. It can be calculated according to equation (4.1.7) directly from the Reynolds stresses distributions over the depth for the developed flow $x > x_d$ as

$$C_D = \frac{2\left(g i_0 + \dfrac{\partial \overline{u'w'}}{\partial z}\right)}{a\,u(z)^2} \tag{4.1.41}$$

To estimate drag coefficients the following scheme was used. Measured mean velocity and Reynolds stresses distributions were fitted with hyperbolic functions (2.1.51) and (4.1.29) in accordance with the theory described above, that allowed accurate determination of the gradients of Reynolds stress, Figure 4.1.21.

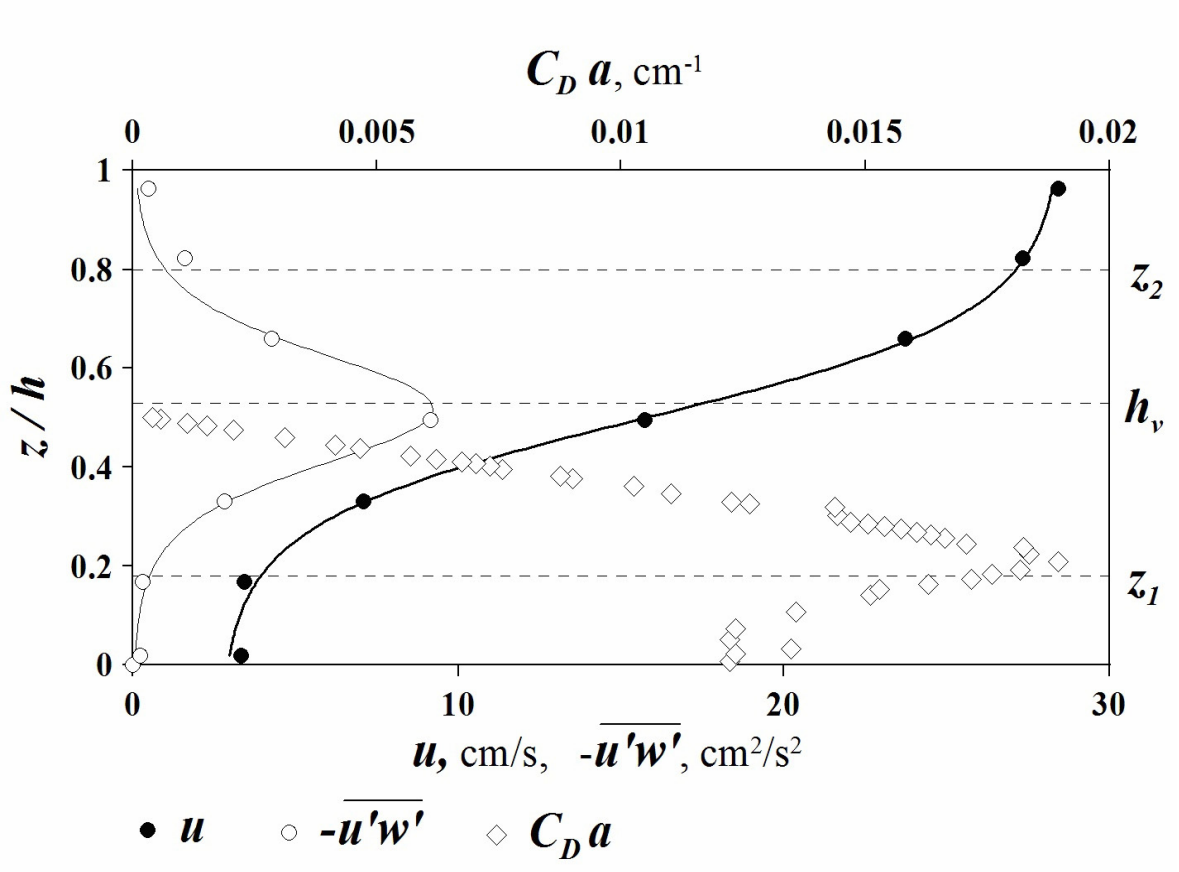

Figure 4.1.21 An example of velocity distribution, shear stress, and drag coefficient over the flow depth (Run 1).

Calculated values of $C_D a$ were practically constant in the area of lower velocity, increased with a maximum, and decreased almost to zero value. The distribution of the plants area a over the depth of the flow is species–specific feature reflecting morphology of the plants. The frontal area of 7 typical plants was measured in 10 cm intervals. The resulting averaged distribution was

fitted to determine the shape function so that the mean vegetation area per unit volume could be 're-distributed' over the depth. The shape function of *Sagittaria sagittifolia* was found to be

$$a = a_{mean}\left[0.1 + 5.63\frac{z}{h_v}\left(1 - \frac{z}{h_v}\right)\right] \tag{4.1.42}$$

with a maximum about the half plants height because of the growth of fresh shorter leaves and 'bunching' of the tissues near the roots. Measured relative areas and their approximation by the shape function (4.1.41) are illustrated in Figure 4.1.22.

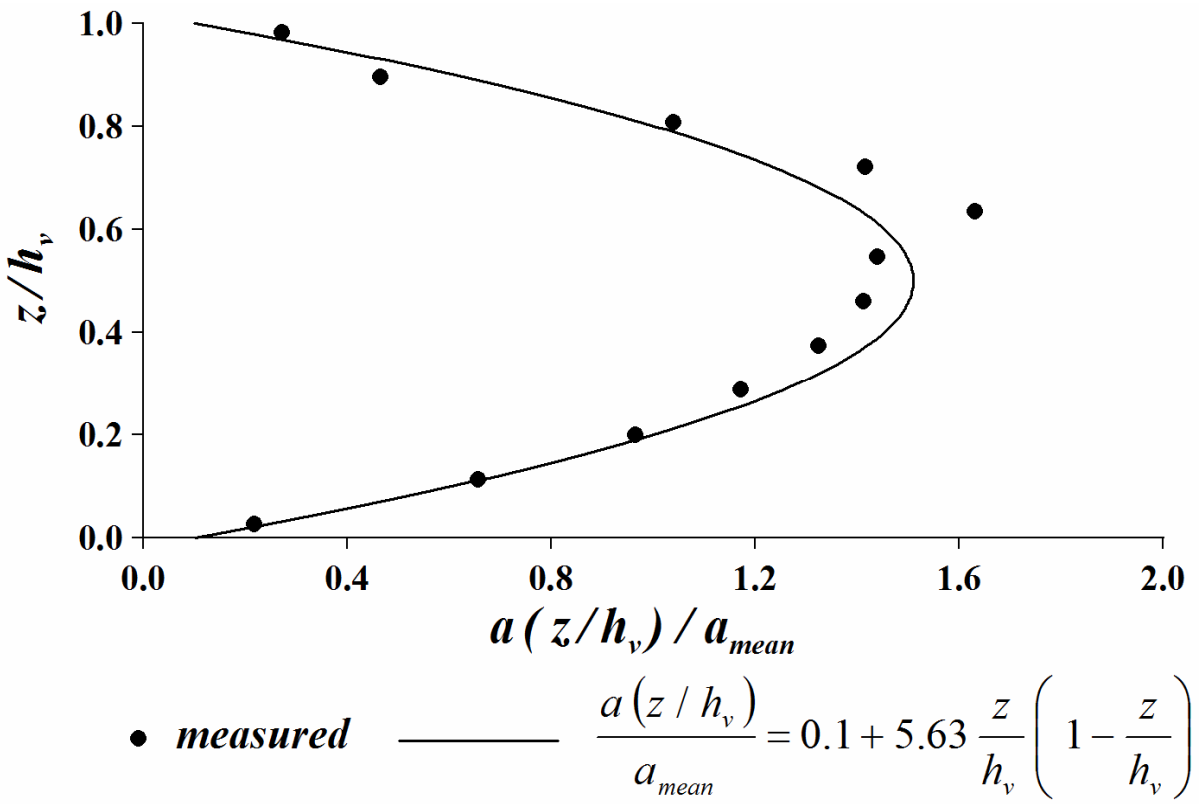

Figure 4.1.22 An example of relative projected area function for *Sagittaria sagittifolia* plants.

Having the shape function (4.1.41) one can readily estimate the values of drag coefficient and its distribution over the river depth. The distribution of drag coefficients over the river depth for all experimental runs is presented in Figure 4.1.23. Obtained data indicate similar trend and magnitudes close to measured in the laboratory studies (Ghisalberti and Nepf 2002).

Spatial distributions of turbulent kinetic energy are even more indicative of the distinctions in spatial dynamics of mixing and boundary layers, as well as in the manifestation significance of population density effect on the structure of flow (Figure 4.1.24). Turbulent kinetic energy increases along the vegetation patch and reaches its maximum in the far downstream. However, the maxima of kinetic energy are located closer to the riverbed near the origin of the vegetation patch, and, similarly to Reynolds stresses, are located at the upper boundary of the vegetation in the far downstream. The changes in magnitude of the energy are also reflecting proportionality to the population density of vegetation, while the pattern of the distribution also attains similarity with the boundary layer without vegetation.

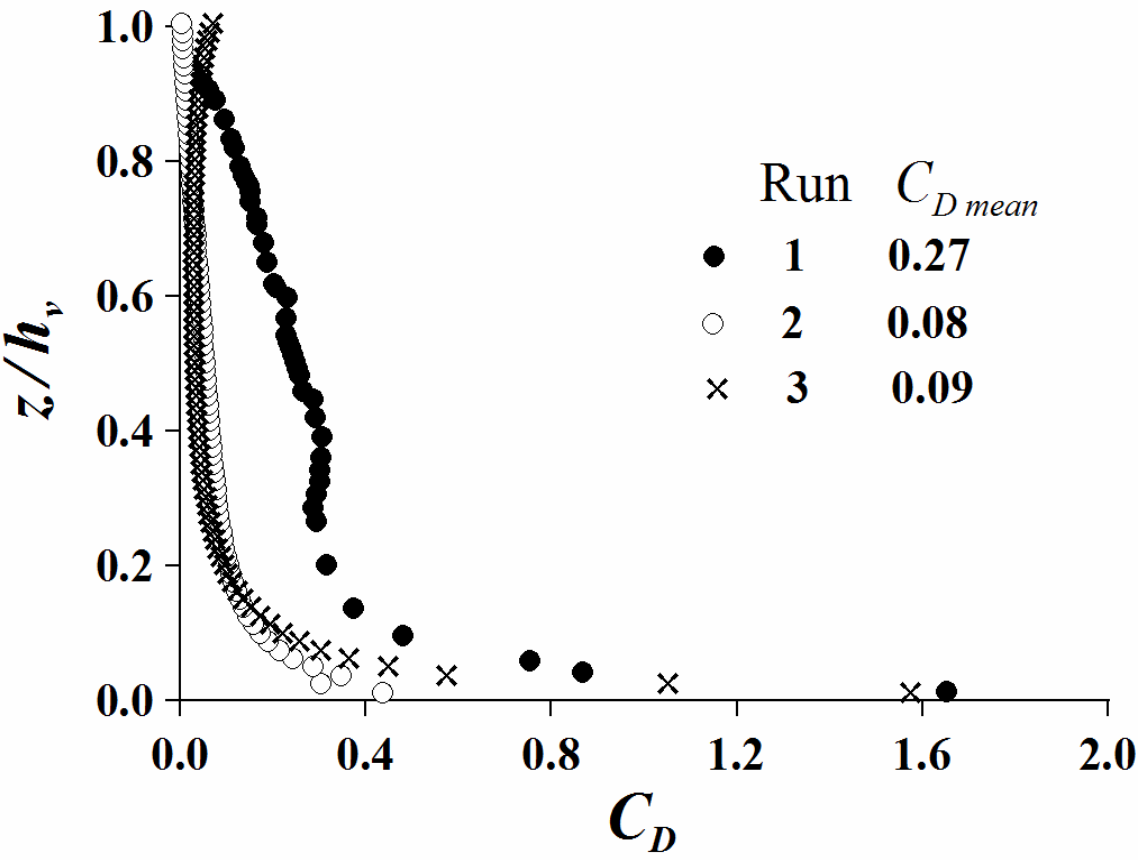

Figure 4.1.23 Distribution of drag coefficient for *Sagittaria sagittifolia* plants over flow depth.

Dissipation rates were computed using measured turbulence spectra and Kolmogorov's relationship (2.1.69) and plotted in Figure 4.1.25. As one can see, the dissipation rates most distinctively of all turbulence statistics outline the effect of vegetation density on the properties of turbulent flow around. Near the origin of the vegetation patch the dissipation rates are distributed similarly as in open channel flows and clearly indicate a characteristic shape described by the semi-empirical equation (Nezu and Nakagawa 1993). Moreover, with decreasing population density (Figure 4.1.25b) a larger region downstream the origin is exhibiting this pattern. The maxima of dissipation rate in the near field ($x < 4$ m, run 1, and $x < 5$ m, run 2) are located near the lower boundary of the mixing layer. In the far field the maximum of dissipation rate as well as the pattern of its vertical distribution vary insignificantly and indicate a steady condition in respect to spatial evolution of dissipation rates.

Measured mean streamwise velocities can be normalized by obtained parameters of the mixing layers and compared with the hyperbolic tangent function (2.1.51). The vertical positions of measuring points were centered in respect to the mixing layer centerline z_0 and scaled with the local width of the mixing layer. Velocity deviations from mean inside the mixing layer were normalized with velocity difference across the flow. Normalized data in Runs 1 and 2 are reasonably collapsed around the hyperbolic function, Figure 4.1.26, while in the Run 3 there was systematical deviation from equation (2.1.51). Noteworthy, that the mean velocity distributions for vertical profiles measured in far downstream of the vegetative patch origin display only minor scatter and the scatter is significantly larger near the origin of the patch. This enlarged scatter is most probably attributed to the stochastic instability of field conditions of measurements rather then physically explainable flow behavior.

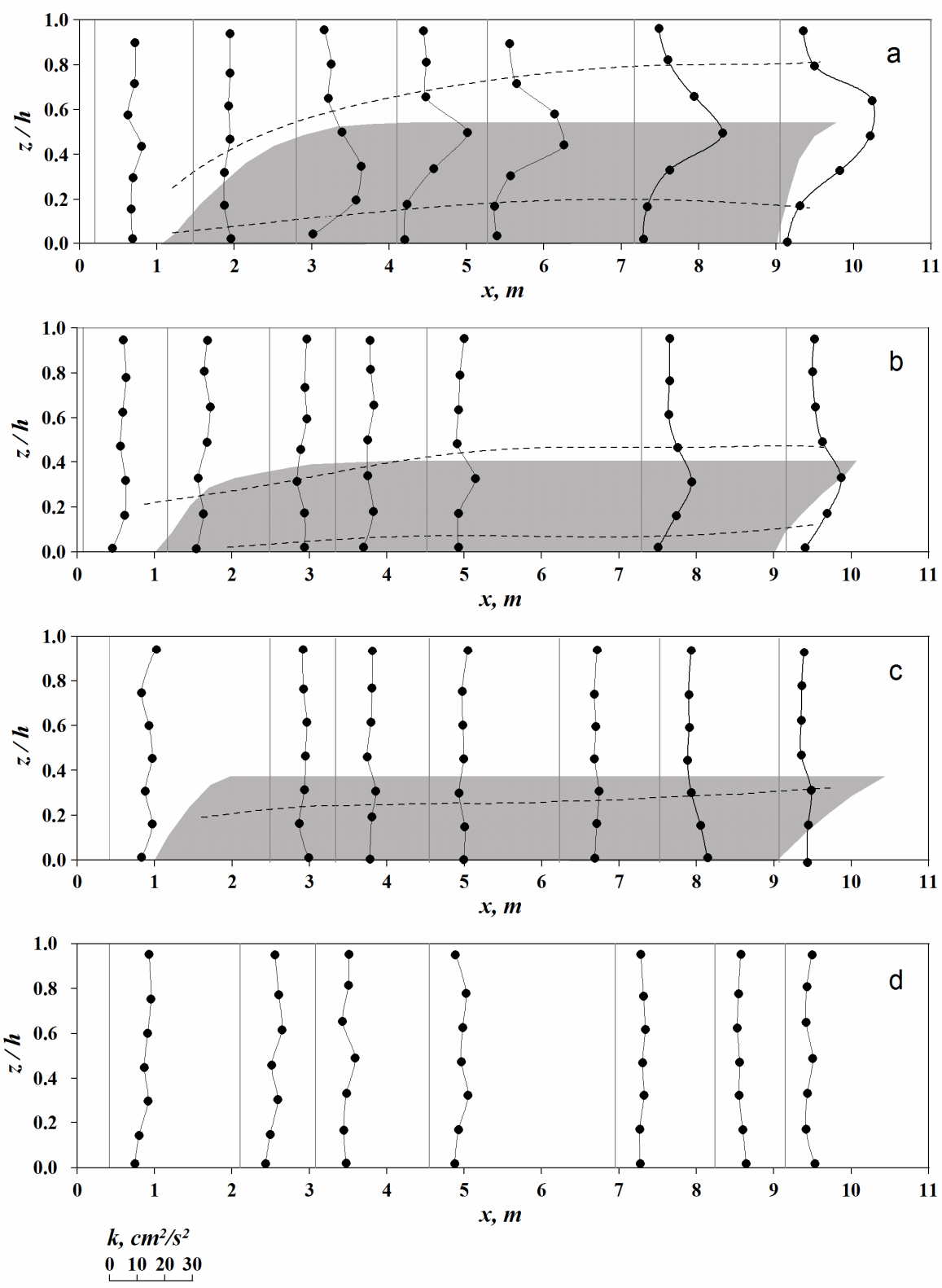

Figure 4.1.24 Vertical profiles of turbulent kinetic energy as a function of position in the experimental vegetation patch: Run 1 (a), Run 2 (b), Run 3 (c), and Run 4 (d), the dashed lines mark the boundaries of the flow layers.

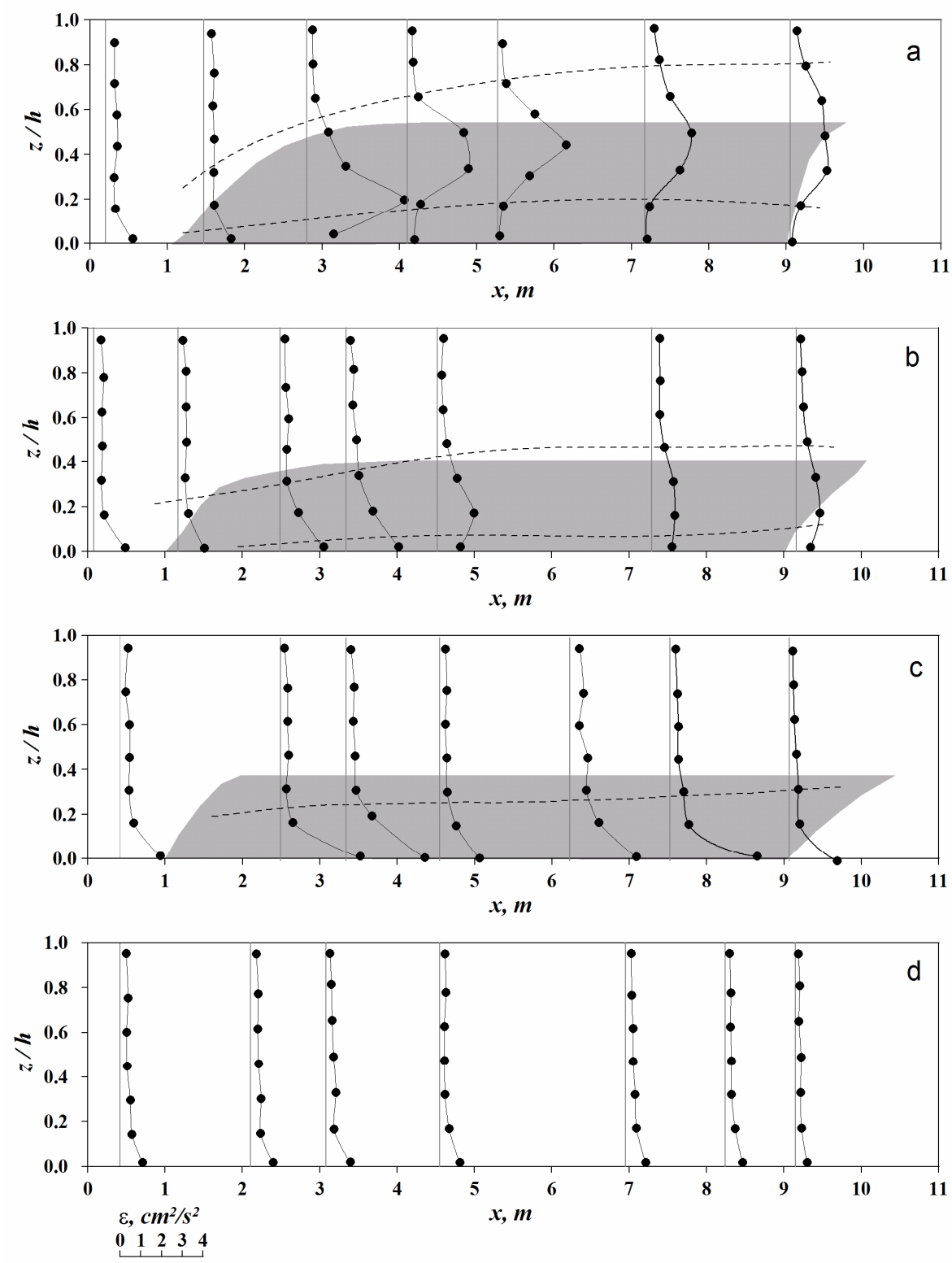

Figure 4.1.25 Vertical profiles of dissipation rates as a function of position in the experimental vegetation patch: Run 1 (a), Run 2 (b), Run 3 (c), and Run 4 (d), the dashed lines mark the boundaries of the flow layers.

Theoretical deductions completed in the subsection 4.1.1, particularly equation (4.1.29) provide the scaling relationship that can be used to generalize measured vertical distributions of Reynolds stresses. The distance from the river bed was scaled in the same way as for mean velocities, and measured values of the Reynolds stresses were normalized by the density of water and the square of velocity difference, Figure 4.1.27. In the vegetation canopy with high population density the normalized measured data are described perfectly by the theoretical function (4.1.29). This collapse and small scatter indicate that constant turbulence viscosity is a good approximate for this flow.

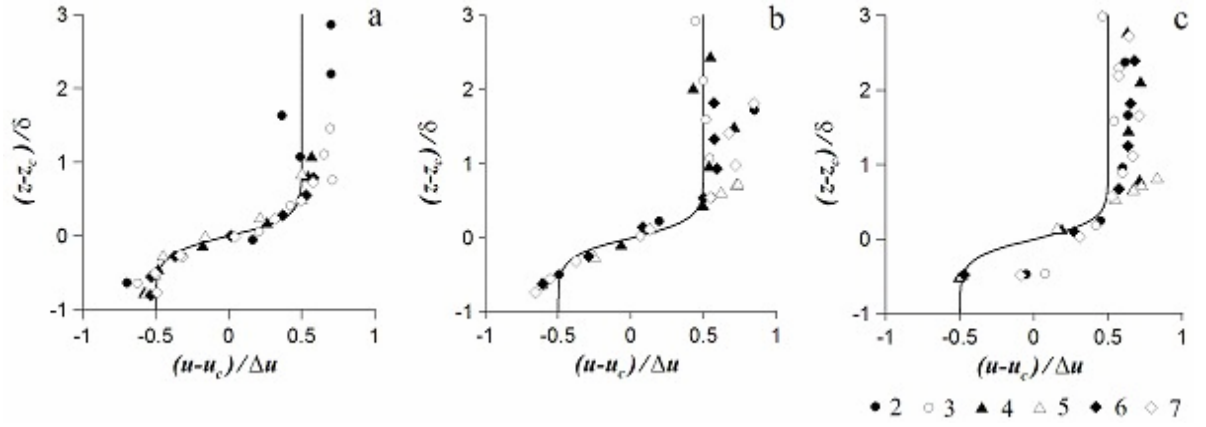

Figure 4.1.26 Vertical distribution of normalized mean streamwise velocity component: a) Run 1; b) Run 2; and c) Run 3.

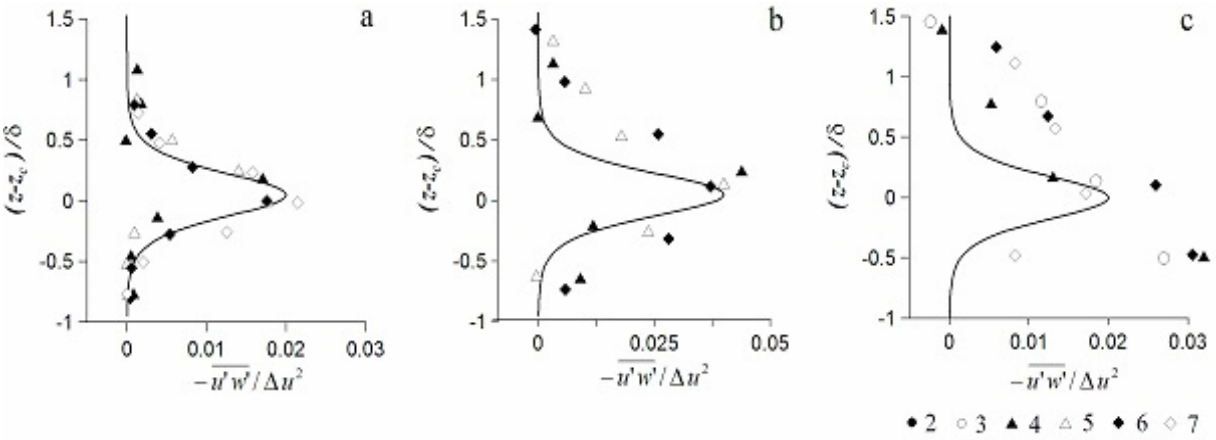

Figure 4.1.27 Vertical distribution of normalized Reynolds stresses: a) Run 1; b) Run 2; and c) Run 3.

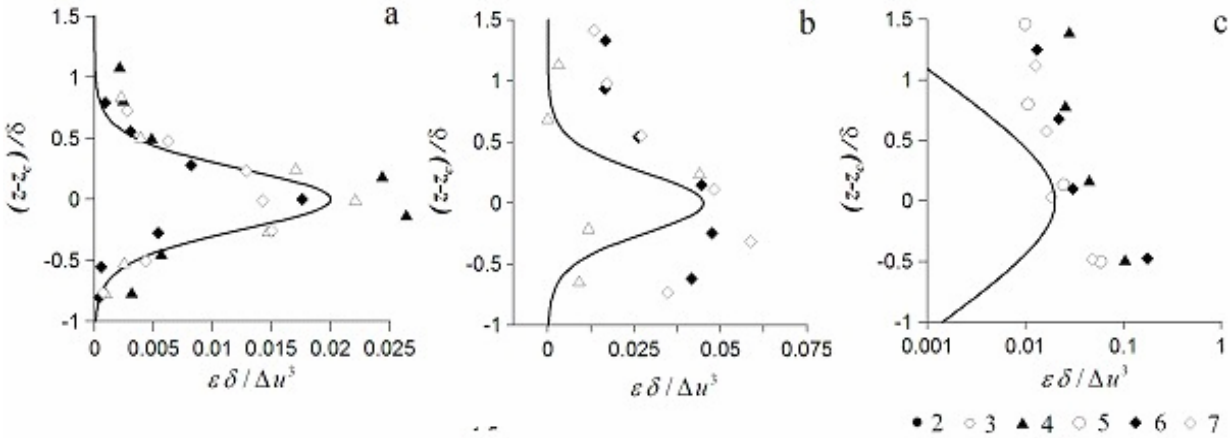

Figure 4.1.28 Vertical distribution of normalized dissipation rates: a) Run 1; b) Run 2; and c) Run 3

Although in the experimental run 2 the data in the far field from the vegetation patch origin indicate agreement with equation (4.1.29), the systematic deviation is evident and mostly pronounced in the flow above the vegetation. Most strong deviations from (4.1.29) appear in the part located near the origin of the patch and are explained by local factors affecting initial development of the flow.

Scaling of obtained dissipation rates completed in accordance with dimensionless analysis presented in the subsection 4.1.1 is shown in Figure 4.1.28. The data indicate again high degree of correspondence in the data set for dense vegetation canopy for Run 1. With progressively decreasing population density systematic deviations occur in the distributions. Most pronounced difference is evidenced for Run 3, Figure 4.1.28c. The grouping of experimental data points in this run reveals boundary layer-like pattern. In general the scaled patterns of principal turbulence statistics exhibit clear and physically interpretable patterns thus revealing distinctive features that vegetation density sets upon flow structure. The flow patterns are comprised between two limiting cases: in dense canopies the flow is best represented by mixing layer model while in sparse vegetation canopy the flow behaves much like perturbed boundary layer.

Visual inspection of measured velocity records inside the vegetative canopy in the experimental patch and in the free flow above the canopy (Figure 4.1.29) indicates distinctive quasi-periodic patterns for the velocity records measured inside the mixing layer. Characteristic for the mixing layers are sweep-like motions corresponding to the fluid being accelerated in the streamwise direction ($u'>0$) and having negative vertical velocities ($w'<0$). These motions exert physical forces on plants and cause motion of the plant blades – monami. The phenomenon is best illustrated by the scaled underwater video records taken synchronously with velocity measurements, Figure 4.1.30. As can be seen on these records the slowed streamwise velocities ($u'<0$) coinciding with positive vertical velocities ($w'>0$), so-called ejection events, cause uplifting of the plant blades, Figure 4.1.30c. Sweep events result in downward motion of the plants blades and bending of the stems. The amplitude of deflection of the plants in average was about 20 cm or about 1/3 of the average patch height. The organized motions control the directed fluxes of momentum and also cause significant alterations of the canopy that increase penetration of momentum inside the canopy.

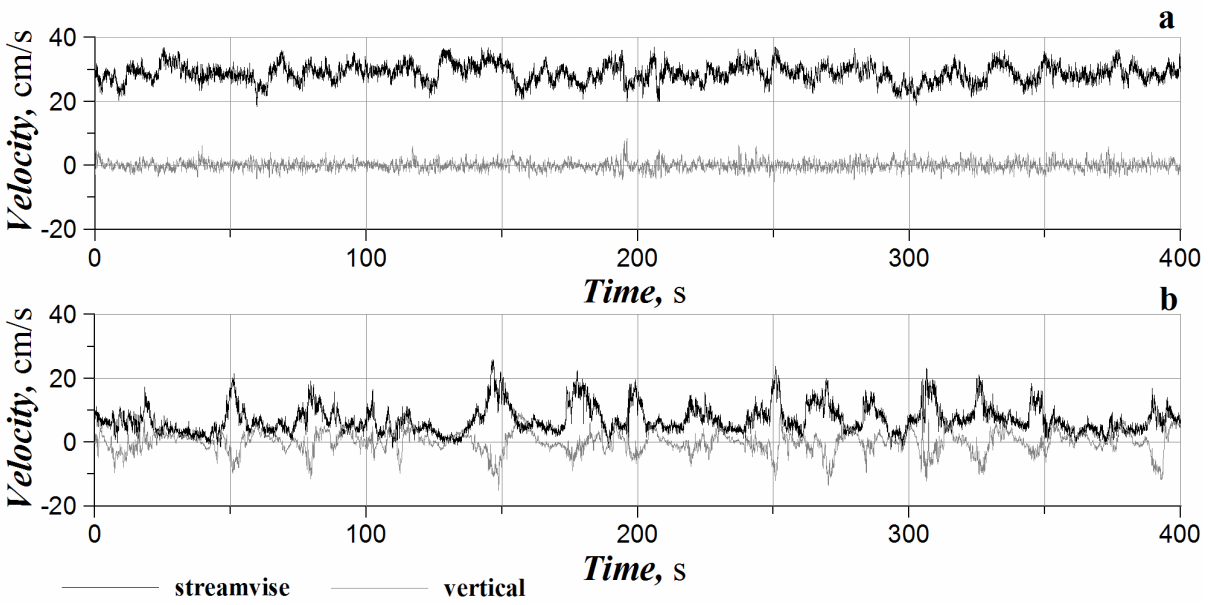

Figure 4.1.29 Flow velocity records measured in the free flow (a), and inside (b) the shear layer region (Run 1, x = 9.1 m, points 7, and 3 respectively)

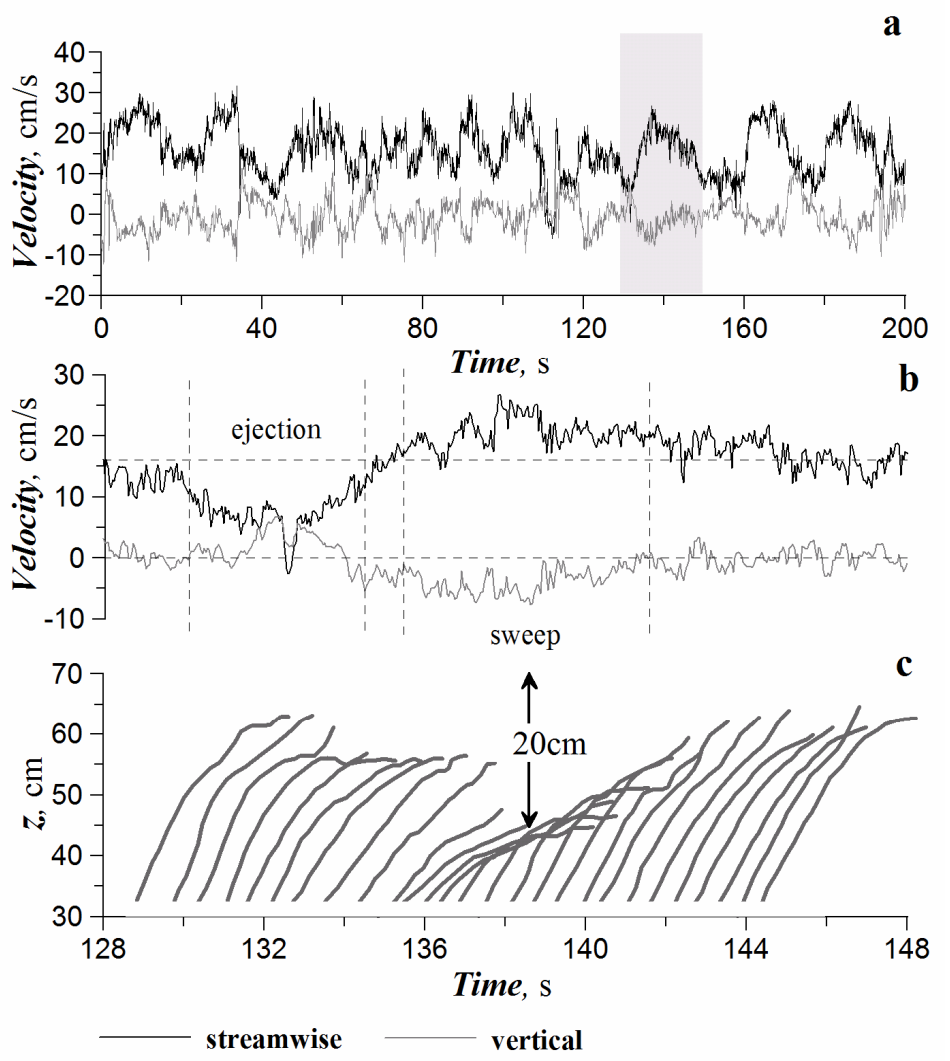

Figure 4.1.30 Flow velocity records measured in the centerline of the mixing layer (a), enlarged part of the record (b), and synchronously recorded trajectory of the plant blade in the patch (c), Run 1.

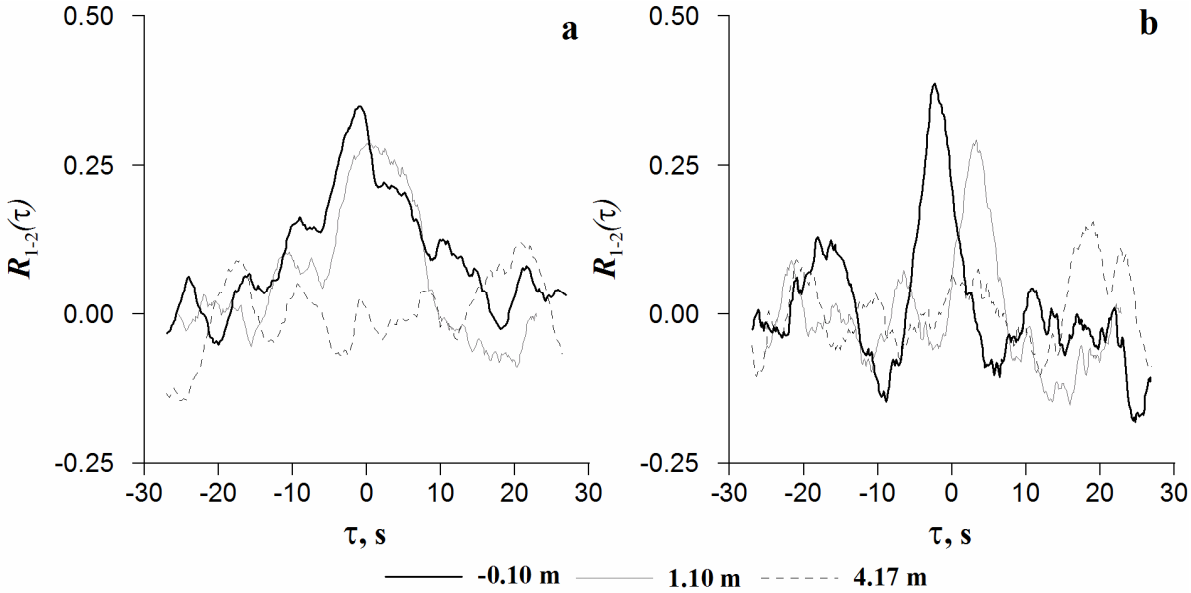

Figure 4.1.31 Examples of cross-correlation functions for streamwise velocity (a), and vertical velocity components (b), experimental Run 1.

Hence, the following analysis of the experimental data will concentrate on the quantitative assessment of the coherent structures and the effect that the population density of vegetation sets upon these organized motions. We will use the method of two-point cross-correlation functions described in the Section 2.1.4, equation (2.1.70) to map the temporal and spatial patterns of structures with the aim of obtaining characteristic spatial scales of the organized motions without necessity to rely on frozen turbulence hypothesis.

Typical two-point cross-correlation functions obtained in this study are shown in Figure 4.1.31. The functions display systematic decrease in the maxima of correlation at increasing lag distances – a pattern reported to be characteristic for most of shearing turbulent flows. The ordinates of two-point cross-correlation functions at $\tau = 0$ represent the value of correlation at a given displacement Δx, Δy, and can be mapped to obtain spatial patterns of coherent structures.

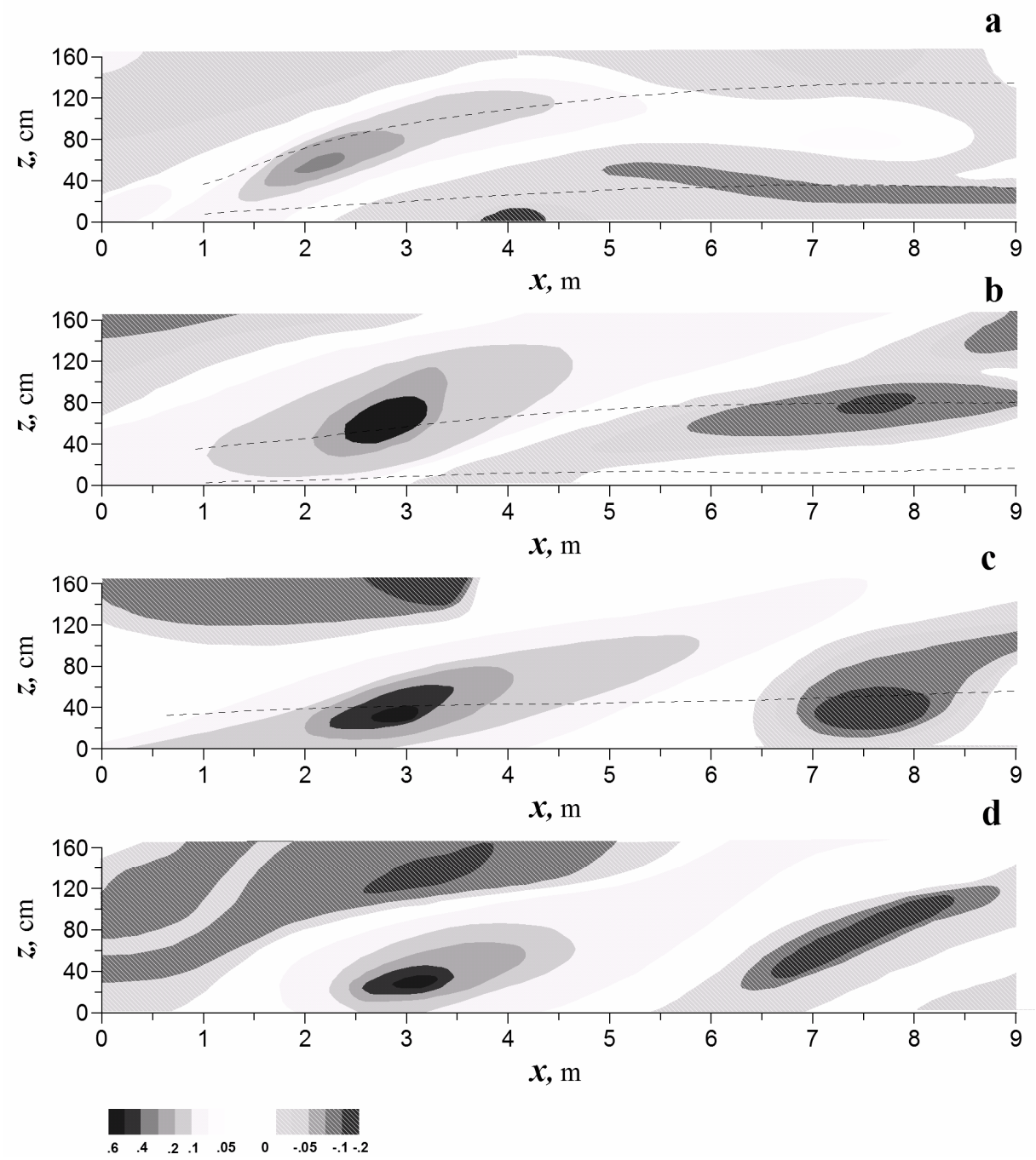

Figure 4.1.32 Spatial two-point correlation maps for streamwise velocity component: Run 1 (a), Run 2 (b), Run 3 (c), and Run 4(d), the dashed lines mark the boundaries of the flow layers.

The correlation maps for streamwise velocity component are shown in Figure 4.1.32, and for vertical component in Figure 4.1.33. The spatial correlation maps depict evidently the pattern representative for mixing layers – three distinctive zones of positive correlation values mark the positions of coherent structures along the mixing layer (Figure 4.1.33a). The zones are elongated in the streamwise direction and their vertical extent corresponds to the width of the mixing layer, though the spatial arrangements of the zones indicate that they are centered along the upper boundary of the vegetative canopy at the near field of the mixing layer origin. In the far field ($\Delta x > 4.5$ m) the center of coherent structures is aligned with the central position of the mixing layer. With decreasing population density of the vegetation patch and respectively decreasing resistance (roughness) of the flow, the spacing between centers for area of flow with positive correlations became larger, Figure 4.1.33b).

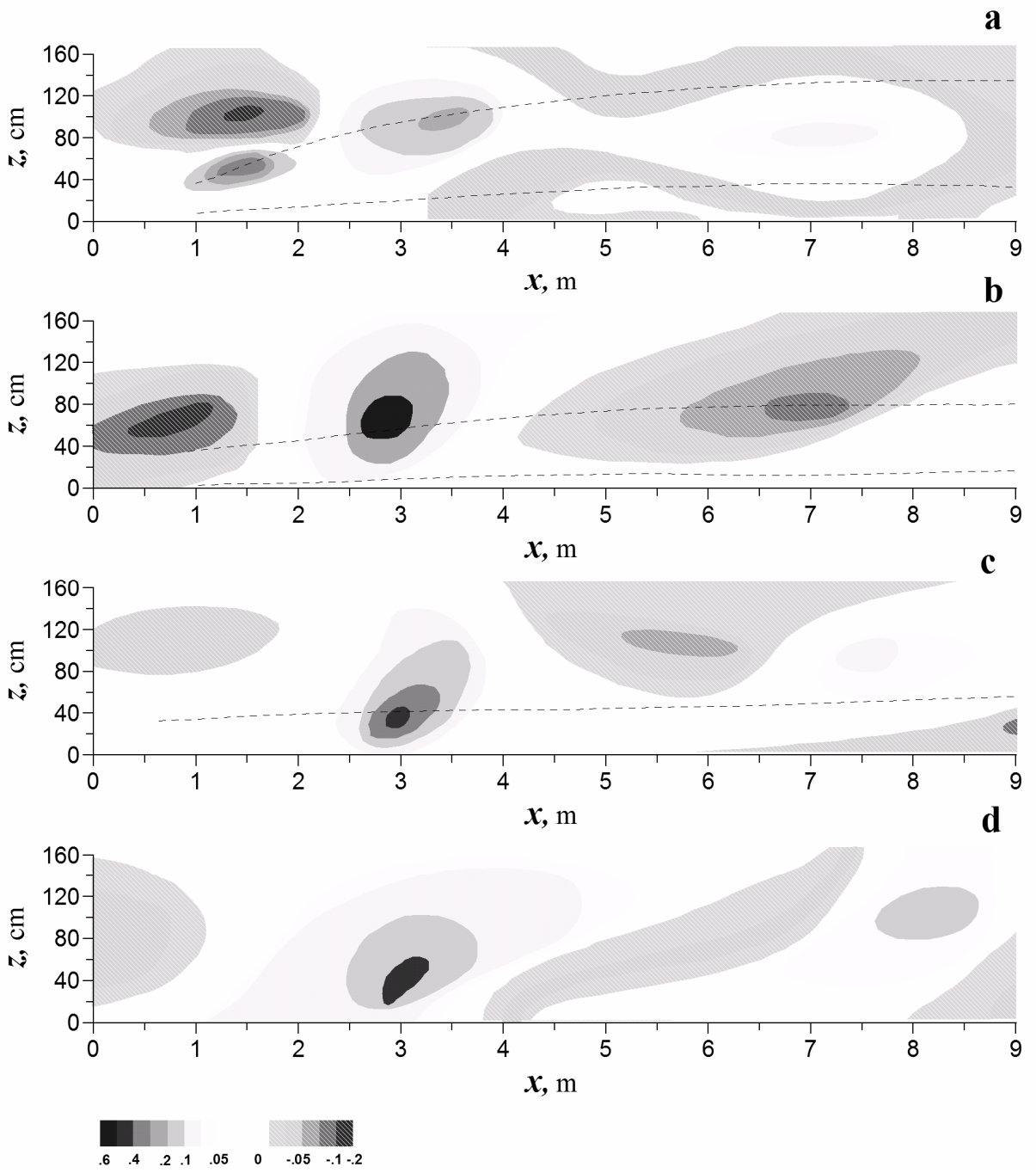

Figure 4.1.33 Spatial two-point correlation maps for vertical velocity component: Run 1 (a), Run 2 (b), Run 3 (c), and Run 4(d), the dashed lines mark the boundaries of the flow layers.

At lowest densities the flow structure resembles more the pattern of boundary layer structure with characteristic narrow band segmentation and evident uplift of the second positive maxima toward the free surface. This uplift is indicative for ejection events and cause well-known and frequently reported phenomenon of boils on the free surface of the flow (Nezu and Nakagawa 1993).

Obtained two-point correlation maps provide comprehensive source of qualitative information and also some valuable quantitative information about spatial scales related to organized motions. More close and detailed quantitative information can be gained using the spectral analysis of velocity records together with analytical tools capturing phenomenology.

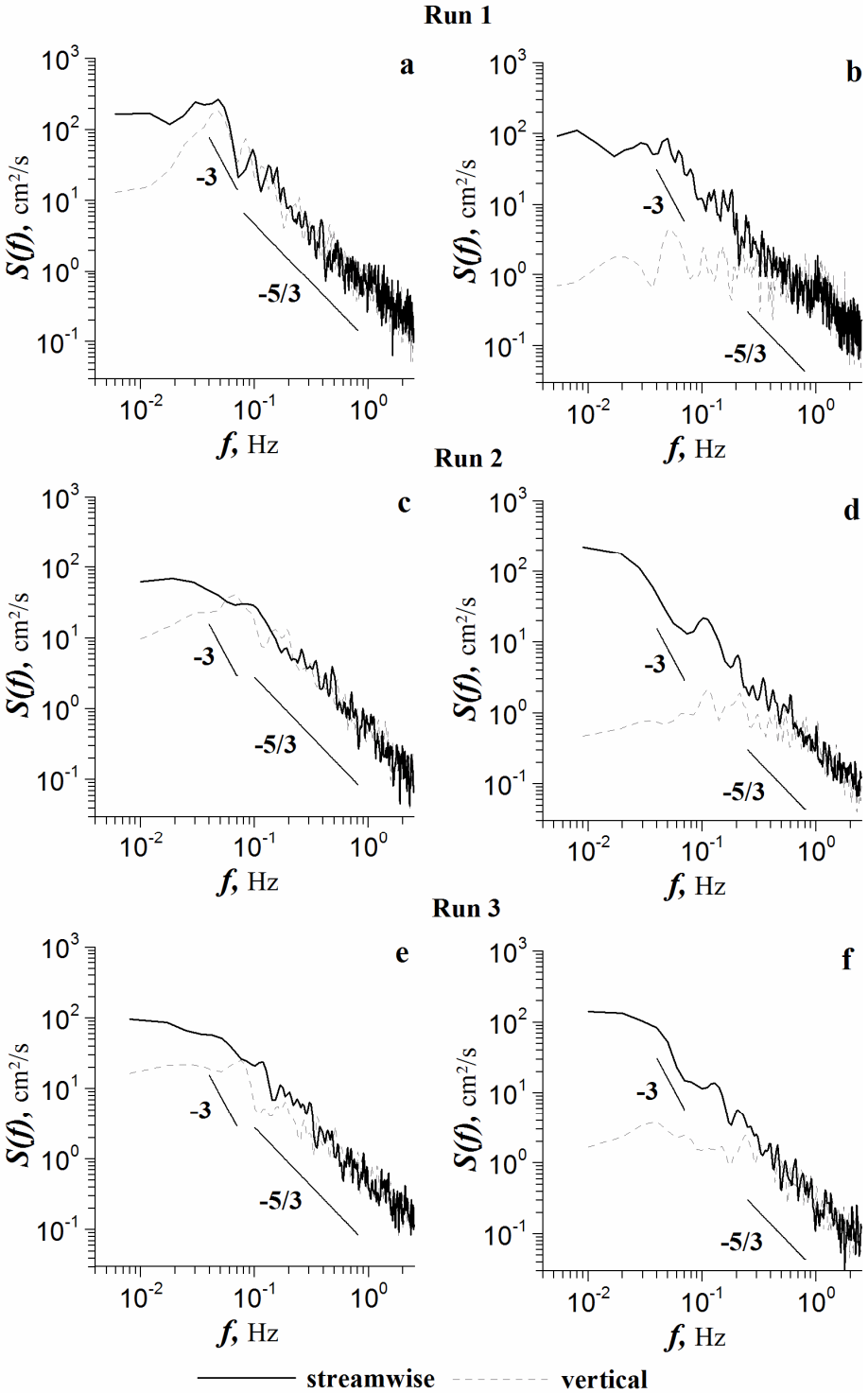

Figure 4.1.34 Examples of turbulence spectra measured near the center of the mixing layer (a, c, e) and in the free flow over the vegetation patch (b, d, f), vertical 7 for all Runs.

Examples of spectral densities measured in the different parts of the flow are shown in Figure 4.1.34. The spectral densities measured inside the area occupied by the mixing layers (Figure 4.1.34a) resemble those reported for laboratory studies (Ghisalberti and Nepf 2002).

A distinctive peak is evidently present at low frequencies (f=0.05 Hz) on both spectra measured in free flow over and inside the mixing layer, though the spectral densities of vertical velocity in the free flow are 100 times smaller than inside the layer. The spectral densities reveal the presence of an inertial subrange -5/3 at higher frequencies ($f > 0.1\,\mathrm{Hz}$ inside, and $f > 0.8\,\mathrm{Hz}$ in free flow) while at lower frequencies the spectral density decay seems to follow the -3 law which might be indicative of turbulent energy being transferred in average to larger scales.

At this point, as sufficient evidence and necessary quantitative information on coherent structures was presented, the analysis of the model (4.1.37) performance can be completed. The main characteristics of the mixing layer and additional necessary information, as well as results of computations according to equations (2.1.52) and (4.1.37) are presented in Table 4.1.3.

Table 4.1.3 Characteristics of the mixing layer, turbulent stresses, resistance factors, measured and predicted frequencies of coherent structures.

x, m	$\delta(x)$, m	Δu, m/s	u_c, m/s	τ/ρ, cm^2/s^2	c_f	f, Hz		
						measured	(2.1.52)	(4.1.37)
Run 1								
5.4	0.85	0.22	0.16	7.0	0.055	0.090	0.042	0.063
7.3	0.95	0.22	0.15	9.0	0.080	0.070	0.035	0.062
9.2	1.05	0.24	0.16	10.0	0.078	0.050	0.034	0.058
Run 2								
4.0	0.57	0.11	0.19	4.6	0.026	0.080	0.075	0.064
7.1	0.63	0.11	0.19	2.3	0.013	0.040	0.068	0.047
8.9	0.61	0.11	0.19	4.2	0.023	0.050	0.070	0.059
Run 3								
6.3	0.42	0.10	0.20	2.0	0.010	0.060	0.107	0.065
7.6	0.46	0.11	0.20	3.2	0.017	0.062	0.097	0.073
9.0	0.51	0.10	0.19	2.0	0.011	0.075	0.083	0.054

Comparison of measured and predicted frequencies for coherent structures indicates that equation (2.1.52) predicts the frequency with accuracy of about 50%, while equation (4.1.37) - with accuracy of about 20% in the far field. Taking into account the fact that mixing layers over submerged vegetation in the near field are very different from the canonical mixing layers (as the velocity difference is formed in the far field), the model (4.1.37) can be considered as adequate to describe the phenomenon.

The spatial scale can be also obtained from the correlation map (Figure 4.1.33a) as the distance between the centers of positive correlation regions in the far field ($L_c = 3.5\,\mathrm{m}$) and hence the accuracy of the estimate is slightly larger than 20%. Up to now the value of the coefficient of proportionality was always equal to 1 assuming perfect agreement with frozen turbulence hypothesis. The slight underestimate of the spatial scale can be most probably attributed to the fact that coherent structures propagate faster than the mean velocity in the mixing layer. This fact was stressed in laboratory investigations (Ghisalberti and Nepf 2002) as the precondition for development of monami motions in submerged vegetation. In fact the video records obtained synchronously with instrumental (ADV) measurements also revealed monami

motions (magnitude of about 20-30 cm) directly related to the ejection and sweep phases of structures.

4.2 Structure of Flow in a River Section: field measurement study

In this section we apply the knowledge gained from the completed theoretical analysis and experimental field studies to examine the structure of flow in a natural section of the river. Measurements were taken for both vegetation free and vegetated conditions allowing direct comparison and illustrating the structure of flow in a section in the vegetative mosaic.

4.2.1 Program of field measurements

The program of field measurement studies was designed to obtain a data set that will make possible examination of turbulent flow structure in a cross-section of a river with and without vegetation at the same water level. Such data set provides direct assessment for the effect of vegetation on the bulk flow structure and fine-scale structure of turbulence as well. A measurement section through the vegetative mosaic provides information on both the structure of flow in vegetated patches and vegetation free paths.

Detailed measurements were carried out on the experimental river reach near Freienbrink (Figure 3.1.1, Figure 3.1.3, Figure 3.1.4) in the cross-section 4 (Figure 4.2.1).

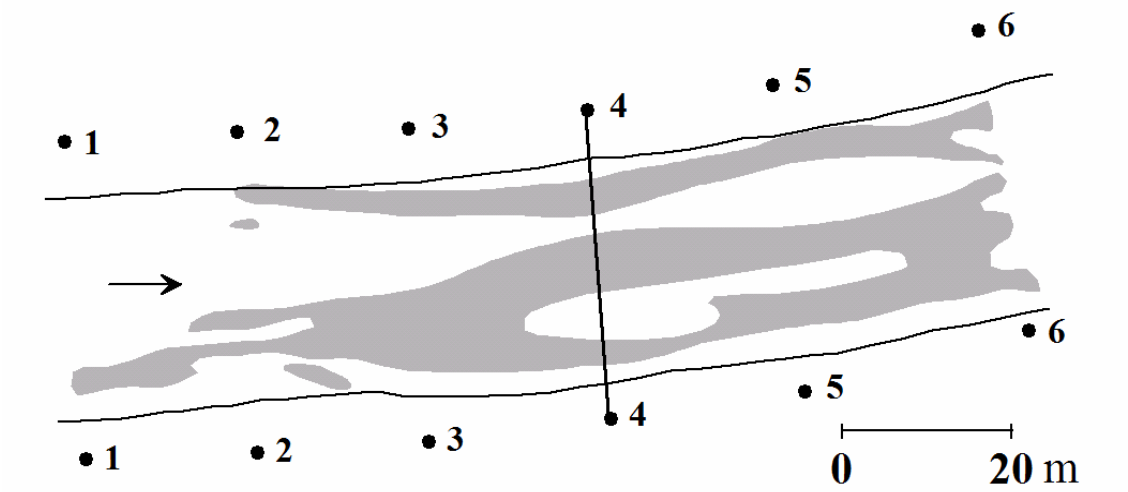

Figure 4.2.1 Location of measuring cross-section on the experimental river reach (shadowed area outlines vegetation patches for 15.07.05, and the circles and number indicate cross-sections).

First data set was measured on 15 of July, 2005 when the river was vegetated, and the second one on 19 of April, 2006 in unvegetated flow when the water level was practically the same as it was in the vegetated channel (Table 4.2.1).

Table 4.2.1 Bulk characteristics of the flow during field measurement studies

Date	Q, m^3/s	U, m/s	B, m	h, m	S $\times 10^5$	c_f	n, $s/m^{1/3}$	Fr	Re $\times 10^{-5}$
15.07.05	6.34	0.21	23.4	1.29	8.00	0.046	0.051	0.06	2.71
19.04.06	15.6	0.50	23.4	1.33	7.96	0.008	0.022	0.14	6.65

These measurements were carried out using the same measuring protocols and are identical in spatial resolution and amount of detail, therefore the following description applies to both cases. Each set of measurements comprised of 15 vertical profiles nearly uniformly distributed

across the river width (Figure 4.2.2). Thus the profiles were separated about 1.25 m apart. Each vertical profile included 11 measuring points uniformly distributed along the water column. In each point three-dimensional velocity vectors were collected by ADVs sampling over a period of 4 minutes at the sampling rate of 25Hz.

Additionally to the measurements of flow velocities the measurements of the riverbed bathymetry and continuous monitoring of the water levels and slopes were carried out. In vegetated channel the distribution of vegetation cover was mapped in a cross-section and the areas upstream and downstream of the section. A set of underwater video-records and photographs with a scaling screen was performed near the vegetation patches of the cross-sections providing information on length, morphology and density of the vegetation.

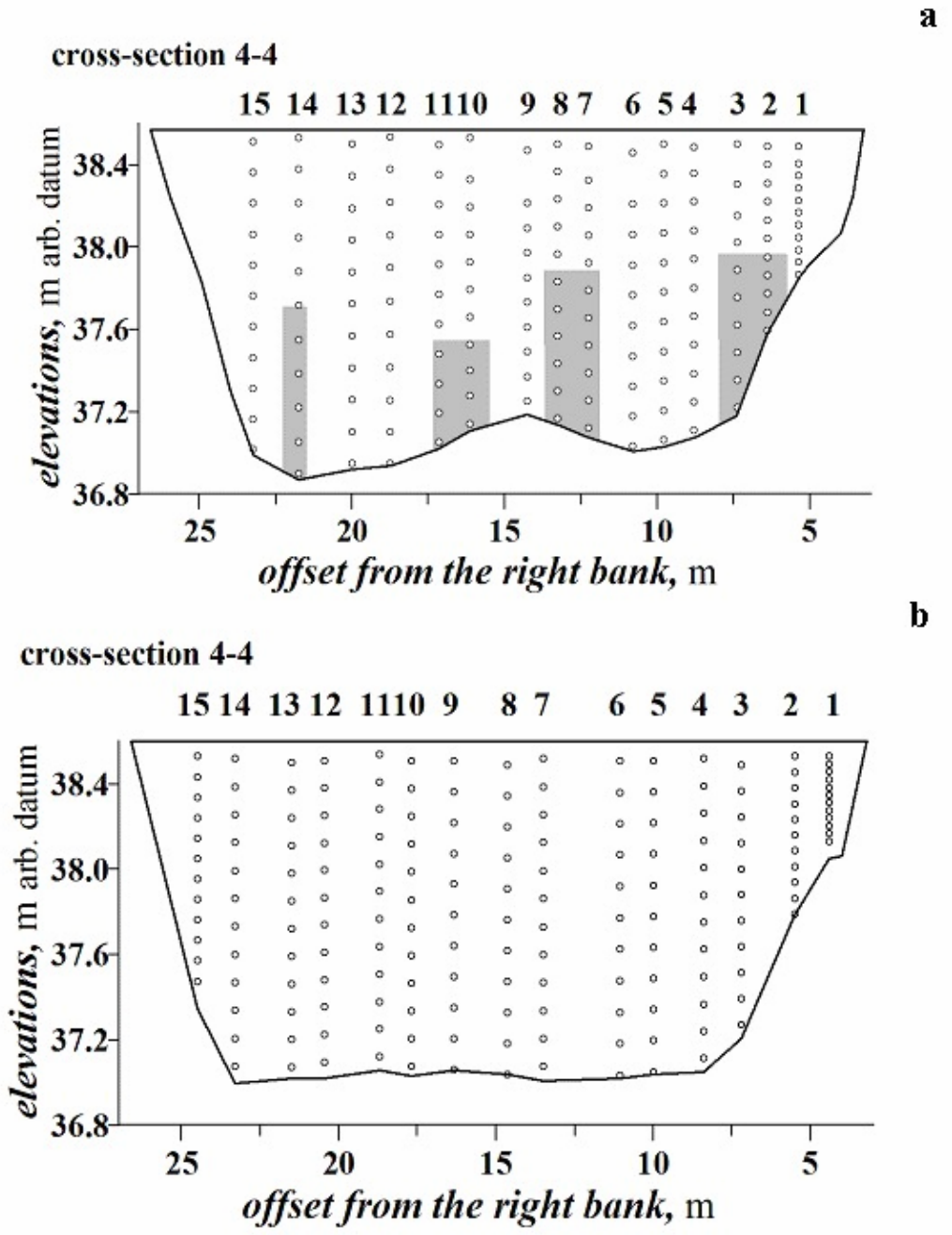

Figure 4.2.2 Distribution of vertical profiles and measuring points in the cross-section of the river in vegetated channel (a), and vegetation-free channel (b). Shadow areas indicate area colonized by plants.

4.2.2 Field measurements: results, comparison, and analysis

This section first examines overall patterns of mean and turbulence characteristics of the flow in the cross-section and qualitatively compares these patterns for vegetation-free and vegetated conditions. Quantitative comparison in frame of the hydrodynamic models of the fluvial channel flow (2.1.24-2.1.35) and the model of analogous mixing layer (2.1.45-2.1.56) were performed for individual vertical profiles. Finally, the conclusions are given in respect to the correspondence between the results of experimental study and measurements using both qualitative comparison and quantitative analysis.

Distributions of time-mean velocities in the experimental cross-section of the Spree River are shown in Figure 4.2.3a and Figure 4.2.4a. In case of vegetation-free flow the distribution exhibits regular and symmetric (relative to the centerline) pattern, Figure 4.2.3a. The velocity maximum appears in the central part closer to the flow surface and gradually reduces towards the riverbed and banks. Maximal gradients are observed in the near bed region. This pattern suggests the applicability of logarithmic law (2.1.29) at least for the central part of the flow. Most probably that close to the banks where the velocity isovels attain steeper vertical slopes, the flow cannot be accurately reproduced by the two-dimensional schematization as the three dimensional effects due to the transversal shear became stronger (2.1.24).

In the vegetated channel in the same cross-section with about the same water level the distribution of time-mean velocities became more inhomogeneous, Figure 4.2.4a. The velocity maximum is reduced almost two times as compared to the vegetation-free flow and its location in the cross-section coincides with the free path in the vegetative mosaic (Figure 4.2.1). Large velocity gradients are observed not only near the riverbed in the free path of the mosaic, but also on the margins of the vegetation patches.

Because of accumulation of fine sediments in the vegetated area and slight scouring in the free path the riverbed geometry was different in these two situations. However, in general these differences in the riverbed geometry seem to be devising the minor effect on the mean flow structures as compared to the primary effect of vegetation.

The turbulent kinetic energy distributions are shown in Figure 4.2.3b and Figure 4.2.4b. In the flow free of vegetation (Figure 4.2.3.b) turbulent kinetic energy pattern is regular, almost symmetrical relative to the central axis of the flow. Kinetic energy is minimal near the free surface of the flow and gradually attains its maximum in the narrow band near the riverbed and banks with a maximum observed in the central part. The distribution in general is a bit asymmetrical in appearance as some isolines are shifted somewhat more toward the riverbed in the left-hand part of the channel. This slight asymmetry is explained by a large scale spatial variation of the flow characteristics on the reach due to the presence of large scale morphological features as starving alternate bars. Regular pattern of flow characteristics suggests that such flow can be relatively easy reproduced by Reynolds average numerical models such as (2.1.8)-(2.1.9).

Distribution of turbulent kinetic energy in the vegetated river (Figure 4.2.4b) is very different from the pattern described above. The domain of the flow appears to be distinctively segmented according to the location of the vegetation patches. Indeed, the zones of maximal turbulent kinetic energy are located approximately on the top margins of the vegetative patches. The flow in the free path of vegetative mosaic (left-hand part of the channel) resembles the unvegetated flow only to a limited extent. The distinctive zone of maximal kinetic energy located exactly on the bed in vegetation-free flow (Figure 4.2.3b) is missing in the free path (Figure 4.2.4b) where the maximal values of energy appear to be shifted upward in the water column. Interesting that regardless of the general reduction of the velocity magnitude about two times, and general reduction of the level of turbulent kinetic energy, the maximal values appear to be as large as in the case of the free flow. This observation indicates the strengths of turbulent organized motions - coherent structures, formed on the interfaces between vegetation and flow.

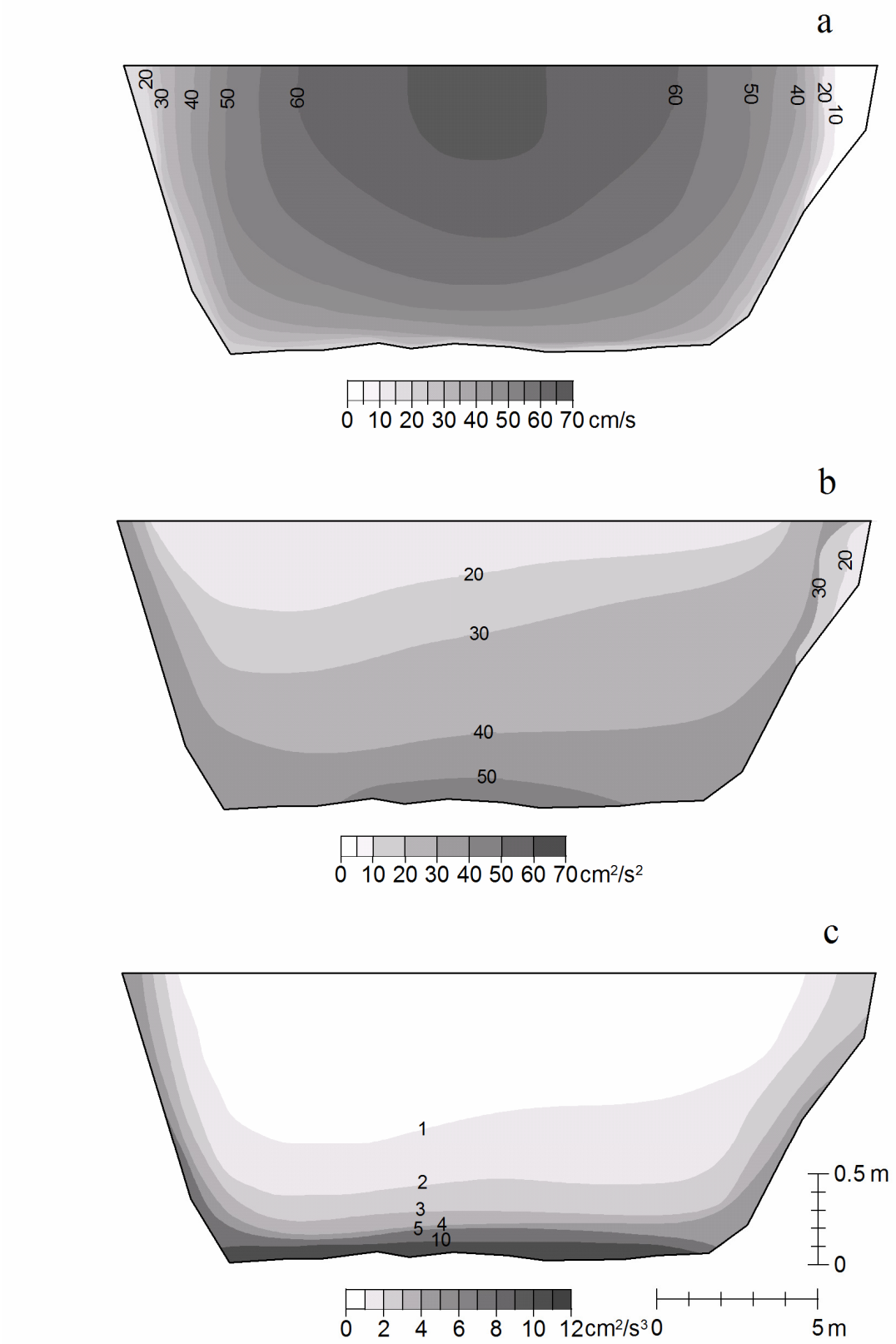

Figure 4.2.3 Distribution of mean streamwise velocity (a), turbulence kinetic energy (b), and dissipation rate (c) in the river cross-section, April 2006.

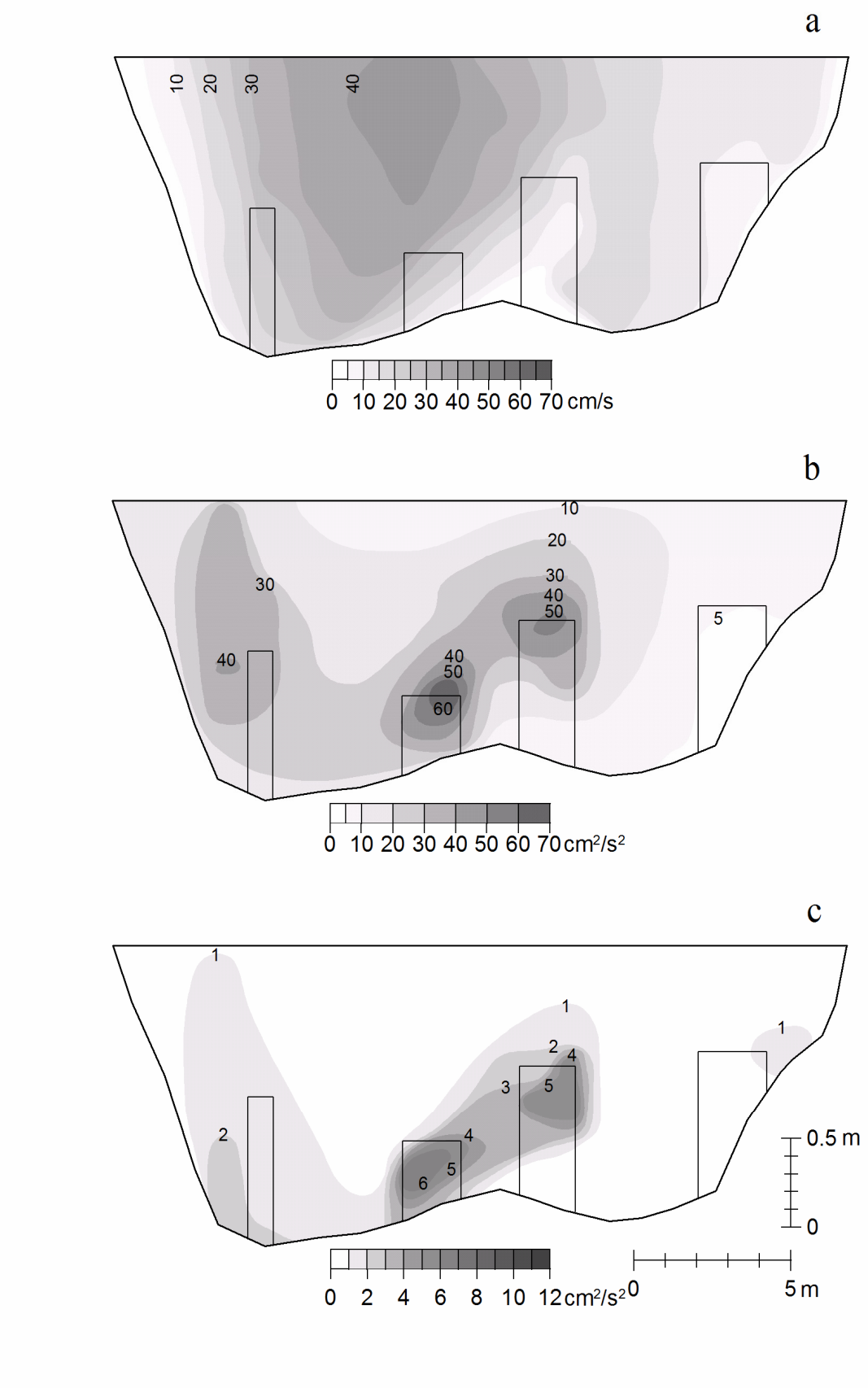

Figure 4.2.4 Distribution of mean streamwise velocity (a), turbulence kinetic energy (b), and dissipation rate (c) in the river cross-section with submerged vegetation, July 2005 (rectangles indicate position and mean deflected height of vegetation).

Patterns of dissipation rates of turbulent kinetic energy are shown in Figure 4.2.3c and Figure 4.2.4c. The values of dissipation rate were computed in accordance with (2.1.68)-(2.1.69) using special interactive tools of the ExploreV software. In the vegetation-free flow (Figure 4.2.3c) the dissipation rate is very small in the central part away from the riverbed and banks. It is gradually increasing to the maximal values which are located in a close proximity to the riverbed and riverbanks. The pattern is almost symmetrical and somewhat identical to the pattern of turbulent kinetic energy. This similarity is indicative of the local equilibrium state in which production of turbulence is balanced by its dissipation (2.1.8).

In the vegetated river cross-section the pattern of dissipation rates is indicating the distinctive segmentation (Figure 4.2.4c). Spatially the zones of maximal dissipation rates coincide with the location of vegetative patches, though in contrast to the zones of kinetic energy they appear to be shifted somewhat downward inside the vegetative patches. The values of maxima are close but somewhat smaller than the corresponding values in the vegetation-free flow. These differences in the locality and magnitudes can be indicative of some deviations from the state of local equilibrium between production of turbulent energy and its dissipation. Some additional terms of balance equation (2.1.8) – (2.1.9), such as advection of turbulence can be significant. As it was anticipated through the experimental studies (Section 4.1), the state of local equilibrium can be attained at some distances (3-4m) downstream from the leading edge of a vegetative patch. Thus, this observation indicates that understanding of flow behavior in the area where flow evolves has important implication for the analysis and interpretation of the field measurements. The pattern of dissipation rate in the free path of the vegetation mosaic is characterized by significantly decreased values and absence of the distinctive maximum near the river bed.

Turbulence characteristics discussed in this subsection have provided general overview of the flow and depicted the transformations imposed by the vegetation cover. Deeper insight into the kinematic structure of the flow can be obtained by examining spatial distributions of turbulent fluxes of momentum represented by different components of the Reynolds stress tensor. The patterns of the Reynolds stress tensor components in the cross-section of vegetation-free flow and flow with vegetation are shown in Figure 4.2.5 and Figure 4.2.6 respectively.

Distribution of $-\overline{u'w'}$ component is presented in Figure 4.2.5a and Figure 4.2.6a. In unvegetated river section the distribution of stresses exhibits very regular pattern (Figure 4.2.5a). The maximal values of $-\overline{u'w'}$ are observed near the riverbed and gradually, almost uniformly across the channel width, decreasing toward the free surface. The character of the pattern suggests applicability of the simplified model (2.1.26) for the most part of the river cross-section. The exempt are the areas in vicinity to the riverbanks that is explained by additional three-dimensional effects that are accounted by the complete model (2.1.24).

In the vegetated channel the areas of maximal shear stress $-\overline{u'w'}$ are located at the upper layers of vegetation patches (Figure 4.2.6a). The absolute values of maximal stresses there appear to be even somewhat larger than those generated by the bed friction in vegetation-free flow. Moreover, the stresses distribution inside the densest vegetative patch is characterized by a region of negative values indicative of enhanced turbulent flux toward the river bed that can substantially increase the sedimentation processes. Apparently the data in Figure 4.2.6a demonstrate dominance of the vegetation-induced shear against the bed-generated shear.

The transversal Reynolds stresses components $-\overline{u'v'}$ are shown in Figure 4.2.5b and Figure 4.2.6b respectively for flows without and with vegetation. A distinctive feature demonstrated already by the pattern of $-\overline{u'v'}$ is the strict symmetry in respect to the central axis of the channel. The central part of the river, approximately 1/3 of the river width, is demarcated by zero values of the transversal fluxes of momentum.

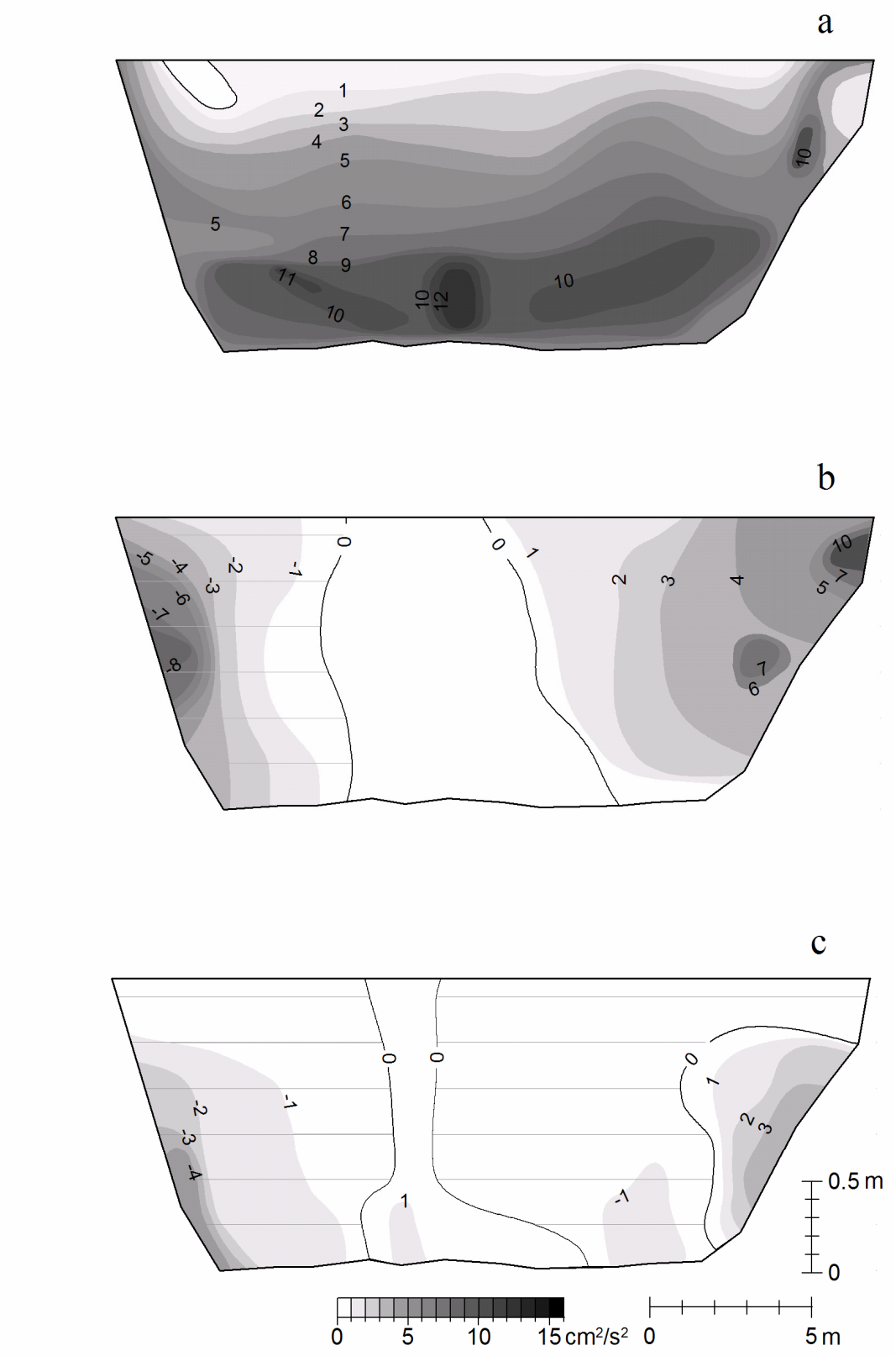

Figure 4.2.5 Distribution of turbulent stresses $-\overline{u'w'}$ (a), $-\overline{u'v'}$ (b), and $-\overline{v'w'}$ (c) in the river cross-section, April 2006.

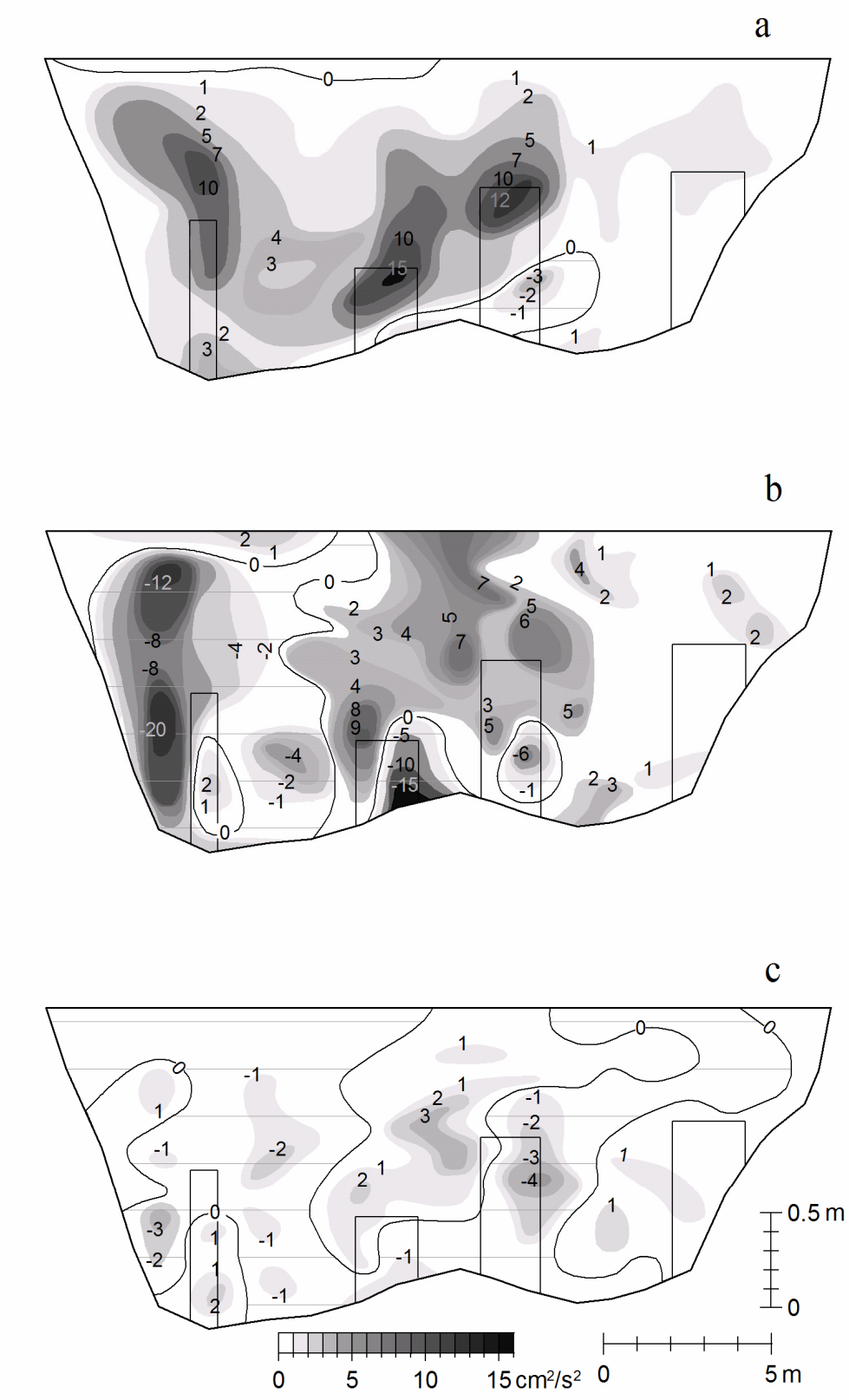

Figure 4.2.6 Distribution of turbulent stresses $-\overline{u'w'}$ (a), $-\overline{u'v'}$ (b), and $-\overline{v'w'}$ (c) in the river cross-section with submerged vegetation, July 2005 (rectangles indicate position and mean deflected height of vegetation).

Because of specific definition of the coordinate system (Figure 2.1.2), the values of stress take negative sign on the left part of the channel. The maxima of the transverse shear stresses are located at the banks of the channel and are distributed nearly uniformly over the river depth. They gradually decrease to zero on the border of the central section. The magnitude of the maxima is close to the values generated by $-\overline{u'w'}$ components. Thus the distributions in Figure 4.2.5a,b provide insight into relative importance of terms in equation (2.1.24).

Essentially different distribution of the transverse shear stresses $-\overline{u'v'}$ is observed in the river channel with vegetation (Figure 4.2.6b). In this case the zones of maximal stresses are observed on the sides of vegetation patches, and hence are indicative of transverse (horizontal) shear layers formed by the patches. The magnitude of those maxima of the transverse shear stresses is about two times smaller than the correspondent values of $-\overline{u'w'}$ component over the same patches (Figure 4.2.6a). The spatial scales of the zones with distinctive transverse shear are much smaller as compared to the unvegetated conditions (Figure 4.2.5b) where they can attain almost 1/3 of the river width. In vegetated channel their size corresponds to the spatial scale of the vegetation patches and free paths.

The distributions of $-\overline{v'w'}$ are shown in Figure 4.2.5c and Figure 4.2.6c. In the unvegetated channel they reveal distinctive symmetrical pattern. The maxima appear at the corners of the channel where the riverbed conjugates with the riverbanks. As these components of the Reynolds stress are indicative of the rotational motions, the spatial patterns thus reveal the presence of secondary circulation at the corners as it was demonstrated by laboratory and numerical computations for the open-channel flows (Nezu and Nakagawa 1993). In general, however, the values of this component are much smaller (1/4-1/3) than other component of Reynolds stress.

In the vegetated channel the spatial distribution of $-\overline{v'w'}$ component is clearly aligned with the spatial distribution of the vegetative patches (Figure 4.2.6c). The zones of maximal stress are located at the sides of the vegetative patches indicating that secondary circulations are promoted at the interfaces between the vegetation and the free paths in the vegetation mosaic. These secondary currents are of a great importance for mixing and transport processes because they are primarily responsible for mechanical dispersion of substances in the vegetation mosaics.

To summarize the overview of the measurements we should point out that the obtained results, as indicated by the patterns of mean flow and turbulence, agree with the qualitative predictions of available theoretical schemes. Therefore at this point we can pass from the qualitative analysis and comparison to more rigorous quantitative examination.

The vertical profiles of flow characteristics measured in the flow without vegetation and in the vegetation-free paths of the mosaic were analyzed using the theoretical framework described in the Section 2.1.2, equations (2.1.24)-(2.1.35). Parameters of the theoretical models deduced from the experimental profiles are summarized in Table 4.2.2. Theoretical framework of the analogous shear layers (Section 2.1.3) expanded through completed theoretical analysis (Section 4.1) served for the data analysis of vertical profiles measured inside the vegetation patches of the mosaic. The results of this analysis are summarized in Table 4.2.3

The generalization of the vertical profiles was achieved by scaling the experimental data and further subdivision of the data set into certain categories according to the models and the degree of correspondence between measured and modeled data. The distributions of mean streamwise velocities over the flow depths in flow without vegetation are presented in Figure 4.2.7. The profiles measured in the central part of the flow without vegetation (Figure 4.2.7c) are perfectly described by logarithmic law (2.1.29) with the universal von Karman constant 0.41 (Table 4.2.2), the value reported for many laboratory studies. Systematic deviations of measured data from equation (2.1.29) are pronounced in the upper layer of the flow $0.7 < z/h < 1.0$ for verticals located close to the riverbanks, Figure 4.2.7a, b (Table 4.2.2).

Table 4.2.2 Parameterization of velocity and turbulence profiles measured in the river cross-section without vegetation and in the free paths between vegetation patches.

NN	$\frac{2y}{B}$	$\bar{u}$, cm/s	u_*, cm/s	k	z_0, cm	c_f	h, m	n, s/m$^{1/3}$
				vegetation free flow (19.04.06)				
1	0.90	7.1	2.71	0.41	4.13	0.291	0.52	0.081
2	0.80	34.7	2.04	0.41	1.07	0.007	0.85	0.023
3	0.66	40.1	2.00	0.41	1.29	0.005	1.43	0.028
4	0.56	44.6	3.98	0.41	0.42	0.016	1.52	0.026
5	0.42	49.0	4.56	0.41	0.44	0.017	1.60	0.025
6	0.33	51.0	4.56	0.41	0.45	0.016	1.62	0.024
7	0.12	51.6	3.55	0.41	0.11	0.009	1.56	0.023
8	0.02	54.8	3.26	0.41	0.04	0.007	1.60	0.022
9	-0.12	55.7	3.88	0.41	0.11	0.010	1.58	0.022
10	-0.24	52.5	3.50	0.41	0.08	0.009	1.55	0.023
11	-0.32	52.1	4.01	0.41	0.21	0.012	1.52	0.023
12	-0.47	50.0	3.67	0.41	0.16	0.011	1.56	0.024
13	-0.56	47.1	3.55	0.41	0.17	0.011	1.56	0.025
14	-0.72	42.5	3.52	0.41	0.30	0.014	1.58	0.029
15	-0.82	32.4	3.14	0.41	0.58	0.019	1.23	0.032
				flow in free paths of vegetation mosaic (15.07.05)				
1	0.81	15.5	1.50	0.41	0.28	0.019	0.74	0.047
4	0.52	12.4	1.56	0.41	3.46	0.032	1.50	0.095
5	0.44	14.5	1.71	0.41	2.67	0.028	1.54	0.082
6	0.35	17.2	1.55	0.41	0.71	0.016	1.57	0.070
9	0.05	24.0	3.40	0.41	2.67	0.040	1.39	0.046
12	-0.33	34.2	2.20	0.41	0.10	0.010	1.63	0.036
13	-0.44	31.7	2.69	0.41	0.38	0.014	1.65	0.039
15	-0.71	15.5	4.47	0.41	18.0	0.166	1.59	0.078

Table 4.2.3 Parameterization of mean velocity and turbulence vertical profiles measured inside the vegetation patches.

NN	$\frac{2y}{B}$	u_c cm/s	Δu, cm/s	δ, m	c_f	h_v, m	h, m	n, $s/m^{1/3}$
2	0.73	7.9	8.8	0.62	0.032	0.56	1.00	0.113
3	0.64	10.5	4.3	1.00	0.018	0.98	1.39	0.106
7	0.22	17.5	15.0	0.48	0.078	0.84	1.51	0.067
8	0.14	16.9	29.0	0.82	0.070	0.69	1.43	0.067
10	-0.11	25.5	27.0	0.73	0.046	0.42	1.47	0.045
11	-0.19	29.4	26.5	0.42	0.028	0.32	1.55	0.041
14	-0.58	28.0	11.5	1.21	0.018	1.01	1.70	0.046

The distributions of normalized shear stress $-\overline{u'w'}/u_*^2$ in accordance with (2.1.26) are shown in Figure 4.2.8. Similarly to the mean velocity profiles the shear stresses agree with theoretical predictions in the central part and are scattered more in the area close to the banks.

Measurements completed in the free paths of the vegetative mosaic (Figure 4.2.9a,b, and Figure 4.2.10a,b) also exhibit general agreement with logarithmic law (2.1.29), but indicate a greater scatter and some specific deviations. The deviations are pronounced in the free path formed behind an upstream vegetation patch in the right-hand part of the channel (Figure 4.2.1). The maximum of the shear stress appears to be shifted to the mid-depth of the flow (Figure 4.2.10b). A smaller secondary maximum can be observed near the riverbed indicating a characteristic profile of internal boundary layer. Obviously, this internal boundary layer develops behind the vegetation patch and is also pronounced in the mean velocity profile (Figure 4.2.9b). Thus the results of this measurement study confirm the applicability of the same open-channel flow model (2.1.25), (2.1.29) to characterize flow in free paths of the vegetative mosaic.

The comparison of vertical profiles for streamwise velocities measured inside the vegetation patches and their approximation with hyperbolic tangent function (2.1.51) are shown in Figure 4.2.9c. The data again reveal an agreement between measured and predicted values, with some evidence for grouping of points respective to the population density of the patch where measurements were taken. Measured shear stresses scaled as suggested in the Section 4.1 $-\overline{u'w'}/\Delta u^2$ are presented in Figure 4.2.10c. They also confirm an agreement with the deduced scaling relationship 4.1.29, though the enlarged scatter in the data is certainly attributed to the spatial non-homogeneity of population density of macrophytes.

Additionally to the parameters of the models, Table 4.2.2 and Table 4.2.3 contain the information on friction factor defined in accordance with (2.4.4-2.4.10), and values of Manning's coefficient of resistance (2.4.6). It appears that in vegetation free flow the values of Manning's coefficient correspond accurately to the values 0.025 usually suggested for natural streams by various literature sources. However, when the flow in free path or in partly blocked path is concerned, the data indicate strong difference in spite of the fact that the correspondent friction factors indicate reasonable agreement. This peculiarity of roughness parameters will be discussed and explained in more detail in the Chapter 7, but here we should point out that the discrepancy in description of flow resistance by those two different parameters reveal the limits of applicability of Manning's parameter for vegetated flow conditions. At the same time we should point out on the agreement between friction coefficients reported for experimental field studies and field measurements.

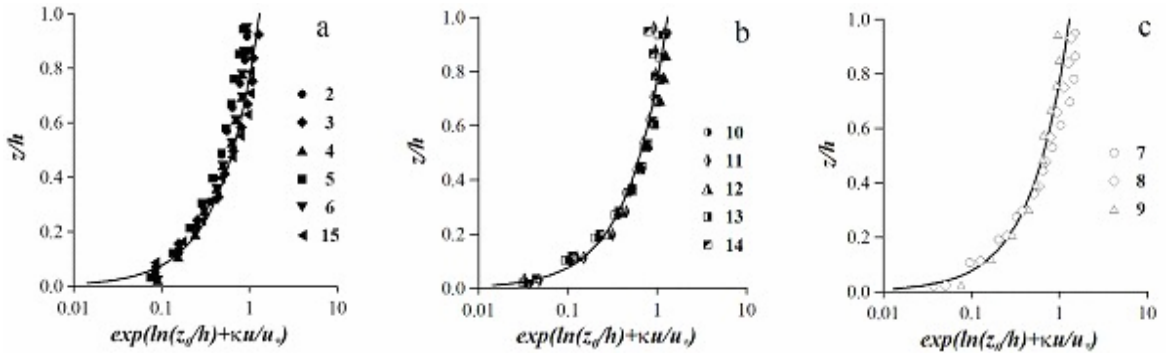

Figure 4.2.7 Vertical distribution of mean normalized streamwise velocity in channel without vegetation: a) in area closer to the banks; b) at the interface between central part and banks; and c) in the central part.

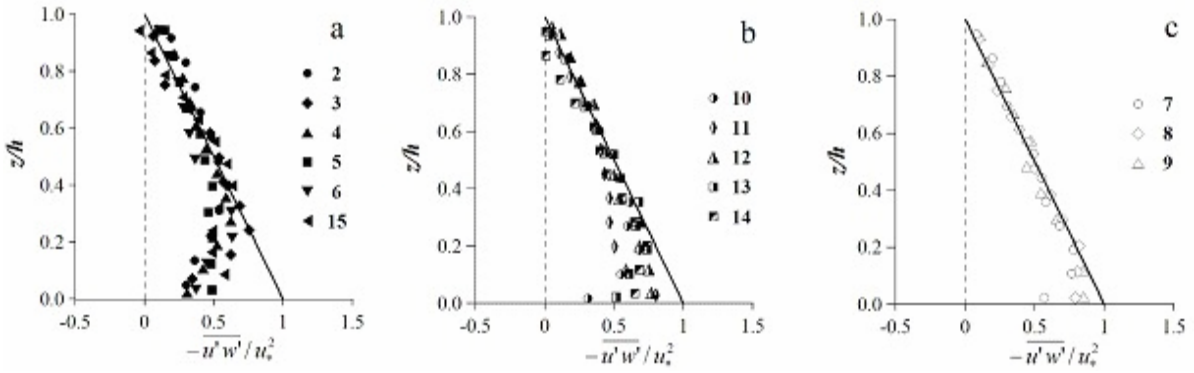

Figure 4.2.8 Vertical distribution of shear stresses in channel without vegetation: a) in area closer to the banks; b) at the interface between central part and banks; and c) in the central part.

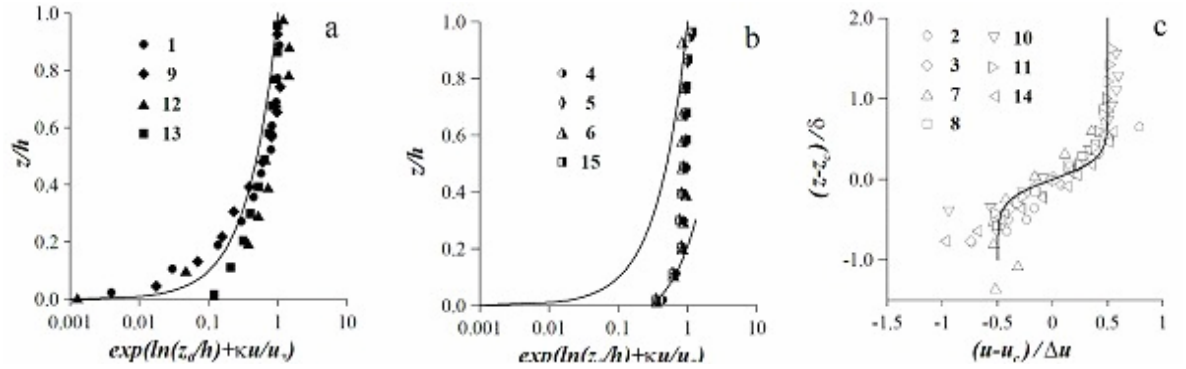

Figure 4.2.9 Vertical distribution of mean normalized streamwise velocity: a) in free paths; b) in partly blocked free paths; and c) inside vegetation patches.

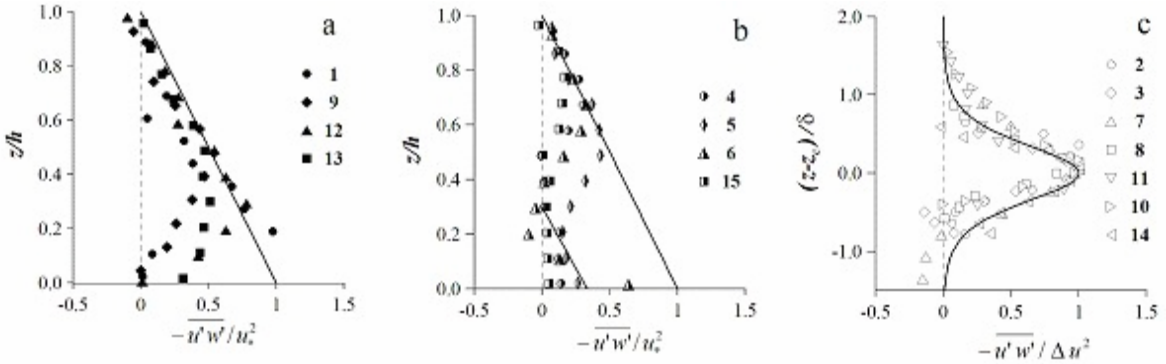

Figure 4.2.10 Vertical distribution of normalized shear stresses: a) in free paths; b) in partly blocked free paths; and c) inside vegetation patches.

4.3 Implications for Transport and Mixing Processes

In this section we summarize the knowledge gained through the theoretical, field experimental works and observations in order to outline implications of flow-plants interactions for transport and mixing processes. This intermediate summary is written to help the understanding of links to other parts of the study, particularly the plants biomechanics and ecology.

Field experiments completed in this study indicate that population density of vegetation plays a crucial role in formation of distinctive hydrodynamics patterns – analogous mixing or boundary layer flows. At sufficiently large population densities (more than 5 plants per square meter with biomass 32 g/m^2 dry weight) the flow can be arranged into analogous mixing layer. At this condition, when the patch is sufficiently long (more than 5 meters in length), a zone of longitudinal exchange can develop, that serves as a dead zone in longitudinal dispersion model. The spatial extent of the longitudinal exchange zone and the rates of exchange in it are dependent on the following factors:

- the deflected height of the vegetation patch;
- the penetration depth of turbulence into the vertical exchange zone;
- population density of vegetation and its drag coefficients;
- the spatial size of a patch.

Deflected height of vegetation is the parameter directly linked to the bio-mechanical properties of plants and their interaction with the flow through the drag force. In this thesis, Chapter 5, Section 5.2.1 we rigorously reconsider the balance of forces and propose a theoretical relationships expressing relations between bending angle, biomechanical properties of plants and flow dynamics. Coupling the proposed hydrodynamical models (4.1.1)-(4.1.17) in the iterative manner provides possibility for prediction of deflected height for the patch of vegetation. The penetration depth in the patch was also shown to depend on the vegetation density and for this study is given in terms of empirical estimates for investigated range of population densities. However, we are confident that it is possible to develop an advanced theoretical model for penetration depth using a combined knowledge on the coherent structures and plants biomechanics. This problem was too immense to explore in frame of this study due to time limitations and is scheduled for further studies.

5 PHENOLOGICAL DYNAMICS OF *SAGITTARIA SAGITTIFOLIA* IN A RIVER

Previous research conducted over the last decade on the Spree River indicates that communities of aquatic plants on the river are dominated by only few species of macrophytes (Schulz et al. 2003). Among them *Sagittaria sagittifolia* – a polymorphic freshwater plant became even most abundant because of its advanced adaptive capabilities. The fact that *Sagittaria sagittifolia* comprised about 80% of the total biomass harvested in the biological monitoring program of this research allows focusing the discussion only on this species. Concentrating on the dominant species in this research allows for more detailed understanding of phenological dynamics of this plant and its consequence for flow-vegetation interactions. In this Chapter we first consider the general features of the individual plants, then we give an overview of the program of field studies and observations, and later the results of field measurements and observation completed during this research project will be presented (Section 5.1). Theoretical approach to the modeling of biomass dynamics and its spatial distribution is described in the Section 5.2, while the implications of these theoretical and experimental studies for transport and mixing processes are discussed in the Section 5.3.

5.1 *Sagittaria sagittifolia*: physiology and ecology

In this Section we present general description of the plant species *Sagittaria sagittifolia*, the program of field studies, and the results of completed field investigations. These materials will serve as the factual basis for the theoretical analysis completed in the following section.

5.1.1 Aquatic macrophyte Sagittaria sagittifolia

Arrowhead (Sagittaria sagittifolia) is a herbaceous perennial plant naturally native throughout temperate regions of Asia and Europe. *Sagittaria* is known by a variety of names, including arrowhead, duck potato, katniss, kuwai, and wapatoo. The plant is highly adoptable in morphology and physiology to changes in the environment.

As all the *Alismaceen*, *Sagittaria sagittifolia* produces generally leaves of two types – linear primary foliage leaves which depending on different environmental conditions can develop into submerged leaves, swimming leaves, or air leaves. Submerged leaves are flexible, usually up to 80 cm long and 2 cm broad (1, 4 Figure 5.1.1), some are reported to grow up to 3m long. The air leaves are rigid, with rectangular or triangular cross-sections (2, 3, Figure 5.1.1) and arrowhead-shaped leaf blade above water level (5, Figure 5.1.1) Flowers (6, Figure 5.1.1) are carried by the rigid inflorescence axis above water surface, in August they develop into seeds (7, Figure 5.1.1). Varieties of forms, different types of leaves enable the plants to tolerate relatively deep flows and large fluctuations of the water level. The plants start to grow in spring underwater and will remain growing when water recedes in summer. *Sagittaria sagittifolia* reproduces by achenes and vegetatively by whole, immature plants and underground tubers (Figure 5.1.2). Seeds float easily and can be carried long distances downstream, and tubers winter in the ground and reproduce during the vegetative period. When washed out of the ground during flood period, the tubers can also float on the surface.

Figure 5.1.1 Leaves of *Sagittaria sagittifolia*

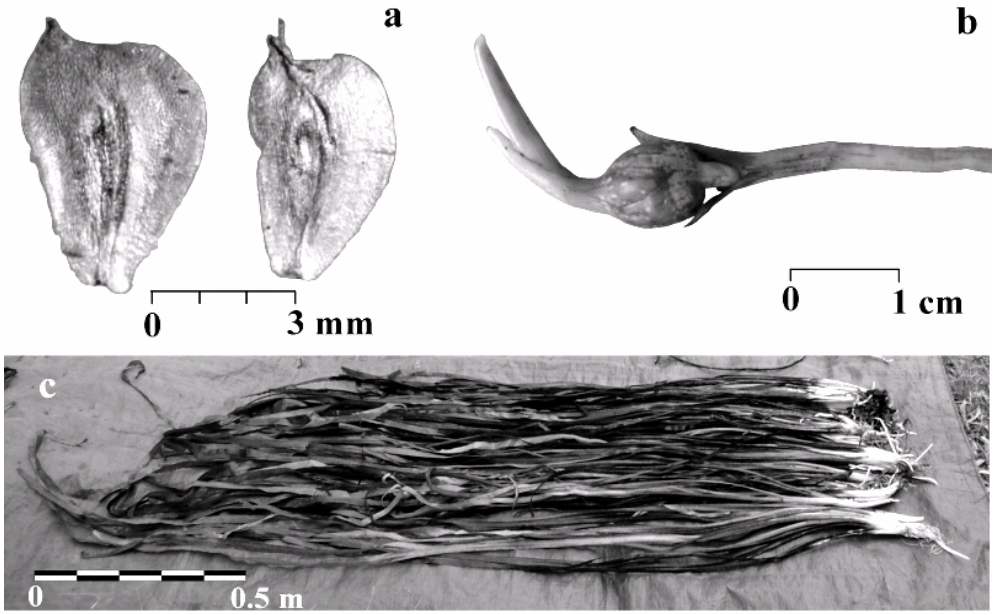

Figure 5.1.2 Seeds (a), tubers (b) and plants (c) of *Sagittaria sagittifolia*

5.1.2 Program of field studies and observations

Field studies and observations for this study were carried out on a representative river reach of the Spree River near the village of Freienbrink (Figure 3.1.1). The field studies were aimed at obtaining the following factual information:

- phenological dynamics of individual plants and its integral representation by biomass;
- seasonal dynamics of vegetative cover of the riverbed;
- biomechanical properties of the individual plants.

A systematic approximately biweekly monitoring survey program for the macrophytes spatial distribution and biomass was completed during spring-autumn 2004. Three additional episodic surveys were performed during summer of 2005 and in August 2006. These additional surveys were carried out during experimental studies of the flow-vegetation interactions (2005), and during the studies of particulate matter resuspension (2006). The study of biomechanical properties was performed in the end of August and beginning of September 2007.

For determination of plants biomass, the plants were harvested in a corridor of 1-m wide across the whole river section, thus making a quadrant size about 1x20 m. The corridor was marked by two rows of topographical sticks and by chains stretched across the river on the bottom (Figure 5.1.3). These marks guided a diver during manual collection of the plants. Plants were harvested with roots which were later separated from stems. The biomass in our study includes only the stems and leaves.

Mapping of the macrophytes patches was performed on the reach about 150 m long equipped with a geodetic base composed of permanent and temporal cross-sections. Seven permanent cross-sections spanned the length of the reach on intervals about 20 long. The sections were fixed at both banks by a pair of metal monuments embedded into concrete pillows. The coordinates of the monuments were measured on an arbitrary coordinate system with a total station. During measurements a marked still tag-line was stretched between monuments, and offsets from monuments to vegetation patches were recorded thus providing the coordinates of the patches. The measurement network was refined by placing additional temporal cross-sections between permanent sections. This system of cross-sections also served as a topographical basis for riverbed surveys.

Figure 5.1.3 Plants harvesting in a cross-section of the river.

The results of the surveys were processed to obtain the spatial distributions of the vegetation patches along the river reach. The spatial distributions were developed by spatial interpolation of the measured coordinates of the patches assisted with additional intermediate drawings and photographs taken during the field surveys. High quality digital maps of the vegetation contours were obtained in the result of the post-processing stage.

The harvested macrophytes were processed in two stages. First they were measured to obtain morphology of the individual plants: the length, and width of the blades, the number of blades, and the diameter of the stem near the roots. The plants were weighted on scales to obtain the wet weight. Later, on the second stage, they were dried in the laboratory and weighted to obtain the dry weight.

The study of biomechanical properties of the plants included harvesting of the macrophytes and their testing. The tests included determination of buoyancy, rigidity, and the surface area of the plants. The buoyancy tests were conducted by means of simple volumetric measurements of the submerged plants. To determine rigidity the cantilever and the loop methods were applied. The area of plants was determined using the digital photographs of the plants fixed on a scaled template surface. In the laboratory the photographs were processed with image-processing software to obtain the surface area of the plants at equidistant height increments from the base of the stems.

5.1.3 Results of field studies and observations

Vegetative period for *Sagittaria sagittifolia* starts on the Spree River in the mid May and continues through the summer and first half of the autumn. Figure 5.1.4 illustrates the characteristic dynamics of individual plants and the biomass growth and decay of *Sagittaria sagittifolia* on the experimental river reach of Spree near the village of Freienbrink. The following important features can be conjectured from these data. First, the leaves of the plants grow relatively fast during the first two-three weeks of the vegetative period and remain practically of the same length till beginning of the autumn. At the same time the leaves number plot (Figure 5.1.4c) indicates an increase during August. This increase can be explained by the observation that in August (also the most low water period) the plants shoot more of the rigid stems carrying air leaves and flowers (3, 5 Figure 5.1.3). This behavior is also confirmed by the plot representing dynamics of the plant diameter near the root which exhibits practically synchronous increase (Figure 5.1.4d).

The specific features of physiology and morphology of the plants have obvious implications for the biomechanical properties of the individual plants. Thus in the beginning of the vegetative period the plants are more streamlined objects that easily reconfigure by the action of flow. This allows plants to sustain considerable physical forces exerted during high flow events. As the flow recedes during the late summer, the plants can maintain more stiff structures that will sustain flow and maintain higher reproduction rates by dispersing seeds. This “intelligent” behavior drastically complicates the interactions between the flow and the plants. The same plant species behave as submerged vegetation with high reconfiguration abilities minimizing resistance during the first phase of vegetative period and later they transform into the rigid emergent vegetation packed densely with the submerged leaves that maximizes resistance and produces considerable backwater effect.

The reasons by which plants form the vegetation patches are apparently obvious. Aquatic forms of the *Sagittaria sagittifolia* plants grow on relatively soft substrates that are suitable for reproduction by the vegetative propagation. Therefore a solitary plant developing from a wintered tuber or a seed will soon produce the child plants in the radius of 10÷20 cm (length of rhizomes). Although a solitary plant produces practically no effect upon the surrounding flow, the neighboring plants maintain mutual sheltering and additional mechanisms of interaction with the flow resulting in the considerable changes of the flow structure.

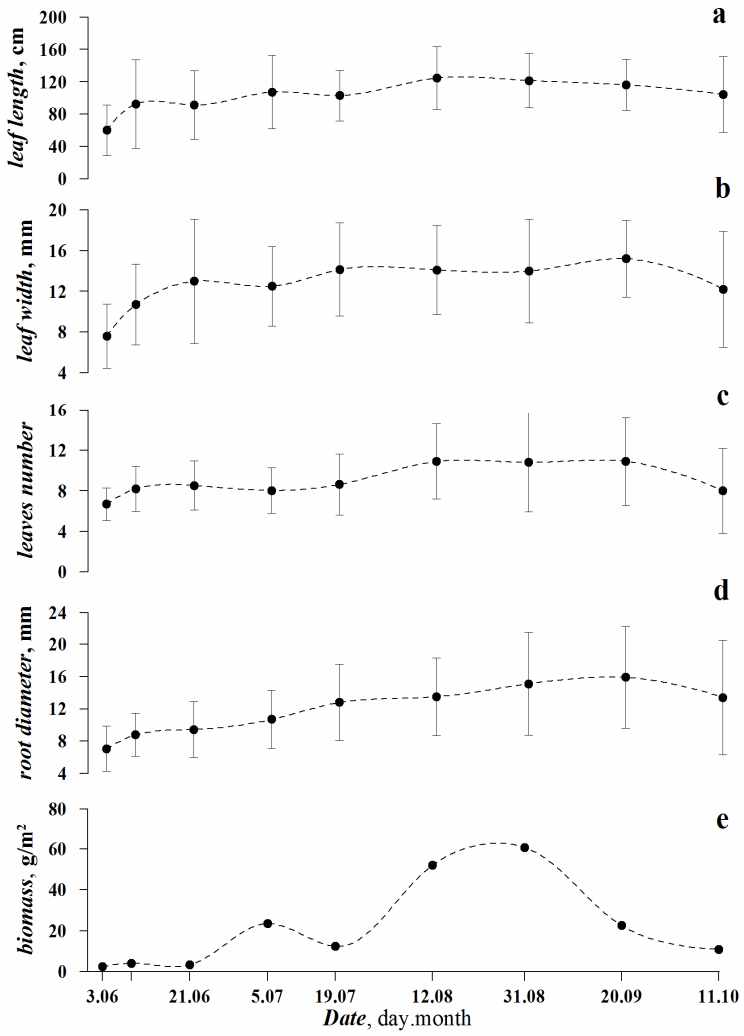

Figure 5.1.4 Dynamics of plants morphology during vegetative period: (a) length of leaves; (b) leaves width; (c) number of leaves; (d) diameter of roots, and (e) biomass (dry weight)

As the flow area became progressively contracted by the growing plants its directions became diverged out of the plants while the magnitude of the flow grows to compensate for the continuity of flow. This causes an enhanced scouring of the riverbed material at the margins of the vegetated areas and limits further spreading by the underground propagation. Therefore at a certain stage of the vegetation development appears a defined pattern of the vegetation distribution composed of relatively uniform units – the vegetation patches.

The dynamics of the vegetative cover can be explored with the successive maps of the area occupied by the plants. To create such maps the data of the systematic biweekly measurements carried out in the permanent cross-sections in the experimental reach near Freienbrink were used, Figure 5.1.5. The patches of vegetation initially appear as the narrow (1÷2m in width), elongated (length up to a 100m) stripes that widen and merge during the vegetative period. It is important to note that density of vegetation inside the strips is very non-uniform. This spatial (mainly lateral) expansion of patches reflects the gradual seasonal reduction of the flow in the river and can be viewed as an adjustment of the plants communities to the varying conditions of the environment.

To provide quantitative assessment of flow-plants interactions on the level of communities requires the joint analysis of changes of the hydraulic variables (discharge, velocity, depth) and characteristics of the vegetation cover (dynamics of area occupied by plants, dynamics of characteristic scales of vegetative patches like transversal and longitudinal extensions, and height).

An example of a vegetative mosaic observed on the experimental reach of the Spree River is shown in Figure 5.1.6. Because of high transparency of water (very low turbidity), and shallowness of the channel (mean depth is comparable with the length of individual plants) the mosaic develops as a dense but incomplete pattern. The reason for incompleteness is the high mobility of the riverbed composed of fine sediments (mean diameter of the sand is 0.6 mm). At the same time one can perceive from the photograph (Figure 5.1.6) that shadowing by the terrestrial vegetation and exposition of the river channel itself are also the factors contributing to the pattern development.

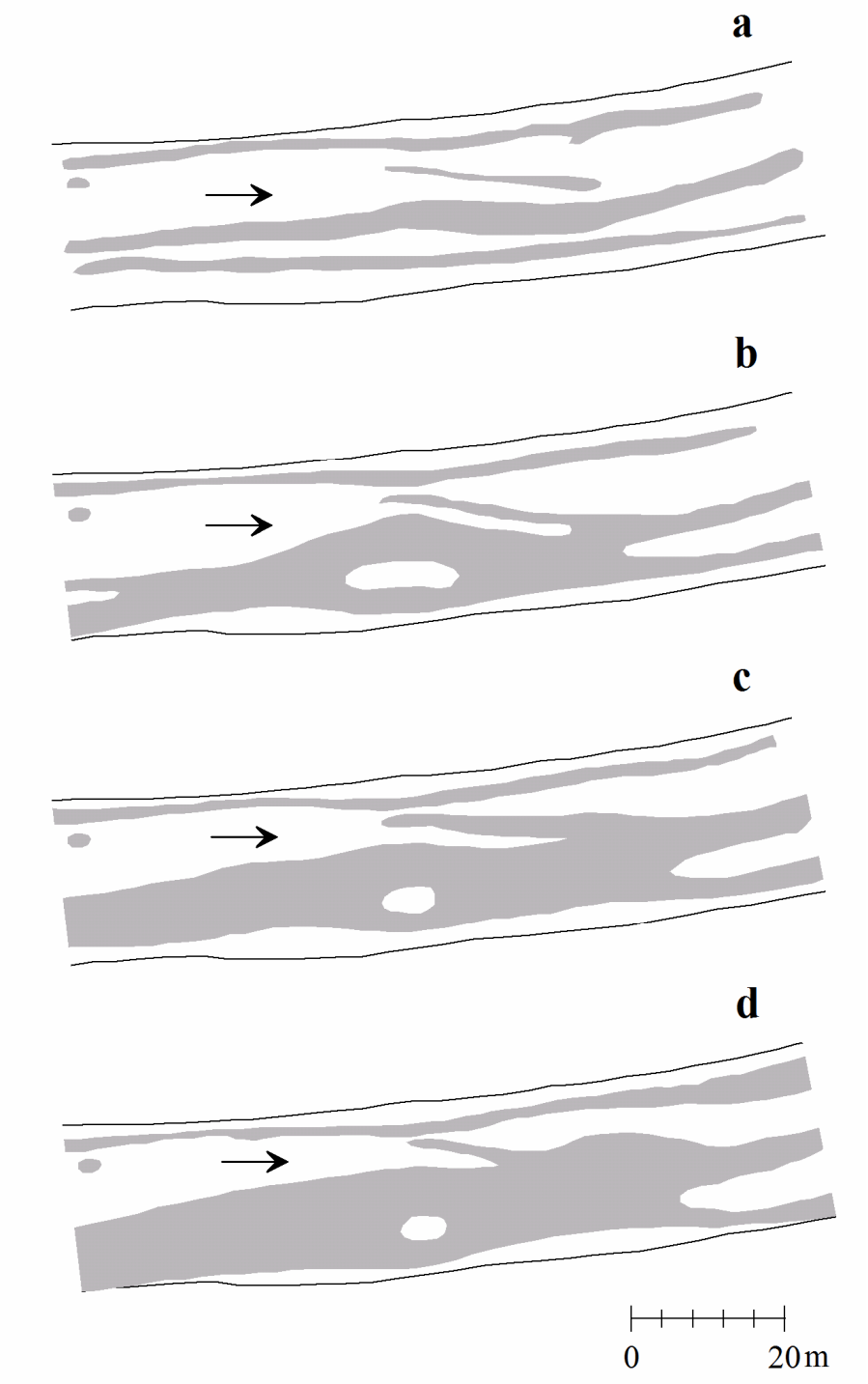

Figure 5.1.5 Growth of the area covered by plants during the vegetative period: (a) 03.06, (b) 21.06, (c) 19.07, and (d) 12.08 (date correspond to biomass sampling in Figure 5.1.4)

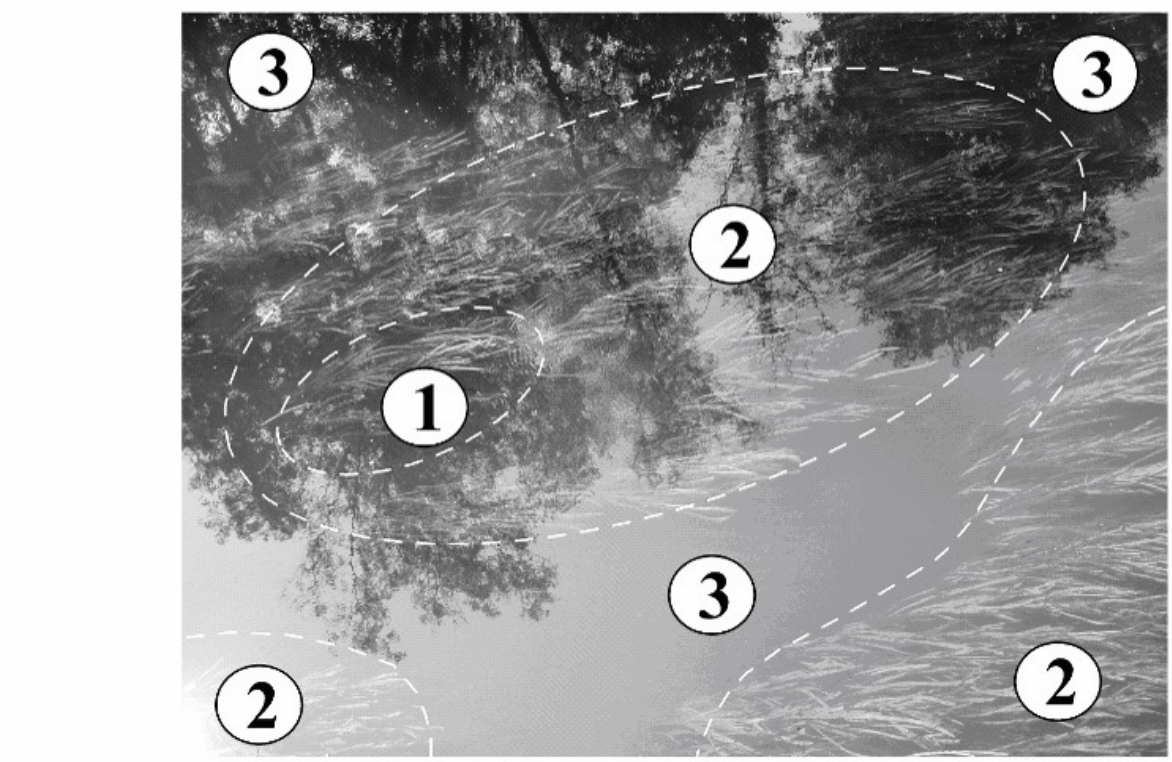

Figure 5.1.6 Characteristic pattern of vegetative mosaic formed by *Sagittaria sagittifolia* in the Spree river (1- individual plant, 2 - vegetative patch, 3 - free path).

Analysis of cross-sectional distributions of vegetation density and the plants morphology (Figure 5.1.7) reveal that the highest densities of vegetative canopies were observed at the riverbanks with the southern exposition (Figure 5.1.7a), the leaves of the plants were also as twice as long in comparison with leaves near the bank with northern exposition (Figure 5.1.7b).

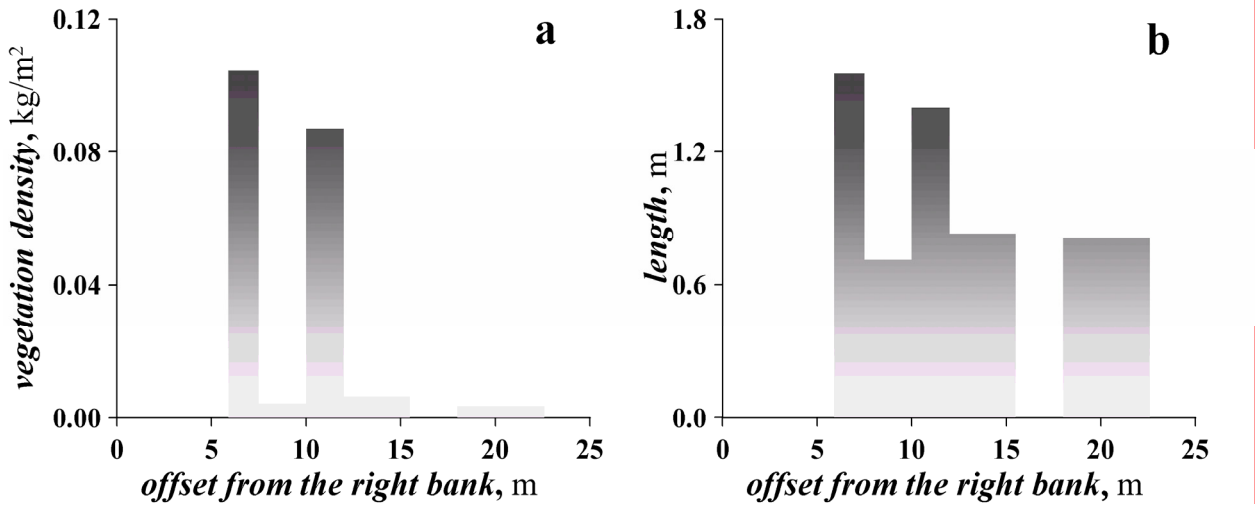

Figure 5.1.7 Distributions of vegetation density and plants morphology across the experimental river reach on the Spree river near Freienbrink.

5.2 Theoretical Analysis of Phenological Cycle of *Sagittaria sagittifolia*

The content of this Section concerns with the theoretical analysis of physical forces acting upon an individual plant of *Sagittaria sagittifolia* (Subsection 5.2.1) and development of the theoretically based model for the biomass growth (Subsection 5.2.2). After construction of the

model for the biomass dynamics the analysis is expanded to the theoretical understanding and comprehending the dynamics of growth of the individual plants and their assemblages – patches and mosaics (Subsection 5.2.3).

5.2.1 Balance of forces acting on individual plant

Let us schematize an individual plant as a flexible cantilever beam of length L. When the beam attains a dynamically stable position, the drag force F_d is counteracted by the buoyancy force F_B and the inner force of the plant F_R due to flexural rigidity of the tissue (Figure 5.2.1).

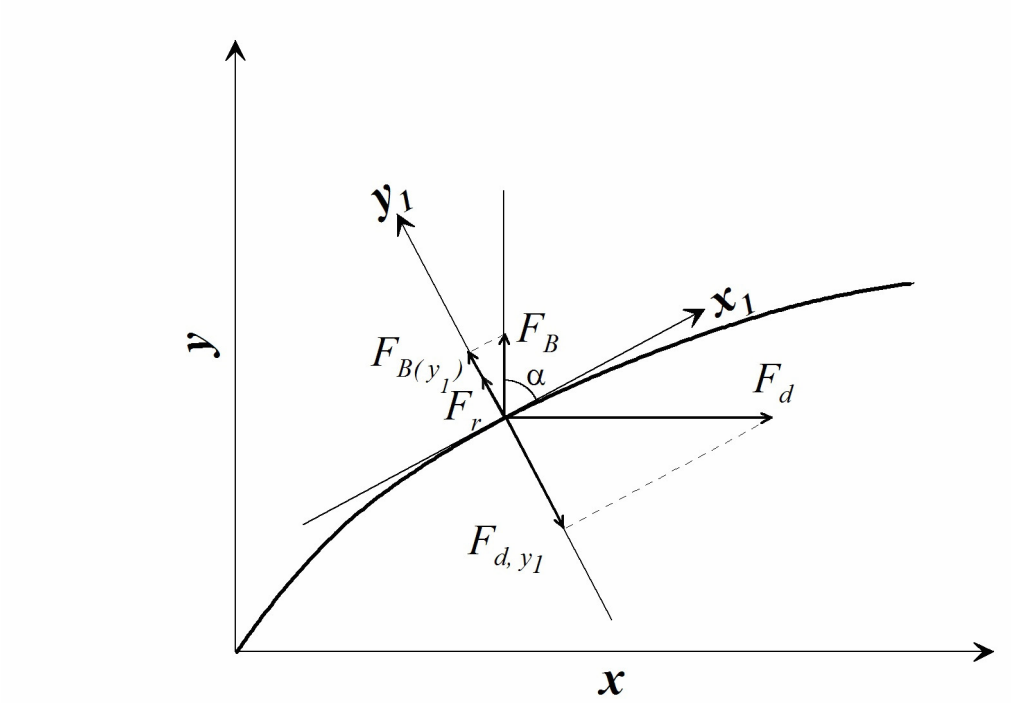

Figure 5.2.1 Balance of forces acting upon a model plant of *Sagittaria sagittifolia.*

Introducing a modified coordinate system in which axis x_1 is directed tangentially to the surface of the model plant, one obtains the balance of forces in dynamically equilibrium state of the plant

$$F_d \cos\alpha = F_B \sin\alpha + F_r \tag{5.2.1}$$

Defining the drag force conventionally as $F_d = 0.5\rho C_D a \overline{u(a)}^2$, where C_D is drag coefficient reflecting the skin and form drag properties of the object, a is the area of the object projection onto the plane perpendicular to the flow, and u is the mean velocity acting on the object. For the model plant deflected by the flow the bending angle determines the projected area in accordance with

$$a = dL\cos\alpha \tag{5.2.2}$$

Respectively the buoyancy force we define as

$$F_B = g\, dL\, d_p\, (\rho - \rho_p) \tag{5.2.3}$$

where d_p is thickness of the plant, and ρ_p is its density. Resistance due to the flexural rigidity for the small deflections ($\alpha < 20°$) is defined as

$$F_r = \frac{3EI_a}{dL^2}\sin\alpha = F_R \sin\alpha: \quad F_R = \frac{3EI_a}{dL^2} \tag{5.2.4}$$

Rearranging (5.2.1) with the terms defined by (5.2.2)-(5.2.4) one obtains

$$0.5\rho C_D\, dL\overline{u(a)}^2 \cos^2\alpha = g\, dL\, d_p\,(\rho - \rho_m)\sin\alpha + \frac{3EI_a}{dL^2}\sin\alpha \tag{5.2.5}$$

which can be further rewritten as

$$\cos^2\alpha - \frac{(F_B + F_R)}{F_d}\sin\alpha = 0 \tag{5.2.6}$$

or simply defining $\phi = 0.5\left(F_B + F_R\right)/F_d$ transforms (5.2.6) into

$$\cos^2\alpha - 2\phi\sin\alpha = 0 \tag{5.2.7}$$

Coefficient ϕ represents the ratio between the sum of buoyancy and rigidity forces, determined by biomechanical properties of the plant, and drag force exerted by the flow. Solutions of quadratic equation (5.2.7) are: $\sin\alpha_{1,2} = \frac{-2\phi \pm \sqrt{4\phi^2+4}}{2} = \pm\sqrt{\phi^2+1} - \phi$. From physical considerations $\sin\alpha$ should be positive, and hence we obtain general solution of (5.2.7) in the following form

$$\sin\alpha = \sqrt{\phi^2+1} - \phi \tag{5.2.8}$$

Further analysis now will concentrate on examining the behaviour of (5.2.8) in the special cases.

Case 1 Let us consider first the plants of considerable rigidity ($F_R \geq F_B$). In this case equation (5.2.8) can be solved for the small deflections $\left(\alpha \leq 20^\circ\right)$ and F_R is determined by (5.2.4). Graphically the relation for special case 1 is shown in Figure 5.2.2.

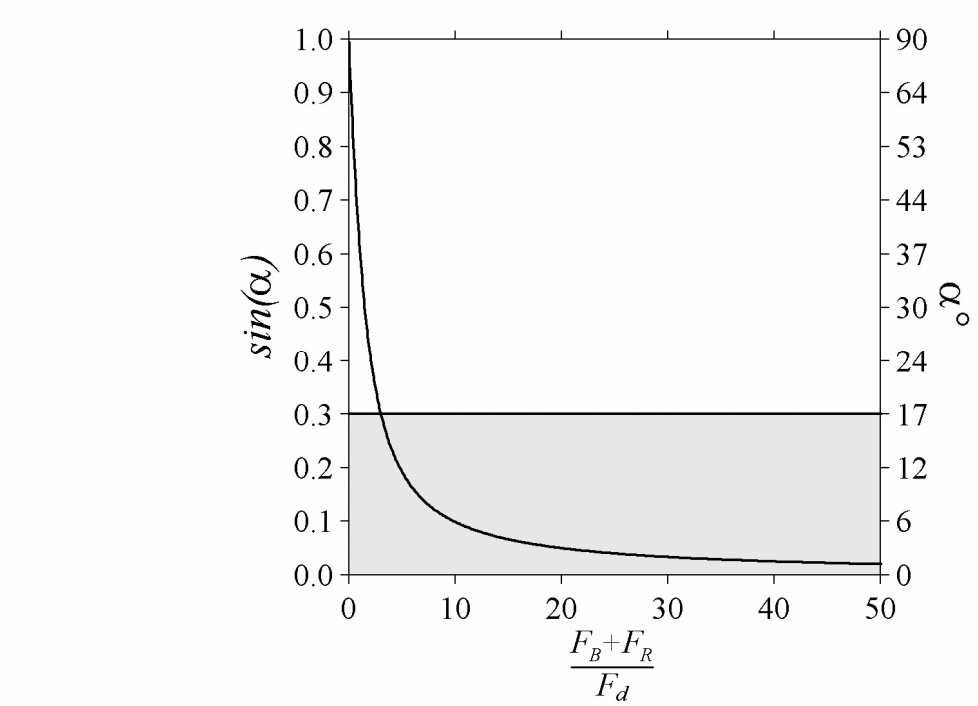

Figure 5.2.2 Deflection angle as a function of ratio of driving forces. The solutions for rigid vegetation are valid at small deflections (shaded area).

Case 2 Now for the highly buoyant flexible plants $F_R << F_B$, coefficient a will be determined as $\phi = 0.5F_B / F_d$ and the solutions of equation (5.2.8) will be valid for all deflection angles. For flexible plants in flowing waters the natural conditions of the environment result in $\phi = 0.5F_B / F_d \le 1$ and $\alpha \ge 30°$ (Sand-Jensen 2003). For these conditions (5.2.8) can be simplified to

$$\sin\alpha = 1 - \phi \qquad (5.2.9)$$

Functions (5.2.8) and (5.2.9) solved for flexible plants deflected to the angles larger than 30° from vertical are presented in Figure 5.2.3.

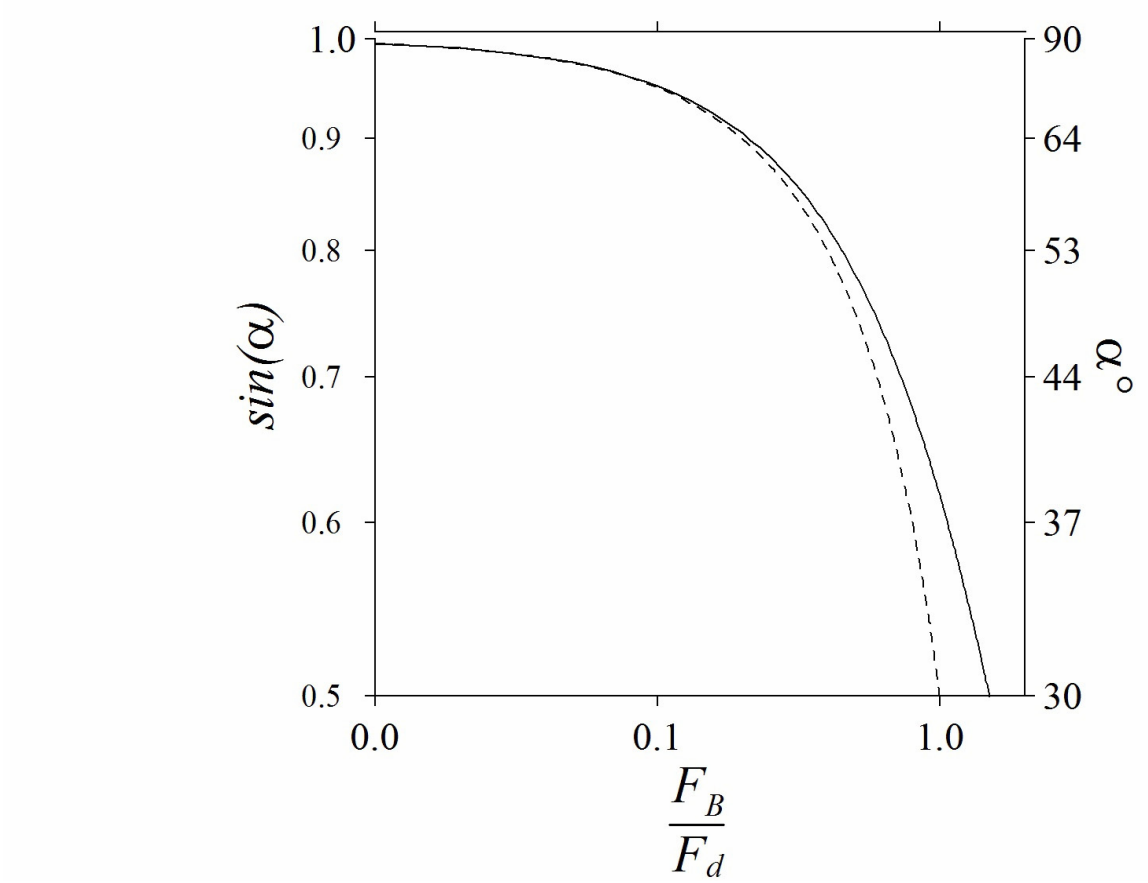

Figure 5.2.3 Deflection angle as a function of ratio of forces for flexible plants, solid line corresponds to (5.2.8), and dashed line to (5.2.9).

The ratio of buoyancy to the drag force $\phi = g\,d_p\left(1-\rho_m/\rho\right)/C_D\,\overline{u(a)}^2$ depends on the drag coefficient, velocity squared, the thickness and density of the plants. For large deflection angles the plants became streamlined and respectively the dependence of the drag on Reynolds number can be neglected. As a consequence, the ratio ϕ will depend only on the velocity squared as $\phi = b\bar{u}^{-2}$, where $b = g\,d_p\left(1-\rho_m/\rho\right)/C_D$ can be considered as a constant for the given flexible species for large deflection angles. Comparison of the measured and predicted angles of deflection for our experimental study (Chapter 4, Section 4.1) is presented in Table 5.2.1 ($C_D = 0.5$).One can see that for our experiments the buoyancy exceeds the rigidity forces by the factor of 8 times that explains applicability of the theoretical approach described in the Case 2, equation (5.2.9). A perfect agreement between predicted and measured data confirms applicability of the developed theory to the analysis of our experimental data set.

Table 5.2.1 Parameters of the forces balance for the experimental runs.

Run	F_r, N×10^6	F_B, N×10^6	b, m^2/s^2	u, m/s	ϕ	$\sin\alpha$ / α°	
						predicted	measured
1	4.78	39.0	0.004	0.16	0.193	0.825 56°	0.832 55°
2	4.78	39.0	0.004	0.19	0.077	0.925 68°	0.912 66°
3	4.78	39.0	0.004	0.20	0.069	0.932 69°	0.925 67°

Although results of our experimental study agree with the theoretical prediction by model (5.2.8), the rigorous examination requires more measured data with the different ratios between buoyancy and rigidity. Unfortunately, data on the density and rigidity of the aquatic plants are scarce to find in the literature. However, recently some studies on bending of the macrophytes have been performed by Carollo et al. (2005) and O'Hare et al. (2007). Characteristic for the vegetative species scaling parameter b can be determined from the deflection angle dependence on the flow velocity. With this approach the data from the literature sources together with our own data are summarized in Table 5.2.2.

Table 5.2.2 Estimates of parameter b from published data.

Source	Vegetative species	Symbol	b, m^2/s^2	r^2
O'Hare et al. 2007	*S. emersum*	●	0.0039	0.98
	R. pseudofluitans	▲	0.0025	0.96
	C. stagnalis	■	0.0007	0.99
	M. spicatum	◆	0.0010	1.00
	P. x zizii	★	0.0008	0.99
Carollo et al. 2005	grass mixture			
	Run1	✳	0.0192	0.99
	Run2	×	0.0218	0.99
	Run3	✲	0.0276	0.69
Present study	*S. Sagittifoliq* calculated fitted	○	 0.0028 0.0026	0.90

The deflection angles as the functions of flow velocities, scaled with the parameter b are shown in Figure 5.2.4. It should be noted that because literature sources (Table 5.2.2) do not provide information on the density and the rigidity of plants tissue, parameter b was estimated cumulatively and includes the impact of the rigidity. Relatively high values of b for the grass mixture (experiments of Carollo et al. 2005), *S. emersum* and *R. pseudofluitans* (O'Hare et al. 2007) possibly appear due to the higher rigidity and the fact that the rigidity impact became more pronounced for the smaller velocities. This effect is most probably captured by the two outlying points of *S. emersum* and *R. pseudofluitans,* Figure 5.2.4.

Theoretical analysis completed in this section yielded the theoretical model (5.2.8) describing interactions of the individual plants with the flow. Comparison of the theoretical predictions with the experimental observations of present study and some data gathered from the literature sources confirms the applicability of the model. The model is capable of description for the different plants species – rigid and buoyant and contrary to the previous empirical approaches (Sand-Jensen 2003), that suffered dimensional problems (Sukhodolov 2005; Green 2005; Statzner et al. 2006), provides physically tractable framework describing the reconfiguration

properties of the flexible freshwater macrophytes. Obtained solution is of a great importance for determination of the height of submerged vegetative patches for certain species of vegetation at a certain flow situation represented by the bulk flow velocity.

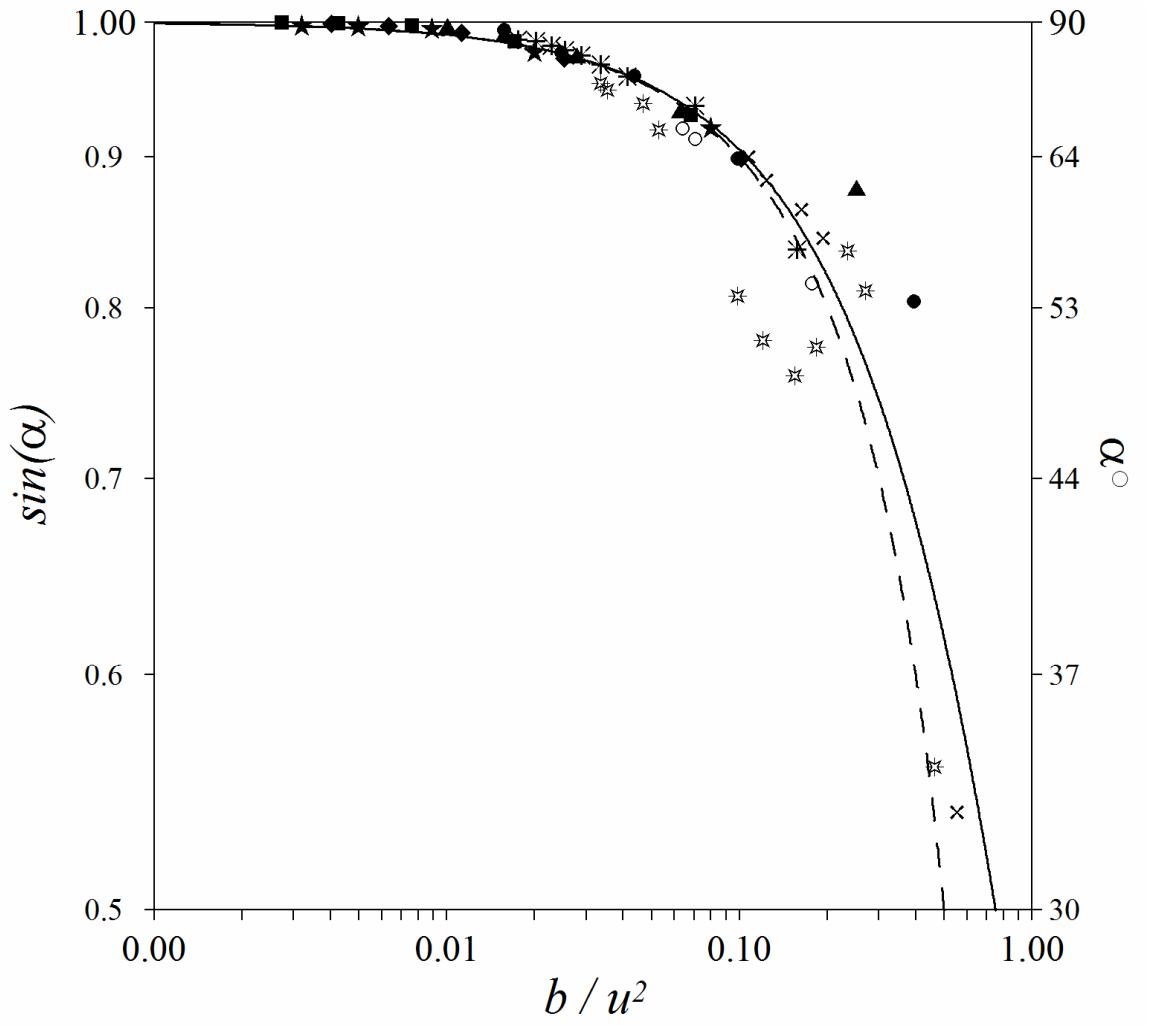

Figure 5.2.4 Deflection angle as a function of flow velocity, solid line corresponds to (5.2.8), and dashed line to (5.2.9), symbols explanation is presented in Table 5.2.2.

5.2.2 Biomass growth and senescence

As it was anticipated in the previous chapters, the development of the aquatic plants depends on a number of environmental quantities: solar irradiance, water temperature, nutrient concentration in the water column and sediments, and the flow velocity. Obviously, the solar irradiance is one of principal variables because of its value for the photosynthesis. In fact water temperature can be perceived as an integral parameter representative for the solar irradiance, and hence as a primary driving parameter of the system. The relation between water temperature and the solar irradiance is illustrated in Figure 5.2.5.

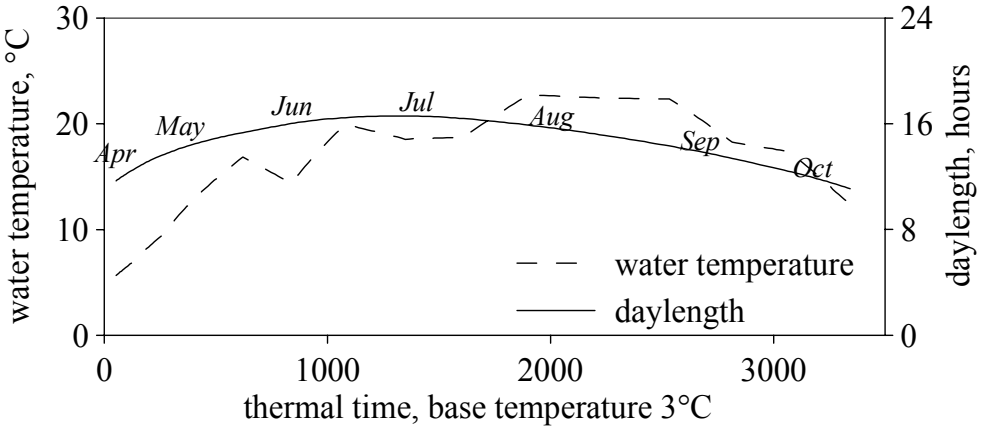

Figure 5.2.5 Water temperature and day length as function of thermal time.

In this plot we use the thermal time with a base temperature of 3°C, equation (2.3.25). The observations of the phenological cycle of *Sagittaria sagittifolia* together with the data on water temperature were used here to obtain the characteristic threshold values for the phenological stages (Table 5.2.3).

Table 5.2.3 Phenological cycles of *Saggittaria sagittifolia* (field data, the Spree River, 2004) and *Vallisneria americana* (Best et al. 2001)

Developmental phase	*Saggittaria sagittifolia*		*Vallisneria americana*	
	Julian day	day-degree 3°C	Julian day	day-degree 3°C
tuber sprouting	65-119	1-260	0-105	1-270
leaf expansion and maturation	119-230	260-2047	106-227	271-2072
max biomass	230	2047	227	2072
senescence	231-323	2050-≈3100	228-365	2073-3167
senesced	323	≈3100	365	3167

In Table 5.2.3 is also presented the phenological cycle of *Vallisneria americana* (Best et al. 2001) for the comparison. The obtained phenological classification establishes a background for modeling the seasonal dynamics of the vegetation cover. Noteworthy, that data in Table 5.3 indicate very similar characteristics. Indeed aquatic form of *Saggittaria sagittifolia* exhibits striking similarity in plant morphology with *Vallisneria americana.* The similarity of phenological cycle most probably indicate the similarity of environmental conditions and life struggling adaptation mechanisms developing by different plants that allow for optimal functioning of the individual plants.

Within the life cycle of a plant the total growth duration can be divided into the three sub-phases: an earlier accelerating phase, a linear phase and a saturation phase for ripening (Goudrian and von Laar 1994). For the aquatic plants these phases are followed by a decay and a wash-out. In the earlier phases of the plants growth, the classical exponential model with constant relative growth rate, equation (2.3.13) has to be an asymptote. Respectively, the net relative growth rate (NRGR) should fulfill the demands summarized in the Table 5.2.4.

Table 5.2.4 Net relative growth rates corresponding to the phases of the plants development.

Developmental phase	biomass	NRGR
leaf expansion: accelerative	exponential growth	constant (positive)
leaf expansion: linear	linear growth	decrease
maximum biomass	maximum	0
beginning of senescence	linear decline	decrease
senescence, wash-out	exponential decline	constant (negative)

Now, assuming symmetry of biomass curve relative to its maximum, we can conclude on equality of the relative growth rates values for the growth and decay parts of the curve. The behaviour of such curve and its characteristics is best represented (from a mathematical point of view) by a hyperbolic tangent function. Indeed, the inflection point of the hyperbolic tangent function corresponds to the argument value of zero. Thus, the thermal time of the maximum biomass $T_{B\max}$ can be used to normalize the thermal time values. To avoid the thermal time dimension day*°C under hyperbolic tangent thermal time $T_B = T - T_{\max}$ should be normalised by the maximum relative growth rate $R_{\max}$, then the function for relative growth rate is

$$\frac{1}{B}\frac{dB}{dT} = -R_{B\max}\tanh\left(T_B R_{B\max}\right) \tag{5.2.10}$$

Integration equation (5.2.10) for the normalized thermal times provides a solution

$$B = B_{\max}\sec h\left(T_B R_{B\max}\right) \tag{5.2.11}$$

To be justified theoretically equation (5.2.11) must meet the following conditions (Birch 1999):

- the function must express the exponential dependence at the small sizes or low densities;
- the function has to be suitable for estimating the maximum relative growth rate which is an important role of the growth models.

As we can see both conditions are fulfilled in the case of the proposed hyperbolic secant function (5.2.11). It tends to the exponential function at low biomass density, and allows estimation of the maximum relative growth rates. To verify the proposed model (5.2.11) we will perform its comparison with the observed data (Figure 5.1.4) and the following theoretical (exponential and Verhulst logistic function, and the model (2.3.22) by Werker and Jaggard 1997) and empirical exponential function (2.3.23) proposed by Wilson et al. (2007). The results of the biomass curve modelling are presented in Figure 5.2.6 and Table 5.2.5.

Available theoretical growth models (Figure 5.2.6 and Table 5.2.5) represent an asymptote for the full curve of the growth and senescence. Although they describe quite well the initial stage of the macrophytes growth, they fail to reproduce the maturation and senescence stages. It is also either impossible with these models to estimate the thermal time for the biomass maximum or the models overestimate it. The model for the growth and senescence proposed by Werker and Jaggard (1997) has four parameters B_{max}, T_{max}, $R_{\min}$, and k, giving more flexibility for modeling asymmetric curves, but also more complexity, so that fitting of experimental data has to be done in steps and the data set must be measured with enough resolution for obtaining physically meaningful values of $R_{\min}$ and k. The empirical function model (2.2.23) approximates the measured data set quite well, however, for the small densities of vegetation it does not tend to the classical models of growth. The reason may be that these functions can be obtained assuming a linear decline of the relative growth rate from its maximum to the minimum value, and therefore it lacks an initial period of the constant relative growth rate characteristic for the theoretical models of growth.

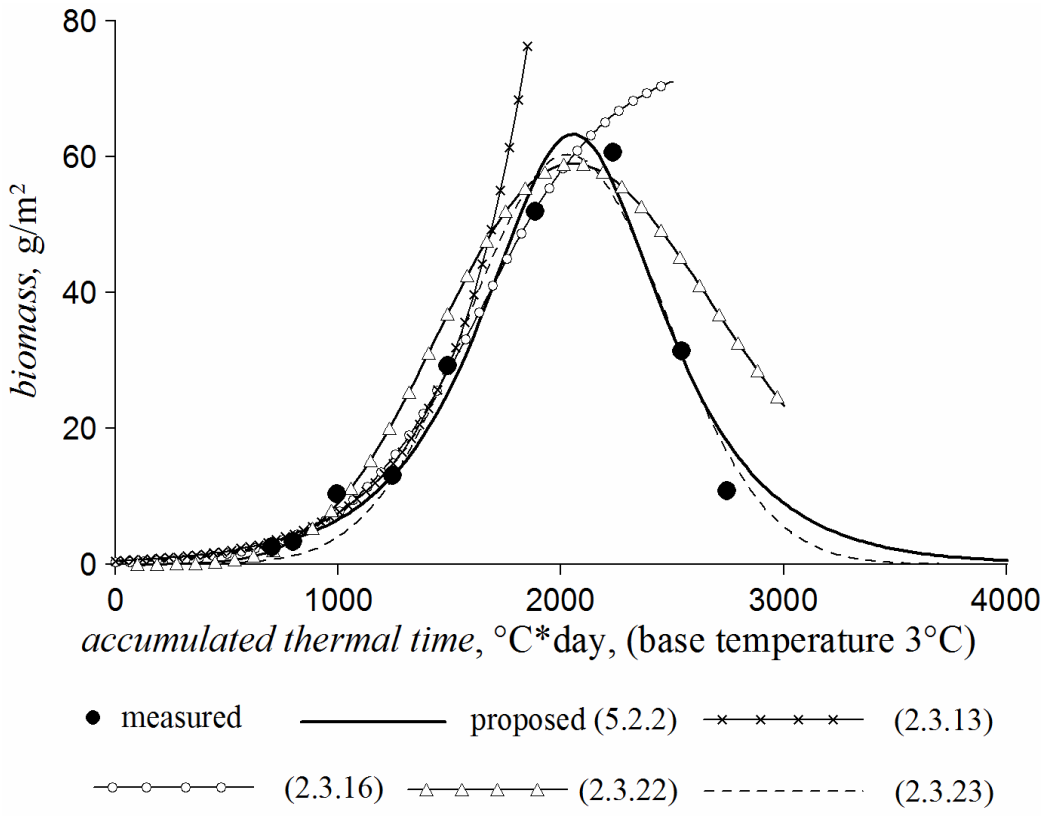

Figure 5.2.6 Comparison of theoretical and empirical formulae of biomass growth with measured data.

Table 5.2.5 Results of the application of the theoretical and empirical models to the growth of *Sagittaria sagittiflolia*.

Model		Model parameters									
		equation	fitted inter-val	B_0	B_m	T_{max}	T_m	k	R_{min}	R_{max}	coef. of det., R-sq.
Theoretical	exponen-tial (2.3.13)	$B = B_0 e^{kT}$	700-1700	0.5	-	-	-	0.0027	-	0.96	0.96
	Verhulst (2.3.16)	$B = \frac{B_{max}}{1 + e^{-k(T-T_m)}}$	700-2055	0.3	75	-	1639	0.0034	-	0.99	0.99
	Werker and Jaggard (1997) (2.3.22)	$B = B_{max}\left(e^{R_{min}(T-T_{max})} - \frac{R_{min}}{k}\left(1 - e^{-k(T-T_{max})}\right)\right)$	700-2743	-	63	2040	-	0.00073	-0.0035	0.74	0.74
Empirical	Wilson et al. (2007) (2.3.23)	$B = B_{max} e^{-0.5k(T-T_{max})^2}$	700-2743	-	60	2040	-	0.0022	-	0.96	0.96
Proposed	hyperbolic secant (5.2.11)	$B = B_{max} \sec h\left(k(T - T_{max})\right)$	700-2743	-	63	2055	1724	0.0028	-0.0028	0.0028	0.96

The proposed hyperbolic secant function (5.2.11) describes the measured biomass curve accurately (Table 5.2.3, Figure 5.2.7a) and provides easier mathematical analysis of the biomass growth curve. For example, the rate of the biomass growth can be readily assessed using the proposed model (5.2.10-5.2.11) as

$$\frac{dB}{dT} = -B_{\max} R_{B\max} \tanh\left(T_B R_{B\max} \right) \sec h\left(T_B R_{B\max} \right) \tag{5.2.12}$$

The function (5.2.12) has two extremes with coordinates $x = \pm 0{,}881$ (Figure 5.2.7b). It can be also seen in Figure 5.2.7b, that function (5.2.12) provides additional information on the phases of the plants development. The left maximum clearly indicates the threshold between periods of elongation and expansion of the individual plants and the period of maturation and flowering.

The study by Sand-Jensen (1993) in which growth of macrophytes patches was examined, and our own observations of the patch dynamics (see example in Figure 5.1.5) reveal enhanced patch expansion in the period from April to July. This way the enhanced expansion of patches occurs mainly in the period of intensive macrophytes growth. The thermal time value corresponding to the end of this period determines the position of the maximum in the corresponding growth curve for the area colonized by the plants.

Now we are heading to the most crucial point of the theory development as we going to hypothesize on a relation between dynamics of biomass and colonized area during the period of the enhanced development of vegetation cover. The hypothesis is that the colonization area growth curve can be also modelled by a hyperbolic secant function. The value of the thermal time, corresponding to the maximum growth rate of the biomass can be determined by taking the second derivative from (5.2.11) and equating it to zero

$$T_{A\max} = T_{B\max} - 0.881 \frac{1}{R_{B\max}} = 1724 \tag{5.2.13}$$

hence

$$T_A = T - T_{B\max} + 0.881 \frac{1}{R_{B\max}} \tag{5.2.14}$$

and equation for the colonized area dynamics is

$$A^* = A_{\max} \sec h \left(\left(T - T_{B\max} + 0.881 \frac{1}{R_{B\max}} \right) R_{A\max} \right) \tag{5.2.15}$$

here $A^* = A_{veg} / A_{total}$ is relative vegetated area where A_{veg} is vegetated area, A_{total} is the area of the river reach. Rearranging (5.2.15) yields

$$A^* = A_{\max} \sec h \left(\left(T_B R_{B\max} + 0.881 \right) \frac{R_{A\max}}{R_{B\max}} \right) \tag{5.2.16}$$

Notation and parameters of the model describing phenological dynamics of area colonized by plants are summarized in Table 5.2.6. The relationship between normalized coordinates for biomass and area integrally reflects a complex of biological relationships: relationships between shoots and rhizome biomass, rhizome biomass and horizontal elongation rate of rhizomes (Duarte and Sand-Jensen 1990; Marba and Duarte 1998). Investigation of the relationship between biomass and occupied area needs further studies on fractal dimension of the stands (area-perimeter relationship), shoot biomass-shoot density, shoot density-rhizome biomass ratios and rhizome elongation velocities (Duarte and Sand-Jensen 1990; Marba and Duarte 1998).

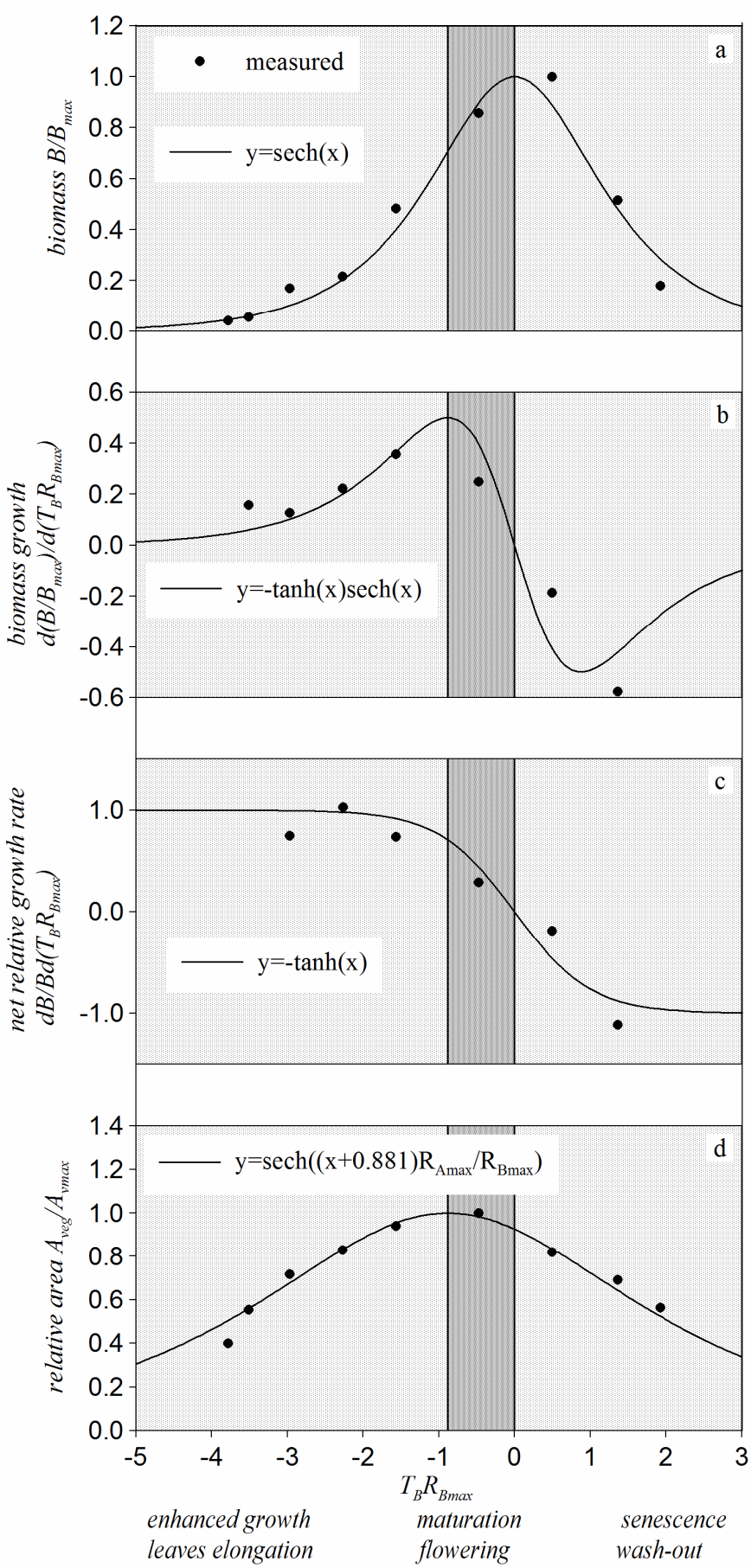

Figure 5.2.7 Application of the proposed model to the growth of *Sagittaria sagittifolia*.

Table 5.2.6 Summary on the model parameters

Parameters	Notation	Modelled Value	Fitted Value
day-degree sum corresponding to the maximum of relative area	$T_{A\max}$	1724	1763
maximum of relative area	$A_{\max}$	0.70	0.69
growth rate	$R_{A\max}$	0.00129	0.00127
coefficient of determination, R-squared	R^2	0.95	0.96

5.2.3 Dynamics of vegetative patches and mosaic

Analysis of dynamics of vegetative patches and mosaic in this subsection is only concerned with the qualitative description of the processes and determination of principal controlling factors. This analysis is the result of systematic observations completed on the river reaches. Quantitative description requires synthesis with other involved disciplines and will be concerned in other part of the thesis.

Observations on the experimental river reach near the village Freienbrink show that during October –May the macrophytes population is drastically reduced and the flow is practically free from the effect of vegetation. This period is usually characterized by high water discharges and intensive bedload transport in form of the sand waves (details are presented in the Chapter 7). Active erosion and deposition associated with the motion of sand waves affect the sediments to the substantial depth – up to 15÷20 cm and redistribute tubers of wintering plants. Sensitivity of tubers to preferential deposition results in accumulation of tubers in the troughs of the sand-waves (Figure 5.2.8a).

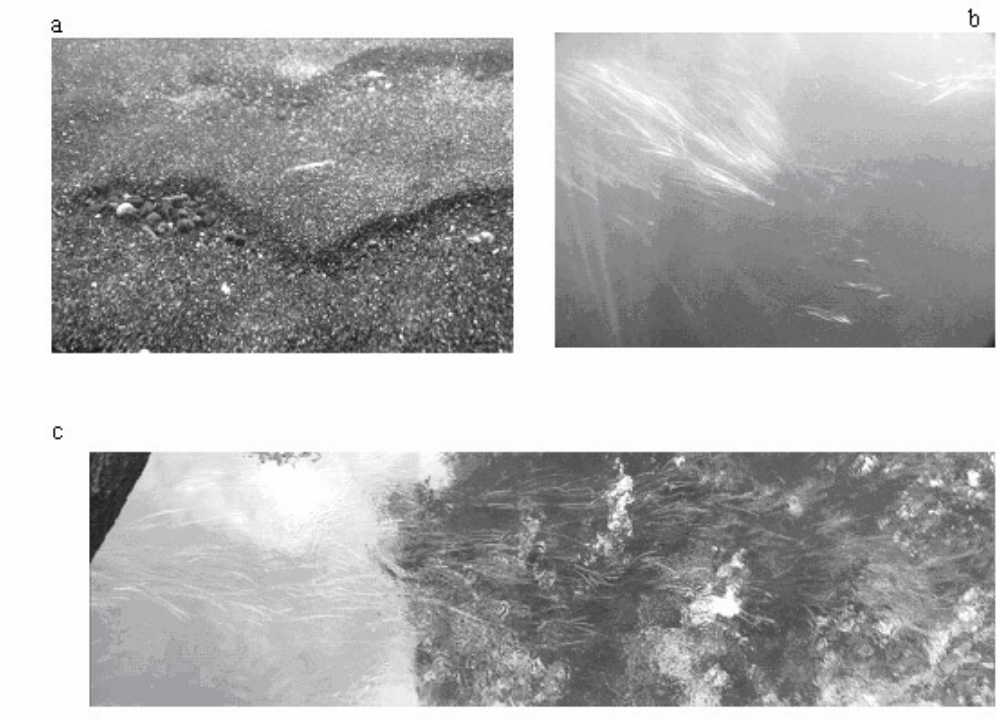

Figure 5.2.8 Deposition of tubers in the trough of a sand-wave (a), initiation of vegetation growth (b), and fully developed patch of vegetation at the pick of biomass (c).

Later in spring when the bedload transport reduces, deposited tubers sprout the leaves and the initial distribution of plants reflects the patterns of previous preferential deposition of tubers (Figure 5.2.8b). During the summer plants increase density of population by intensive vegetative propagation mainly in the downstream direction forming long but narrow patches (Figure 5.2.8c).

Variability of hydraulic regime of the river during the vegetative period greatly affects the structure of vegetative mosaic by shaping the patches into singular units via wash out of the single plants from the free paths of the mosaic. However, prolonged periods of low water can reduce the total biomass on account of physical damage of individual plant leaves. Such situations usually occur after prolonged high water periods when plants develop long flexible leaves which after sudden reduction of water level became exposed at the free surface of the flow.

The observations described above allow drawing of a conceptual model describing the dynamics of vegetative patches and mosaics in terms of individual plants and communities – a more discrete description as compared to the quantitative model describing dynamics of integral area occupied by macrophytes (5.2.16). In this conceptual model we propose that at the end of vegetative season, when the parts of the plants exposed out of substrate will be mechanically dislodged by the flow, initial distribution of plants tubers can be assumed uniform (Figure 5.2.9).

Figure 5.2.9 Spatial distribution of *Sagittaria sagittifolia* tubers at the end of the vegetation period (a), during active bedload transport period (b), and during vegetative period (c).

During winter season and intensive bedload transport period the tubers will be shifted by the flow and deposited in accordance with the patterns of bedforms or sand waves (Figure 5.2.9b). Knowledge on hydrodynamics of flow and associated with it morphodynamic processes can provide the estimates of characteristic spacing between the accumulated tubers. Obviously, that larger sand waves will be capable to trap more tubers and initially to form more dense populations that can sustain physical forcing by flow and maintain further colonization by propagating the rhizomes (Figure 5.2.9c).

This simple conceptual model however allows figuring out some quantitative estimates for characteristic sizes of patches and their dynamics during vegetative period. Thus in the beginning of vegetation growth patches will be represented by assemblages of individual plants accumulated on relatively small area. As the leaves of plants grow fast in two first weeks the size of the patches may reach the length comparable to the length of individual plants (around 1.5 – 2 meters). These initial patches will be separated by free paths about 3 to 4 depth of flow (4 to 6 meters). At the peak of biomass the rhizomes of the plants will fill out the spaces between initial patches forming longer strips. At the same time the extension of the strips and their size will be controlled by other factor: larger-scale morphology of the riverbed (riffles and pools sequences), and by the effect of local factors as shadowing from the terrestrial vegetation. On our experimental river reach the maximal size of the continuous dense patches (strips) was around 10-15 m.

5.3 Implications for Transport and Mixing Processes

The developed model of the biomass growth (5.2.11) parameterised for the phenological cycle of dominant species of macrophytes Table 5.2.6, and accomplished with the model for average colonization area (5.2.16) provide enough information for estimating the principal parameter of the dead zone model – the relative dead zone volume ε. The output of the biomass model is also important for the determination of population density of vegetation which was shown to be one of the controlling factors for the interactions of the turbulent flow and vegetative patches (Chapter 4).

The model describing the biomechanical interactions of individual plants with the flow (5.2.8-5.2.9) provide the bridge between properties of plants and physical forces exerted by flow giving as an output the bended height of the vegetation patch. There is now the only one step left in determining the dead zone volume ε - to subtract the portion of patch volume through which the vertical exchange of momentum goes from the portion of the average patch volume. As it was already discussed in the Chapter 4, the extent of the zone of vertical exchange of momentum and mass can be deduced by estimating the penetration depth for the certain density of vegetation using the model of analogous mixing layer. The model of biomechanical interactions (5.2.8-5.2.9) has also important implications for estimating resistance of the vegetated channel and hence for estimation of mean velocities.

The knowledge gained in respect to the dynamics of elements of vegetative mosaic, particularly regarding initial scales of patches and their maximal limits together with the knowledge on hydrodynamics inside the vegetation (Chapter 4) provides the possibilities for estimating characteristic residence times inside the vegetation patches. This is the second valuable parameter necessary for accurate description of the dead zone effect.

To conclude this chapter we should point out to the fact that at this point we have gathered substantial theoretical and empirical knowledge about hydrodynamical aspects of vegetated flow in a lowland river and physical and ecological aspects of interactions between flow and flexible submerged vegetation. This knowledge is sufficient for making prognostic estimates for the consequence of bio-physical interactions in respect to the transport and mixing processes in frame of the longitudinal dispersion model with dead zones which is the scope of the present research. In the next chapter we are going to perform estimates of the parameters of the dead zones using developed models and to compare the results of prediction with the results of direct experimental measurements.

6 LONGITUDINAL DISPERSION IN A RIVER REACH WITH SUBMERGED VEGETATION

In this Chapter we synthesize the knowledge gained in the involved disciplines to comprehend the consequences of complex interactions between principal physical and biological components of the fluvial ecosystem for transport and mixing of substances. The results of theoretical and experimental research described in the previous chapters of the thesis will be summarized to show how do parameters of the transport and mixing model evolve during vegetative season. The results of the theoretical analysis are compared to the direct experimental observations of the transport phenomena. The program of experimental observations is described in the Section 6.1, and the analysis of the obtained results is presented in the Section 6.2. Theoretical analysis of dispersion process in vegetation mosaic is discussed in the Section 6.3. Numerical modeling of the longitudinal dispersion with dead zones is concerned in the Section 6.4, and in the Section 6.5 we show how the results of the study can be applied to understand transport of suspended matter and phytoplankton.

6.1 Program of Field Tracer Experiments

The aim of experimental studies presented in this Chapter was to obtain a data set that can be used for validation of the developed theoretical concepts regarding transport and mixing processes in a river reach subjected to seasonal growth of aquatic vegetation. This ultimate goal of the research was achieved by carrying out tracer experiments.

The tracer experiments were carried out during May – August 2005 on the downstream part of the Spree River, Figure 3.1.1b. The program of field measurements included observations of the downstream changes of a tracer cloud after instantaneous injection, and a set of hydrometric and morphologic measurements. The concentration of the tracer, flow rate and cross-sectional profiles of the riverbed elevations were measured in each experiment. The solution of uranin was injected from a bridge as a surface line across the channel. Each injection consisted of 400 g of uranin AT dissolved in about 700 L of river water. The time of injection was within 20 s interval and can be considered as an instantaneous. Solution of uranin AT dye is ecologically harmless and permitted for scientific purposes in the natural environments. However, because of its sensitivity to the sunlight, uranin solution exposed to the bright sun decays relatively rapidly. To prevent considerable losses of the tracer because of photolysis the experiments were performed during the night time. The concentrations were measured with a pair of fluorometers (Section 3.2.2), one of which was set in a stationary location close to the cross-section of release and another one was moved by a motorboat.

In total three tracer experiments were conducted. Their time-table was arranged to capture the characteristic changes occurring during vegetation season and they were respectively completed at the beginning of the season (mid of May), at the period of exponential growth (end of June), and at the maximum of vegetation biomass (mid of August). The examples of obtained concentration distributions are shown in Figure 6.1.1. The concentration curves exhibit characteristic decay of concentration maximum and the growth of asymmetry characteristic for the effect of dead zones. A summary of hydraulic and morphological variables for the field tracer studies is presented in Table 6.1.1.

Parameters of the longitudinal dispersion model evaluated with optimization technique (2.2.21) are summarized in Table 6.1.2.

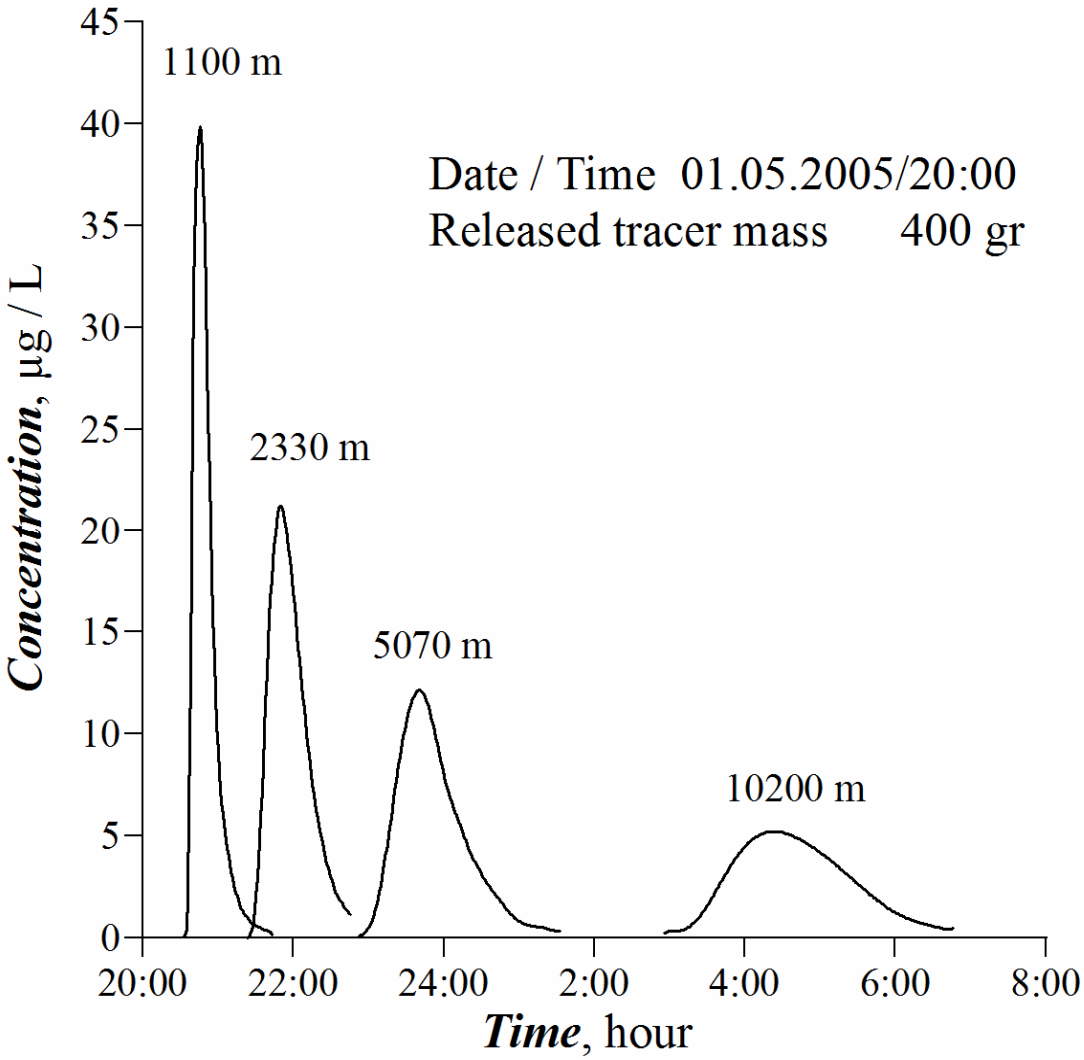

Figure 6.1.1 Examples of measured concentration curves.

Table 6.1.1 Hydraulic and morphometric characteristics of the river reach.

NN	date	Q,, m^3/s	B, m	h, m
1	11.05	9.0	25	1.06
2	30.06	2.8	23	0.87
3	10.08	7.5	27	1.54

Table 6.1.2 Parameters of the dead zone model.

NN	U, m/s	D, m^2/s	э	T_d, min
1	0.34	11.5	0.01	29.1
2	0.14	8.0	0.03	0.08
3	0.18	18.0	0.15	2.50

6.2 Results and Analysis

The comparison of measured and predicted values for the central moments of concentration distributions are shown in Figure 6.2.1-Figure 6.2.3. It can be seen from these figures that the analytical solutions (2.2.18)-(2.2.20) approximate spatial distributions of measured moments quite accurately. Specifically the first two moments are prescribed with the deviations less than 5%. The scatter in the measured data about theoretical prediction (2.2.19) for the third central moment is about 20%. This scatter is explained by the sensitivity of numerical estimates of the third moment to the imperfections of the measuring procedures. Thus, because of limited number of fluorometers some units were moved to the downstream sections and the tails of concentration curves were cut on non-zero value. There were also the errors associated with the calibration procedures of fluorometers.

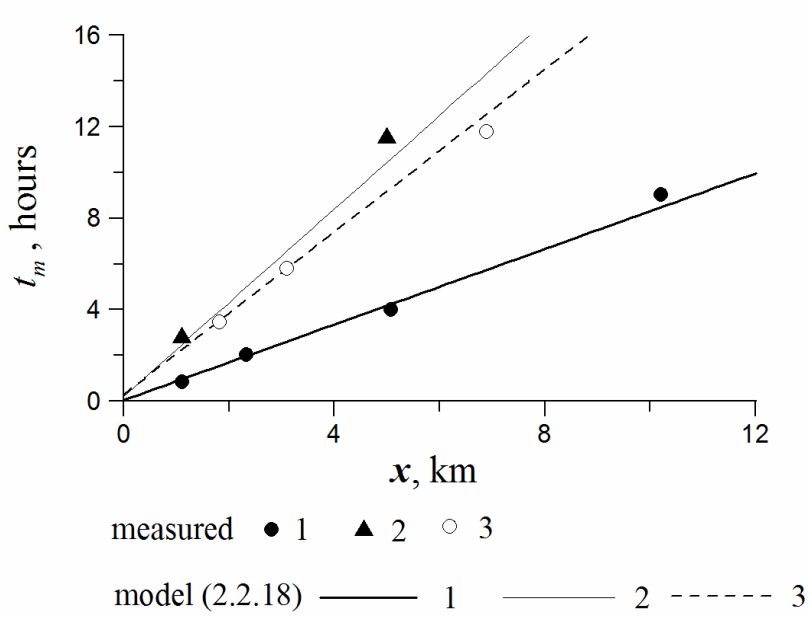

Figure 6.2.1 Downstream evolution of the first central moment (mean travel time) of the concentration cloud.

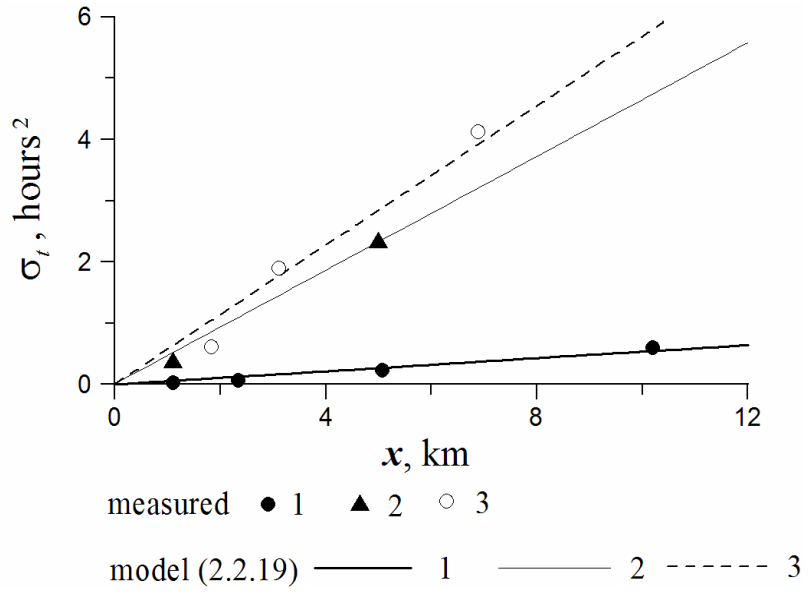

Figure 6.2.2 Downstream evolution of the second central moment (variance) of the concentration cloud.

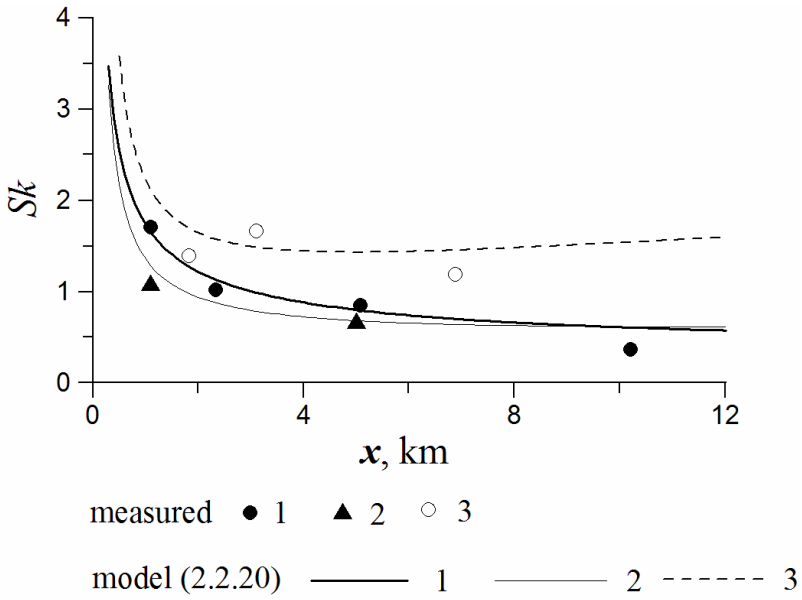

Figure 6.2.3 Downstream evolution of the third central moment (skewness) of the concentration cloud.

The results of the tracer studies indicate substantial reduction of mean flow velocities during the vegetative period (Table 6.1.2). At the same time the data reveal a systematic increase in the values of dead zone volume and decrease of penetration times.

To understand better the effect that dead zones cause on the mixing and transport processes it is useful to compare experimental data with predictions from classical model of longitudinal dispersion: $\text{э} = 0, T_d = \infty$ in equation (2.2.8). Assuming instantaneous injection of the tracer, the downstream evolution of dimensionless maximal concentration is described as (Sukhodolov et al. 1997)

$$\frac{2A\sqrt{\pi DB/U}\,C_{\max}}{M_T} = \frac{1}{\sqrt{x/B}} \tag{6.2.1}$$

where $A = hB$ is cross-section area, and M_T is mass of the injected tracer. The tracer studies in natural streams (Sukhodolov et al. 1997) indicate that equation (6.2.1) is satisfied quite accurately for the distances $x/B > 70$. Comparison of scaled measured maximal concentrations of uranin with the predictions from relation (6.2.1) is demonstrated in Figure 6.2.4. For comparison in Figure 6.2.4a the data set obtained in rivers with minor effect of dead zones (Sukhodolov et al. 1997) is shown. The data set in Figure 6.2.4a demonstrates that the experimental points collapse on the line corresponding to the right side of equation (6.2.1) revealing that the dispersion stage of the process was obtained after initial mixing at the distances shorter than $x/B < 70$. In contrast, the data obtained on the Spree River (Figure 6.2.4b) indicated that though the dispersion process was attained at the distances $x/B < 70$, the data points deviated systematically from equation (6.2.1) at $x/B > 70$ revealing significant decrease in maximal concentrations. This systematic decrease is easily perceived from the numerical computations (Figure 2.2.1a) and addressed to the effect of dead zones.

A dimensionless form for the variance of the tracer cloud is obtained from the definition of the dispersion coefficient

$$D = \frac{U^3\,\sigma_t^2}{2B}\frac{1}{x/B}, \quad \frac{U^3\sigma_t^2}{2DB} = x/B \tag{6.2.2}$$

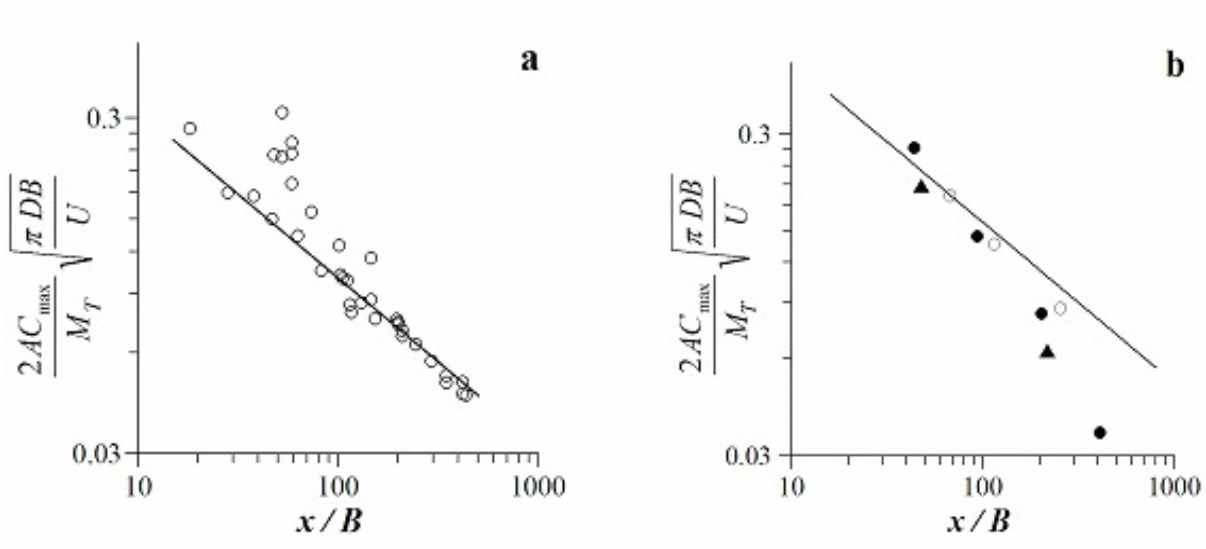

Figure 6.2.4 Dimensionless peak concentrations along the experimental river reaches; (a) with minor effect of dead zones (from Sukhodolov et al. 1997), and (b) present study -significant effect of dead zones.

The measured downstream growth of the tracer cloud and its comparison with the linear relation (6.2.2) are shown in Figure 6.2.5. A systematic deviation from the classical dispersion process (Figure 6.2.5b) is also evident at this plot. The size of the tracer cloud is evolving at higher rate than linear and, hence, equation (6.2.2) significantly underestimates the variance of the distribution.

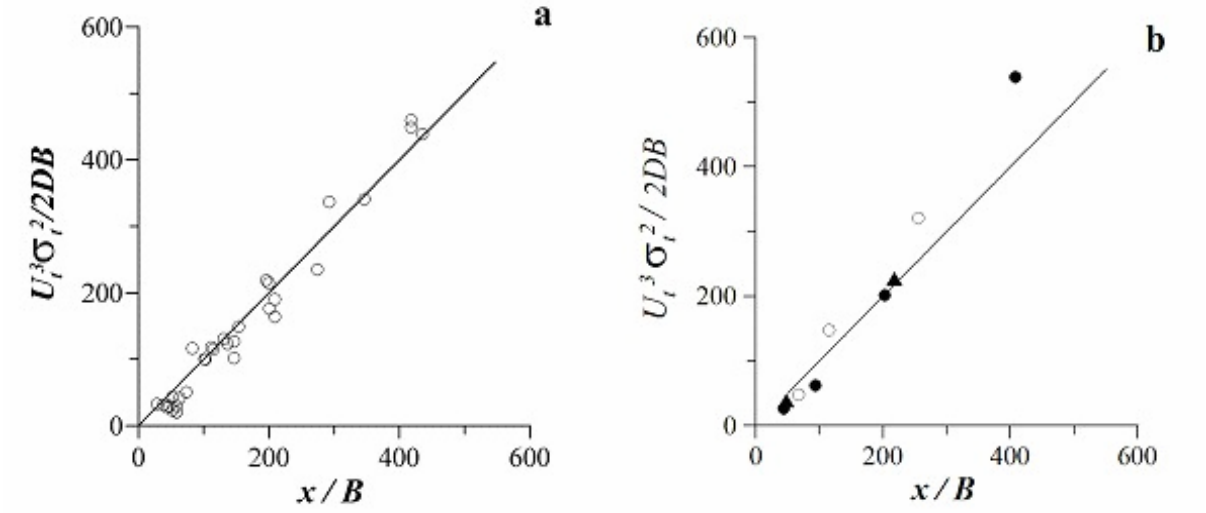

Figure 6.2.5 Dimensionless variances along the experimental river reaches; (a) with minor effect of dead zones (from Sukhodolov et al. 1997), and (b) significant effect of dead zones.

Relationship for the skewness in the longitudinal dispersion model was obtained by Sukhodolov et al. (1997) in the form similar to (2.2.13) but relating dimensions of the channel

$$Sk \sim \left(\frac{U\,h}{D}\right)^{-1/2}\left(\frac{x}{B}\right)^{-1/2} \tag{6.2.3}$$

The measured skewness data normalized in accordance with (6.2.3) are plotted in Figure 6.2.6. The data reveal systematic deviations from (6.2.3) indicating that only in the channel free of vegetation the trend similar to the longitudinal dispersion model was observed. In vegetated channel the skewness was approaching constant state along the river reach.

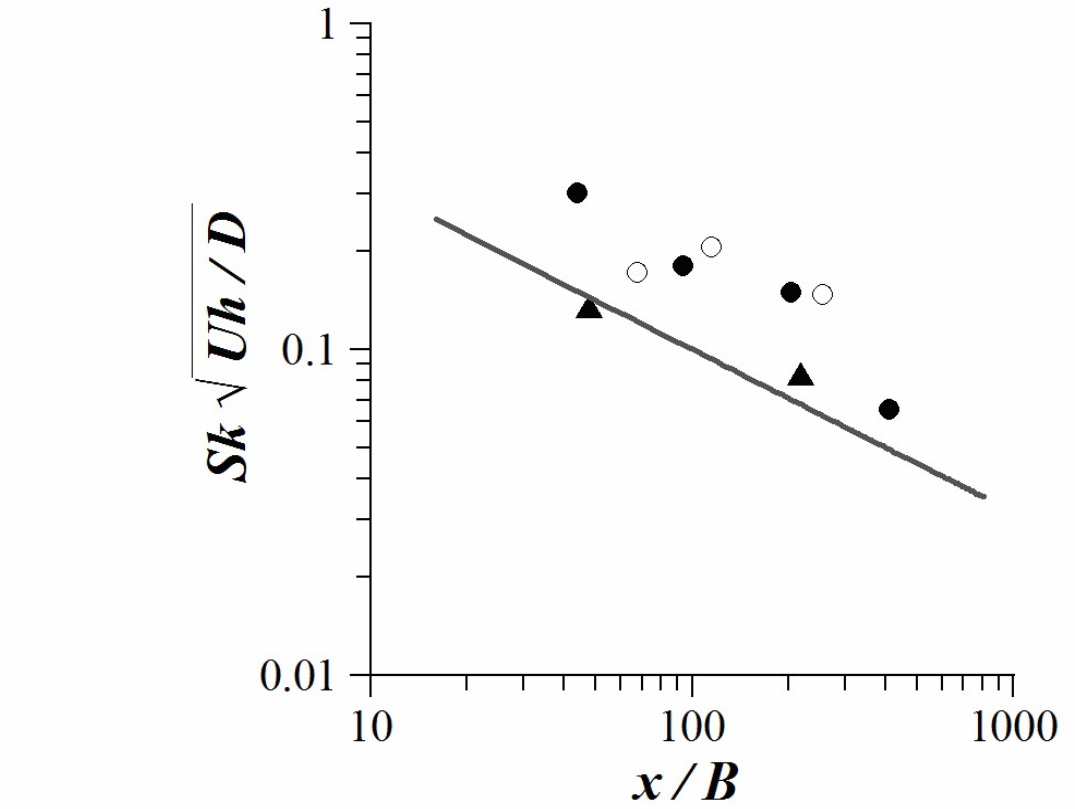

Figure 6.2.6 Variation of dimensionless skewness coefficients along the river reach.

The analysis presented above was focused on the behavior of the central moments of the concentration distribution curves because it is impossible to analyze the distribution curves with analytical methods directly. However, useful information can be obtained exploring similarity properties of concentration curves (Sukhodolov et al. 1997). The simplest way to obtain normalized concentration curves $C^* = f(t^*)$ is (Chatwin 1980)

$$t^* = \frac{t-\mu}{\sigma_t} \sim \frac{t-t_p}{\sigma_t},\ C^* = C/C_{\max} \tag{6.2.4}$$

where asterisk indicates dimensionless variables. The dimensionless concentrations curves are shown in Figure 6.2.7 together with the dimensionless solution for the longitudinal dispersion model without dead zones.

The concentration curves exhibit distinctive similarity in their pattern though they are obviously asymmetric and systematically deviate from the longitudinal dispersion model. However, the main differences are observed for small concentrations $C < 0.5C_{\max}$ while at the concentration level $C = 0.5C_{\max}$ the width of the concentration cloud is close to that of the longitudinal dispersion model. This last fact is indeed crucial for the analysis in frame of the longitudinal dispersion model as it indicates that the meaning of dispersion coefficient is not discarded.

The parameterization of the longitudinal dispersion coefficient was already discussed in detail in the Section 2.2.4, and there it was shown that this parameter can be simply related to the bulk flow velocity as an integral velocity scale and to the river width as a representative spatial scale, equation (2.2.29). Heterogeneity of velocity and flow bathymetry distributions defines the coefficient of proportionality in (2.2.29). Measured values of the dispersion coefficient and the values computed from flow parameters according to (2.2.29) are shown for comparison in Figure 6.2.8. The data of tracer studies completed in small rivers of Moldova are also indicated in this plot (Sukhodolov et al. 1997). Close correspondence between measured and predicted value of

the dispersion coefficient can be reported for the flow without vegetation (experiment 1). In vegetated channel measured values of the dispersion coefficient were significantly higher than those predicted with equation (2.2.29).

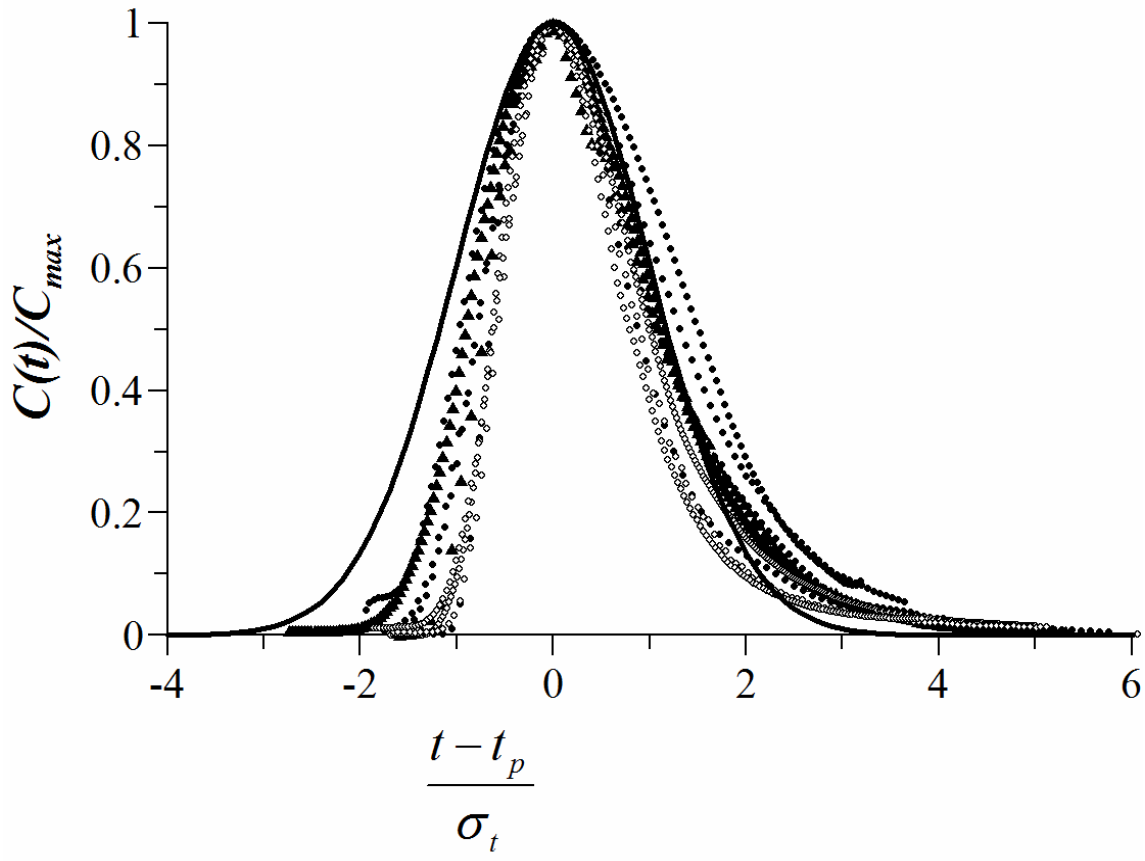

Figure 6.2.7 Similarity of normalized concentration curves and their comparison with the longitudinal dispersion model (solid line).

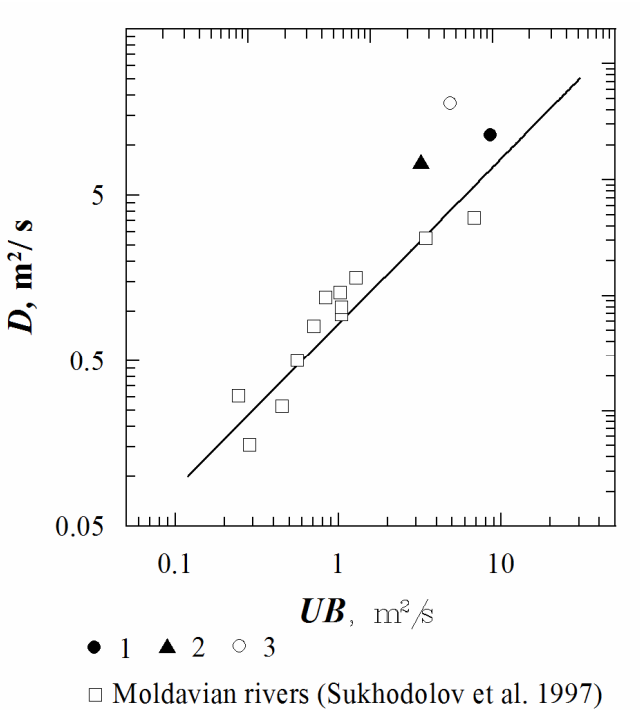

Figure 6.2.8 Relation between flow parameters and dispersion coefficient.

6.3 Effect of Vegetation on Dispersion: theoretical analysis

The results of the study indicate that downstream evolution of the temporal moments of the concentration curves is accurately predicted by the model of longitudinal dispersion with dead zones. Comparison of measured temporal moments with predictions of the classical theory of longitudinal dispersion indicated unacceptably large discrepancies.

Specific parameters of the dead zone model, dead zone volume and penetration time, exhibited a distinct behavior during the vegetative period. As might be expected, the relative volume of dead zone was increasing from 1% in May to 15% in August. Correspondently, the biomass growth (dry weight per area of the river channel) has indicated increase from 5 to 60 g/m^2. However, the penetration time – characteristic time scale of tracer residence in the dead zone decreased from 30 minutes to 2.5. Phenomenologically the observation can be explained only by metamorphoses of dead zone. In early spring the dead zones are represented predominantly by recirculation zones formed because of the flow separation on the irregularities of banks (Figure 6.3.1). A precondition for formation of recirculation zone is to have substantial velocity of the main stream. Although such dead zones have considerable dimensions and retention times about 30 minutes, they are sparsely distributed on the river reach and respectively their relative volume is small.

Figure 6.3.1 A typical dead zone at the left bank of the Spree River near Mönchwinkel.

During the vegetation period the dead zones are formed by blocking effect of submerged and emergent vegetative canopies occupying substantial part of the river cross-section though the penetration time of these dead zones is comparable with the time scales of wakes developing behind the plant canopies and ranges from 5 s to 3 minutes. The metamorphosis scheme for the dead zones type is presented in Figure 6.3.2.

In vegetated channels additionally to the heterogeneity of the mean velocity field the liquid particles are dispersed by mechanical dispersion (Nepf 1999). Mechanical dispersion is introduced on a patchy mosaic scale by the tortuousity of free passes between vegetation patches. An example of particle dispersion in vegetative mosaic is shown in Figure 6.3.3.

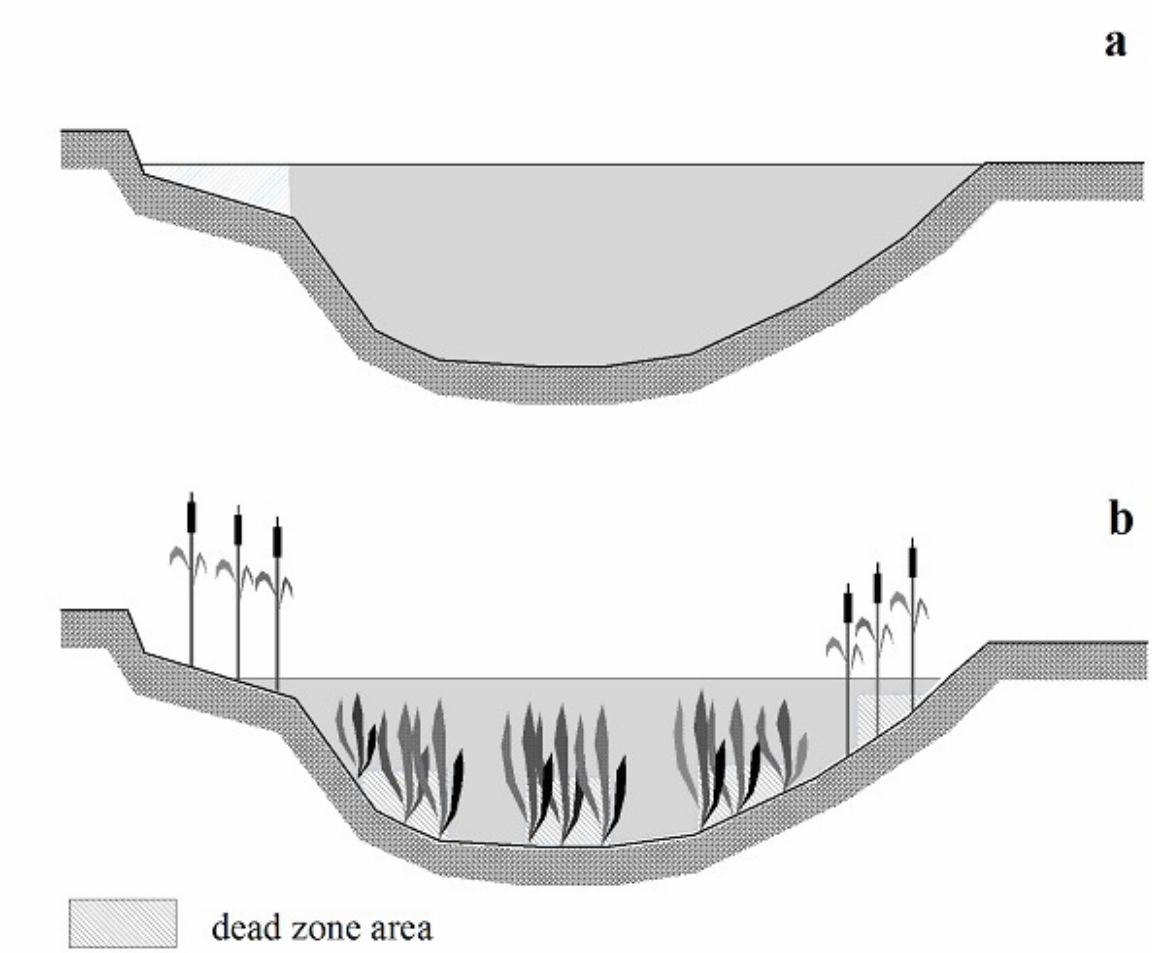

Figure 6.3.2 Seasonal metamorphosis of the dead zone type in a lowland river; (a) dead zone formed in free channel with flow separation on bank protrusion, and (b) stagnant zones beneath the vegetation canopies.

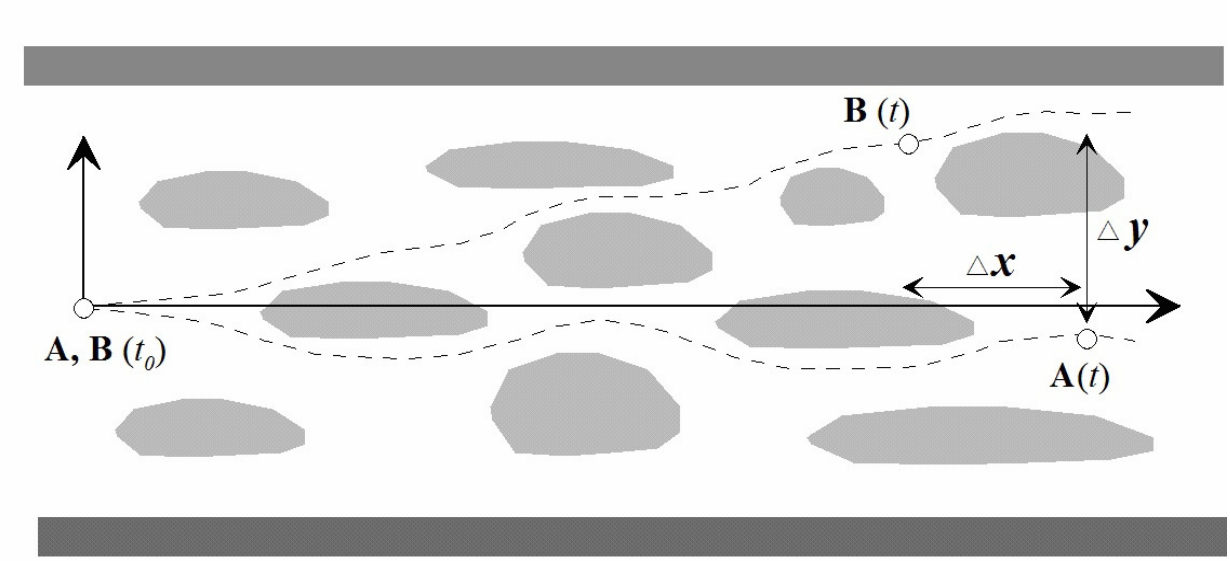

Figure 6.3.3 Mechanical dispersion in a vegetative patchy mosaic (adopted from Nepf 1999).

The processes of mechanical and shear dispersion are independent, their variances and hence contribution to the total longitudinal dispersion process can be considered as additive and expressed as

$$D = \sigma_u^2 T_L + \sigma_m^2 T_m \tag{6.3.1}$$

where σ_m^2 and T_m are variance and time Lagrangian scale of mechanical dispersion. The time scale T_m can be represented as

$$T_m = \gamma \frac{b}{U} = \gamma \frac{э B}{U} \tag{6.3.2}$$

where γ is scaling parameter, b is width of vegetative dead zone. Velocity variance for mechanical dispersion is proportional to the velocity difference between the flow in vegetative canopy and in a free flowing path or over the macrophytes. As our field experimental studies and measurements show that velocity difference normalized by mean velocity is varying between 0.8 and 1.2 depending on the vegetation density and hence can be accepted as equal to mean velocity and

$$\sigma_m^2 T_m = \gamma э UB \tag{6.3.3}$$

Finally, the expression for the longitudinal dispersion in vegetative reaches is presented as

$$D = (\alpha_u^2 \beta_B + \gamma э)\, UB \tag{6.3.4}$$

Scaling parameter γ represents a characteristic dimensionless length scale and characterizes an average distance between patches in the canopy mosaic relative to the characteristic length-scale of the dead zone. The scaling parameter thus is a variable which value depends on the vegetation density and its spatial distribution. At first approximation this dependency can be expressed as $\gamma = f(э)$. Note that the relationship should be reciprocal – the spacing is large in the sparse vegetative canopies and decreases with growth of the dead zone parameter. The available experimental data suggest the following relationship

$$\gamma = 63 \exp(-7.6 э) \tag{6.3.5}$$

Subtracting the impact of mechanical dispersion in the vegetative mosaic, one can rescale the data already presented in Figure 6.2.8, Figure 6.3.4.

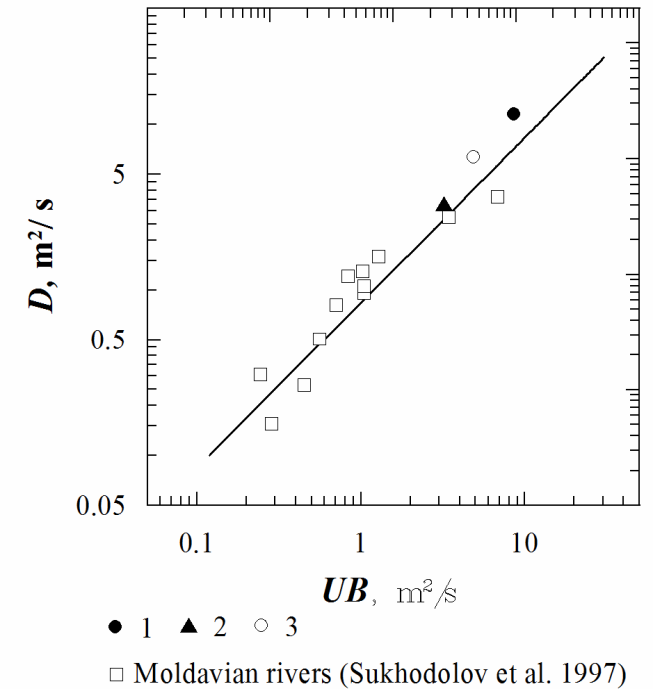

Figure 6.3.4 Relation between flow parameters and dispersion coefficient (effect of vegetation is subtracted).

Present experimental data and their analysis contribute to the understanding of complex transport and mixing processes in the vegetated river reaches. A quantitative characterization of the impact provided by vegetation on main parameters of the longitudinal dispersion model is achieved because of deeper understanding of changes in mean velocity and velocity differences caused by vegetation, and consequences of those changes for the process of dispersion represented with dispersion coefficient.

6.4 Numerical Modeling and Comparison with Measurements

In this Section we illustrate application of the developed theory to predict parameters of the longitudinal dispersion model (Subsection 6.4.1), and on the next step the obtained parameters are used in the numerical computations simulating completed tracer experiments for the direct comparison of the predicted and observed concentration curves (Subsection 6.4.3). The details of numerical method are presented in the Subsection 6.4.2.

6.4.1 Predicting parameters of the model

The parameters of the coupled model can be determined using the following scheme:

- temperature records are processed to compute degree-day indexes;
- using relationships (5.2.11) and (5.2.16) the mean population density of vegetation in the patches and the total area occupied by the macrophytes in an average cross-section of the river are obtained;
- with the model of vegetation and for assumed hydraulic data (5.2.8) the deflected height of plants is estimated by performing iterative computation (iterations are necessary to make the correspondence between vegetation and altered hydraulics);
- for known deflected height applying shear layer model the penetration depth is estimated and based on that parameter the thickness of an average dead zone is estimated;
- for provided mean velocity in the free path and density of vegetation and drag coefficients mean velocity in the dead zone is computed;
- the average length of a patch is determined based on the information about density of macrophytes and the stage in the vegetative period, and evaluate the characteristic residence time in vegetative dead zones;
- finally, the longitudinal dispersion coefficients are determined using the information about volume of dead zones, characteristic velocity scale in free paths and width of the river (6.3.4-6.3.5).

Guided by the computational scheme described above we have performed two sets of computations to address the seasonal dynamics of the longitudinal dispersion model parameters. These sets correspond in time to the tracer experimental studies and can be referred as end-June and mid-August sets of parameters. The details about the parameters and their estimates are summarized in Table 6.4.1, and Table 6.4.2.

Table 6.4.1 Predicted characteristics of the vegetation cover and flow hydraulics.

	T_B, degree-day	B, g/m^2	L_v, m	A_p/A	U_c, m/s	α, degree	h_v, m	L_p, m
end June	1100	8	0.9	0.48	0.12	55	0.63	0.7
mid August	2000	62	1.20	0.72	0.16	62	0.64	10

Table 6.4.2 Predicted characteristics of the analogous mixing layer model over vegetation cover and the longitudinal dispersion model with dead zones.

	δ, m	h_p, m	Q, m^3/s	h, m	U, m/s	U_v, m/s	D, m^2/s	э	T_d, min
end June	0.70	0.57	3.0	0.90	0.14	0.11	8.5	0.03	0.1
mid August	1.15	0.46	8.0	1.60	0.18	0.06	21.2	0.13	3.0

Comparing the results of predicted parameters for the dead zone model (Table 6.4.2) with measured (Table 6.1.2) shows that parameters are estimated with the accuracy about 20% which is satisfactory precision for most of practical computations. Now it is possible to apply obtained parameters to the numerical computations to predict the distribution of the substance along the river reach in main channel and in the dead zone in any desirable moment of time having that the concentration of a substance is provided at some entrance cross-section of the river. The aim of numerical computation in the context of the thesis is to illustrate how small uncertainties in model parameters will affect distributions of substances in particular cross-sections along the river.

6.4.2 Numerical method

A three step computational method (Abbott and Minns 1998; Rowiński et al. 2004) was used here to solve numerically equations (2.2.14)-(2.2.15). The solution is obtained in result of multi-staging procedure during which some processes are "frozen" or "locked" while the other is implemented. The general scheme of the method is represented in Figure 6.4.1.

The computational domain is represented by a rectangular grid spaced by spatial increments Δx. The state of variables at certain moment of time t_0 is provided along the whole computational domain and represents initial conditions C_i^n, where *i* is an index defining spatial position of the grid node, and *n* is the index defining temporal variable in the computational domain. Temporal changes of concentration $C(x_0, t)$ in the section at the beginning of the grid x_0 provide a set of boundary conditions C_0^n. Using central difference discretization scheme one can obtain algebraic equations approximating original system of partial differential equations (2.214)-(2.2.15).

For computing advection process one simply applies translation

$$C_i^{n+1} = C_{i-1}^{n+1} \text{ when the grid is specified as } \Delta t = \Delta x / U \tag{6.4.1}$$

The second step includes computations of dispersion processes and effect of the dead zone on the flow in the main channel

$$C_i^{n+1} = \left(1 - \frac{2D\Delta t}{\Delta x^2} - \frac{э}{T_d}\Delta t\right) C_i^n + \frac{D\Delta t}{\Delta x^2}\left(C_{i+1}^n + C_{i-1}^n\right) + \frac{э}{T_d}\Delta t\, C_{d\,i}^{\ n} \tag{6.4.2}$$

It should be noticed that concentrations C_i^{n+1} obtained at the first step (6.4.1) are used as the known values C_i^n at the second step (6.4.2). At the third step the balance of mass is solved for the dead zone using fourth-order Runge-Kutta method. General form of equations describing the balance (Figure 6.4.1) is

$$\frac{d\,\mathbf{y}}{d\,t} = \mathbf{f}(t, \mathbf{y}) \tag{6.4.3}$$

where $y_1 = C$, $y_2 = C_d$, $f_1(t, \mathbf{y}) = (y_2 - y_1)э / T_d$, and $f_2(t, \mathbf{y}) = (y_1 - y_2)/T_d$.

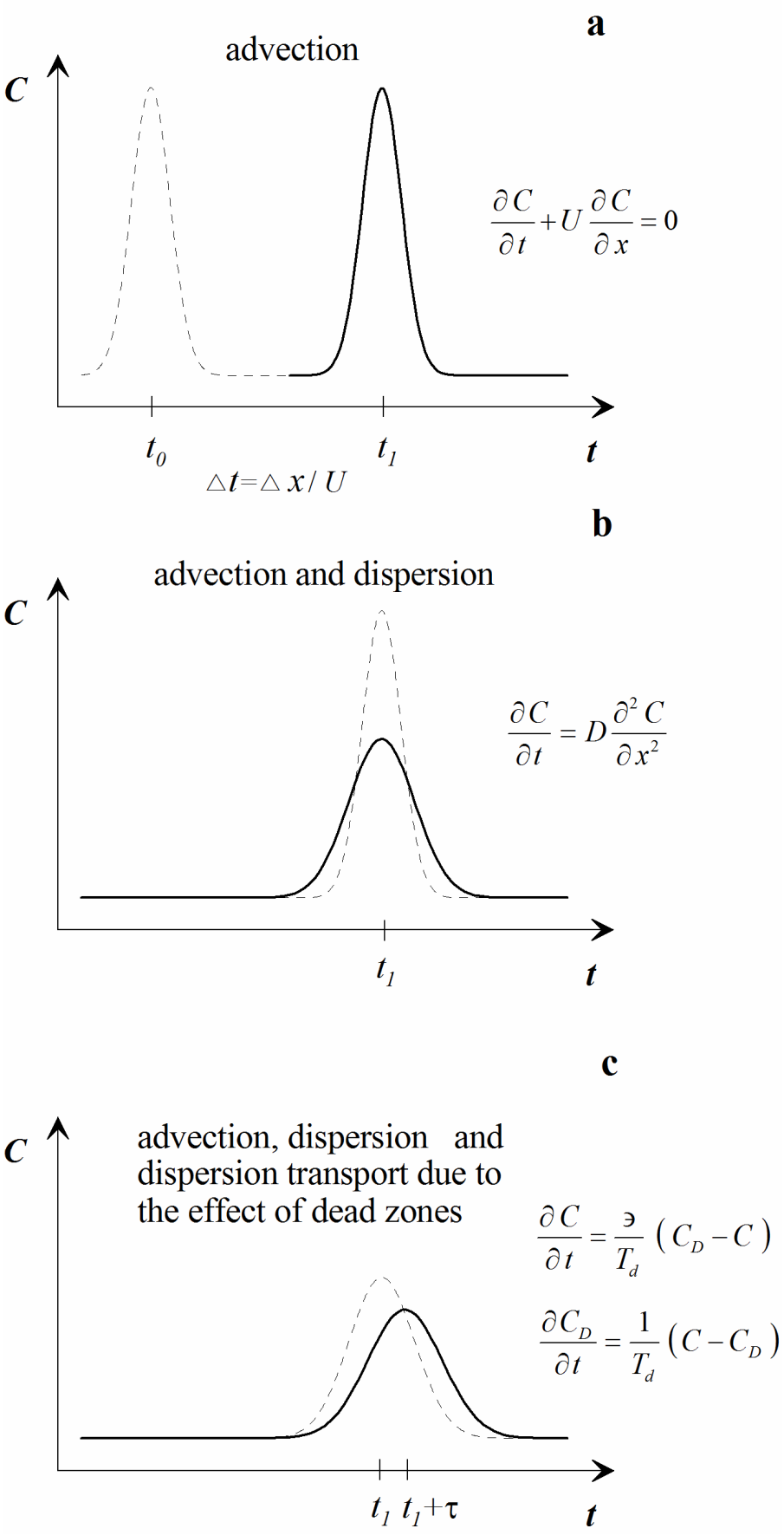

Figure 6.4.1 Schematic representation the three step computational method (after Rowiński et al. 2004).

The Runge-Kutta method assumes iterative solution for problem (6.4.3) while a stable result is obtained. A computation for single iteration may be represented as

$$\mathbf{k}_1 = \Delta t\, \mathbf{f}\left(t_i, \mathbf{y}^n\right),\ \mathbf{k}_2 = \Delta t\, \mathbf{f}\left(t_i + \frac{\Delta t}{2}, \mathbf{y}^n + \frac{\mathbf{k}_1}{2}\right) \tag{6.4.4}$$

$$\mathbf{k}_3 = \Delta t\, \mathbf{f}\left(t_i + \frac{\Delta t}{2}, \mathbf{y}^n + \frac{\mathbf{k}_2}{2}\right),\ \mathbf{k}_4 = \Delta t\, \mathbf{f}\left(t_{i+1} + \frac{\Delta t}{2}, \mathbf{y}^n + \mathbf{k}_3\right) \tag{6.4.5}$$

$$\mathbf{y}^{n+1} = \mathbf{y}^n + \frac{1}{6}\left(\mathbf{k}_1 + 2\mathbf{k}_2 + 2\mathbf{k}_3 + \mathbf{k}_4\right) \tag{6.4.6}$$

A computer code incorporating algorithms described by (6.4.1)-(6.4.6) was written using object-oriented model and implemented in Pascal 6.0 computer language. Numerical method and the developed code were validated and verified using analytical solutions (2.2.18)-(2.2.20), the results of validation are partly illustrated in Figure 2.2.1.

Boundary condition for numerical computations were obtained using a synthetic gaussian curve with integral mass of tracer correspondent to mass of injected uranin for each experiment. The time and spatial lags were computed for every individual cross-section to insure proper correspondence between them and hence to minimize the error related to the numerical uncertainties of the method.

6.4.3 Results of computation and comparison

The goal of numerical computation described in this section was to demonstrate the overall completeness of the approach as well as for learning application of numerical methods for modeling transport and mixing processes. Because we showed before that the main parameters of the model were predicted with sufficient accuracy (Table 6.1.1) we expected to obtain general agreement between modeled and measured results. Therefore comparison of numerical results presented here should reflect basic problems associated with the numerical computations rather than the problem with the proposed theoretical model.

Numerical modeling was performed only for the situations when the river channel was with submerged vegetation (experiment 2, and 3) using parameters predicted by the developed theoretical approach, Table 6.4.1 and Table 6.4.2. The results of numerical computations are shown together with the results of measurement studies in Figure 6.4.2, and Figure 6.4.3. As it was anticipated before, the overall agreement between measured and modeled concentration curves can be concluded. However, some characteristic features can be noticed from the presented plots. The performances of the model in terms of match between measured and predicted concentration curves are vividly better at short and medium distances (times) from the section of the release of tracer. This fact reflects both the problems associated with a simplified presentation of the computational domain and explicit method used for computation, but also indicates larger errors in measured data at long distances and smaller concentrations. Moreover, there were small losses of tracer in measurements due to necessity to cut the trailing edges of concentration curves to compromise between number of measured curves and completeness of individual measurements. Thus the results of numerical modeling can also help to evaluate the quality of experimental measurements which can be concluded as being commensurate to the goals of this study.

Developed numerical code is convenient for scientific estimates and as the demonstrational tool for teaching the numerical methods, but for the practical purposes it has to be supplied with more comprehensive and robust methods of discretization for the governing partial differential equations. For example more accurate, fully implicit Cranck-Nicholson scheme will provide more general solution for variable bulk flow characteristics (Rowiński et al. 2004).

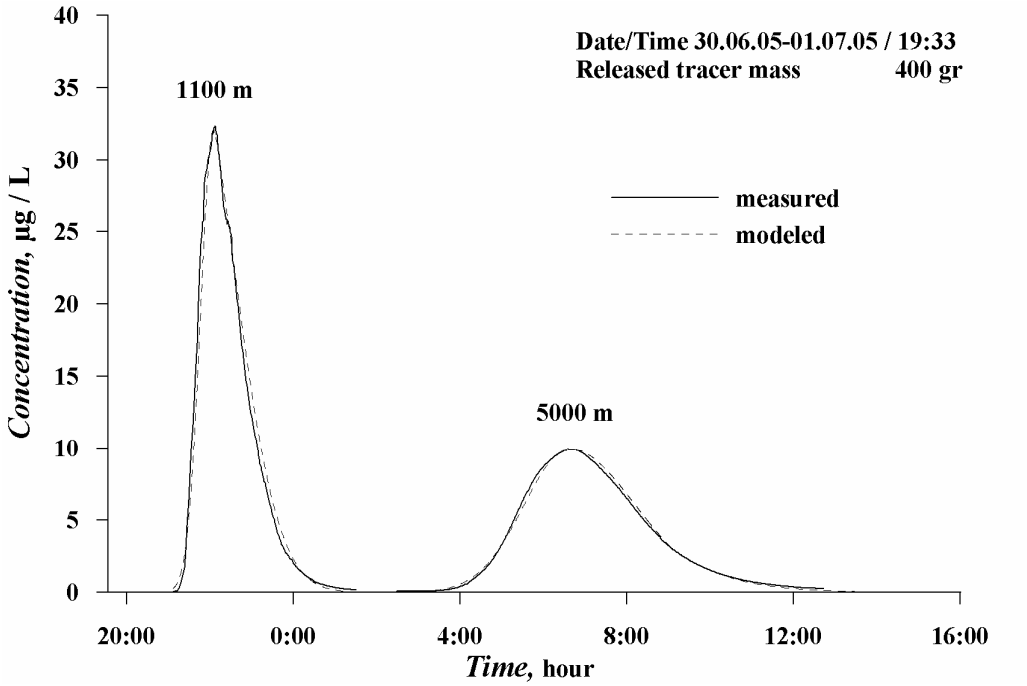

Figure 6.4.2 Comparison of measured and numerically computed concentration curves, Spree River, experiment 2.

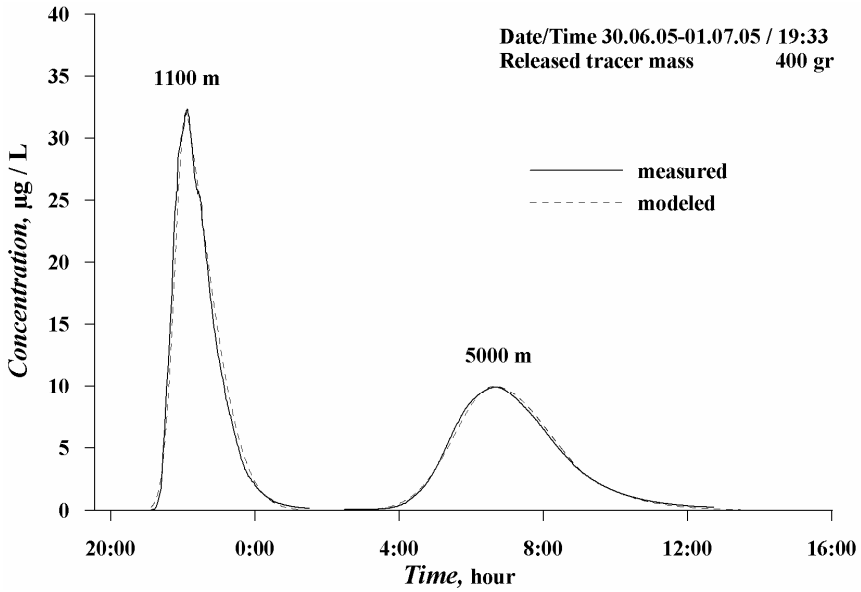

Figure 6.4.3 Comparison of measured and numerically computed concentration curves, Spree River, experiment 3.

6.5 Implications for Transport of Particulate Suspended Matter

Transport of a particulate suspended matter represents an important process in fluvial ecosystems because it determines the fluxes of nutrients, accumulation and release of organic material representing the source of food for the aquatic organisms. The classical longitudinal dispersion model which was rigorously examined in this Chapter provides the convenient framework for understanding driving mechanisms and the effect that aquatic flexible vegetation sets upon the transport and mixing processes. However, the model concerns only conservative substances which total mass remains constant in the volume of water where it is dispersed. To

account for non-conservative substances the model should include additional specific terms describing the change in the mass of injected substance. Assuming that decay or increase of mass is proportional to the concentration of the substances, the system (2.2.14)-(2.2.15) can be modified to as

$$\frac{\partial C}{\partial t} + U\frac{\partial C}{\partial x} - D\frac{\partial^2 C}{\partial x^2} = \frac{э}{T_d}\left(C_d - C\right) + K_m \tag{6.5.1}$$

$$\frac{\partial C_d}{\partial t} = \frac{\left(C - C_d\right)}{T_d} - K_d \tag{6.5.2}$$

where K_m and K_d are decay/increase rates of the substance in the main flow and the dead zone respectively. The decay of substance mass can occur on account of sedimentation processes while increase of concentration can be observed for living microscopic organisms or plants (phytoplankton). Therefore the model (6.5.1) – (6.5.2) can serve as the basis for the studies of phytoplankton-macrophytes interactions with distinctive separation for production and transport of phytoplankton and its settling in the sink zones represented by the vegetation patches.

The settling flux can be represented by Krone equation (Krone 1962), the decay rate due to sedimentation can be represented as

$$K_d = \frac{C_d\, w_s}{L_d}\left(1 - \frac{\tau}{\tau_c}\right) \tag{6.5.3}$$

where w_s is settling velocity of the suspended particulate matter, L_d is characteristic length scale of the dead zone, and τ, τ_c are actual and critical shear stresses. Equation (6.5.3) can be further simplified taking in account the knowledge gained about the dead zones formed in the vegetation patches. Indeed, the vegetative dead zones are characterized by nearly zero shear stresses while the characteristic length scale can be represented by the multiplicative product of residence time and characteristic longitudinal velocity scale u_d. Velocity u_d is related, as it was shown in the Chapter 4, to the drag coefficient of plants and population density within the patch. Respectively equation (6.5.3) will be rewritten as

$$K_d = \frac{C_d\, w_s}{T_d\, u_d} \tag{6.5.4}$$

and hence equation (6.5.2) converts to

$$\frac{\partial C_d}{\partial t} = \frac{\left[C - C_d\left(1 + w_s / u_d\right)\right]}{T_d} \tag{6.5.5}$$

Although the deposition (sedimentation) flux is relatively easily represented in terms of the dead zone model and characteristics of suspended sediments, the decay/increase rate for the main channel is more difficult to formalize. However, for the case when only sedimentation processes are present, the increase rate for the main channel can be represented analogously to (6.5.4). For many rivers application of this approach can be practically relevant – for example to describe the transport and sedimentation processes in a vegetated river reach downstream a river confluence where tributary with increased concentration of suspended sediments discharge into the river. However, in more general case such as the transport of cohesive organic sediments and phytoplankton the model needs to account for the biological growth of algae.

In the next chapter we will apply theoretical considerations and obtained experimental data to analyse the morphodynamic processes and particularly sedimentation processes in the vegetative mosaic. Additional information related to consequences of morphodynamic processes and sedimentation/resuspension can be found in the Chapter 8.

7 MORPHODYNAMICS AND HYDRAULICS

The program of field observations on morphodynamic processes and flow hydraulics is described in the Section 7.1. The Section 7.2 is dedicated to the analysis of field measurements and comparison of morphodynamic processes in the channel free of vegetation and changes in these processes due to the seasonal growth of submerged vegetation. Similar analysis is completed for hydraulics of the investigated river reach, and the implication of hydraulic regime and morphodynamic processes for the biological processes are discussed in the Section 7.3.

7.1 Program of Field Measurements

The discussion of theoretical backgrounds on morphodynamic processes and flow hydraulics (Chapter 2, Subsection 2.4.2) already outlined that changes in morphodynamic processes reflect the changes in hydraulic regime and are primary connected to the subtle alterations in hydrodynamic structure of the flow. However, the temporal scales of morphodynamic processes are in general much longer than temporal scales of in-stream processes and hence the response is somewhat delayed by the inertia of the fluvial system. Therefore the strategy for studying morphodynamic processes differs from the strategy of studies of turbulent flows or dispersion processes. Essentially the program of research was composed of regular but non-frequent surveys of the riverbed morphology and of more frequent measurements of bulk hydraulic characteristics of the flow. Additionally for the periods of more intense morphodynamic changes we have performed special case studies exploring the dynamics of bedforms.

Riverbed surveys for the whole experimental river reach near the village Freienbrink were performed in the channel free of vegetation, at the maximum of vegetation biomass, and after the vegetative period. Measurements of riverbed elevations on arbitrary coordinate system were performed in cross-sections regularly spaced around 10m apart along the river reach. In each cross-section water depth was measured at points spanned on intervals of 1 m. Measurements were guided by marked steel tag-lines stretched between permanent monuments with known coordinates on the arbitrary system and were performed with a wadding rod. Elevations of flow free surface on the arbitrary coordinate system were also monitored during surveys allowing for further conversion of depth readings into riverbed elevations. The results of surveys were transformed into a series of cross-sectional profiles and digital maps using software tool as GRAPHER 6, and SURFER 7.

Two different types of additional specialized riverbed surveys were performed to address the problems of bedload transport and morphodynamic processes in the channel free of vegetation at high water discharges characteristic for winter season, and to explore formation of specific accumulations at vegetation patches. The studies of the first type required frequent detailed surveys of riverbed elevations in longitudinal sections allowing for tracing the kinematics of individual bedforms (ripples and sand waves), while the studies of morphodynamic processes within vegetation patches required surveys with enhanced spatial resolution.

The surveys of longitudinal profiles were performed using a measuring frame as a guide, Figure 7.1.1. An acoustic Doppler velocimeter sampling in a mode of an echosounder for a boundary profile was propagated along the guiding frame and taking very accurate readings of bed elevations every 5 cm. These surveys were relatively quick and lasted for the 12 m long profile only about 10 to 15 minutes. Surveys were repeated every 4 hours yielding the records of the riverbed relief. During the intervals between surveys of longitudinal profiles three detailed

profiles of turbulence characteristics were measured at three characteristic positions along a sand wave: in the trough, at the crest, and a stoss side of the wave. Velocities were measured in 20 points at each vertical profile. Near the riverbed the space between points was around 1 to 2 cm and the distance was increased to 5-6 cm in upper layers of flow. The measurements were collected at 25Hz for a sampling period of 5 minutes at each point.

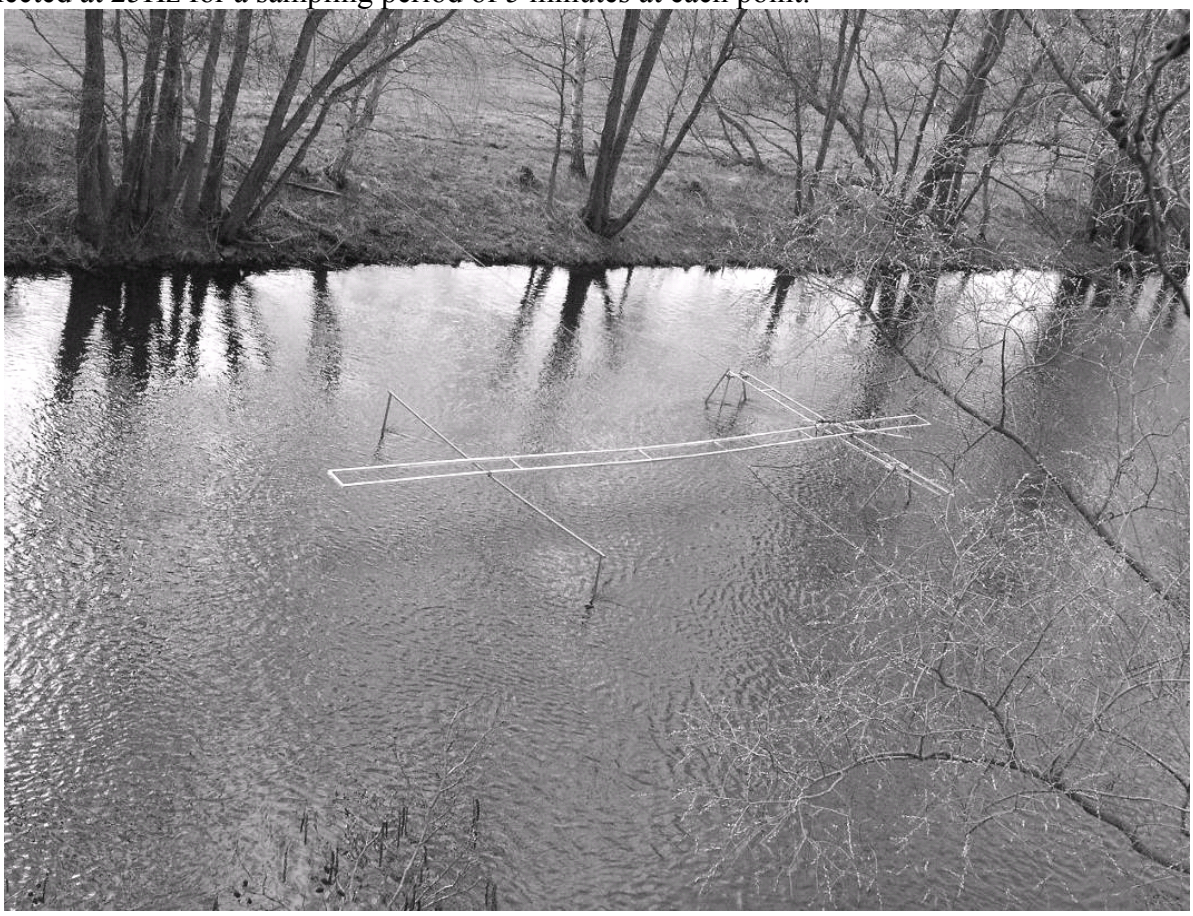

Figure 7.1.1 Guiding frame for surveying the longitudinal profiles.

Detailed surveys of riverbed elevations on a dense spatial grid were performed using a total station and direct measurements of planar coordinates and elevations around patches of macrophytes. Density of the grid was around 10×10 cm resolving fine details for selected parts in the vegetative mosaic. Morphometric measurements in this case were also accomplished with the surveys of riverbed material by taking sediment cores in the free paths of vegetative mosaic and within a vegetation patch.

Hydraulic observations comprised regular measurements of the free surface slope of the flow on the reach, water level, and a bulk velocity of the flow. The slopes were measured by taking water level readings on four gauging stations uniformly distributed along 300 m of the experimental reach. Each gauging station was equipped with 5 measuring piles enabling appropriate measurements of water level in wide range of water stages – from low to high (within 1.5 m of the amplitude). The elevations of the piles were accurately measured with a total station to gain precision around ±1mm yielding minimal accuracy in determination of the slope around 15% for smallest observed slopes. At high flow conditions and largest slopes accuracy was about 3 to 5%. The piles were regularly (minimum twice a year) checked for changes in elevations because of possible mechanistic displacements. Bulk velocity of the flow was measured using the flow tracing technique. A slag injection of the uranin solute was performed at the beginning of 300 long river reach and a response curve at the downstream end of the reach was recorded with the BackScat fluorometer. Velocity was determined by relating

length of the reach to the amount of time that concentration cloud spent to pass the reach. The time of a peak in concentration curve was used as the estimate of the travel time of the cloud.

7.2 Results and Analysis of Field Measurements

Field observations of morphodynamic processes and flow hydraulics completed in this study indicated two principal stages in the regime of investigated river reach. First, during the winter season (mid November – mid April) hydraulic regime of the river is characterized by high water discharges (10 to 25 m^3/s) transported in unvegetated channel and causing intensive bedload transport that predominantly occurs in the form of propagating ripples and sand waves. Second stage of the hydraulic regime is primarily affected by vegetation period (mid May – mid October) and characterized by low water discharges (3 to 5 m^3/s) with great reduction of the bedload transport and dominancy of suspended sediment transport. Though, during occasional high water events during summer period, an intensification of bedload transport might produce very specific morphological forms. The content of this section therefore is focused on comparative analysis of morphological structures caused by shift of dominancy of suspended sediment transport over bedload on the same river reach and explanation for the changes in respect to the flow structure.

7.2.1 Comparative analysis of morphodynamic processes

Characteristic longitudinal profile of riverbed elevations obtained in beginning of May 2002 (Sukhodolov and Sukhodolova 2005) in the central part of the experimental river reach indicates presence of a relatively wide spectrum of bedforms, Figure 7.2.1.

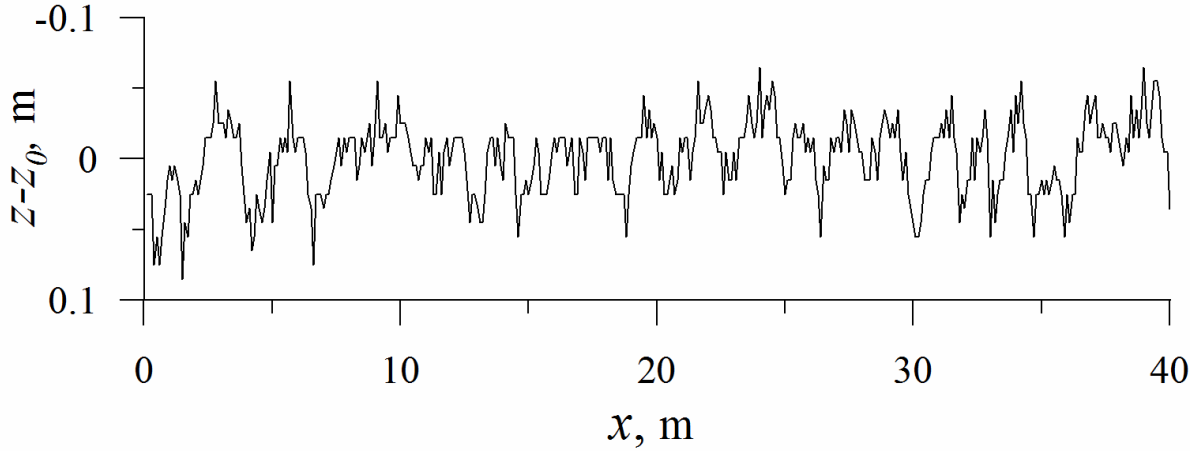

Figure 7.2.1 An example of a longitudinal profile of the riverbed.

The largest nearly symmetrical forms range in their length from 10 to 15 m and are superimposed with smaller slightly asymmetrical forms of 4 to 6 m long. Even much shorter ripples of around 50 cm in lengths are evident on the backs of sand waves. The height magnitudes are ranging from 15 to 20 cm for the larger bedforms, 5 to 15 cm for intermediate sand waves, and around 3 to 5 cm for the ripples. In horizontal plain the larger bedforms represent oblique (20-30° in respect to flow direction) features relatively regularly spaced in longitudinal direction and spanning around half of the river width, Figure 7.2.2a. Intermediate sand waves and ripples were oriented nearly perpendicular to the local direction of the flow, Figure 7.2.2b.

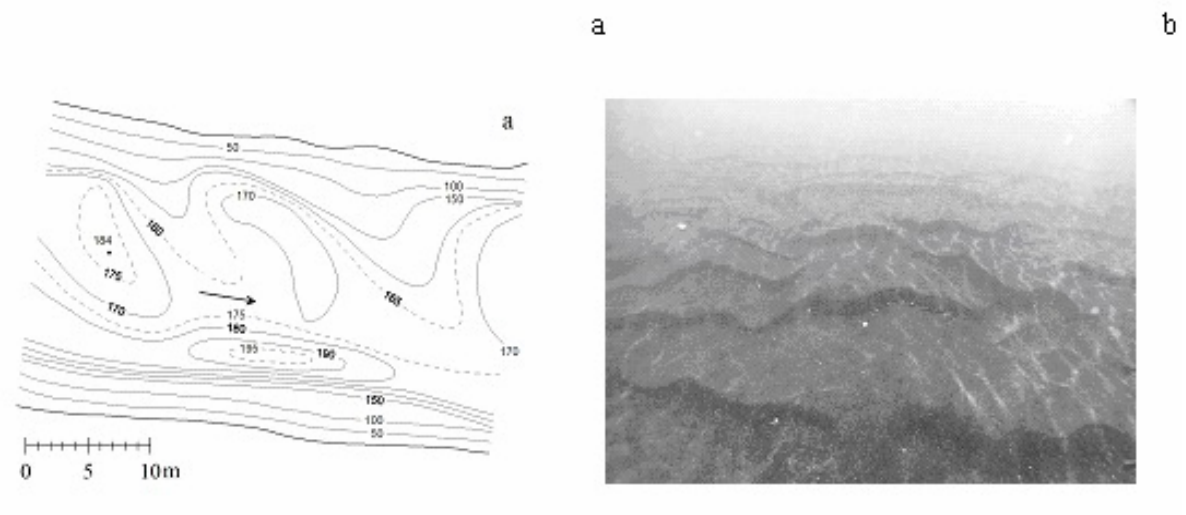

Figure 7.2.2 Planar geometry of bedforms (a), and an underwater photograph of ripples (b).

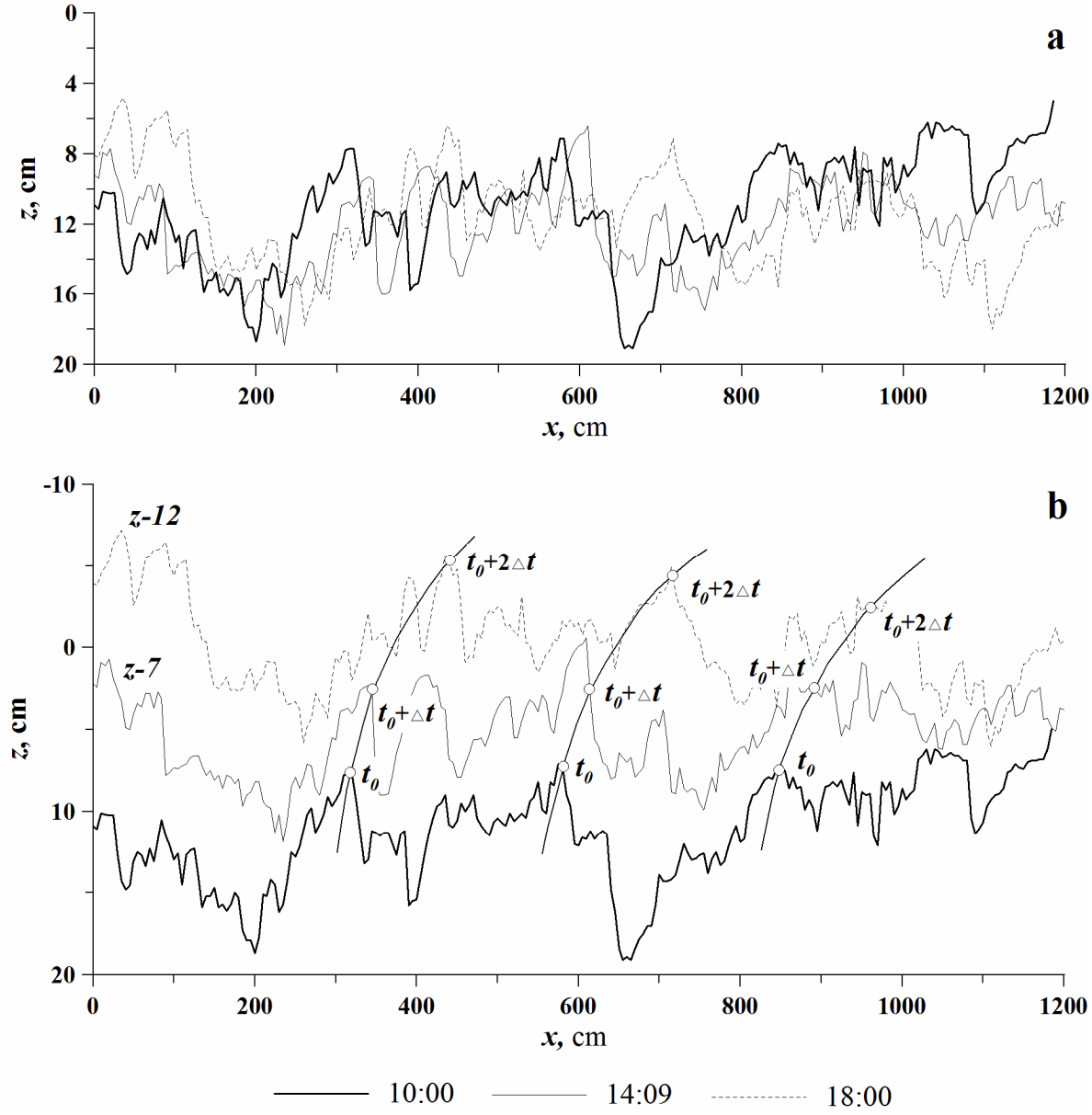

Figure 7.2.3 Longitudinal profiles of riverbed elevations measured in the central part of experimental river reach, mid April 2006.

Now we will explore dynamics of sand waves by analysis of time evolution of the longitudinal profiles, Figure 7.2.3. In Figure 7.2.3a three profiles presented in the same coordinate system outline the magnitude of changes in the riverbed elevations at particular points. Separation of profiles by shift in mean elevation (Figure 7.2.3b) allows examining the propagation of the individual sand waves by tracing the characteristic points of the waves as depicted by the connecting dashed lines for time moments $t_0, t_0 + \Delta t, t_0 + 2\Delta t$. One can see from the profiles that there is certain nonlinearity in the sand wave's dynamics of their transformations during propagation. These transformations obviously are a sort of dispersion in these advection-diffusion processes. Neglecting diffusion of sand waves by averaging over the whole period and over the ensemble of waves we can define a characteristic speed of sand waves propagation called waves celerity S_W

$$S_W = \overline{X} / \Delta\overline{T} \tag{7.2.1}$$

where $\overline{X}$ is averaged distance traveled by the bedforms, and $\Delta\overline{T}$ is averaged period of travel. An estimate of sand waves celerity for our experiments equaled $S_W = 4.2 \times 10^{-5}$ m/s which indicates relatively high rates of the local deformations of the riverbed. Indeed riverbed elevation can change about 15 cm during 8 hours, Figure 7.2.3.

To understand the dynamics of sand waves we need to take a closer look into the spatial structure of flow over the sand waves. Mean streamwise velocity profiles are shown in Figure 7.2.4 and corresponding turbulent shear stresses $-\overline{u'w'}$ in Figure 7.2.5.

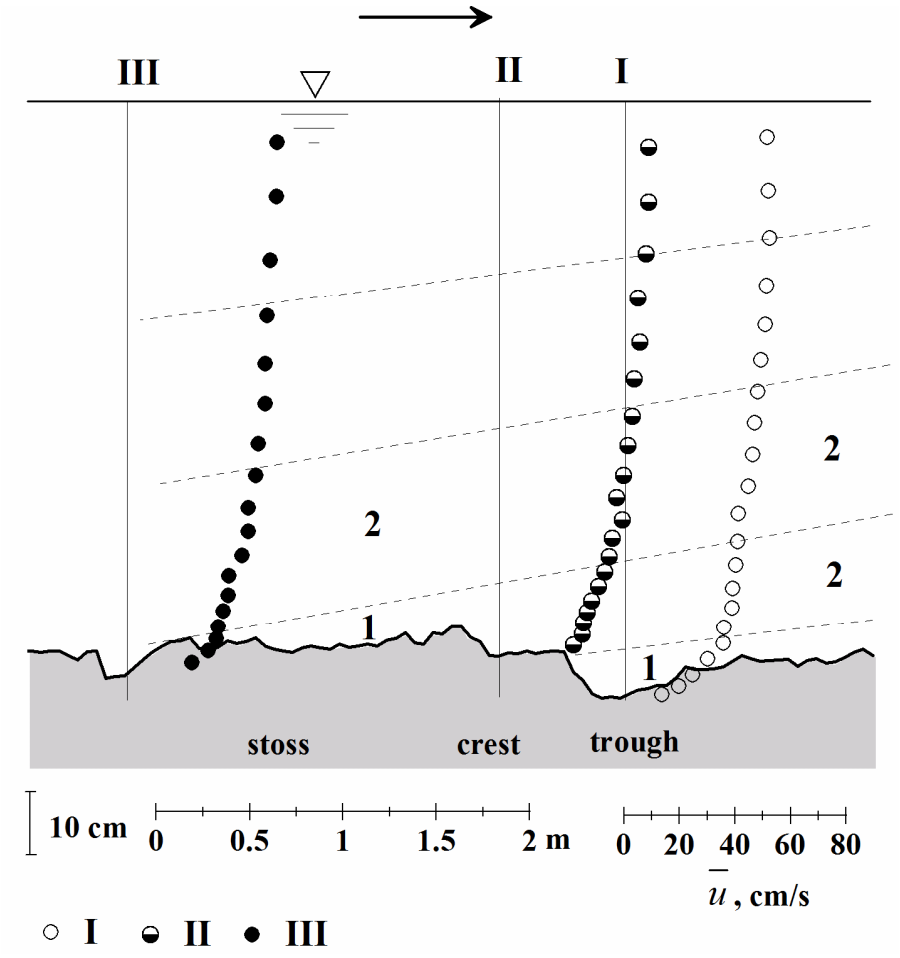

Figure 7.2.4 Distributions of mean streamwise velocity along a sand wave, mid April 2006.

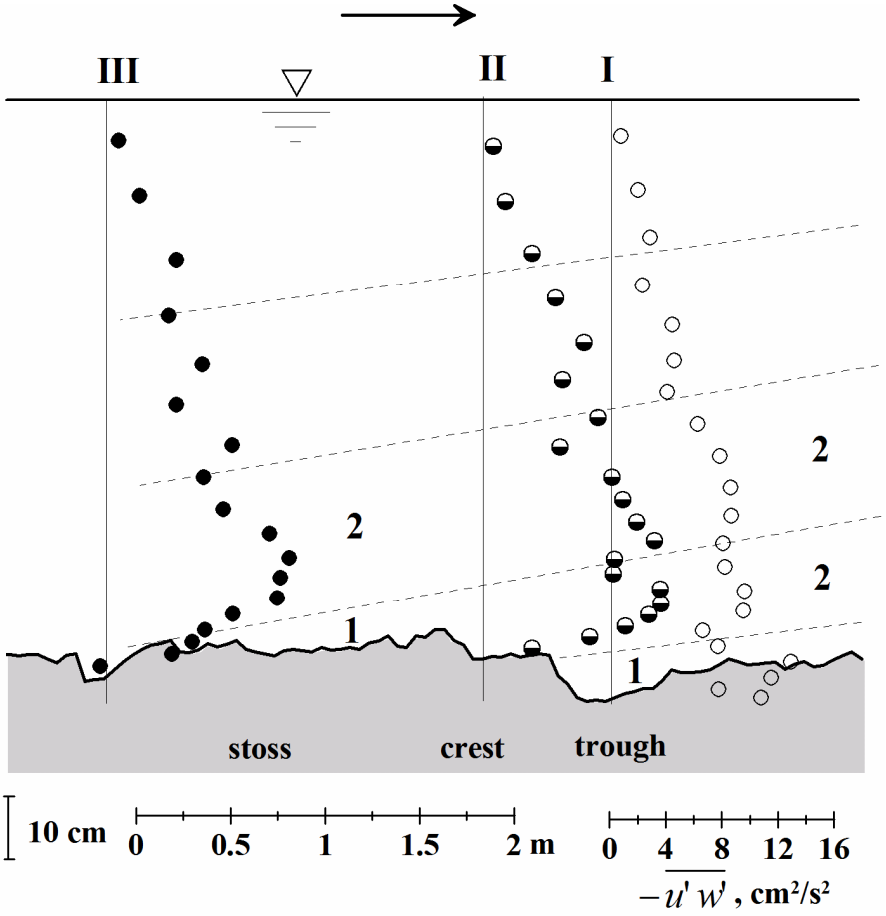

Figure 7.2.5 Distributions of turbulent shear stresses along a sand wave, mid April 2006.

Characteristic feature of these profiles is a distinct segmentation of profiles into a series of staked layers (Nelson et al. 1993; Sukhodolov et al. 2006). The segmentation reflects the development of internal boundary layers (1) along the stoss sides of the waves and the separation of these layers at the crests where they became wakes (2) spreading above the wave troughs, Figure 7.2.4, and Figure 7.2.5. Segments are characterized by approximately the same gradient of mean velocity and stresses, while the boundaries between layers are demarked by changes in the velocity gradients and the abrupt discontinuities in the stress values. The highest velocity gradients are observed near the riverbed at a trough of the sand wave. Distributions of shear stresses display even more evidently that the highest stresses occur in the trough very close to the riverbed – practically within millimeters from the riverbed, while at stoss side stresses are zero at the same distance from bed and the maximum of stress is displaced at relatively large distance. Knowledge of the mean velocity profile and turbulence characteristics together with information on spatial scales of sand waves allow direct comparison for estimated value of sand waves celerity with a prediction from a semi-empirical relationship (Nikora et al. 1997)

$$S_W = 0.019\, Fr^{2.9} \overline{U} = 0.019 \times 0.14^{2.9} \times 0.56 = 3.6 \times 10^{-5} \text{ m/s} \qquad (7.2.2)$$

and one can see that equation (7.2.2) predicts celerity fairly well with the accuracy about 15%.

From the profiles measured on 10:00 and 18:00 it is possible to compute the volumes of the transported material and to estimate the bedload discharge related to a square meter of the riverbed accepting commonly used value for density of sand $\rho_s = 2500$ kg/s and porosity of the material as 0.8. In our case the discharge was $q_b = 0.012$ kg/s. Application of Meyer-Peter and Müller formula (2.4.16) with $d_{50} = 0.6$ mm and shear velocity value $u_* = 3.7$ cm/s (Figure 7.2.5)

yields predicted value for $q_b = 0.031$ kg/s. Thus equation (2.4.16) overpredicted the bedload discharge about 2.5 times. The discrepancy most probably accounts for the fact that bedload transport in our case is more discrete as compared to laboratory studies mostly used to define parameters of Meyer-Peter and Müller formula.

Analysis of flow structures provides, together with the information on kinematics of sand waves considered above, some understanding for the mechanisms of bedload transport. Thus, the strong physical forces act on the sedimentary grains in the middle part of the sand wave trough. These forces destabilize and lift grains into the flow where they saltate to the stoss side and land. A weak transport in the form of ripples transports grains at shorter distances along the stoss toward the crests where they either saltate or avalanche into the upper part of the trough. Therefore the sand waves propagate mainly by erosion at the middle and downstream parts of the trough and avalanching and accumulation of saltated particles at the upstream part of the trough. Peculiar feature could be figured out from Figure 7.2.4, and Figure 7.2.5 - the geometry of river bed topographically does not notably change between stoss, crest, and the trough. Indeed, one can hardly tell the difference because of superimpositions of different waves and ripples while the spatial distribution of turbulence characteristics provides a clear picture. Velikanov (1958) suggested a hypothesis that spatial scales of sand waves are primary connected to the characteristic scales of coherent structures, and in our case they can be estimated using equation (2.1.41), providing for measured flow parameters value $L_C / h = 6.2$ or ≈ 9.5 m, which appears to be an upper range of the measured sand waves.

Underwater visual observations of riverbed relief showed that after mid May with development of vegetation sand waves and ripples disappear gradually in time. The river bed became more uniform, and the upper layer of sand became coated with a venire of fine sediments and a biofilm. Presence of vegetation causes intensive deposition of suspended material and local aggravations of riverbed, Figure 7.2.6.

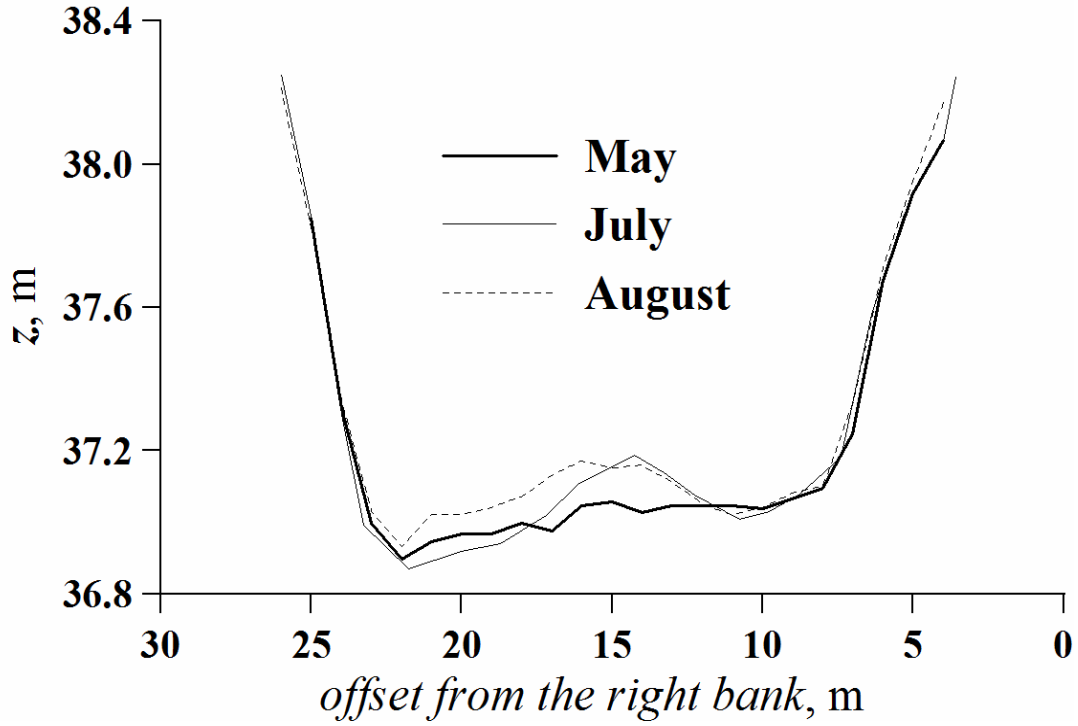

Figure 7.2.6 Dynamics of the riverbed relief in a cross-section through the vegetation period 2005.

Appearance of a vegetation patch in the middle of the channel caused a slight scour in a free path on the left part of the channel, which was later covered with deposits because of the lateral spreading of the vegetation. Detailed spatial surveys of riverbed relief around a patch of

macrophytes allowed accurate mapping of depositional bedform, Figure 7.2.7. Distribution of the grain size of the riverbed material across the bedform (Figure 7.2.7) is shown in Figure 7.2.8. One can see that unimodal grain size composition inside the bedfrom is dominated by fine material with the $d_{50} = 0.4\,\text{mm}$, while on the margins of the bedform in the regions of free path the distributions are bimodal and represented by a mixture of coarser material with the $d_{50} = 5\,\text{mm}$ which creates an armoring layer for the finer material. Therefore this type of bedforms was created by selective depositions and retention of finer sediments inside the patch and erosion on the margins of the patch and was a result of highly variable hydraulic conditions enabling entrainment of particles about 0.4 mm into the transport.

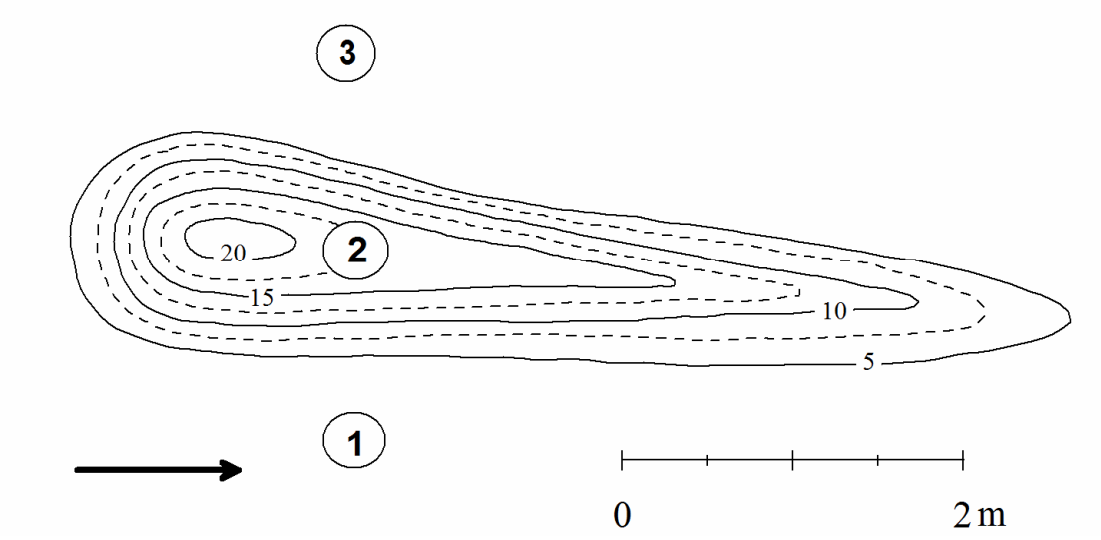

Figure 7.2.7 A bedform measured around a patch of vegetation in beginning of July (circles with numbers indicate positions of sediment samples for granulometric analysis).

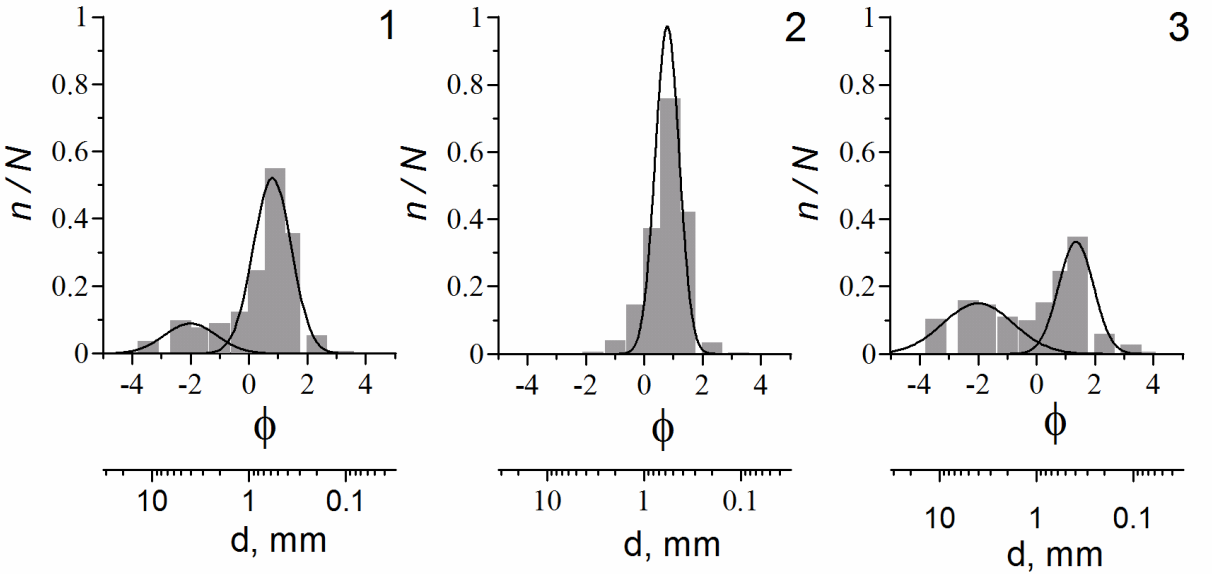

Figure 7.2.8 Spectra of grain sizes across a depositional bedform formed in a patch of vegetation.

However, more common mechanism by which riverbed relief is modified in lowland vegetated reaches under moderately varied hydraulic conditions is deposition of material inside the vegetative patches. A map of river bed changes occurred between initiation of vegetation growth and its maximum is shown in Figure 7.2.9.

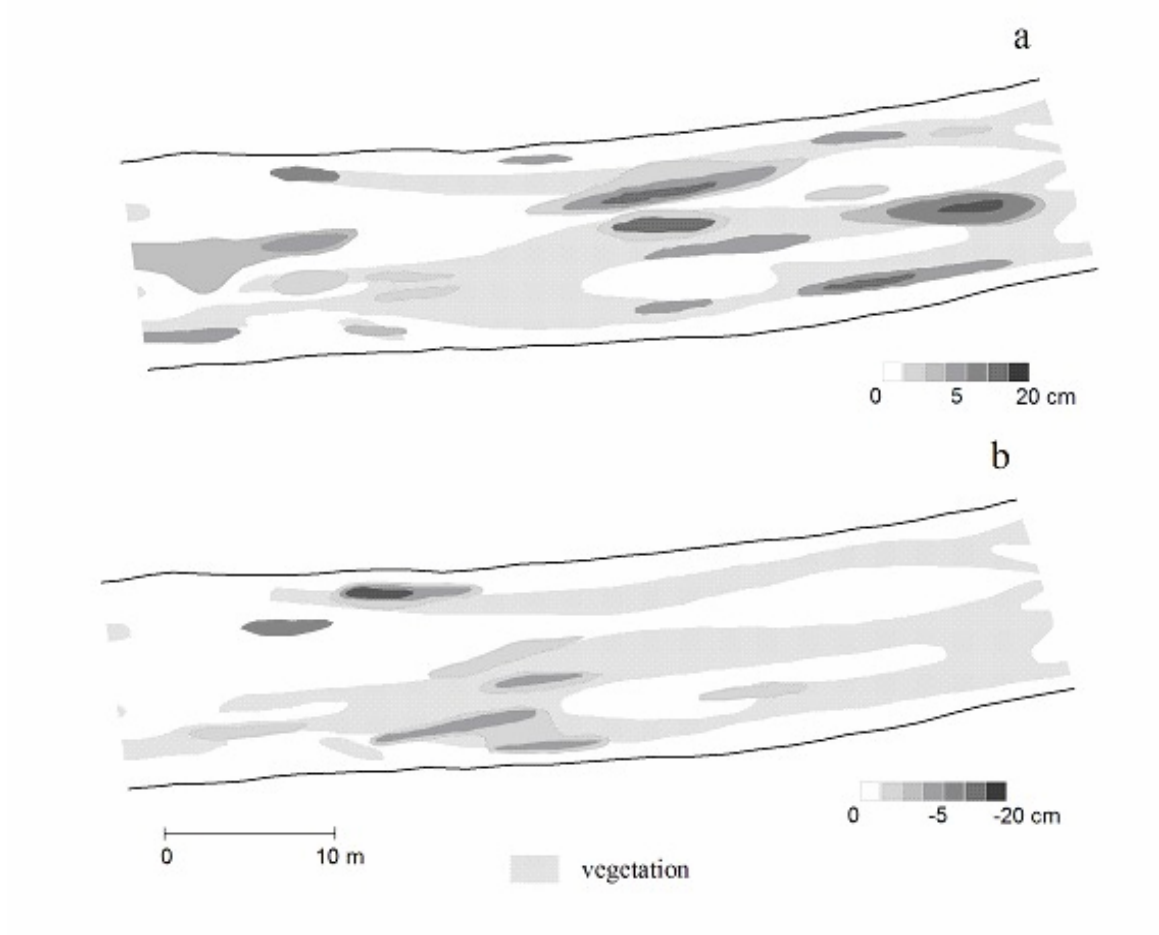

Figure 7.2.9 Differences in riverbed elevations: (a) deposition, and (b) erosion patterns for the period April-August 2005.

Deposition of the riverbed material is highly inhomogeneous inside the vegetation mosaic depicted by contours in Figure 7.2.99. The dominated accumulation forms are mostly located inside the vegetated areas, while larger erosion forms were occurring on the margins of vegetation patches and in the free paths. Some accumulation of material in the free paths and erosion inside vegetated areas indicate the transport of the bed material which was most probably occurring at episodic high flow events. The pattern of accumulated material inside the vegetation patch is important for revealing the spatial size of effective dead zones inside the vegetation.

The depositional flux q_s is represented by the conventional Krone's equation (Krone 1962)

$$q_s = \overline{C} u_s \left(1 - \frac{\tau_0}{\tau_c} \right) \tag{2.7.3}$$

where $\overline{C}$ is mean concentration of suspended sediments, u_s is settling velocity, τ_0, and τ_c are bed shear stress, and critical shear stress respectively. As it was shown in Chapters 4 and 6, inside the zone of longitudinal transport the turbulent stresses are practically zero and hence equation (2.7.3) can be reduced to only account for concentration and settling velocity. Previous studies (Prochnow et al. 1997) provide estimates for a range of settling velocities for cohesive sediments in the Spree River and characteristic suspended concentrations, Table 7.2.1. With the data from Table 7.2.1, applying equation (2.7.3) for one-dimensional flow with zero bedload discharge, and accounting for average porosity of cohesive organic matter as 60%, one obtains a layer of deposition around 10-15 cm for the period of 3 months – a value agreeable with observations. Thus, to summarize the results of morphodynamics studies we can conclude that we have obtained important quantitative information about characteristic fluxes of particulate

matter for investigated river reach and evaluated the effect of vegetation on morphodynamic processes.

Table 7.2.1 Characteristics of the suspended sediments in the Spree River

Date	u_s, m/h	$\overline{C}$, mg / L	γ_s, %	ρ_s, kg/m^3	Δz, cm
17.08.1992	4.93	14.8	60	1600	17
31.08.1992	1.80	28.7	60	1600	12
23.08.1993	4.89	11.1	60	1600	13

7.2.2 Comparative analysis of river hydraulics

Theoretically, as it was shown in the Subsection 2.4.1, the effect of vegetation is pronounced on the following bulk characteristics of flow: 1) decrease of bulk velocity of flow; 2) increase of water depth on the reach; and 3) decrease of the slope of the free surface. All these changes are observed when the flow characteristics of the same river reach are compared at the same water discharges in vegetation-free channel and in vegetated channel respectively. A perfect illustration to the seasonal variations of integral characteristics on the investigated river reach is presented in Figure 7.2.10, where the water stage relationship measured in the control section Grosse Tränke, located 5 km downstream Fürstenwalde (Figure 3.1.1a) are plotted together with a biomass growth curve computed using the model (5.2.11). For the same water discharge the water level can change for more than 1 m, and for lower discharges that are normally observed during summer (≈ 3 m^3/s) it ranges within 20-25 cm.

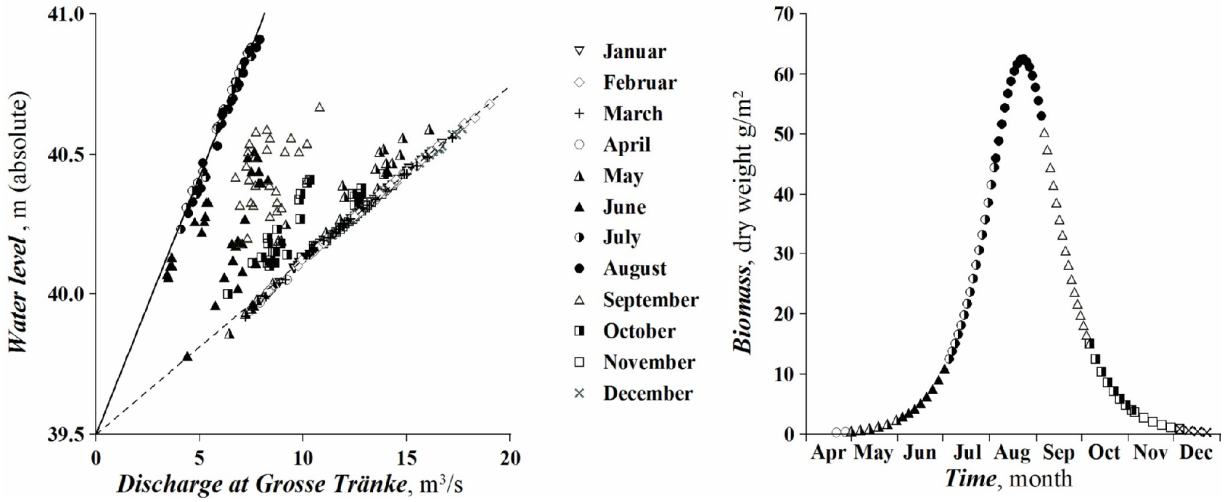

Figure 7.2.10 Stage relationships for a control section Grosse Tränke and a biomass growth curve for submerged macrophyte *Sagittaria sagittifolia.*

A mass colonization of the Spree River by submerged macrophytes *Sagittaria sagittifolia* began about 15 years ago and was caused by the changes in complex industrial utilization of waters. Before 1990th the Spree River was accepting waters pumped from the mines of brown coal in Lusatians, and in beginning of 90th when the exploration of mines was closed, the hydrological and chemical regimes of the Spree were greatly altered. In the period 1992-1995, a period when submerged macrophytes were not abundant on the Spree River and dominated by other species than *Sagittaria sagittifolia,* a series of hydraulic measurements was completed on

the experimental reach near Freienbrink (Prochnow et al. 1997). The results of those studies illustrating hydraulic regime of the river in the channel free of vegetation and vegetated channel (measurements of the present study) are presented in Figure 7.2.11.

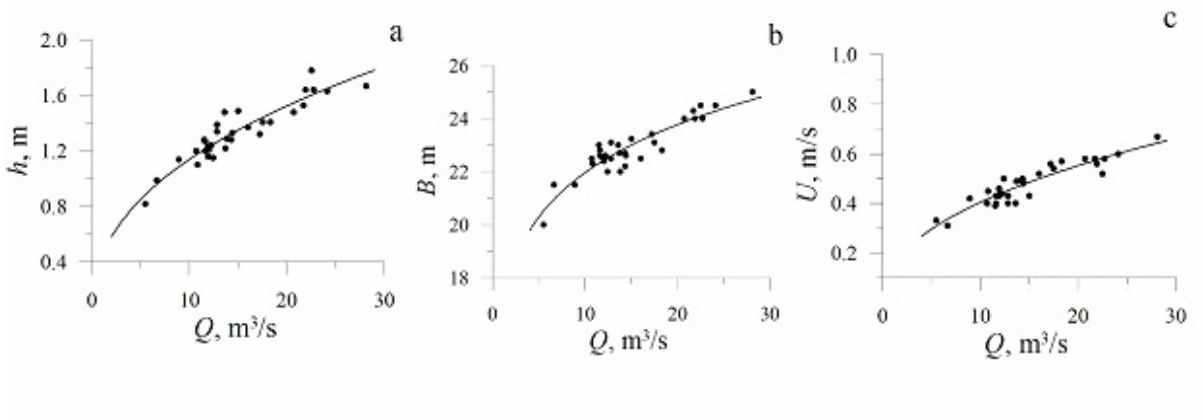

Figure 7.2.11 Relation between bulk flow velocity (a), river width (b), mean depth (c) water discharge in the Spree River near Freienbrink (measurements 1991-1995).

The effect of relative riverbed roughness on the slope of flow free surface in vegetation-free conditions is shown in Figure 7.2.12. The data on that plot are represented in the dimensionless form: the slopes are normalized by the maximum slope of riverbed on the reach, and the flow depths are scaled on heights of macroforms of riverbed which on average were $\Delta h = 0.25$ m.

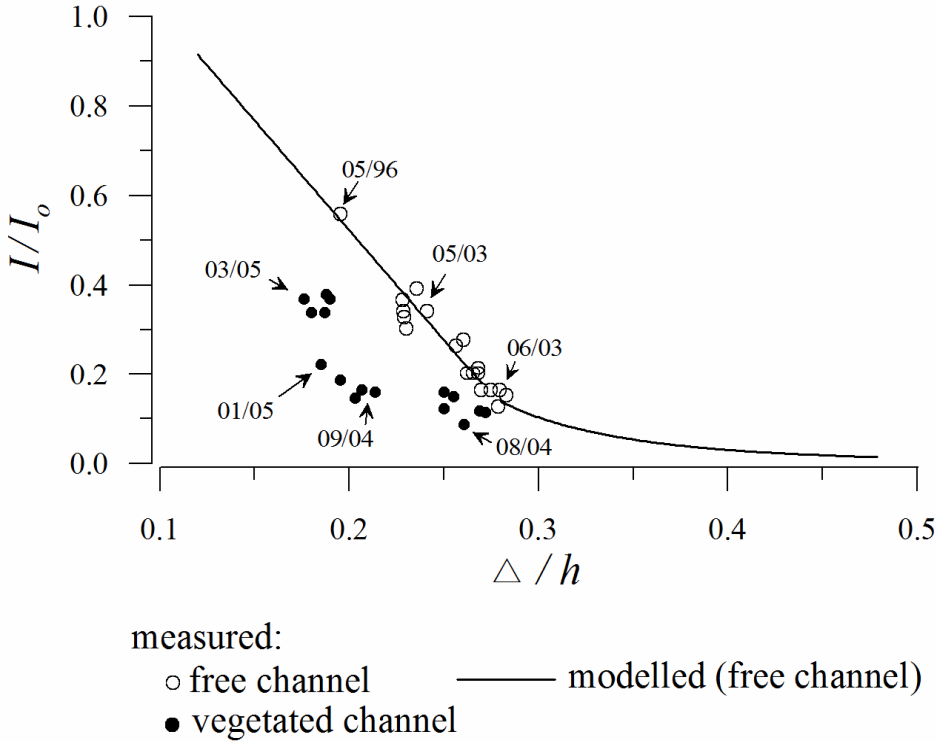

Figure 7.2.12 Seasonal changes of the free surface slope in the Spree River near Freienbrink.

A solid line in Figure 7.2.12 represents the relationship for the slope modeled using equations for flow without vegetation (2.1.24), (2.1.26), and (2.1.29) and the data set depicted in Figure 7.2.11. The data points follow a linear decline of the slope for small relative roughness values $0.1 \geq I / I_0 \geq 0.28$ and the effect of relative roughness (submergence) on slope is stabilized when the roughness elements are larger than 0.3 river depth. The slopes asymptotically decline to zero values for submergence $\Delta h / h \rightarrow 1$ physically meaning absence of surface flow when the water level is at height of roughness elements. The slopes measured in the vegetated

channel are significantly reduced in comparison with a free flow, as it was expected from the theoretical analysis presented in the Section 2.4.1. The channel resistance, represented by n from Chezy-Mannings formulae (2.4.5-2.4.6) and plotted as a function of $U\,h$ (Figure 7.2.13), is also indicating enlarged values of resistance for the vegetated channel as compared to the unvegetated conditions. The solid line in Figure 7.2.13 was computed for the free channel using equations (2.4.5-2.4.6) and best fits to the data in Figure 7.2.11-Figure 7.2.12. It can be seen that measurements completed in 2004-2005 in the unvegetated channel agree with the prediction and follow the trend (2.4.5-2.4.6). However, the data measured in vegetated channel display no obvious relationship, presenting rather a cloud of points. This may reflect the fact that the $n-U\,h$ method is most probably inappropriate in the case. Indeed, for the same type of vegetation experimental data of flume studies are usually scaled on any of a specific $n-U\,h$ curve of the family. According to a standard diagram suggested by USDA (1947), the tested grasses were subdivided into 5 classes, Figure 7.2.14.

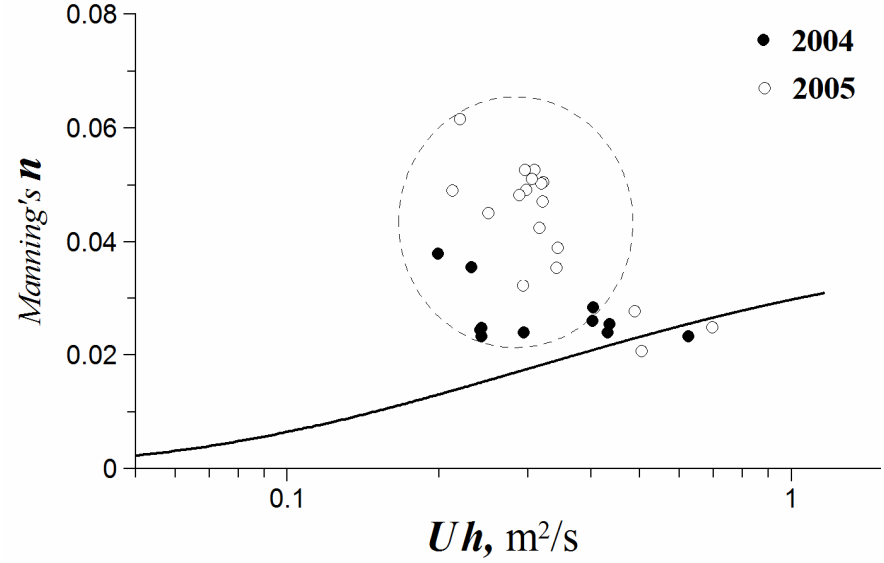

Figure 7.2.13 Comparison of $n-U\,h$ curves for the vegetation free (solid line) and vegetated channel.

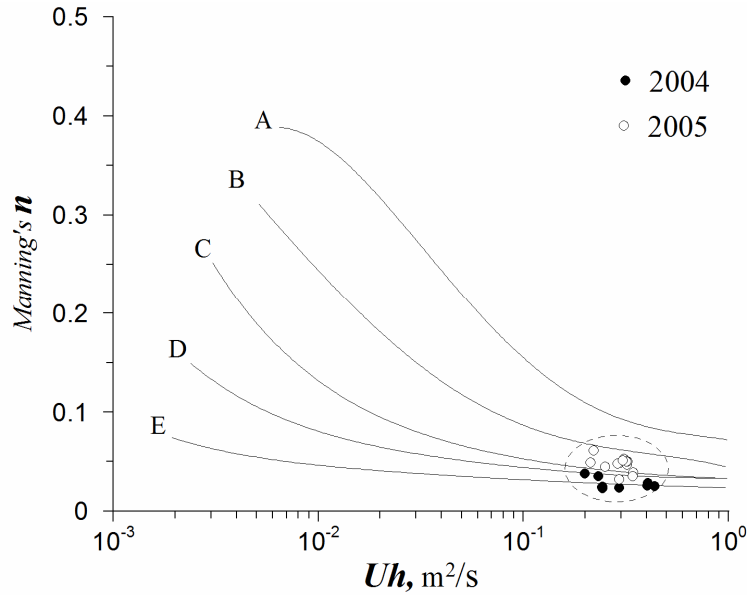

Figure 7.2.14 Comparison USDA $n-U\,h$ retardance curves with the data of present study (only vegetated channel).

Recently Wilson (2007) compared the results of her study and indicated a perfect scaling by $n-U\,h$ curves. Although in our case the data were represented by the same species of vegetation and measured in the same river reach, they display no collapse on a specific curve, thus confirming the conclusion about inappropriateness of the diagrams.

Retardance curves were obtained in laboratory channels with relatively large slopes $I_0 \approx 0.1-1\%$ and considering only effect of rigidity for both rigid and flexible vegetation (Kouwen and Uny 1973; Wilson 2007). In our study the slopes were less than 0.01% or even more than 10 times smaller of the lowest available limit. At larger slopes ($I_0 \approx 0.1-1\%$) the changes in slope due to vegetation resistance are insignificant and hence do not affect estimates of the shear stresses from equation $\tau_0 = \rho g\left(h-h_v\right)I$. Therefore values of Manning's coefficient are reasonably estimated and representative for certain type of vegetation in laboratory experiments and they are incorrect for our data of lowland river condition because of two reasons: 1) the shear stress is estimated incorrectly due to slope change, and 2) Chezy coefficient is not scaling on factor one sixths of the channel depth as the depths is increasing due to vegetation effect.

Despite widespread usage of Manning's coefficients due to the gap of knowledge on channel resistance, these coefficients are difficult to generalize because of their dimensionality and primarily relation to a certain and very specific model of turbulence (boundary layer or open-channel flow) that was shown by laboratory and present field studies (Chapter 4) to be inappropriate in lowland rivers with small slopes and flexible vegetation. More appropriate parameter is the friction factor (2.4.10), because it is dimensionless and is not restricted to a specific turbulence model. Though there is a problem here in determination of shear stresses and density of vegetation as the main factors defining resistance of the channel. A possible alternative for direct measurements of turbulent stresses can be the estimation of velocity difference and density of vegetation with further evaluation of stresses from the scaling relationships developed for shear layer model (4.1.20) and estimating reconfiguration of plants (the reduction of projected area because of deflection) with the developed model (5.2.8). The estimates of resistance (dashed curves) and comparison with data of completed experiments are shown in Figure 7.2.15.

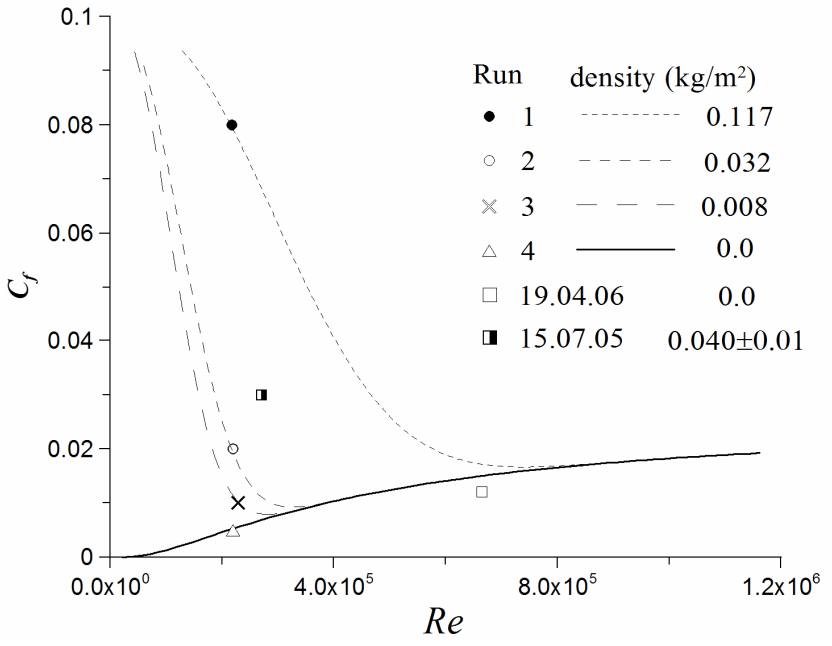

Figure 7.2.15 Modeling friction factors as the functions of density of vegetation and its projected area as function of bending angle (dashed lines) and comparison with results of field experiments (symbols), and field measurements (Table 4.2.1-4.2.2, 4.2.3).

In contrast to the semi-empirical retardance curve method $n - U\,h$ this approach provides physically sound background accounting for main physical and bio-mechanical parameters of flow and vegetation. It can be easily expanded to describe seasonal changes during vegetation period by modeling density of vegetation with biomass model: equations (5.2.11) – (5.2.16). Unfortunately in our field experiments we were restricted by hydraulic conditions in a narrow range of Reynolds numbers thus lacking possibility for more rigorous direct comparison of modeled results and observations. Nevertheless, the approach can be used for planning and interpretation of further studies that we hope will address the problem in detail.

7.3 Implications for Biological and Transport Processes

Results of field observations and experimental investigations presented in this chapter provide deeper insight into mechanisms driving biological and physical processes in lowland rivers during the vegetation season. In contrast to the terrestrial vegetation and some other aquatic species the annual succession of *Sagittaria sagittifolia* population can be greatly altered by morphodynamic processes, particularly by development and propagation of bedforms – ripples, and sand waves.

Terrestrial vegetation and riparian forms of vegetation such as reeds mostly form stable populations that change density of the cover mainly by loosing leaves. Exceptions can be usually observed only on the eroded slopes and in arid regions on the loose soils. In rivers at higher flow rates alluvium almost always became loose and actively transported. Bedload transport causes temporal erosion of upper layer of sediments (about 20 cm thick) exposing plants tubers and entraining them into motion. Because the flow structure over bedforms is characterized by reduced velocities in sand waves troughs, coarse organic particulate matter is retained in those areas as illustrated in Figure 5.2.8a. Therefore despite of seemly randomness of the processes, the knowledge on morphodynamic processes might provide very important information on the initiation of vegetation cover development. A possible way to determine initial density of vegetation distribution is to relate the spatial pattern to wave lengths of dominant bedforms (sand waves). Unfortunately we still know only few about how the tubers of the plants are distributed over the sediment depth and how are they entrained and transported, and therefore we have to leave this problem for future studies.

Studies of depositional and scouring patterns in vegetative mosaic, an example of which is shown in Figure 7.2.9, provide a great deal of information on spatial arrangement of the vegetative patches, free paths and their actual capabilities on altering flow condition and promotion of sedimentation. Interesting property of erosion/deposition patterns is their certain large scale periodicity causing large scale (order of 2÷3 river width) perturbation of flow field. Development of such large scale perturbations is analogous to evolution of bedforms into alternation or crescent bars and might result in certain increase of flow resistance and reduction of the slope of the riverbed. This study and some recent investigations (Sand Jensen 1998) provided only first insight into this important issue, but development of modern surveying techniques relaying on differential global positioning systems might provide possibilities for routine high resolution surveys of large river reaches.

Investigation of river hydraulics and particularly the problem of resistance in a natural stream with seasonal growth of vegetation completed in frame of this study indicates, that conventional methods developed in result of experimental studies completed in flumes with large slopes (I ≈0.1÷1%) and accounting only for rigidity of vegetation are inappropriate for conditions of lowland rivers with small slopes (I ≈0.01%) with flexible buoyant vegetation. To develop practical methods of computation of flow resistance for such conditions requires refined approaches for determination of turbulent shear stresses and relationships between characteristics of vegetation cover and flow. The model developed in this study represents a first promising step

in that direction but requires for rigorous experimental validation which at the moment is hindered by the lack of field experimental data. Nevertheless, obtained quantitative and qualitative information about resistance of the channel and its seasonal changes allows for improvement of the modeling of hydraulic characteristics, such as bulk flow velocity and mean flow depth, and is important for application in the scientific practice.

8 APPLICATIONS OF THE RESULTS

This Chapter illustrates the application of theoretical knowledge and experimental material gained through this research to complex multidisciplinary studies of ecological and biological processes carried out in IGB. In the Section 8.1 the studies of retention of nutrients and chemicals and conditions of their entrainment into suspension are discussed in respect to the spatial variability within the vegetation mosaic. Application of the longitudinal dispersion model as a theoretical framework explaining development of juvenile fish communities is illustrated in the Section 8.2.

8.1 Retention Processes in River Channels

The transport function of waters in a river, as an agent to deliver phosphorus and nitrogen (called nutrients because of their crucial role for living organisms), is one of the principal mechanisms driving the fluvial ecosystems. An important feature of nutrients is that they are mostly included into the sediments via different compounds, rather than dissolved in the water, and hence their transport is very susceptive to the sedimentation and resuspension processes. As it was already shown in the Chapter 7, vegetation is on the control of sedimentation and erosion patterns in the vegetation mosaics. Therefore it is very valuable to illustrate quantitatively the implications of sedimentation and resuspension processes for the retention and transport of nutrients. Here we present some selected results of a multidisciplinary study addressing to some extent the topic and completed in IGB under supervision of Dr. A. Kleeberg with our participation (Kleeberg et al. 2008).

This field experimental and measurement study was designed to investigate the thresholds of resuspension for the riverbed sediments, to quantify resuspended fluxes of nutrients, and their chemical composition and distribution of substances within the vegetation mosaic. The study was completed in August 2006 on the experimental reach near Freienbrink and included *in situ* resuspension experiments, sampling of the riverbed sediments with sediment cores, and concurrent measurements of the flow and its turbulence characteristics. Two sets of measurements were performed at one location inside a vegetation patch (average biomass dry weight 0.112 kg/m^2), and in a free path of the vegetation mosaic. Sediment resuspension experiments were performed with an erosion chamber (Gust 1990). The device creates a certain level of a shear force on the riverbed by stirring water inside the chamber, Figure 8.1.1. The water was pumped through the chamber to determine turbidity and to sample the water for further chemical analysis in a laboratory. Each experimental run consisted of the measurements at 11 levels of the shear velocity increased from 0 to 0.34, 0.53, 0.85, 1.11, 1.34, 1.55, 1.69, 1.90, 2.09, 2.26 and to 2.42 cm/s for 20 minutes for every measurement. Turbidity was recorded at sampling rate of 0.17 Hz by a Forward Scatter Turbidimeter TF 10-512 (Optek-Danulat, Essen, Germany). An integrated water sample was taken during the entire period of each step in the shear velocity. Four undisturbed sediment cores were collected inside a patch and in a free path with a sediment corer (UWITEC©, Mondsee, Austria) and sliced to obtain a range of depths as 0-0.5, 0.5-1, 1-2, 2-4, 4-6 cm. The details of chemical processing procedures can be found in the paper by Kleeberg et al. (2008).

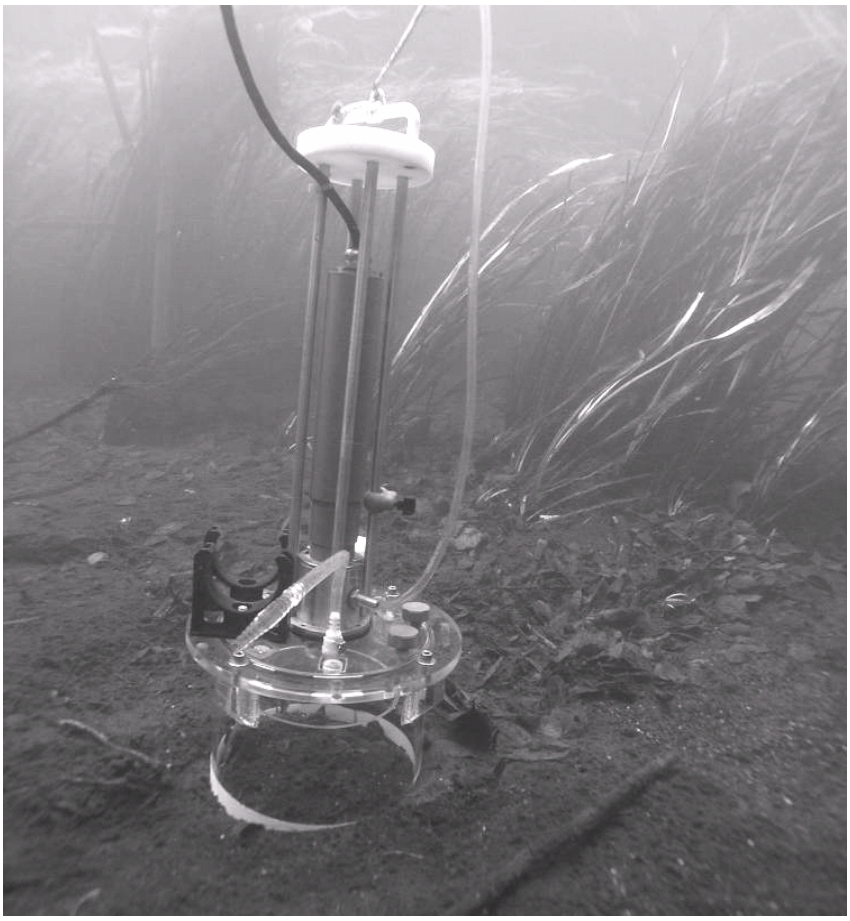

Figure 8.1.1 Resuspension chamber for *in situ* testing of the riverbed sediments deployed in a free path of the vegetation mosaic (flow from lower left to upper right side).

Sedimentary composition of the surface veneers inside the vegetation patch and in the free path of mosaic was distinctly different (Figure 8.1.2). Inside the patch the sediments were moist, loose, and fine graded. Respectively in the free path the sediment was coarser (Figure 8.1.2a), with heavier dry weight and contained lesser organic matter (Figure 8.1.2b). The content of total phosphorus, nitrogen, and iron in the upper layer of sediments (between 0 and 3 cm) was 2-3 times higher in the samples taken inside the patch as compared to the samples in the free path (Figure 8.1.2c-e). Deeper into the sediment layer the contents were not that different. This analysis also supports a choice of a threshold of ±2.5 cm in the riverbed elevation that was applied to differentiate accumulation and erosion patterns (Figure 7.2.9). The vertical stratification of the sediment composition reflects the features in temporal dynamics of the macrophytes patch and hence the flow adjustments. Indeed, at early stages when the density of vegetation was not high enough to dump turbulent resuspension of the fine material, only the coarser sediments were accumulated and their chemical composition only slightly differed by a small amount of fine organic matter (Figure 8.1.2a-b).

Reckoning that average size of a patch is about 1.5×10 m (Figure 7.2.9) with a thickness of chemically reach layer of 2.5 cm, and porosity of the river bed material 0.6 (muddy incompact substrate) and specific weight about 1.600 kg/m^3 one can estimate amount of retained substances in a patch. Thus the estimate per average patch yields 0.53 kg of phosphorus, 0.84 kg for total nitrogen, 11.4 kg of organic carbon, and around 5.2 kg of total iron. Averaging over total area of the experimental reach 20×50 m and 10 patches depicted by deposition layers more than 2.5 cm in riverbed elevation (Figure 7.2.9) provides bulk characteristic of retention as 5.3 g/m^2 for phosphorus, 8.4 g/m^2 for total nitrogen, 114 g/m^2 of organic carbon, and 52 g/m^2 of total iron.

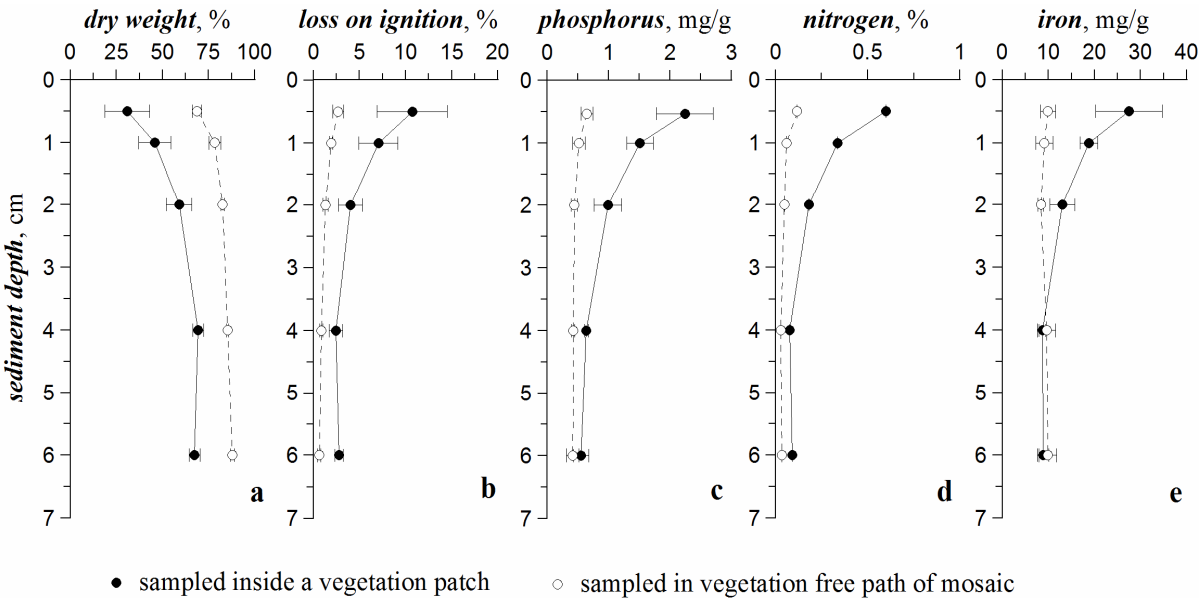

Figure 8.1.2 Chemical composition of riverbed sediments in a vegetation mosaic, August 2006

The resuspension experiments completed with the resuspension chamber indicated large difference between properties of riverbed material deposited inside the vegetation patches and riverbed material in the free path of the mosaic. When chamber was installed inside the patch, the concentration of particulate matter in the chamber increased even at small shear velocities (<0.5 cm/s), then with further increase of shear velocity SPM slightly decreased and was continuously rising in response to increase of shear velocity (Figure 8.1.3a).

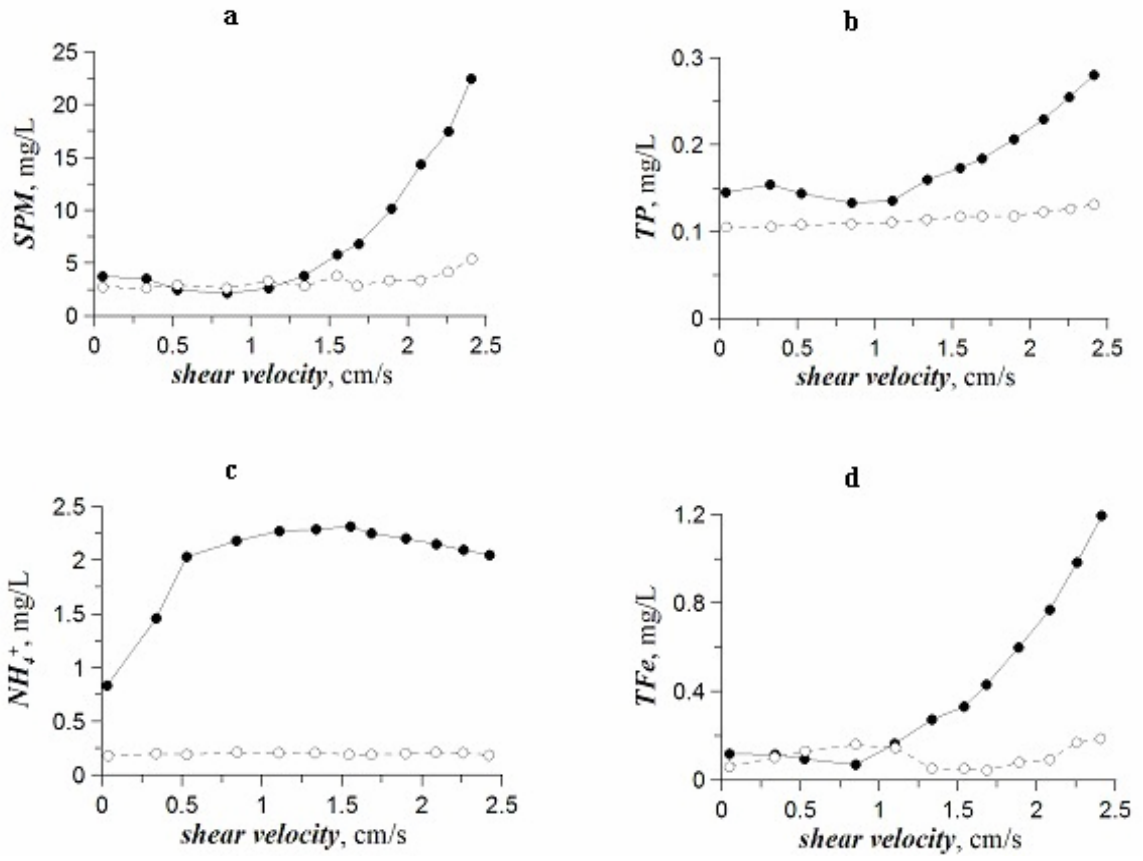

Figure 8.1.3 Results of resuspension tests for sediments on the riverbed inside vegetation patches (filled circles), and in vegetation-free path of mosaic (open circles): (a) suspended particulate matter; (b) phosphorus; (c) nitrate; (d) total iron.

In the free path there were no significant systematic changes in the SPM concentration until a threshold in the shear velocity of about 2 cm/s was reached (Figure 8.1.3a). In general SPM concentration increased 6 times at the shear velocity level of 2.5 cm/s in comparison with the initial concentration at the nearly zero shear velocities inside the vegetation patch. In vegetation-free path of mosaic SPM concentration increased only 2 times. Respectively, with increasing concentrations at increasing shear velocities the chemical content of water in the chamber was showing increase of concentrations for different constitutions (Figure 8.1.3). Although total phosphorus and total iron indicated patterns of response similar to SPM, the NH^{+}_{4} was reaching maximum concentration at 0.5 cm/s and was practically constant all over the range of shear velocities (Figure 8.1.3c).

Analysis of chemical composition of the riverbed deposits together with the resuspension experiments provides important clues to the processes that formed the deposits. The results of this study, however, need to be considered with the knowledge gained from studies of hydrodynamics (Section 4.2), morphodynamics (Section 7.2), and phenological dynamics of vegetation (Section 5.2). Completed studies show that riverbed deposits in the free paths of the vegetation mosaic as well as in the deeper layers of deposits inside the vegetation patches are formed similarly at conditions of intensive bedload transport and therefore are nearly identical in their chemical composition. Some small differences can be explained by the difference of biological and chemical processes evolving in sedimentary deposits during vegetative period when sediments are at rest. High sensitivity of riverbed material inside vegetation patch to the physical forcing by turbulence indicates that for developing appropriate rates of deposition a relatively high density of vegetation should be established. From field experimental studies it can be concluded that the biomass of *Sagittaria sagittifolia* mast be at least larger than 0.050 kg/m^2 dry weight , and population density of more than 10 plants per square meter. Analysis of biomass growth (Chapter 5) indicates that favorable conditions for deposition processes in terms of biomass and population density can be only attained for the short periods of about 3-4 weeks (usually during August), thus outlining the time scales for intensive deposition processes and retention of chemicals due to vegetation.

8.2 Dynamics of Juvenile Fish Communities

Though many studies concerned habitat preferences of early juvenile fish, comparative analyses of swimming performance of fish larvae doubts larvae ability for maintaining position in the river flow and hence to choose the habitats. As a consequence, the juveniles will be distributed randomly by turbulent flow on the initial stage, and the match of suitable nurseries will depend on heterogeneity of the banks large scale geometry or availability of flow stagnation zones (dead zones) in aquatic vegetation mosaic which can also act as the refuge. Therefore the longitudinal dispersion model can be considered as a tool to interpret the spatio-temporal patterns of juvenile fish assemblages, e.g. downstream of a spawning site. In this section the swimming performances of juvenile fish are compared to characteristic flow velocities, than some simplifications of longitudinal dispersion model are introduced in respect to boundary conditions and then modelled patterns discussed together with some results of the field observations on juvenile fish assemblages. This study was an IGB internal interdisciplinary research supervised by Dr. C. Wolter (Wolter and Sukhodolov 2008).

Swimming performance of fish, an ability to support certain speed during time period until fatigue (endurance time), determines availability of shelter, food, and possibility to escape predation. Conventionally swimming performance classified as sustained if mean speed maintained for more than 200 minutes, prolonged (60 to 200 minutes), critical (less than 60 minutes), and burst swimming for the period shorter than 20 seconds (Webb 1975). Although variety of biological and physical factors define swimming performance (Webb 1975; Hammer 1995), the most important one is the size of fish (Hammer 1995; Domenici 2001). Recent

generalization of 168 studies completed on 75 freshwater fish species indicated range of critical speed from 5 to 13 cm/s, and from 6 to 20 cm/s for burst speeds for freshly hatched larvae 6 to 15 mm long (Wolter and Arlinghaus 2003, 2004). For these performances juveniles can travel distances as long as 180-500 m in critical speed, and 1.2-4 m in bursting speed. Considering characteristic interval of bulk flow velocities in a typical lowland river as the Spree River ranging from 20 to 45 cm/s one can see that for the critical endurance period the fish will be moved by flow 700 to 1600 m downstream. Even developing maximal burst speeds the fish would not be able to approach a river bank if travelling in the central part of the river. Moreover, it might be almost impossible for fish to overcome local turbulent pulsations and to pass through distinctive interfacial zones as mixing layers developing between main flow and recirculation zones near banks or between transit flow and vegetated patches.

The straight comparison of speeds and travelled distances implies that fish might intelligibly choose to move long time straight against current in a search of a preferential habitat, which is probably unlikely for many reasons. Moreover, empirical evidence of downstream drift of juvenile fish in rivers is documented in many studies. Harvey (1987) reported that centrarchids and cyprinids smaller than 10 mm were extremely susceptible to downstream displacement by flow. Peaking drift patterns have been observed early in the season when most of larvae were small: in the lower River Elbe (Ösmann 2003), in the Czech lowland rivers Morava and Kyjovka (Reichard et al. 2002), and in the Austrian Danube (Zitek et al. 2004).

Though species differentiate in their behavioural strategies and ontogenetic development, their larvae nevertheless leave the spawning substrate and enter water column when the yolk sac is almost exhausted (Bardonnet 2001). At that moment the larvae became exposed to hydrodynamic forces, especially strong at the interfaces between the flow and riverbed substrate or riparian vegetation, it can be accidentally displaced by currents. Hatching and emergence of juvenile fish is normally observed during a certain period that might be considered as substantially long in comparison with characteristic temporal scales of transport processes in natural streams. For instance, hatching occurs during 4-8 weeks while characteristic time scale on the river reach, residence time, is about 2-3 days. At these conditions it is possible to approximate hatching rate as a constant ($\partial C / \partial t = 0$) and the concentration of hatched fish in the stream as very gradually changing along the river reach ($\partial^2 C / \partial x^2 = 0$). Moreover, the dead zone will be considered as the sink area and respectively only the mass balance in the transit flow is concerned. These assumptions allow simplifications of equation (2.2.15)

$$U \frac{dC}{dx} = \frac{\text{э}}{T_d}\left(C_d - C\right) \tag{8.2.1}$$

Further assumption is to consider a relationship between concentration of juvenile fish in the transit flow and in the non-transit flow (dead zones) $C_d = \gamma C$, and to rewrite (8.2.1)

$$U \frac{dC}{dx} = -\frac{\text{э}(1-\gamma)}{T_d} C . \tag{8.2.2}$$

Equation (8.2.2) now can be easily integrated to obtain distribution of juvenile fish concentration along the river reach in the transit flow

$$C(x) = C_0 \exp\left(-\frac{(1-\gamma)\text{э}}{U T_d} x\right) \tag{8.2.3}$$

that describes decrease in number of juvenile fish in the transit flow due to retention in the non-transit portions of the flow. Knowing this function of streamwise coordinate x one easily obtains the number of individual juvenile fish retained at a certain cross-section of the river assuming that the concentration is representing a number of fish in a certain volume of water.

To obtain the concentration of juvenile fish in the dead zones one can rewrite (8.2.3) as

$$C_d = C_0(x_0) - C(x) = C_0(x_0)\left[1 - \exp\left(-\frac{(1-\gamma)э}{U T_d}x\right)\right] \tag{8.2.4}$$

Normalizing the concentration of juvenile fish in the dead zones by the concentration of hatched fish and substituting the volume concentrations by the number of fish settled in the dead zones N_s and number of hatched fish N_0 yields

$$\frac{N_s}{N_0} = 1 - \exp\left(-\frac{(1-\gamma)э}{UT}x\right) \tag{8.2.5}$$

Characteristic behavior of the model (8.2.5) is illustrated in Figure 8.2.1. To solve equation (8.2.5) the value for the parameter γ was set to equal 0.1 assuming that only 1/10 of juvenile fish entering the dead zones will retain there for the period substantially long to maintain considerable swimming performance. This value corresponds to the observations at groyne fields, that only about 0.1 of the groyne field area serve as an effective storage area with long receptivity capabilities (Engelhardt et al. 2004). Calculations with equation (8.2.5) particularly indicate that number of fish retained in the dead zones increases an order of magnitude with an increase of volume of dead zones of three times. Substantial increase of settled juvenile fish is also notable with an increase of the dead zones retention time (Figure 8.2.1). These results agree with general considerations and the next step is obviously comparison, at least qualitative, with field juvenile fish surveys.

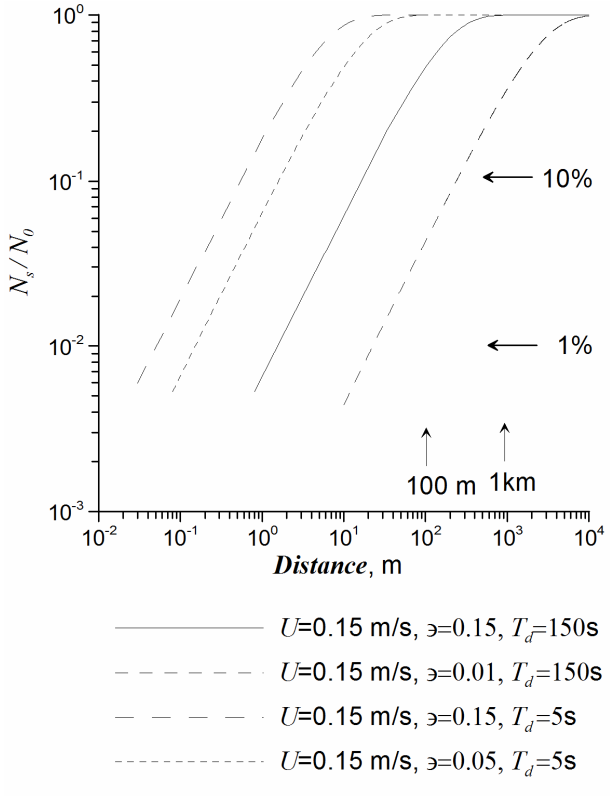

Figure 8.2.1 Effect of dead zones on settling of juvenile fish assemblages in the river reaches of a typical lowland river.

Field studies of juvenile fish communities were completed by our colleagues from the IGB and here we briefly outline their findings and comparison with the modeling and the results of this study. Detailed information about fish surveys and processing of results is presented in Wolter and Sukhdolov (2008). Young-of-the-year or 0+ fishes were sampled from a boat using an electrofishing unit. Three sites were selected within the stretch of the Spree River described

above: downstream of the bridge at Mönchwinkel, near Spreewerder, and at Spreeau (Figure 3.1.1). At each site two times 50 points were fished during daytime, at May, 27th and at June, 10th, 2006. Altogether 300 points have been sampled and in total 898 0+ fishes caught belonging to four species: 344 silver bream, *Blicca bjoerkna* (L.), 329 roach, *Rutilus rutilus* (L.), 122 bleak, *Alburnus alburnus* (L.), and 103 perch, *Perca fluviatilis* L.. In all four species total length differed significantly between sampling dates, mostly increased from May 27th to June 10th: mean ± standard deviation: silver bream 7.44±0.61 mm compared to 12.76±1.93 mm ($p<0.001$, *t* test), roach 14.46±0.50 mm – 20.85±1.63 mm ($p<0.001$), and perch 19.22±1.88 mm – 30.84±4.061 mm ($p<0.05$).

The longitudinal dispersion model predicts a decreasing density of fish in the dead zones with increasing distance downstream of the imaginary model origin, i.e. a spawning place and area of hatchling emergence (Figure 8.2.2a, Figure 8.2.3a), as well as an increasing cumulative number of 0+ fish trapped in the dead zones (Figure 8.2.2b, Figure 8.2.3b). At both sampling dates, the observed differences in mean fish densities between sites were not significant ($p>0.05$, ANOVA). The density distribution of bleak and silver bream in May and of bleak in June corresponded well with the model predictions, whilst the opposite was observed for perch and roach (Figure 8.2.2b, Figure 8.2.3b).

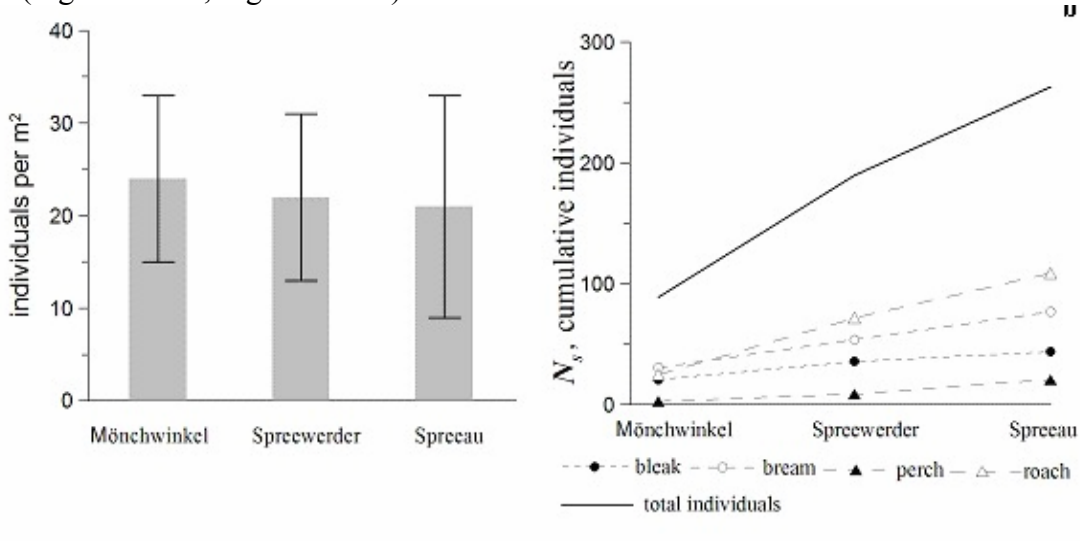

Figure 8.2.2 Distribution of juvenile fish density (a), and cumulative number of retained juveniles along the river reach, May 2006.

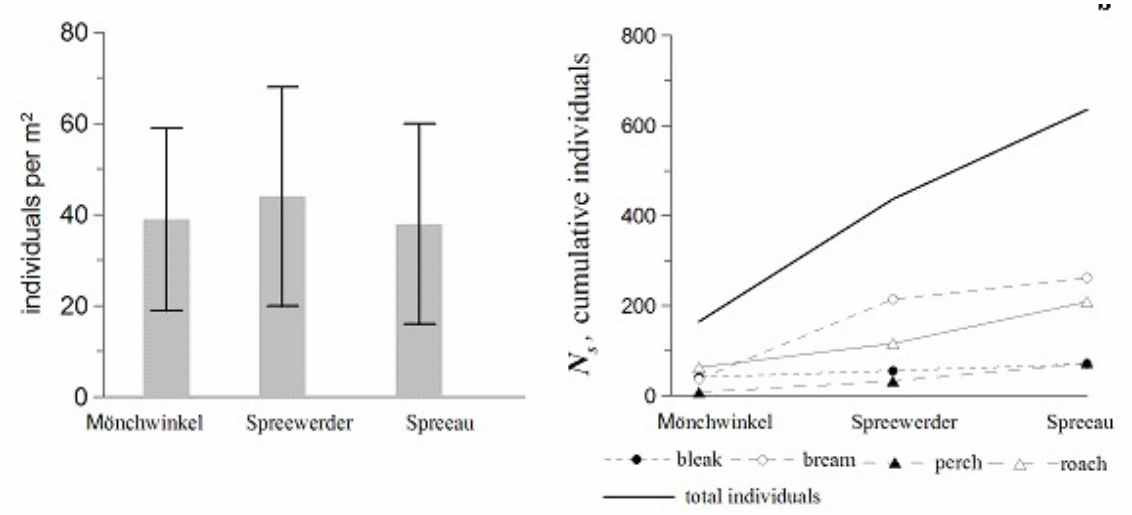

Figure 8.2.3 Distribution of juvenile fish density (a), and cumulative number of retained juveniles along the river reach, June 2006.

The apparent mismatch between the observed and predicted densities of fish species at the sampling sites resulted from multiple spawning sites. In its present form, the hydrodynamic distribution model assumes a single origin of fish in the main flow to be transported downstream. This initial amount of fish (particles) in the flow becomes partially distributed in the dead zones and the remaining further distributed downstream. The higher the fish density in the flow, the higher the proportion of fish advected to dead zones and the higher their densities therein. With increasing distance from the source, the fish density in the flow becomes lower and the total number of fish already trapped in dead zones increases.

In a natural river stretch fish spawning doesn't occur at a single site only. Spawning of bleak and silver bream has been observed 200 m upstream of the first sampling site at the bridge Mönchwinkel. However, it is also known to occur along the emerged vegetation between Mönchwinkel and Spreeau as well as further downstream. Accordingly, several spawning places between the sampling sites contribute emergent hatchlings to the overall accidentally displaced fish larvae resulting in the observed discrepancy between predicted and sampled fish densities.

9 DISCUSSION AND CONCLUSIONS

The study described in this thesis concerns a multidisciplinary research of complex physical and biological processes in the natural streams. The focus of the study was to gain an advanced knowledge on wide spectrum of processes and to obtain refined theoretical models for their essentials and mutual interactions. The primary goal of the research was to investigate the effects of submerged flexible vegetation on the turbulent flow and its consequences for transport and mixing processes with further implications for morphodynamics, biology, and ecology in lowland rivers. Methodologically it was achieved through a synergy between theoretical analysis, field experimental investigation and observations, and numerical modeling. Although because of scarceness of time and resources the research was limited to only particular river reach and dominated species of plants, the fundamental character of the approach allows generalization of the results on a sound theoretical background and thus gives a longer way to the acquired data sets and gained knowledge. Application of recently developed theoretical concepts in frame of present study bridges a gap between highly idealized laboratory studies, even more idealized numerical computations, and very coarse observations in natural conditions. In this respect the study is original, novel, opening new prospective and outlining specific problems that should be challenged by further studies.

Turbulent river flow represents a physical environment for biota in a fluvial ecosystem and can directly interact with its biological components by mechanical impact, or affects them indirectly through the alterations of transport functions of the vital matters. Mechanical interactions generally mean that living organisms create certain obstructions to the flow current and thus simply block the flow and hence alternate its structure. Among many species of aquatic organisms only the macroscopic plants (macrophytes) are capable for maintaining stable, abundant populations that can affect the river flows during long periods on the large spatial scales. Although rivers with their strong and very variable currents provide extremely harsh conditions for the rooted plants, macrophytes have developed certain strategies helping them proliferate in the fluvial systems. Most competitive species, often invasive for regions with the changing climate or the water management strategies, via ability to polymorphism produce terrestrial, riparian, and even aquatic forms strongly differentiating by properties of their tissues, morphology, and phenology. Aquatic macrophytes are usually flexible, and streamlined tolerating strong physical forcing from current and avoiding damages of the stems and dislodgement in response to the floods. This ability is reflecting mutual relationship between the flow and plants which makes the most remarkable difficulty for the quantitative assessment of the river flows with the submerged flexible vegetation. Therefore up today relatively little was known about turbulent flows in the river reaches with submerged vegetation, and the knowledge was mainly gained from the laboratory studies. In our study we approached the problem by studying flow in a natural lowland river subjected to the seasonal growth of submerged vegetation.

Previous studies of mechanical interactions considered balance of forces maintained by drag from the current and response of a plant by rigidity of its tissue. This was traditional approach for terrestrial vegetation and is the efficient way to describe interactions of many riparian and emergent forms of the aquatic plants. However, as it was acknowledged in some recent investigations and rigorously examined in this study, for the submerged flexible macrophytes flow drag can be effectively counteracted by buoyancy of plants tissue. Reconsideration of the physics of interaction provided us with the general theoretical solution of the problem that was verified using the results of original field investigations completed in this study and some

previous published results. Development of this theory is a very important result of the study because it significantly contributes to the scientific curriculum and will stipulate further developments in the nearest future. Moreover, together with the understanding that during phenological cycle the biomechanical properties of plants undergo fundamental changes switching from buoyancy to rigidity dominated by plants architecture, the theory provides the ways for explaining different behavior of the plants and allows to avoid ambiguities in the analysis and interpretation of observations in the natural conditions.

To obtain deeper insight into the complex structure of turbulent flow evolving over a patch of flexible submerged vegetation in a natural stream, an original field experimental study was carried out and its results were examined in the context of an analytical framework provided by the hydrodynamic model of a mixing layer. The model was expanded by the theoretical analysis of evolution of mixing layer through the understanding how do interactions of the flow and the vegetation in a patch produce velocity shear across the flow depth as well as evolution of the shear in the downstream direction. Obtained theoretical solution is linked to the theoretical description of biomechanical properties for flexible buoyant vegetation through the bending angle and the effect of vegetation density via drag forces. These findings provide previously missing links between hydrodynamic and biomechanical aspects of the problem and thus establish a basis for the development of unified theory of flow-plants interactions. Detailed analysis of structural properties of mixing layer allowed suggesting a phenomenological model for organized turbulent fluxes popularly called coherent structures. The model related basic flow parameters and properties of vegetative cover and is capable of realistic prediction for scales of the coherent structures. It has also a great potential for further theoretical examination of monamic motions, or waving, of the plants specifically by coupling it with the biomechanical model developed for the flexible buoyant plants. Unfortunately this interesting topic was left here untouched because of the lack of time and resources for additional investigations.

Though understanding of interactions between the flow and plants itself is a key to development of the theoretical approaches, they are of lesser importance for general ecological problems which mainly concern indirect alternations of the environment by changes in the transport functions of oxygen, nutrients, and suspended particulate matter. Recognizing the merits of this part of the problem for ecological studies – the primary focus of multidisciplinary research carried in IGB, the main line of the thesis is aligned with this direction and examines consequences of flow – plants interactions in respect to one-dimensional approach to modeling of transport and mixing in rivers. This one-dimensional approach known as longitudinal dispersion model has an extension called dead zone model which allows describing effects of prolonged retention in non-transit or stagnant zones of the flow. Although this model was developed three decades ago, its practical relevance was always hindered by difficulties to predict the model parameters such as characteristic volume of dead zones, specific time of residence for substance in the dead zone, and longitudinal dispersion coefficient. In this study we reexamined the structure of flow in vegetation mosaic and proposed possible quantitative approaches to infer the model parameters for known type of vegetation. Coupling of developed theory of flow-plants interactions with a phenological model of biomass growth which was also proposed in this study provided nearly complete approach to the problem. Indeed, possibility to predict most important features of the flow dynamically during vegetative period makes the approach an objective tool for the ecological studies. Moreover, because basic properties of the plants phenology are locked on a degree-day parameterization, the approach became a tool for studies concerned consequences of climatic change on the ecology and hydraulics of the lowland rivers.

In contrast to terrestrial vegetation, aquatic plants colonizing river channels in many cases are forced to reestablish spatial distribution of their population every year. This is caused by distinctive properties of the hydrological cycle – the periodic flooding during spring and because of development of the river network in alluvial deposits actively transported during the flooding

events. The knowledge of morphodynamic processes is therefore indispensable for predicting initial conditions for the vegetation growth. In this study we have explored only some aspects of fluvial morphodynamics such as bedload transport in form of sand waves and ripples. This brief study nevertheless yielded valuable information about thickness of sedimentary layer subjected to intensive bedload transport as well as the amplitudes and rates of bedload transport, and levels of physical forces driving this transport. Morphological surveys regularly completed during vegetation period yielded maps of riverbed changes due to deposition and erosion processes. Accumulation bedforms were unambiguously related to the spatial arrangement of vegetative mosaic and location of patches with maximal population density and biomass.

In contrast to previous, mostly laboratory, studies experimental part of this research was carried out in natural field conditions in a typical lowland river. The difference in experimental conditions was mainly pronounced through the small slopes of the riverbed, relatively large depths, and small bulk velocities. Indeed, most of experimental laboratory studies were completed in flumes with much higher slopes (0.1-1%), depth smaller than 0.5 m and velocity higher than 20 cm/s. Such experimental conditions eliminated some important features occurring in lowland rivers with the small slopes. Although due to the limitations in the amount of experimental data it was not possible in this study to propose and test more refined method for predicting resistance for conditions of lowland rivers with small slopes and affected by submerged flexible vegetation, nevertheless the study outlined the shortcomings of some conventional approaches and hinted to how a refined method can be developed.

During completion of this research program a series of the concurrent research projects was running in IGB directly or indirectly related to the problems of vegetated river flows, transport of cohesive suspended matter, retention and remobilization of nutrients and chemical substances, and the dynamics of juvenile fish communities. These research activities required provision of expertise gained from this study to plan field measurements and samples, to post-process and interpret the results, and finally to advance models for those processes. The results appear to be very beneficial both for the dissertation thesis because they uncovered some additional aspects or provided more solid support for choice of parameters, and for concurrent research projects as the study provided theoretical and experimental framework for them.

The topic of research described in this thesis is very broad and concerned by wide community of river engineers, biologist, hydrologists, geomorphologists, and ecologists. Therefore we hope that the results presented here will attract the audience with different educational backgrounds, and to help this audience better understand the material an extended introduction into essentials of involved disciplines was also presented in the chapter on theoretical background of the study.

BIBLIOGRAPHY

Abt et al., 1994: Abt S.R., Clary W.P., and Thornton C.I. 1994. Sediment deposition and entrapment in vegetated streambeds. Journal of Irrigation and Drainage Engineering *120*, 1098-1111.

Abbott and Minns, 1998: Abbott M.B., and Minns A.W. 1998. Computational Hydraulics, Ashgate, Aldershot.

Armstrong et al., 2003: Armstrong N., Planas D., and Prepas E. 2003. Potential for estimating macrophyte surface area from biomass. Aquatic Botany *75*, 173-179.

Bardonnet, 2001: Bardonnet A. 2001. Spawning in swift water currents: implications for eggs and larvae. Archiv für Hydrobiologie Suppl. *135*, 271-291.

Beltaos, 1980: Beltaos S. 1980. Longitudinal dispersion in rivers. Journal of Hydraulic Division *106*, 151-172.

Bencala et al., 1990: Bencala K.E., McKnight D.M., and Zellweger G.M. 1990. Characterization of transport in an acidic and metal-rich mountain stream based on a lithium traces injection and simulations of transient storage. Water Resources Research *26*, 989-1000.

Best et al., 2001: Best E.P.H., Buzzelli C.P., Bartell S.M., Wetzel R.L., Boyd W.H., Doyle R.D., and Campbell L. K. P. 2001. Modeling submersed macrophyte growth in relation to underwater light climate: modeling approaches and application potential. Hydrobiologia *444*, 43-70.

Birch, 1999: Birch C.P.D. 1999. A new generalized logistic sigmoid growth equation compared with the Richards growth equation. Annals of Botany *83*, 713-723.

Brown and Roshko, 1974: Brown G.L, and Roshko A. 1974. On density effects and large structure in turbulent mixing layers. Journal of Fluid Mechanics *64*, 775-816.

Burke and Stolzenbach 1983: Burke R.W., and Stolzenbach K.D. 1983. Free surface flow through salt marsh grass. MIT-Sea Grant Report MITSG, Massachusetts Institute of Technology, Cambridge, Massachusetts, 83-16.

Cantwell, 1981: Cantwell B.J. 1981. Organized motion in turbulent flow. Annual Review of Fluid Mechanics *13*, 457-515.

Capers, 2000: Capers R.S. 2000. A comparison of two sampling techniques in the study of submersed macrophyte richness and abundance. Aquatic Botany *68*, 87-92.

Carollo et al., 2002: Carollo F.G., Ferro V., and Termini D. 2002. Flow velocity measurements in vegetated channels. Journal of Hydraulic Engineering *128*, 664-673.

Carollo et al., 2005: Carollo F.G., Ferro V., and Termini D. 2005. Flow resistance law in channels with flexible submerged vegetation. Journal of Hydraulic Engineering *131*, 554-564.

Carr et al., 1997: Carr G.M., Duthie H.C., and Taylor W.D. 1997. Models of aquatic plant productivity: a review of the factors that influence growth. Aquatic Botany *59*, 195-215.

Champion and Tanner, 2000: Champion P.D., and Tanner C.C. 2000. Seasonality of macrophytes and interaction with flow in a New Zealand lowland stream. Hydrobiologia *441*, 1-12.

Chatwin, 1980: Chatwin P.C. 1980. Presentation of longitudinal dispersion data. Journal of Hydraulic Division *106*, 71-83.

Choi and Kang, 2004: Choi S.-U., and Kang H. 2004. Reynolds stress modeling of vegetated open-channel flows. Journal of Hydraulics Research IAHR *42*, 3-11.

Chu and Babarutsi, 1988: Chu V.H., and Babarutsi S. 1988. Confinement and bed-friction effects in shallow turbulent mixing layers. Journal of Hydraulic Engineering *114*, 1257-1274.

Clarke, 2002: Clarke S.J. 2002. Vegetation growth in rivers: influences upon sediment and nutrient dynamics. Progress in Physical Geography, *26*, 159-172.

Compertz, 1825: Compertz B. 1825. On the nature of the function expressive of the law of human mortality, and on the new mode of determining the value of life contingencies. Philosophical Transactions of the Royal Society *182*, 513-585.

Cox and Palmer, 1948: Cox M.B., and Palmer V.J. 1948. Results of Tests on Vegetated Waterways and Method of Fields Application. Miscelanous Publication MP-12, Oklahoma Agricultural Experimental Station, Stillwater, Oklahoma, 1-43.

Cui and Neary, 2002: Cui J., and Neary V.S. 2002. Large eddy simulation (LES) of fully developed flow through vegetation. IAHR 5th International Conference on Hydroinformatics, Cardiff, Wales.

Czernuszenko and Rowinski, 1997: Czernuszenko W., and Rowinski P. 1997. Properties of dead-zone model of longitudinal dispersion in rivers, Journal of Hydraulic Research *35*, 491-504.

Czernuszenko et al., 1998: Czernuszenko W., Rowinski, P.M., and Sukhodolov A.N. 1998. Experimental and numerical validation of the dead-zone model for longitudinal dispersion in rivers. Journal of Hydraulic Research *36*, 269-280.

Davis and McDonnel, 1997: Davis J.F., and McDonnel A.J. 1997. Development of a partitioned-biomass model for rooted macrophytes growth. Aquatic Botany *56*, 265-276.

Day, 1975: Day T.J. 1975. Longitudinal dispersion in natural channels. Water Resources Research*, 11*, 909-918.

Domenici, 2001: Domenici P. 2001. The scaling of locomotor performance in predator-prey encounters: from fish to killer whales. Comparative Biochemistry and Physiology A *131*, 169-182.

Downing and Anderson, 1985: Downing J.A. and Anderson M.R. 1985. Estimating the standing biomass of aquatic macrophytes. Canadian Journal of Fishery and Aquatic Science *42*, 1860-1869.

Duarte and Sand-Jensen, 1990.: Duarte C.M., and Sand-Jensen K. 1990. Seegrass colonization: biomass development and shoot demography in Cymodocea nodosa patches. Marine Ecological Progress, Ser. *67*, 97-103.

Eastgate, 1966: Eastgate W.I. 1966. Vegetated stabilization of grassed waterways and dam bywashes. MS. thesis, Univ. of Queensland, St. Lucia, Australia.

Elder, 1959: Elder J.W. 1959. The dispersion of marked fluid in turbulent shear flow. Journal of Fluid Mechanics *5*, 544-560.

Engelhardt et al. 2004: Engelhardt C., Krüger A., Sukhodolov A., and Nicklisch A. 2004. A study of phytoplankton spatial distributions, flow structure and characteristics of mixing in a river reach with groynes. Journal of Plankton Research *26*, 1351-1366.

Engelund and Hansen, 1972: Engelund F., and Hansen E. 1972. A Monograph on Sediment Transport in Alluvial Streams*,* Teknish Forlag, Copenhagen, Denmark.

Erduran and Kutija, 2003: Erduran K.S., and Kutija V. 2003. Quasi-three-dimensional numerical model for flow through flexible, rigid, submerged and non-submerged vegetation. Journal of Hydroinformatics *5*, 189-202.

Finnigan, 2000: Finnigan J. 2000. Turbulence in plant canopies. Annual Review Fluid Mechanics *32*, 519–571.

Fischer, 1967: Fischer H.B. 1967. The mechanics of dispersion in natural streams. Journal of Hydraulic Division *93*, 187-215.

Fischer-Antze et al., 2001: Fischer-Antze T., Stoesser T., and Olsen N.R.B. 2001. 3D numerical modeling of open-channel flow with submerged vegetation. Journal of Hydraulic Research *39*, 303-310.

Fonseca et al., 2007: Fonseca M.S., Koehl M.A.R., and Kopp B.S. 2007. Biomechanical factors contributing to self-organization in seagrass landscapes. Journal of Experimental Marine Biology and Ecology *340*, 227-246.

Fukuoka, 1971: Fukuoka S. 1971. Longitudinal Dispersion in Sinous Channels. Ph.D. thesis, University of Iowa.

Gantes and Sánchez, 2001: Gantes H.P., and Sánchez Caro A. 2001. Environmental heterogeneity and spatial distribution of macrophytes in plain streams. Aquatic Botany *70*, 225-236.

Gaylord and Denny, 1997: Gaylord B., and Denny M.W. 1997. Flow and flexibility I. Effects of size, shape, and stiffness in determining wave force on the stipitate kelps Eisenia arborea and Pterygophora californica. Journal of Experimental Biology *200*, 3141-3164.

Ghisalberti and Nepf, 2002: Ghisalberti M. and Nepf H.M. 2002. Mixing layers and coherent structures in vegetated aquatic flows. Journal of Geophysical Research *170*, 10.1029/ 2001JC000871.

Ghisalberti and Nepf, 2004: Ghisalberti M. and Nepf H.M. 2004. The limited growth of vegetated shear layers. Water Resources Research *40*, W07502, doi:10.1029/2003WR002776.

Glover, 1964: Glover R.E. 1964. Dispersion of Dissolved and Suspended Materials in Flowing Streams. Professional Paper 433-B, U.S. Geological Survey, Reston, VA.

Godfrey and Frederick, 1970; Godfrey R.G., and Frederick B.J. 1970. Dispersion in Natural Streams. Professional Paper 433-K, U.S. Geological Survey, Reston, VA.

Goldstein, 1938: Goldstein S. 1938. Modern Developments in Fluid Dynamics. 1, Claredon Press, Oxford, 297-309.

Goudrian and van Laar, 1994: Goudrian J., and van Laar H.H. 1994. Modeling potential crop growth processes., Kluwer Academic, Dordrecht.

Green, 2005: Green J.C. 2005. Modelling flow resistance in vegetated streams: review and development of new theory. Hydrological Processes *19*, 1245-1259.

Green, 2006: Green J.C. 2006. Effect of macrophyte spatial variability on channel resistance. Advances in Water Resources *29*, 426-438.

Gregory and Gurnell, 1988: Gregory K.J., and Gurnell A.M. 1988. Vegetation and river channel form and process. In: Viles H.A. (edr.) Biogeomorphology, Basil Blackwell Ltd., Oxford, 1-42.

Grinvald and Nikora, 1988: Grinvald D.I., and Nikora V.I. 1988. River Turbulence. Gidrometeoizdat, Leningrad.

Grishanin, 1979: Grishanin K.V. 1979. Dynamics of Channel Flows. Hydrometeoizdat, Leningrad.

Gurnell and Midgley, 1994: Gurnell A.M., and Midgley P. 1994. Aquatic weed growth and flow resistance: influence on the relationship between discharge and stage over 25 year river gauging station record. Hydrological Processes *8*, 63-73.

Gust, 1990: Gust G. 1990. Method of generating precisely-defined wall shear stresses. US Patent Number: 4.973.1651990.

Haber, 1982: Haber B. 1982. Über den Erosionsbeginn bei der Überströmung von flexibilen Rauheitselementen. Mitteilungen des Leichtweiss-Institutes für Wasserbau der Technischen Universität Braunschweig, *Heft 74*.

Hammer, 1995: Hammer C. 1995. Fatigue and exercise tests with fish. Comparative Biochemistryand Physiology A *112*, 1-20.

Harman and Finnigan, 2007: Harman I.N., and Finnigan J.J. 2007. A simple unified theory for flow in the canopy and roughness sublayer. Boundary-Layer Meteorology *123*, 339-363.

Harvey, 1987: Harvey B.C. 1987. Susceptibility of young-of-the-year fishes to downstream displacement by flooding. Transactions of the American Fisheries Society *116*, 851-855.

Herb and Stefan, 2003: Herb W. R., and Stefan H.G. 2003. Integral growth of submersed macrophytes in varying light regimes. Ecological Modeling *168*, 77-100.

Ho and Huerre, 1984: Ho C.M., and Huerre P. 1984. Perturbed shear layers. Annual Review Fluid Mechanics 16, 365-424.

Horvath, 2004: Horvath T.G. 2004. Retention of particulate matter by macrophytes in first-order stream. Aquatic Botany *78*, 27-36.

Jackson, 1976: Jackson R.G. 1976. Sedimentological and fluid-dynamic implications of the turbulent bursting phenomenon in geophysical flows. Journal of Fluid Mechanics 77, 531-560.

Jenkins and Watts, 1968: Jenkins G.M., and Watts D.G. 1968. Spectral analysis and its applications. Holden-Day, Merrifield.

Jirka, 2001: Jirka G.H. 2001. Large scale flow structures and mixing processes in shallow flows. Journal of Hydraulic Research *39*, 567-573.

Jirka, 2004: Jirka G.H. 2004. Mixing and dispersion in rivers. In: RiverFlow 2004, M. Greco, A. Carravetta & Della Morte (eds.), A. Balkema, 1, 13-27.

Klaven, 1968.: Klaven A.B. 1968. Kinematic structure of the turbulent flow. Transactions of the State Hydrological Institute, Gidrometeoizdat, Russia, 134-141.

Kleeberg et al., 2008: Kleeberg A., Sukhodolov A., Sukhodolova T., and Köhler J. 2008. Dynamic of riverine matter deposition, resuspension and respective phosphorus entrainment within a vegetation mosaic. (in review).

Kolmogorov, 1942: Kolmogorov A. N. 1942. Equations of motion of an incompressible turbulent fluid. Izvestiya Akad. Nauk SSSR *6*, 56–58.

Körner and Kühl, 1996: Körner S., and Kühl H. 1996. Development of submerged macrophytes in the treated sewage channel Wuhle (Berlin, Germany). Int. Revue ges. Hydrobiol. *81*, 385-397.

Kouwen et al., 1969: Kouwen N., Unny T.E., and Hill. H.M. 1969. Flow retardance in vegetated channels. Journal of the Irrigation and Drainage Division *95*, 329-341.

Kouwen and Unny, 1973: Kouwen N.and Unny T.E. 1973. Flexible roughness in open channels. Journal of the Hydraulic Division *99*, 713-728.

Kouwen and Li, 1980: Kouwen N., and Li R.M. 1980. Biomechanics of vegetative channel linings. Journal of the Hydraulics Division *106*, 1085-1103.

Kouwen, 1992.: Kouwen N. 1992. Modern approach to design of grassed channels. Journal of Irrigation and Drainage Engineering *118*, 733-743.

Kozerski, 2002: Kozerski H.-P. 2002. Determination of areal sedimentation rates in rivers by using plate sediment trap measurements and flow velocity – sediment flux relationship. Water Research *36*, 2983-2990.

Krone, 1962. : Krone R.B. 1962. Flume studies of the transport of sediment in estuarial shoaling processes. Hydraulic Engineering Laboratory and Sanitary Engineering Research Laboratory. University of California, Berkeley.

Lee et al., 2004: Lee J.K., Roig L.C., Jenter H.L., and Visser H.M. 2004. Drag coefficients for modeling flow through emergent vegetation in the Florida Everglades. Ecological Engineering *22*, 237-248.

Lightbody and Nepf, 2006: Lightbody A.F., and Nepf H.M. 2006. Prediction of velocity profiles and longitudinal dispersion in emergent salt marsh vegetation. Limnology and Oceanography *51*, 218-228.

Lohrmann et al., 1994: Lohrmann A., Cabrera R., and Kraus N.C. 1994. Acoustic-Doppler velocimeter (ADV) for laboratory use. In: Fundamentals and Advancements in Hydraulic Measurements and Experimentation, New York, 351-365.

López and García, 2001: López F., and García M.H. 2001. Mean flow and turbulence structure of open-channel flow through non-emergent vegetation. Journal of Hydraul. Engineering ASCE *127*, 392-402.

Lumley, 1981: Lumley J.L. 1981. Coherent structures in turbulence. In R.E. Meyer (ed.) Transition and Turbulence, Academic, New York.

Madsen, 1993: Madsen J.D. 1993. Biomass techniques for monitoring and assessing control of aquatic vegetation. Lake and Reservoir Management *7*, 141-154.

Madsen et al., 2001: Madsen J.D., Chambers P.A., James W.F., Koch E.W., and Westlake D.F. 2001. The interaction between water movement, sediment dynamics and submerged macrophytes. Hydrobiologia *444*, 71-84.

Marba and Duarte, 1998: Marba N., and Duarte C.M. 1998. Rhizome elongation and seegrass clonal growth. Marine Ecological Progress, Ser. *174*, 269-280.

Matthes, 1947: Matthes G.H. 1947. Macroturbulence in natural stream flow. In: Transactions of American Geophysical Union *28*, 255-265.

Michalke, 1965: Michalke A. 1965. On spatially growing disturbances in an inviscid shear layer. Journal of Fluid Mechanics *23*, 521-544.

Mommer et al., 2005: Mommer L., de Kroon H., Pierik R., Bögemann G.M., and Visser E.J.W. 2005. A functional comparison of accumulation to shade and submergence in two terrestrial plant species. New Physiologist *167*, 197-206.

Monin and Yaglom, 1971: Monin A.S., and Yaglom A.M. 1971. Statistical fluid mechanics. Vol. 1: Mechanics of turbulence. MIT Press, Cambridge.

Murota et al., 1984: Murota A., Fukuhara T., and Sato M. 1984. Turbulence structure in vegetated open channel flows. Journal of Hydroscience and Hydraulic Engineering *2*, 47-61.

Nadaoka and Yagi, 1998: Nadaoka K., and Yagi H. 1998. Shallow water turbulence modeling and horizontal large-eddy computation of river flow. Journal Hydraulic Engineering *124*, 493-500.

Naot et al., 1996: Naot D., Nezu I., and Nakagawa H. 1996. Hydrodynamic behavior of partly vegetated open channel. Journal of Hydraulic Engineering ASCE *122*, 625-633.

Neary, 2003: Neary V.S. 2003. Numerical solution of fully developed flow with vegetative resistance. Journal of Engineering Mechanics *129*, 558-563.

Nelson et al., 1993: Nelson J.M., McLean S.R., Wolfe S.R. 1993. Mean flow and turbulence fields over two-dimensional bed forms. Water Resources Research *29*, 3935-3953.

Nepf, 1999: Nepf H.M. 1999. Drag, turbulence, and diffusion in flow through emergent vegetation. Water Resources Research *35*, 479-489.

Nepf and Vivoni, 2000: Nepf H.M., and Vivoni E.R. 2000. Flow structure in depth-limited, vegetated flow. Journal of Geophysical Research *105*, 28,547-28,557.

Nezu and Nakagawa, 1993: Nezu I., and Nakagawa H. 1993. Turbulence in open-channel flows. A.A. Balkema, Rotterdam, Netherlands.

Niklas, 1992: Niklas K. J. 1992. Plant biomechanics: an engineering approach to plant form and function. University of Chicago Press, Chicago, Illinois, USA.

Nikora et al., 1997: Nikora V.I., Sukhodolov A.N., and Rowiński P.M. 1997. Statistical sand waves dynamics in the one-directional water flows. Journal of Fluid Mechanics *351*, 17-39.

Nikora and Goring, 1998: Nikora V.I., and Goring D.G. 1998. ADV measurements of turbulence: can we improve their interpretation? Journal of Hydraulic Engineering *124*, 630-634.

Nordin and Troutman, 1980: Nordin C.F., and Troutman B.M. 1980. Longitudinal dispersion in rivers: The persistence of skewness in observed data. Water Resources Research *16*, 123-128.

O'Hare et al., 2007: O'Hare M., Hutchinson K.A., and Clarke R.T. 2007. The drag and reconfiguration experienced by five macrophytes from a lowland river. Aquatic Botany *86*, 253-259.

Olesen and Sand-Jensen, 1994: Olesen B., and Sand-Jensen K. 1994. Patch dynamics of eelgrass Zostera marina. Marine Ecology Prog. Ser. *106*, 147-156.

Ösmann, 2003: Ösmann S. 2003. Vertical, lateral and diurnal drift patterns of fish larvae in a large lowland river, the Elbe. Journal of Applied Ichthyology *19*, 284-293.

Paw et al., 1992: Paw U K.T., Brunet Y., Collineau S., Shaw R.H., Maitani T., Qiu J., and Hipps L. 1992. On coherent structures in turbulence above and within agricultural plant canopies. Agricultural and Forest Meteorology *61*, 55-68.

Pedersen, 1977: Pedersen F.B. 1977. Prediction of longitudinal dispersion in natural streams. Hydrodynamics and Hydraulics Engineering Series Paper N. 14, Technical University of Denmark.

Peifang and Chao, 2007: Peifang W., and Chao W. 2007. Nutrients removing by arrowheads in different growing periods in the transition zone between land and rivers. Water Resources *34*, 471-477.

Peterson et al., 2004: Peterson C.H., Luettich R.A., Micheli F., and Skilleter G.A. 2004. Attenuation of water flow inside seagrass canopies of differing structure. Marine Ecology Progress Series *268*, 81-92.

Pope, 2000: Pope S.B 2000. Turbulent Flows*,* Cambridge University Press, Cambridge.

Plate and Quraishi, 1965: Plate E., and Quraishi A. 1965. Modeling of velocity distributions inside and above tall crops. Journal of Applied Metheorology *4*, 400-408.

Pringle et al., 1988: Pringle C.M., Naiman R.J., Bretschko G., Karr J.R., Oswood M.W., Webster J.R., Welcomme R.L., and Winterbourn M.J. 1988. Patch dynamics in lotic systems: the stream as a mosaic. Journal of North American Benthological Society *7*, 503-524.

Prochnow et al., 1997: Prochnow D., Bungartz H., Engelhardt C., Krüger A., Sauer W., Schild R., and Thiele M. 1997. Schweb- und Schadstoffe der unteren Spree 1994-1996, Modellirung und Simulation des dynamischen Verhaltensvon Schwebstoffen in eutrophen Fließgewässern. Berichte des IGB, *Heft 3,* Berlin.

Raupach and Thom, 1981: Raupach M.R., and Thom A.S. 1981. Turbulence in and above plant canopies. Annual Review of Fluid Mechanics *13*, 97-129.

Raupach et al., 1989: Raupach M.R., Finnigan J.J., and Brunet Y. 1989. Coherent eddies in vegetation canopies. Proc. of 4th Australian Conference on Heat and Mass Transfer, Christchurch, New Zealand, 9-12 May 1989.

Raupach et al., 1996: Raupach M.R., Finnigan J.J., and Brunet Y. 1996. Coherent eddies and turbulence in vegetation canopies: the mixing-layer analogy. Boundary-Layer Meteorology *78*, 351-382.

Ree and Palmer, 1949: Ree W.O., and Palmer V.J. 1949. Flow of water in channels protected by vegetative linings. Bulletin of Soil Conservation Service, US Dept. of Agriculture *967*, 1-115.

Reichard et al., 2002: Reichard M., Jurajda P., and Ondračkova M. 2002. Interannual variability in seasonal dynamics and species composition of drifting young-of-the-year fishes in two European lowland rivers. Journal of Fish Biology *60*, 87-101.

Richards, 1959: Richards F.J. 1959. A flexible growth function for empirical use. Journal of Experimental Botany *10*, 290-300.

Righetti and Armanini, 2002: Righetti M., and Armanini A. 2002. Flow resistance in open channel flows with sparsely distributed bushes. Journal of Hydrology *269*, 55-64.

Rümmelin, 1913: Rümmelin Th. 1913. Wie bewegt sich fließendes Wasser? Ein neuer Weg zur Erklärung des Problems, Zahn und Jaensch, Dresden.

Rutherford, 1994: Rutherford, J.C. 1994. River Mixing. John Wiley and Sons, New York, N.Y.

Rochusaar and Paal, 1970: Rochusaar L., and Paal L. 1970. The results of the experimental investigation of the longitudinal dispersion coefficient in open channels. Proceedings of Tallin Technical University *289 A*, 6.

Rodi, 1993: Rodi W. 1993. Turbulence models and their application in hydraulics. IAHR Monograph Series.

Rogers and Moser, 1992: Rogers M.M., and Moser R. 1992. The three-dimensional evolution of a plane mixing layer: the Kelvin-Helmholtz rollup. Journal of Fluid Mechanics *243*, 183-226.

Roshko, 1992: Roshko A. 1992. Instability and turbulence in shear flows. Theoretical and Applied Mechanics. (eds.) Bodner S.R., Singer J., Solan A., and Hussain. Proc. of XVIII Int. Congress, Haifa, Israel.

Rouse, 1939: Rouse H. 1939. Experiments on the mechanics of sediment transport. In: Proceedings of 5th International Congress of Applied Mechanics, Cambridge, Massachusetts, 550-554.

Rowiński et al., 2004: Rowiński P.M., Dysarz T., and Napiórkowski J.J. 2004. Estimation of longitudinal dispersion and storage zone parameters. In: RiverFlow 2004, M. Greco, A. Carravetta & Della Morte (eds.), A. Balkema, 2, 1201-1210.

Runkel and Chapra, 1993: Runkel R.L., and Chapra S.C. 1993. An efficient numerical solution of the transient storage equations for solute transport in small streams. *Water Resources Research 29*, 211-215.

Sand-Jensen et al., 1982: Sand-Jensen K., Prahl C., and Stokholm H. 1982. Oxygen release from roots of submerged aquatic macrophytes. Oikos *38*, 349-354.

Sand-Jensen, 1998: Sand-Jensen K. 1998. Influence of submerged macrophytes on sediment composition and near-bed flow in lowland streams. Freshwater Biology *39*, 663-679.

Sand-Jensen and Pedersen, 1999: Sand-Jensen K., and Pedersen O. 1999. Velocity gradients and turbulence around macrophyte stands in streams. Freshwater Biology *42*, 315-328.

Sand-Jensen, 2003: Sand-Jensen K. 2003. Drag and reconfiguration of freshwater macrophytes. Freshwater Biology *48*, 271-283.

Sand-Jensen, 2005: Sand-Jensen K. 2005. Aquatic plants are open flexible structures – a reply to Sukhodolov. Freshwater Biology *450*, 196-198.

Schnauder et al., 2007: Schnauder I., Uijttewaal W.S.J., and Sukhodolov A.N. 2007. Shallow mixing layers at a confluence of parallel streams: field experiments and preliminary results. In: Hydraulic Measurements & Experimental Methods. (E.A. Cowen et al., eds), Proc. Int. Conf. 10-12 Sept. 2007, Lake Placid, USA, 268-273.

Schoppa and Hussain, 2000: Schoppa W., and Hussain F. 2000. Coherent structure dynamics in near-wall turbulence. Fluid Dynamics Research *26*, 119-139.

Schulz et al., 2003: Schulz M., Kozerski H-P., Pluntke T., and Rinke K. 2003. The influence of macrophytes on sedimentation and nutrient retention in the lower River Spree (Germany). Water Research *37*, 569-578.

Shimizu and Tsujimoto, 1993.: Shimizu Y., and Tsujimoto T. 1993. Comparison of flood-flow structure between compound channel and channel with vegetated zone. Proc. 25th Int. Association of Hydraulic Research Congress, Delft, Netherlands.

Smith et al., 1988.: Smith R.D., Pregnall A.M., and Alberte R.S. 1988. Effects of anaerobiosis on root metabolism of the seagrass Zostera marina L. Marine Biology *98*, 131–141.

Spenser and Whitehand, 1993: Spenser D.F, and Whitehand L.C. 1993. Experimental design and analysis in field studies of aquatic vegetation. Lake and Reservoir Management *7*, 165-174.

Stallins, 2006: Stallins J.A. 2006. Geomorphology and ecology: unifying themes for complex systems in biogeomorphology. Geomorphology *77*, 207-216.

Statzner et al., 2006: Statzner B., Lamouroux N., Nikora V., Sagnes P. 2006. The debate about drag and reconfiguration of freshwater macrophytes: comparing results obtained by three recently discussed approaches. Freshwater Biology *51*, 2173-2183.

Statzner and Higler, 1986: Statzner B., and Higler B. 1986. Stream hydraulics as a major determinant of benthic invertebrate zonation patterns. Freshwater Biology *16*, 127-139.

Statzner, 1987: Statzner B. 1987. Ökologische Bedeutung der sohlennahen Strömungsgeschwindigkeit für benthische Wirbellose in Fließgewässern. Habil-Thesis, Univ. Karlsruhe.

Stephan and Gutknecht, 2002: Stephan U., and Gutknecht D. 2002. Hydraulic resistance of submerged flexible vegetation. Journal of Hydrology *269*, 27-43.

Stewart and Thom, 1973: Stewart J.B., and Thom A.S. 1973. Energy budget in pine forest. Q. Journal of Royal Metheorological Society *99*, 154-170.

Stewart, 2006: Stewart H.L. 2006. Hydrodynamic consequences of flexural stiffness and buoyancy for seaweeds: a study using physical models. The Journal of Experimental Biology *209*, 2170-2181.

Stoesser and Rodi, 2004: Stoesser T., and Rodi W. 2004. Large Eddy Simulation of open-channel flow over spheres. In: High performance Computing in Science and Engineering. Nagel W.E, Jäger W., and M. Resch (eds.), Springer.

Stoesser et al., 2006: Stoesser T., Liang C., Rodi W., and Jirka G.H. 2006. Large eddy simulation of fully-developed turbulent flow through submerged vegetation. In: River Flow 2006. R.M.L. Ferreira, E.C.T.L. Alves, J.G.A.B. Leal and A.H. Cardoso (eds.) Proc. of 3rd Int. Conference on Fluvial Hydraulics, September 6-8, 2006, Lisbon, Portugal, V1, 227-234.

Stuart, 1966: Stuart I.M. 1966. A loop test for bending length and rigidity. British Journal of Applied Physics *17*, 1215-1220.

Sukhodolov et al., 1997: Sukhodolov A.N., Nikora V.I., Rowinski P.M., and Czernuszenko W. 1997. A case study of longitudinal dispersion in small lowland rivers. Water Environmental Research *69*, 1246-1253.

Sukhodolov et al., 1998: Sukhodolov A., Thiele M., and Bungartz H. 1998. Turbulence structure in a river reach with sand bed, Water Resources Research *34*, 1317-1334.

Sukhodolov et al., 1999: Sukhodolov A., Thiele M., Bungartz H., and Engelhardt C. 1999. Turbulence structure at an ice-covered river reach with sand bed. Water Resources Research *37*, 2411-2424.

Sukhodolov, 2005: Sukhodolov A. 2005. Comment on drag and reconfiguration of macrophytes. Freshwater Biology *50*, 194–195.

Sukhodolov and Sukhodolova, 2005: Sukhodolov A., and Sukhodolova T. 2005. Morphodynamics and hydraulics of vegetated river reaches: a case study on the Müggelspree in Germany. In: River, Coastal and Estuarine Morphodynamics. G. Parker and M.H. Garcia (eds.), Proc. of the 4th IAHR Symposium, 4-7 October 2005, Urbana, Illinois, USA, 1, 229-236.

Sukhodolov and Sukhodolova, 2006: Sukhodolov A., and Sukhodolova T. 2006. Evolution of mixing layers in turbulent flow over submersible vegetation: field experiments and measurement study. In: River Flow 2006. R.M.L. Ferreira, E.C.T.L. Alves, J.G.A.B. Leal and A.H. Cardoso (eds.) Proc. of 3rd Int. Conference on Fluvial Hydraulics, September 6-8, 2006, Lisbon, Portugal, V1, 525-534.

Sukhodolov et al., 2006: Sukhodolov A.N., Fedele J.J., and Rhoads B.L. 2006. Structure of flow over alluvial bedforms: an experiment on linking field and laboratory methods. Earth Surface Processes and Landforms *31*, 1292-1310.

Sukhodolov et al., 2007: Sukhodolov A., and Sukhodolova T. 2007. Coherent structures in river flows over submerged vegetation: experimental study in a lowland river. In: Hydraulic Measurements & Experimental Methods. (E.A. Cowen et al., eds) Proc. Int. Conf. 10-12 Sept. 2007 , Lake Placid, USA, 172-177.

Sukhodolova et al., 2004: Sukhodolova T., Sukhodolov A., and Engelhardt C. 2004. A Study of turbulent tlow structure in a partly vegetated river reach. In: RiverFlow 2004*,* M. Greco, A. Carravetta & Della Morte (eds.), A. Balkema, 1, 469-478.

Sukhodolova et al., 2006: Sukhodolova T., Sukhodolov A., Kozerski H-P., and Köhler J.. 2006. Longitudinal dispersion in a lowland river with submersible vegetation In: River Flow 2006. R.M.L. Ferreira, E.C.T.L. Alves, J.G.A.B. Leal and A.H. Cardoso (eds.) Proc. of 3rd Int. Conference on Fluvial Hydraulics, September 6-8, 2006, Lisbon, Portugal, 1, 631-638.

Takatera and Shinohara, 1994: Takatera M., and Shinohara A. 1994. An analysis to compare conventional methods for estimating bending rigidity of fabrics. Journal of Textil Machinery Society of Japan *47*, 250-258.

Tukker, 1997: Tukker J. 1997. Turbulence structures in shallow free-surface mixing layers. PhD. Thesis, Rotterdam, the Netherlands.

Taylor, 1953: Taylor G.I. 1953. Dispersion of soluble matter in solvent flowing slowly through a tube. Proc. R. Soc. London, Ser. A *219*, 186-203.

Taylor, 1954: Taylor G.I. 1954. The dispersion of matter in turbulent flow through a pipe. Proc. R. Soc. London, Ser. A *223*, 446-468.

Tennekes and Lumley, 1972: Tennekes H., and Lumley J.L. 1972. A First Course in Turbulence. Cambridge: MIT Press.

Thackston and Schnelle, 1970: Thackston E.L., and Schnelle K.B. 1970. Predicting effects of dead zones on stream mixing. Journal of Sanitary Engineering *96*, 319-331.

Thom, 1971: Thom A.S. 1971. Momentum absorption by vegetation. Q. Journal of Royal Metheorological Society *97*, 414-428.

Thomann, 1973: Thomann R.V. 1973. Effects of longitudinal dispersion on dynamic water quality response of streams and rivers. Water Resources Research *9*, 355-366.

Thomas, 1958: Thomas I.E. 1958. Dispersion in open-channel flow. Ph.D. Thesis, Northwestern University.

Thornley and Johnson, 1990: Thornley J.H.M., and Johnson I.R. 1990. A mathematical approach to the plant and crop physiology. In: Plant and Crop Modeling, Clarendon press, Oxford, 139-144.

Toerien et al., 1983: Toerien D.F., Gary P.R., Finlayson C.M., Mitchell D.S., and Weerts P. G. J. 1983. Growth models for Salvinia molesta. Aquatic Biotany *16*, 173-179.

Tooth and Nanson, 2000: Tooth S., and Nanson G.C. 2000. The role of vegetation in the formation of anabranching channels in an ephemeral river, Nortern plains, arid central Australia. Hydrological Processes *14*, 3099-3117.

Townsend, 1956: Townsend A.A. 1956. The structure of turbulent shear flow. London: Cambridge University Press.

Tsoularis, 2001: Tsoularis A. 2001. Analysis of logistic growth models. Research Letters of Informatics and Mathematics Society *2*, 23-46.

Tsujimoto, 1999: Tsujimoto T. 1999. Fluvial processes in streams with vegetation. Journal of Hydraulic Research *37*, 789-803.

Uijttewaal and Tukker, 1998: Uijttewaal W.S.J., and Tukker J. 1998. Development of quasi two-dimensional structures in shallow free-surface mixing layer. Experiments in Fluids *24*, 192-200.

Uijttewaal and Booij, 2000: Uijttewaal W.S.J., and Booij R. 2000. Effects of shallowness on the development of free-surface mixing layers. Physics of Fluids *12*, 392-402.

Uittenbogaard, 2003: Uittenbogaard R. 2003. Modeling turbulence in vegetated aquatic flows. International workshop on RIParian FORest vegetated channels: hydraulic, morphological and ecological aspects, Trento, Italy.

Valentine and Wood, 1977: Valentine E.M., and Wood I.R. 1977. Longitudinal dispersion with dead zones. Journal of Hydraulic Division. *103*, 975-990.

Vannote et al., 1980: Vannote R.L., Minshall G.W., Cummings K.W., Sedell J.R., and Cushing C.E. 1980. The river continuum concept. Canadian Journal of Fisheries and Aquatic Sciences *37*, 130-137.

Velasko et al., 2005: Velasko D., Bateman A., and DeMedina V. 2005. A new integrated hydro-mechanical model applied to flexible vegetation in riverbeds. In: River, Coastal and Estuarine Morphodynamics. G. Parker and M.H. Garcia (eds.), Proc. of the 4th IAHR Symposium, 4-7 October 2005, Urbana, Illinois, USA, 1, 217-228.

Velikanov, 1946: Velikanov M.A. 1946. Kinematic structure of turbulent flow in open channel. Bulletin of the Academy of Sciencess of USSR*, X(4)*, 331-340.

Velikanov, 1958: Velikanov M.A. 1958. Channel Process (Background of Theory). Phys-Math. Publ., Moscow.

Verhulst, 1838: Verhulst P.F. 1838. A note on population growth. Correspondances Mathématiques et Physiques *10*, 113-121.

Voulgaris and Trowbridge, 1998: Voulgaris G., and Trowbridge J.H. 1998. Evaluation of the acoustic Doppler velocimeter (ADV) for turbulence measurements. Journal Atmospheric and Oceanic Technology*, 15*, 272-289.

Webb, 1975: Webb P.W. 1975. Hydrodynamics and energetics of fish propulsion. Bulletin of the Fisheries Research Board of Canada *190*, 1-159.

Webster, 1975: Webster J.R. 1975. Analysis of Potassium and Calcium Dynamics in Stream Ecosystems on Three Southern Appalachian Watersheds of Contrasting Vegetation. Ph.D. Thesis, University of Georgia.

Werker and Jaggard, 1997: Werker A.R., and Jaggard K.W. 1997. Modelling asymmetrical growth curves that rise and then fall: application to foliage dynamics of sugar beet (Beta vulgaris L). Annals of Botany *79*, 657-665.

Wilson and Shaw, 1977: Wilson N.R., and Shaw R.H. 1977. A high-order closure model for canopy flow. Journal of Applied Metheorology *16*, 1198-1205.

Wilson et al., 1986: Wilson J.F. Jr., Cobb E.D., and Kilpatrick F.A. 1986. Fluorometric Procedures for Dye Tracing. Applications of Hydraulics 3**,** U.S. Geological Survey, Denver, CO.

Wilson et al., 2007: Wilson D. J., Alm T., Riutta J., Laine K.A., Byrne E.P., Farrell E., and Tuitilla S. 2007. A high resolution green area index for modelling the seasonal dynamics of CO2 exchange in peatland vascular plant communities. Plant Ecology *190*, 37-51.

Wilson 2007: Wilson C.A.M.E. 2007. Flow resistance models for flexible submerged vegetation. Journal of Hydrology *324*, 213-222.

Winant and Browand, 1974: Winant C., and Browand F.K. 1974. Vortex pairing, the mechanism of turbulent mixing-layer growth at moderate Reynolds number. Journal of Fluid Mechanic*s 63*, 237-255.

Wolter and Arlinghaus, 2003: Wolter C., and Arlinghaus R. 2003. Navigation impacts on freshwater fish assemblages: the ecological relevance of swimming performance. Reviews in Fish Biology and Fisheries *13*, 63-89.

Wolter and Arlinghaus, 2004: Wolter C., and Arlinghaus R. 2004. Burst and critical swimming speeds of fish and their ecological relevance in waterways. Berichte des IGB, Berlin, *20*, 77-93.

Wolter and Sukhodolov, 2008: Wolter C., and Sukhodolov A. 2008. Random displacement versus habitat choice of fish larvae in rivers. River Research and Applications *24***,** 661-672.

Wright et al., 1981: Wright J.F., Hiley P.D., Ham S.F., and Berrie A.D. 1981. Comparison of three mapping procedures developed for river macrophytes. Freshwater Biology *11*, 369-379.

Wrigth et al., 1982: Wrigth J.F., Cameron A.C., Hiley P.D., and Berrie A.D. 1982. Seasonal changes in biomass of macrophytes on shaded and unshaded sections of the River Lambourn, England. Freshwater Biology *12*, 271-283.

Wygnanski and Fiedler, 1970: Wygnanski I., and Fiedler H.E. 1970. The two-dimensional mixing region. Journal of Fluid Mechanics *41*, 327-361.

Young and Wallis, 1986: Young P.C., and Wallis S.C. 1986. The aggregated dead zone model for dispersion. In: Water Quality Modelling in the Inland Natural Environment*,* BHRA, Cranfield, 421-433.

Zitek et al., 2004: Zitek A., Schmutz S., and Ploner A. 2004. Fish drift in a Danube sidearm-system: II. Seasonal and diurnal patterns. Journal of Fish Biology *65*, 1339-1357.

LIST OF SYMBOLS

A	cross-section area of the flow	m^2
A_d	dead zone area in transversal plane	m^2
A_{bed}	area of the riverbed on a reach	m^2
A_{veg}	planar area covered by vegetation	m^2
A^*	dimensionless relative area	
a	projected area of the plants per unit volume	m^{-1}
a_{ij}	coefficients of the calibration matrix	
B	river width	m
$B, B_0, B_{\max}$	biomass, initial biomass, and maximal biomass	kg/m^2
b	dimensionless transversal coordinate	
C	Chezy coefficient	$m^{1/2}/c$
C, c	concentration of substances	g/L
C^*	normalized concentration of substances	
C_b	coefficient determining the type of load on a cantilever beam	
C_D	drag coefficient	
C_d	concentration in the dead-zone	g/L
C_k	empirical constant	
C_0	universal constant in -5/3 law	
c_f	friction factor	
C_s	speed of sound in water	m/s
C_w	constant in biomass growth model	
D	longitudinal dispersion coefficient	m^2/s
D_k	dimensionless parameter	
d	diameter of a sedimentary grain, width of a plant	mm
d_{50}	characteristic size of riverbed material	mm
d_p	thickness of a plant	mm
E	elasticity modulus	N/m^2
erf	error function	
e_m	coefficient of molecular diffusion	m^2/s

e_T	coefficient of turbulent diffusion	m^2/s
F_B	buoyant force	N
F_d	drag force	N
F_G	gravity force	N
F_f	friction force	N
F_r	rigidity force	N
f	frequency	Hz
Fr	Froude number	
g	specific gravity	m/s^2
h	flow depth	m
h_v	height of the vegetation layer	m
I_a	second moment of area of the cantilever beam	m^4
I	energy gradient, slope of the free surface	
i_0	slope of the riverbed	
K	curvature of a cantilever	
K_d	decay/increase rate of a substance concentration in dead zone	s^{-1}
K_C	carrying capacity	kg/m^2
K_b	dimensionless ratio between bending load and rigidity	
K_i	coefficient of turbulent dispersion	m^2/s
k	turbulent kinetic energy	$m^2/s2$
K_m	growth/decay rate in the main stream	s^{-1}
L_C	longitudinal scale of coherent structures	m
L_b	bending length	m
L	length of the cantilever beam	m
L	loss of biomass because of decay	kg/m^2
L_x	integral length scale	m
L_T	integral time scale	s
l	length scale	m
M	moment of the bending force	Nm
M_T	mass of injected tracer	kg
n	Manning's coefficient	$sm^{-1/3}$

P	photosynthetic production of biomass	kg/m^2
P_l	lateral load	N
p	pressure	N/m^2
Q	water discharge	m^3/s
q_b	volume unit bedload discharge	m^2/s
q_s	volume unit suspended sediment discharge	m^2/s
R	losses of biomass because of respiration	kg/m2
$R(\tau)$	auto-correlation function	
Re	Reynolds number	
$r(t)$	net rate of biomass growth	s^{-1}
$r(\tau)$	auto-covariance function	m^2/s^2
$r_{1-2}(\tau)$	cross-covariance function	m^2/s^2
S	dimensionless stability parameter	
$S(f)$	spectral function	
Sk	skewness	
St	Strouhal number	
S_s	speed of sound	m/s
S_W	speed of sand waves propagation	m/s
s'	length of segment of the material	m
T_c	period of coherent structures	s
T_d	residence time of the dead zone	s
T	temperature	ºC
T_L	Lagrangian temporal scale of longitudinal dispersion	s
T_m	Lagrangian temporal scale of mechanical dispersion	s
t	time	s
t^*	dimensionless time	
t_p	time of tracer cloud peak	s
U	random variable	m/s
U	bulk velocity of flow	m/s
u	instantaneous velocity, streamwise velocity component	m/s
u_C	mean velocity in the center of the mixing layer	m/s
u_s	settling velocity of suspended sediments	m/s

u_*	shear velocity in vertical plane	m/s
V	volume of submersed body	m^3
V_i	velocity component	m/s
v	transverse velocity component	m/s
v_*	shear velocity in horizontal plane	m/s
W	random variable	
w	vertical velocity component	m/s
w_L	weight of material per unit length	N/m
X	body forces	N
x	spatial coordinate in the longitudinal direction	m
y	spatial coordinate in the transversal direction	m
z	spatial coordinate in the vertical direction	m
z_s	free surface elevation	m
z_0	hydrodynamic roughness parameter	m
α	angle of riverbed slope or a plant deflection	º, rad.
α_C	spreading coefficient	
α_u	coefficient in longitudinal dispersion formulae	
β_B	coefficient in longitudinal dispersion formulae	
β	asymmetry parameter in biomass growth equations	
γ	scaling parameter	
γ_s	porosity of riverbed material	
Δ	height of roughness elements	m
Δu	velocity difference in the mixing layer	m/s
$\Delta\Phi$	phase difference	rad.
$\Delta\overline{T}$	average period of sand waves travel	s
δ	mixing layer width	m
$\delta(t)$	decay loss coefficient for biomass	s^{-1}
δ_x, δ_z	deflections of the cantilever beam	m
ε	turbulent kinetic energy dissipation per unit mass	m/s^3
э	relative volume of dead zones	
ζ	dimensionless horizontal coordinate	
κ	von Karman parameter	
λ	velocity ratio in mixing layer	

$\lambda(t)$	respiration loss rate of biomass	s^{-1}
λ_p	porosity of sediment deposits	
μ	empirical constants	
$\mu(t)$	growth rate of biomass	s^{-1}
μ_n	statistical moments	
η	dimensionless vertical coordinate	
ν	kinematic viscosity	m^2/s
ν_T	turbulent viscosity	m^2/s
ξ	dimensionless transversal coordinate	
π	3.1412…	
Π	turbulence production rate per unit mass	W/kg
ρ , ρ_0	density of water	kg/m^3
ρ_r	relative density	
ρ_s	density of riverbed material	kg/m^3
σ_t^2 , σ_x^2	temporal and spatial variance of the tracer cloud	s^2, m^2
σ	standard deviation of the acoustic noise	m/s
σ_u^2	variance of Lagrangian velocity	m^2/s^2
σ_m^2	variance of Lagrangian velocity due to mechanical dispersion	m^2/s^2
τ_{ij}	shear stress	N/m^2
τ	time lag	s
φ	angle for cantilever bending test	º, rad.
χ	dimensionless streamwise coordinate	
ψ	streamline function	m^2/s
ψ	dimensionless transverse shear stresses	
ϑ	dimensionless penetration depth	
Ω	stability parameter	
∇^2	Laplacian operator	
υ	coefficient representing squared ratio of velocity scales	

LIST OF PUBLICATIONS

Sukhodolova T., Sukhodolov A., and Engelhardt C. 2004. A study of turbulent flow structure in a partly vegetated river reach. In: RiverFlow 2004, M. Greco, A. Carravetta & Della Morte (eds.), A. Balkema, Vol. 1, 469-478.

Sukhodolov A., and Sukhodolova T. 2005. Morphodynamics and hydraulics of vegetated river reaches: a case study on the Müggelspree in Germany. In: G.Parker and M.H. Garcia (eds.) River, Coastal and Estuarine Morphodynamics, 229-236.

Sukhodolov A., and Sukhodolova T. 2006. Evolution of mixing layers in turbulent flow over submerged vegetation: field experiments and measurement study. In: River Flow 2006. R.M.L. Ferreira, E.C.T.L. Alves, J.G.A.B. Leal and A.H. Cardoso (eds.) Proc. of 3rd Int. Conference on Fluvial Hydraulics, September 6-8, 2006, Lisbon, Portugal, Vol. 1, 525-534.

Sukhodolova T., Sukhodolov A., Kozerski H.-P., and Köhler J. 2006. Longitudinal dispersion in a lowland river with submerged vegetation. In: River Flow 2006. R.M.L. Ferreira, E.C.T.L. Alves, J.G.A.B. Leal and A.H. Cardoso (eds.) Proc. of 3rd Int. Conference on Fluvial Hydraulics, September 6-8, 2006, Lisbon, Portugal, Vol. 1, 631-638.

Sukhodolova T., and Sukhodolov A. 2006. Field-scale experiment on the flow dynamics over submerged macrophytes, In: Berichte des IGB, Vol. 23, 65-78.

Sukhodolov A., Sukhodolova T., and H. Bungartz 2006. Turbulence in natural streams. In: J. Studzinski and O. Hryniewicz (eds.) Modelling Concepts and Decision Support in Environmental Systems, 41-56.

Sukhodolov A., Uijttewaal S.W.J., Schnauder I., Sukhodolova T., Erdbrink C., Brevis W., Pusch M., and F. Gabel. 2007. Flow visualization in natural streams: examples and perspectives. In: 32nd Congress of IAHR, 1-6 July 2007, Venice, Italy, Vol. 1, 68.

Zinke P., N.R.B. Olsen, and T. Sukhodolova 2008. Modeling of hydraulics and morphodynamics in a vegetated river reach. River Flow 2008, 3-5 September 2008, Izmir, Turkey (accepted)

ACKNOWLEDGMENTS

The study was completed in the Institute of Freshwater Ecology and Inland Fisheries (IGB) – a multidisciplinary oriented research institution uniting ecologists, hydrologists, chemists, and practitioners. The objectives of research in IGB, the comprehensive expertise, and predominant occupation with processes in nature provided fertile grounds for the study. I am grateful to many people who contributed to my professional development, sheared ideas, resources, and spent time for data collection and processing.

The opportunity for me to participate in this graduate program was provided by Drs. Heinz Bungartz and Hans-Peter Grossart (IGB) through the financial support of Deutsche Forschungsgemeinschaft (BU 1442/1). The program was embedded into the curriculum of Geography Department, Humboldt University, Berlin by Prof. Gunnar Nützmann who also kindly accepted the load to promote the thesis. The daily supervision and guidance on all stages of the research was provided by Dr. Alexander Sukhodolov (IGB).

Many colleagues from IGB discussed parts of the dissertation, helped in carrying out field investigations and preparing the equipment: Jan Köhler, Hans-Peter Kozerski, Martin Pusch, Andreas Kleeberg, Ingo Schnauder, Christian Wolter, Sabine Hilt, Antji Lüder, Nicholas Nikolaevich, Jörg Friedrich, Grit Siegert, Henrik Zwadlo, and Rüdiger Biskupek.

I also appreciated collaboration with Prof. Nils Reidar B. Olsen and PhD student Peggy Zinke from the Norwegian University of Science and Technology, Trondheim.

Through the completion of the graduation program I have got the possibility to participate in the summer school organized by the Institute for Hydrodynamics, University of Karlsruhe and in a Master class on turbulent flows of the RiverFlow2006 international conferences. These short courses as well as the conferences RiverFlow2004, 2006, RCEM 2005, and regular internal workshops in the IGB were important milestones for the development of this thesis.